Structural Investigations of Pro-apoptotic Bcl-2 Family Proteins

Angus David Cowan

ORCID: 0000-0002-9702-7319

Doctor of Philosophy

August 2017

Walter and Eliza Hall Institute of Medical Research

Department of Medical Biology

The University of Melbourne

Submitted in total fulfilment of the requirements of
the degree of Doctor of Philosophy

Abstract

The Bcl-2 protein family regulates the intrinsic apoptotic pathway through an intricate network of protein:protein and protein:membrane interactions. The pathway culminates in the permeabilisation of the mitochondrial outer membrane by the pro-apoptotic effector proteins Bak and Bax, an event that irreversibly commits a cell to death. To facilitate membrane permeabilisation, Bak and Bax undergo a series of conformational changes to convert from inert monomers to membrane-embedded homodimers that nucleate and propagate apoptotic oligomers. While great strides have been made in structurally characterising these conformational changes, questions remain surrounding homodimer interactions with the membrane, oligomerisation, and membrane pore formation. This thesis addresses these questions by providing structures of lipids bound to Bak BH3:groove core homodimers (Chapter 2). These are the first structures of any Bcl-2 family protein in complex with lipid. They reveal symmetric binding sites for phospholipid headgroups and acyl chains. In one structure, adjacent Bak homodimers are cross-linked by the acyl chains of single phospholipids, suggesting homodimer oligomerisation could be mediated by lipid. Bak oligomers could be dissociated with phospholipase A2, supporting a role for lipid in oligomer stability. Collectively, the structures presented here indicate that lipids may play a direct role in Bak oligomerisation.

Like Bak, Bax homodimerises and oligomerises on the mitochondrial outer membrane. The original Bax BH3:groove core homodimer structure was solved as a GFP fusion at low resolution. Here, a tetrameric structure consisting of two Bax BH3:groove core homodimers alone was solved at high resolution (Chapter 3), providing details for canonical interactions in atomic detail. A crystal structure of Bax BH3:groove core homodimers containing lipid was also solved, although the structure could not be refined due to severe twinning. This result demonstrates that Bax core domains also associate with lipid, and provides a starting point for crystal optimisation.

Pro-survival Bcl-2 family proteins antagonise the apoptotic function of Bak and Bax by preventing their activation and sequestering their activated forms. Sequestration of activated Bak and Bax in heterodimeric Mode 2 complexes involves binding of the

Bak/Bax BH3 domain to a conserved hydrophobic groove. Beyond this, little is known regarding the topology of these complexes. The pro-survival protein Bcl-X_L can undergo similar conformational changes to Bak and Bax, but whether it forms BH3:groove heterodimers with Bak/Bax was unknown. Using cysteine cross-linking on mitochondria, I show that Bcl-X_L can form reciprocal BH3:groove heterodimers with Bax, and possibly Bak (Chapter 4). These results challenge a simplistic view of Mode 2 complexes, implicating more extensive interactions beyond the canonical BH3 in groove interface.

Bok is a third potential pro-apoptotic effector protein that shares sequence similarity with Bak and Bax, but its role in apoptosis remains unresolved. To investigate the structure and function of Bok, I developed a recombinant expression system to produce human, rat, and chicken Bok. The first crystal structure of Bok, from the chicken, reveals the canonical Bcl-2 family fold, with deviations that may explain its proposed constitutive activity (Chapter 5). The structure paves the way for mutagenesis studies that will further our understanding of this enigmatic protein.

Declaration

This is to certify that:

i) this thesis comprises only my original work towards the degree of Doctor of Philosophy, except as indicated in the Preface;

ii) due acknowledgement has been made in the text to all other materials used;
and

iii) this thesis is less than 100,000 words in length, exclusive of tables, maps, bibliographies and appendices.

Preface

In accordance with the regulations of the University of Melbourne, I acknowledge that some of the data in Chapter 2 were obtained in conjunction with collaborators at the Walter and Eliza Hall Institute and the Bio21 Molecular Science and Biotechnology Institute. Specifically:

- The lipid mass spectrometry data presented in **Figure 12** and **Table 7** were collected on samples provided to Yepy Rustam (Bio21 Molecular Science and Biotechnology Institute) in the laboratory of Gavin Reid (Bio21 Molecular Science and Biotechnology Institute) and analysed by Yepy Rustam
- SAXS data presented in **Table 2** and **Figure 13** was collected in conjunction with James Murphy (Cell Signalling and Cell Death Division, Walter and Eliza Hall Institute) and analysed by James Murphy
- Chromatograms and Western blots in **Figure 21** were obtained in conjunction with Ahmad Wardak (Structural Biology Division, Walter and Eliza Hall Institute)
- Thin-layer chromatography experiments presented in **Figure 26** were performed in conjunction with Michael Roy (Chemical Biology and Structural Biology Divisions, Walter and Eliza Hall Institute)

All other experiments comprise my own work.

Acknowledgments

I would like to take the time to acknowledge the many people who have helped me during my PhD in one way or another.

First and foremost, I would like to thank my two supervisors, Peter Czabotar and Peter Colman, for their guidance and wisdom. To Peter Czabotar, thank you for teaching me to steer the Synchrotron and sharing my excitement about new results and ideas. Your sharp, analytical and imaginative mind kept me on track when I went meandering off from time to time. To Peter Colman, thank you for taking the time to help me better understand crystallography. I still have much to learn, but your passion and deep knowledge of the discipline are inspiring.

My family has been a constant source of love, support and laughs throughout my PhD and my life. Weekend dinners at home were the place to share triumphs and tribulations. Thanks to my mum, Sally, for looking after me and making sure I looked after myself. Thanks to my brother, Max, for keeping me entertained. Thanks to my dad, Peter, for his advice in science and life, and for comments and proofreading of this thesis. Thank you to my partner, Becky, for her love and friendship, for showing patience and compassion during the bad times, for sharing my excitement in the good times, and for making me laugh every day.

I acknowledge and thank my committee members, the chair Jeff Baboon, Melissa Call and Grant Dewson, for their support, insight and ideas. In particular, I owe much to Grant who took me into his group in the Cell Signalling and Cell Death Division and taught me the art of tissue culture. His comments on this thesis were invaluable. I would also like to thank members of the Dewson laboratory; Iris Tan, Mark Li, Jon Bernardini, and former member Rob Ninnis, for helping me when I was out of my comfort zone, navigating the fifth floor of WEHI.

The Czabotar and Colman laboratories have provided an excellent environment for me to grow as a scientist and a person. I would like to thank the following people: Adeline Robin and Rich Birkinshaw, for advice and help in the lab and out of it; Ahmad Wardak,

the liposome guru, for helping to optimise a number of the experiments presented in this thesis; Michael Roy for his help with thin-layer chromatography experiments; Daisy Luo and former lab member Yan Hong Tan for their help with cloning; former lab member Geoff Thompson who helped orientate me in the lab when I began my PhD. In particular, I would like to thank Jason Brouwer for his encouragement and friendship. Jason inspired me to try things outside science, and it is thanks to him that I joined the Reconciliation Committee and was able to participate in the life-changing experience that I had in the Northern Territory with the organisation Teachabout.

Thank you to the Structural Biology Division for providing a fun and stimulating working environment. Thanks to Matt Call for advice at work and the many conversations shared (and beers bought) on Fridays at the pub. Thanks to Amanda Voudaris for keeping the division running smoothly and helping me organise my scientific forays overseas.

I acknowledge the Walter and Eliza Hall Institute, particularly the Chemical Biology, Cell Signalling and Cell Death, and Molecular Genetics of Cancer Divisions. I made many friends here and it was a great privilege to work with so many gifted scientists and diligent professional staff. The Reconciliation Committee were a great group to work with and I thank them for their friendship.

I would also like to thank and acknowledge collaborators who contributed to this body of work. Thank you to Yepy Rustam and Gavin Reid for their input and expertise in everything lipid. Thank you to James Murphy for the SAXS experiments, advice and deadpan jokes.

I acknowledge the Australian Synchrotron and thank the staff of the MX beamlines. I also acknowledge and thank the C3 facility at CSIRO for the 240 or so crystal trays set up there. Thank you in particular to Janet Newman for running such a stellar facility.

I acknowledge sources of funding during my PhD. Thank you to the Australian Government for my scholarship. Thank you to WEHI for the Edith Moffat Travel Award. Thank you to the organisers of AsCA 2015 and ECM-30 for travel bursaries.

Thank you to the Society of Crystallographers in Australia and New Zealand travel awards for a local and international conference.

Thank you to Callum Lawrence, my dear friend, who introduced me to WEHI and a great many other things as well. It has been a long road from undergrad to doctorate and a privilege to share the journey with you.

Thank you to the pub and dumplings crew for your friendship and the many beers, wines, and MSG-coated dumplings that we shared together. Thanks to Raphael Trenker and Christoph Grohmann, former housemates and fast friends. Thanks to Margs Brennan, Nick Liau, Cyrus Tan, Emma Watson, Katrina Black, Kerstin Brinkmann, Zoe Grant, Che Stafford, Michael Coffey, Loges Krshnan, Robyn Schenk, Tom Hayman, Tash Anstee, Erin Lawrence, Katherine Davies, Sean Hewetson, Nick Chandler, Rhiannon Morris, other people mentioned above, and the many other friends too numerous to list here, for your camaraderie.

Thanks to Mick, Brendan, Jack and Seb. May the Turf Rest in Peace.

Thank you to my close friends Tim, Cam, Sam, Durham, Alice, Matt, Gemma, Emma, Marty, Aric, Johnnie, Stu, Nico, Paul, Helen and Meighan for reminding me of life outside the lab.

Table of Contents

List of Figures

Chapter 1

Chapter 2

Chapter 3

Chapter 4

Chapter 5

List of Tables

Chapter 2

Chapter 3

Chapter 5

Abbreviations

AFM	Atomic force microscopy
BH	Bcl-2 homology
C8E4	Tetraethylene glycol monooctyl ether
CHAPS	3-([3-cholamidopropyl]dimethylammonio)-1-propanesulfonate
CHAPSO	3-([3-cholamidopropyl]dimethylammonio)-2-hydroxy-1-propanesulfonate
COX	Cyclooxygenase
Cryo-EM	Cryo-electron microscopy
CuPhe	Copper phenanthroline
DDM	*n*-Dodecyl-β-D-maltoside
DEER	Double electron-electron resonance
DGS-NTA	1,2-dioleoyl-*sn*-glycero-3-[(*N*-(5-amino-carboxypentyl)iminodiacetic acid)succinyl]
DHPC	1,2-dihexanoyl-*sn*-glycero-3-phosphocholine
DKO	Double knockout
DMPG	1,2-ditetradecanoyl-*sn*-glycero-3-phospho-(1'-rac-glycerol)
DOPC	1,2-dioleoyl-*sn*-glycero-3-phosphocholine
EDTA	Ethylenediaminetetraacetic acid
EPR	Electron paramagnetic resonance
ER	Endoplasmic reticulum
ERAD	Endoplasmic reticulum-associated degradation
FACS	Fluorescence-activated cell sorting
GF	Gel filtration
GFP	Green fluorescent protein

GST	Glutathione S-transferase
HA	Hemagglutinin
HCD	Higher-energy collision-induced dissociation
IMS	Intermembrane space
IP	Immunoprecipitation
IP3R	Inositol 1,4,5-trisphosphate receptors
IPTG	Isopropylthio-β-galactosidase
IRES	Internal ribosome entry site
LLG	Log-likelihood gain
LUV	Large unilamellar vesicles
LysoPC	1-palmitoyl-2-hydroxy-*sn*-glycero-3-phosphocholine
MEF	Mouse embryonic fibroblast
MELB	M-phase egg lysis buffer
MES	2-(*N*-morpholino)ethanesulfonic acid
MOM	Mitochondrial outer membrane
MOMP	Mitochondrial outer membrane permeabilisation
NEM	*N*-Ethylmaleimide
NMR	Nuclear magnetic resonance
O.D.	Optical Density
PBS	Phosphate-buffered saline
PDB	Protein Data Bank
PE	Phosphatidylethanolamine
PEG	Polyethylene glycol
PFP	Pore-forming protein
PI	Phosphatidylinositol
POPC	1-palmitoyl-2-oleoyl-*sn*-glycero-3-phosphocholine

PS	Phosphatidylserine
PVDF	Polyvinylidene fluoride
S200	Superdex 200
S75	Superdex 75
SB	Super Broth
SUV	Small unilamellar vesicle/liposome
TBS	Tris-buffered saline
TBS-T	TBS-Tween
TEN	Tris-EDTA sodium
TFZ	Translation function Z-score
TLC	Thin-layer chromatography
TM	Transmembrane
UPR	Unfolded protein response
WT	Wild type

Chapter 1

Introduction

1.1 Apoptosis

In 1972, John Kerr, Andrew Wyllie and Alastair Currie coined the term "apoptosis" to describe a "little recognised mechanism of controlled cell deletion" (Kerr *et al.*, 1972). The significance and indispensability of this fundamental biological process in multicellular organisms would become apparent in the years to follow. Though cell death had been described previously as a normal part of embryonic development (Glucksmann, 1951; Lockshin and Williams, 1965; Saunders, 1966), Kerr and colleagues were the first to characterise the distinct morphological and biochemical changes that occur during this process, including nuclear and cytoplasmic condensation, fragmentation of the cell and engulfment of cell fragments by phagocytosis (Kerr, 1971; Kerr *et al.*, 1972).

Closely connected to the story of apoptosis is the study of cell lineage and fate in the flatworm *Caenorhabditis elegans* by John Sulston and H. Robert Horovitz in the lab of Sydney Brenner (Sulston and Horvitz, 1977). In this work, the authors observed that of the total number of cells generated during development, 131 were missing from the healthy adult worm. These missing cells underwent programmed cell death, though the genes responsible for execution and regulation of this program were unknown at the time (Sulston and Horvitz, 1977). The genes controlling the worm's apoptotic program were later identified in Horovitz's own lab, including the apoptosis-inducing *ced-3* (cell death abnormal-3) and *ced-4* (cell death abnormal-4) and the apoptosis-inhibiting *ced-9* (cell death abnormal-9) (Ellis and Horvitz, 1986; Hengartner and Horvitz, 1994).

Meanwhile, the *bcl-2* (B-cell lymphoma 2) gene was identified in a human acute pre-B-cell leukaemia cell line (Tsujimoto *et al.*, 1984). The gene, situated on chromosome 18, was placed under the control of the immunoglobulin heavy chain promoter due to the t(14;18) chromosome translocation often observed in B-cell follicular lymphomas (Bakhshi *et al.*, 1985; Bakhshi *et al.*, 1987). This translocation was proposed to result in altered expression of the otherwise native Bcl-2 protein by both transcriptional activation and abnormal posttranscriptional regulation of *bcl-2*

mRNA (Cleary *et al.*, 1986). The oncogenic potential hinted at in these studies was demonstrated in 1988, when David Vaux, in the lab of Jerry Adams and Suzanne Cory, reported the anti-apoptotic and tumorigenic activity of the *bcl-2* gene in haematopoietic cells (Vaux *et al.*, 1988). Bcl-2 was unique among known oncogenes at the time in that it prevented cell death rather than promoting cell division and differentiation. The work on Bcl-2 and apoptosis in *C. elegans* came together when Vaux *et al.* showed that overexpression of Bcl-2 prevented apoptosis in worm cells (Vaux *et al.*, 1992). Following cloning of the ced-9 gene, sequence homology was established between Bcl-2 and ced-9, demonstrating aspects of the cell death program were evolutionarily conserved in vertebrates and invertebrates, with increasing complexity in higher organisms (Hengartner and Horvitz, 1994).

Apoptosis is essential in multicellular organisms for many physiological processes including normal tissue development, maintenance of homeostasis and defence against disease and cytotoxic insults, such as viral infection or UV irradiation. Unsurprisingly then, dysregulation and disruption of the apoptotic program is observed in many different diseases. Viral and bacterial infections often suppress apoptosis to allow for replication in infected cells (Lamkanfi and Dixit, 2010). There are a number of viral homologues of Bcl-2 pro-survival proteins that block the apoptotic pathway to promote infected cell survival (Kvansakul and Hinds, 2013). Suppression of apoptosis is also one of several hallmarks of cancer (Hanahan and Weinberg, 2011). On the other hand, aberrant apoptosis has also been implicated in neurodegenerative disease (Ghavami *et al.*, 2014).

A deep and comprehensive understanding of certain aspects of intrinsic apoptosis at the molecular level has led to the development of novel therapeutics; most notably the BH3-mimetic drug Venetoclax that inhibits Bcl-2 (Souers *et al.*, 2013). Venetoclax has significantly improved the prognosis for patients with chronic lymphocytic leukaemia bearing the 17p deletion (Roberts *et al.*, 2016). The molecular mechanisms that govern apoptosis are a key area of research for treating disease, and further elucidation of these mechanisms will likely lead to more breakthrough treatments.

1.2 The Bcl-2 Protein Family

There are two apoptotic pathways found in mammals that converge at the activation of caspases. Death-receptor mediated, or "extrinsic", apoptosis involves the ligation of death receptors of the tumour necrosis factor receptor gene superfamily by their cognate ligands, leading to activation of caspase-8 and downstream caspases. Mitochondrial, or "intrinsic", apoptosis is mediated by Bcl-2 and related proteins collectively referred to as the Bcl-2 protein family. Bcl-2 family proteins primarily localise to the mitochondrial outer membrane (MOM) where homo- and hetero-typic interactions between these proteins either antagonise or activate apoptosis. Activation of the intrinsic pathway culminates in mitochondrial outer membrane permeabilisation (MOMP), releasing apoptogenic molecules from the intermembrane space (IMS) and committing the cell to death. The subject of this thesis is the Bcl-2 protein family.

Bcl-2 family proteins exhibit either pro-survival or pro-apoptotic functions. There are 6 known pro-survival proteins in mammals: Bcl-2, Mcl-1, Bcl-X_L, Bcl-w, Bfl-1 and Bcl-B. Pro-apoptotic Bcl-2 proteins are divided into two groups. The first group, called the BH3-only proteins, sense and convey apoptotic stimuli and include Bid, Bim, Puma, Noxa, Bad, Bmf, Bik and Hrk. The pro-apoptotic effector proteins Bak and Bax that cause MOMP comprise the second group, and are structurally similar to the pro-survival proteins. Bok, another potential pro-apoptotic effector protein, may also cause MOMP. A delicate balance of protein-protein interactions between these family members governs cell fate (**Figure 1**).

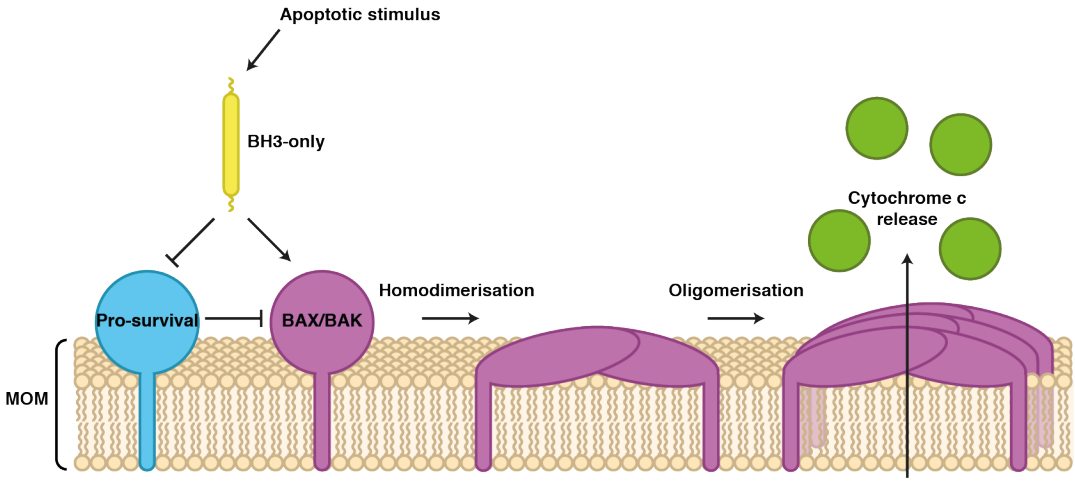

Figure 1. Regulation of intrinsic apoptosis by the Bcl-2 protein family. *Apoptosis is initiated when stress stimuli upregulate and activate BH3-only proteins, (yellow). Pro-survival proteins (blue) sequester and repress Bak and Bax (purple) and are neutralised by BH3-only proteins. Bax and Bak are directly activated by certain BH3-only proteins, inducing conformational changes that lead to homodimerisation. Homodimers assemble into higher-order oligomers and permeabilise the MOM, releasing cytochrome c and other apoptogenic factors and committing the cell to death by apoptosis.*

Bcl-2 family members share short stretches of sequence homology known as Bcl-2 homology (BH) domains (**Figure 2A**). The pro-survival proteins and Bak, Bax and Bok contain BH domains 1-4. BH3-only proteins, on the other hand, contain only the BH3 domain, an amphipathic α-helix important for inter-family interactions that is common to all Bcl-2 family proteins. Structurally, the pro-survival proteins, multi-BH domain effector proteins Bak and Bax, and the BH3-only protein Bid (before it is activated by cleavage) are highly similar despite having different functional roles. Seven α-helices fold around a central hydrophobic helix forming a globular bundle that is, in most cases, anchored to the MOM by a single transmembrane (TM) helix (**Figure 2B** and **C**). A key feature of the fold, formed by amino acids of the BH domains, is a hydrophobic surface groove bounded primarily by α-helices 3, 4 and 5 (**Figure 2C**). Overwhelming binding of pro-apoptotic BH3 domains to both pro-survival and pro-apoptotic hydrophobic grooves leads to MOMP and apoptosis.

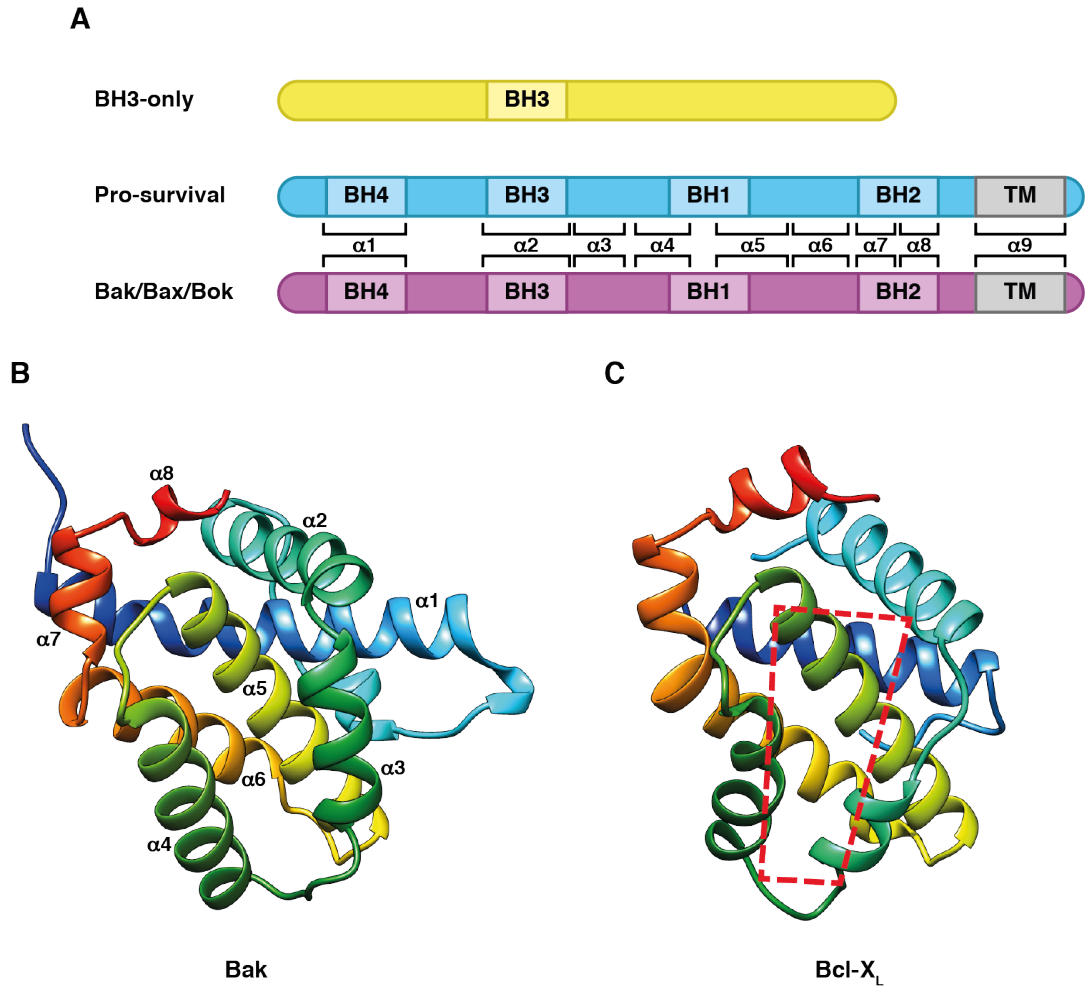

Figure 2. Domain architecture and tertiary structure of Bcl-2 family proteins. ***A)*** *Domain organisation of the 3 sub-families of Bcl-2 proteins. BH domains 1-4 are present in both pro-survival proteins and Bak/Bax/Bok while BH3-only proteins contain only the BH3 domain. The α-helices of the pro-survival proteins and Bak/Bax/Bok are labelled, including the α9 TM helix.* ***B)*** *and* ***C)*** *X-ray crystal structures of Bak (PDB code: 2IMS (Moldoveanu et al., 2006)) and Bcl-X_L (PDB code: 1MAZ (Muchmore et al., 1996)), respectively, in cartoon representation coloured in rainbow (from blue N- to red C-terminus). Each α-helix from 1 to 8 in Bak is labelled and the hydrophobic surface groove that binds BH3-domains is labelled with a red dotted line on Bcl-X_L.*

The intrinsic apoptotic pathway is initiated by a wide range of stimuli that upregulate BH3-only proteins at a transcriptional and/or post-translational level. All BH3-only proteins promote apoptosis by binding to and antagonising the function of pro-survival proteins and some are capable of directly activating Bak and Bax. When pro-survival

proteins, which normally restrain Bak and Bax, are overwhelmed by BH3-only proteins, Bak and Bax homodimerise and oligomerise on the MOM. Oligomerisation results in MOMP, leading to the release of proteins such as cytochrome *c* and SMAC from the IMS (Kluck *et al.*, 1997). Cytochrome *c* forms a complex with Apaf-1 and ATP that binds to and activates caspase-9, forming the "apoptosome". The apoptosome activates effector caspases leading to the degradation of cellular contents.

Chemical inhibition of caspases only slows cell death after MOMP is initiated, and while genetic ablation of caspase activation (by removal of Apaf-1 or caspase 9) prevents short-term apoptotic cell death, it does not confer long-term clonogenic survival of cells (Chautan *et al.*, 1999; Ekert *et al.*, 2004). On the other hand, Bcl-2 overexpression or genetic co-ablation of both Bak and Bax confers long-term clonogenic survival or resistance to a wide range of apoptotic stimuli, respectively (Ekert *et al.*, 2004; Lindsten *et al.*, 2000; Wei *et al.*, 2001). Thus, MOMP is the critical event that commits a cell to death.

1.2.1 Bak and Bax

The tightly regulated effectors of apoptosis Bak and Bax are responsible for MOMP. Both proteins undergo homologous structural transitions during activation and oligomerisation. From inert monomers they transform, via a series of large conformational changes, into membrane-permeabilising oligomers that grow to very large sizes on the MOM.

The first known effector of apoptosis, Bcl-2 Associated X Protein (Bax), was discovered in 1993 by co-immunoprecipitation experiments with Bcl-2 (Oltvai *et al.*, 1993). Overexpression of Bax both accelerated cell death following growth factor removal and countered the protective pro-survival effect of overexpressed Bcl-2 (Oltvai *et al.*, 1993). The authors correctly predicted that Bax was an effector of cell death that was neutralised by the repressor of cell death, Bcl-2 (Oltvai *et al.*, 1993). Two years later, back-to-back publications in *Nature* independently identified Bcl-2 homologous antagonist/killer (Bak) as a Bax-like protein with pro-apoptotic activity (Chittenden *et al.*, 1995b; Farrow *et al.*, 1995; Kiefer *et al.*, 1995). Chittenden *et al.* went on to characterise a motif (the BH3 domain) in Bak, Bax and Bip1 (also known

as the BH3-only protein Bik) critical for both heterodimerisation with Bcl-X_L and the pro-apoptotic activity of the 3 proteins (Chittenden *et al.*, 1995a). The BH3 domain is responsible for the major protein-protein interactions between Bcl-2 family proteins and is discussed further in Section 1.3.

The importance of the pro-apoptotic effectors is evident in many contexts. Other than male sterility in Bax singly deficient mice, mice lacking Bax or Bak display few phenotypic abnormalities (Knudson *et al.*, 1995; Lindsten *et al.*, 2000). The compound loss of both Bax and Bak, on the other hand, has severe consequences including perinatal death and extensive developmental abnormalities (Lindsten *et al.*, 2000). As mentioned above, genetic knockout of both effectors in cells results in resistance to intrinsic apoptotic stimuli, including drug treatment with etoposide and staurosporine, ultraviolet and gamma irradiation, growth factor deprivation and treatment with endoplasmic reticulum (ER) stress-inducing drugs such as tunamycin and thapsigargin (Lindsten *et al.*, 2000; Wei *et al.*, 2001).

The functional redundancy exhibited in studies of Bak/Bax double knockout (DKO) animals and cells is matched by a conserved mechanism of action that has been structurally characterised at the atomic level up to the stage of homodimerisation by X-ray crystallography and nuclear magnetic resonance (NMR) spectroscopy (Brouwer *et al.*, 2014; Czabotar *et al.*, 2013; Moldoveanu *et al.*, 2013). A wealth of cross-linking, electron paramagnetic resonance (EPR) spectroscopy and, more recently, super-resolution microscopy data have contributed to our understanding of the subsequent steps of the MOMP pathway: oligomerisation of Bak and Bax and formation of the apoptotic pore. Many attempts have been made to determine the atomic structures of Bak and Bax oligomers and the apoptotic pore. Unfortunately, due to difficulties in sample preparation and the heterogeneity of Bak and Bax oligomers, our picture of the pore remains low resolution. What is known about Bak and Bax inhibition, activation, homodimerisation and oligomerisation is discussed in Section 1.3.

A balance between survival and cell death by apoptosis is essential for maintenance of homeostasis. In cells required for the continued healthy existence of a given organism, the pro-apoptotic effector proteins are held in check by the pro-survival proteins.

1.2.2 Pro-survival Proteins

The pro-survival proteins repress the apoptotic function of Bak and Bax. These structurally similar proteins set the apoptotic threshold that must be overcome in order for a cell to undergo apoptosis. Removal of pro-survival proteins by gene knockout has demonstrated their importance in mammalian development and maintenance of homeostasis. *bcl-2*-deficient mice, for example, survive to birth but die around 2-3 weeks of age, with the primary cause of mortality being severe polycystic kidney disease that results in renal failure (Fedorov *et al.*, 2006; Veis *et al.*, 1993). Osteoblasts from *bcl-2*-deficient mice are morphologically abnormal and defective in depositing collagen and effecting bone growth (Boot-Handford *et al.*, 1998). The mice also exhibit high levels of apoptosis of lymphoid cells in the spleen and thymus, demonstrating the importance of Bcl-2 in lymphocyte survival (Veis *et al.*, 1993). Deletion of other pro-survival proteins results in phenotypic abnormalities ranging from mild to catastrophic.

The gene for one of these proteins, Mcl-1, was identified in a search for early induction genes during chemically-induced differentiation of a myeloid cell leukaemia cell line (Kozopas *et al.*, 1993). It was the first gene discovered with homology to Bcl-2 and hence the subject of great interest due to the known oncogenic potential of Bcl-2 (Kozopas *et al.*, 1993; Vaux *et al.*, 1988). Knockout of the Mcl-1 gene in mice results in peri-implantation embryonic lethality and a failure to implant *in utero*, necessitating the use of conditional knockout systems to investigate its role in adult animals (Rinkenberger *et al.*, 2000). Mcl-1 is widely required for survival of diverse cell types including lymphocytes, hematopoietic stem cells, neutrophils, neuronal progenitors, hepatocytes and cardiomyocytes (Arbour *et al.*, 2008; Dzhagalov *et al.*, 2007; Opferman *et al.*, 2005; Opferman *et al.*, 2003; Thomas *et al.*, 2013; Vick *et al.*, 2009; Wang *et al.*, 2013).

The *bcl-x* gene was the first Bcl-2 homologue to be identified by low stringency hybridisation using a *bcl-2* DNA probe (Boise *et al.*, 1993). Interestingly, alternative splicing of the gene generates two proteins with opposing functions: a pro-survival splice variant (Bcl-X_L) and a pro-apoptotic splice variant (Bcl-X_S) (Boise *et al.*, 1993). The Bcl-X_S variant is less well characterised and not discussed further. Bcl-X_L, on the

other hand, has been extensively studied in the context of health and disease. Mice deficient for *bcl-x* die around embryonic day 13, displaying extensive apoptotic death of immature neuronal and hematopoietic cells (Motoyama *et al.*, 1995). Bcl-X_L-deficient mice are thrombocytopenic, and the degradation of a limited pool of Bcl-X_L sets the lifespan of mature, circulating platelets (Mason *et al.*, 2007).

Far less is known about the other pro-survival proteins, primarily because their roles appear less critical or because of experimental barriers. Bcl-W knockout mice are healthy but defective in spermatogenesis (Print *et al.*, 1998). Bfl-1/A1 has proven difficult to investigate in mice due to the presence of 3 functional A1 genes, but appears to play a role in lymphocyte survival (Ottina *et al.*, 2012). The mouse homologue of Bcl-B (Boo/Diva) is unusual in that it lacks a BH3 domain and has an altered BH1 domain that is missing a conserved arginine residue critical for pro-survival function (Rautureau *et al.*, 2010). Consequently, mouse Bcl-B does not bind to and sequester pro-apoptotic BH3 domains (Rautureau *et al.*, 2010).

Together, the pro-survival proteins ensure survival of a cell until stress levels reach a critical point and the threshold for apoptosis is overcome. The conveyors of the stress signal are the BH3-only proteins.

1.2.3 BH3-only Proteins

Various stress stimuli upregulate BH3-only proteins at the transcriptional and/or post-translational level. BH3-only proteins repress the anti-apoptotic function of pro-survival proteins, and some are able to directly activate the effector proteins Bak and Bax. Certain BH3-only proteins, including Bim, PUMA and tBid, bind promiscuously to pro-survival proteins, while others display a restricted binding repertoire. With the notable exception of Bim, deletion of individual BH3-only proteins appears to be compensated for by functional redundancy with other BH3-only proteins (Bouillet *et al.*, 1999; Happo *et al.*, 2012).

1.3 Bcl-2 Family Protein-Protein Interactions

The primary protein-protein interaction that conveys the intrinsic apoptotic signal is the binding of BH3 domains to the conserved hydrophobic surface groove (α3-5) present on both pro-survival proteins and multi-BH domain pro-apoptotic effector proteins (see **Figure 2B** and **C**). Hereafter, binding of a BH3 domain to a hydrophobic groove will be referred to as BH3:groove binding. BH3:groove binding events may form stable complexes or induce large conformational change depending on the specific Bcl-2 family proteins involved in the interaction. This section will discuss both cases in structural detail.

1.3.1 Inhibition of Apoptosis by Pro-survival Proteins

The pro-survival proteins inhibit apoptosis primarily by binding and sequestering the BH3 domains of pro-apoptotic Bcl-2 family proteins. Pro-survival protein-mediated inhibition of apoptosis can be categorised as Mode 1 or Mode 2 (**Figure 3**) (Llambi *et al.*, 2011). Mode 1 inhibition involves sequestration of activator BH3-only proteins by pro-survival proteins via a BH3:groove interaction, thereby preventing activation of Bak and Bax. In Mode 2, pro-survival proteins bind to the BH3 domains of activated Bak and/or Bax and prevent their homodimerisation. The relative importance of either mode of inhibition is largely unclear and may vary in different cellular contexts.

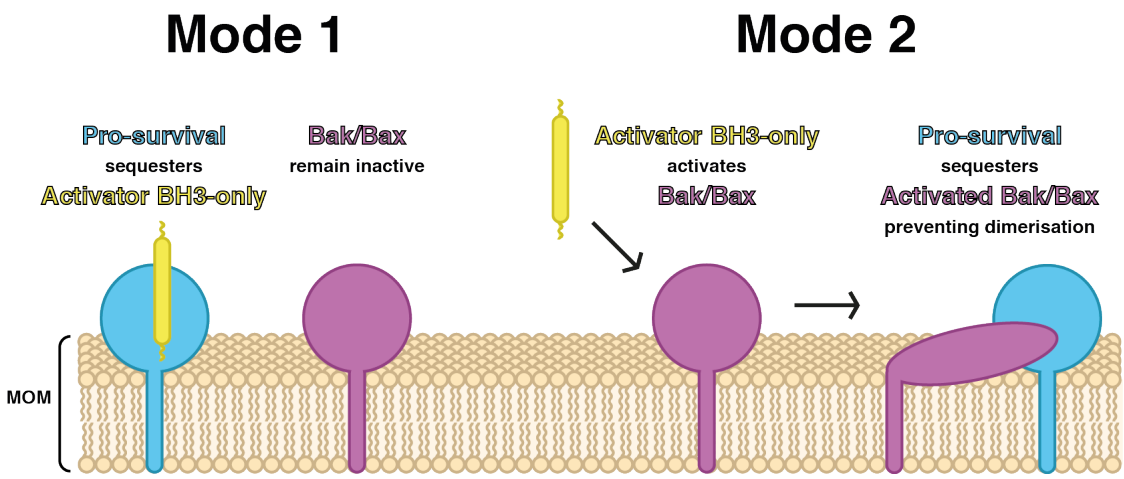

Figure 3. Schematic of Mode 1 vs. Mode 2 inhibition of intrinsic apoptosis. *In Mode 1 inhibition, pro-survival proteins bind the BH3 domain of activator BH3-only proteins, preventing activation of Bak and Bax. Once BH3-only proteins are freed from Mode 1 complexes they activate Bak/Bax. Activation results in exposure of the Bak/Bax BH3 domain that can be sequestered by pro-survival proteins in Mode 2 complexes.*

The first structural view of the BH3:groove interaction was provided in 1997 by Sattler *et al.*, who determined the NMR solution structure of Bcl-X_L in a Mode 2 complex with the Bak BH3 peptide (**Figure 4A**) (Sattler *et al.*, 1997). The stable nature of the BH3:groove interaction has allowed elucidation of many structures of pro-survival proteins in complex with pro-apoptotic BH3 peptides in subsequent years, including X-ray crystal structures showing the canonical BH3:groove interaction at atomic resolution (**Figure 4B**). The BH3 motif is characterised by a series of hydrophobic residues (h1-h4) and a conserved aspartic acid residue that forms an essential salt bridge with an arginine residue in the BH1 domain of its binding partner (**Figure 4C**). The h1-h4 residues project from one side of the α-helical BH3 domain and are received by 4 complementary binding pockets that form the hydrophobic surface groove of an interacting partner protein (**Figure 4C**).

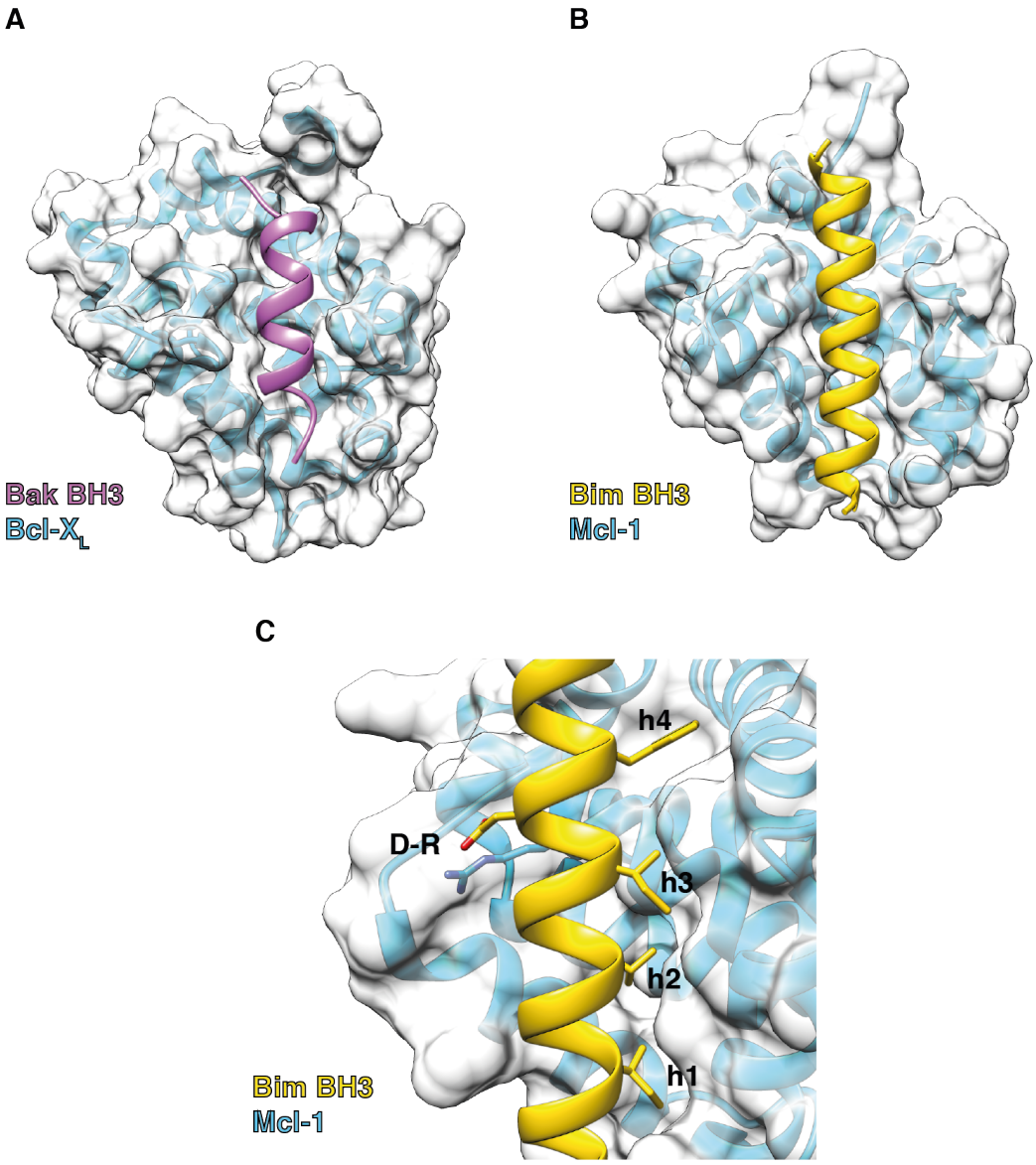

Figure 4. Structural view of the BH3:groove interaction. ***A)*** *and* ***B)*** *X-ray crystal structures of BH3 peptides from Bak (purple) and Bim (yellow) bound to the hydrophobic grooves of Bcl-X_L (PDB code: 1BXL (Sattler et al., 1997)) and Mcl-1 (PDB code: 2NL9 (Czabotar et al., 2007)) (both blue), respectively.* ***C)*** *Bim BH3 peptide binding to Mcl-1 groove as in* ***B****. The conserved hydrophobic residues h1-h4 and D to R salt bridge residues are labelled and shown as sticks.*

Sequence differences within BH3 domains determine the suite of pro-survival proteins that a given pro-apoptotic protein can bind to. For example, Bad binds selectively to Bcl-2, Bcl-X_L and Bcl-W, while Noxa binds Mcl-1 and A1 (Certo *et al.*, 2006; Chen *et al.*, 2005; Kuwana *et al.*, 2005). Bim, tBid and Puma, on the other hand, are

promiscuous and appear to bind to and neutralise all pro-survival proteins (Certo *et al.*, 2006; Chen *et al.*, 2005; Kuwana *et al.*, 2005). Pro-survival proteins also bind to the multi-BH domain effector proteins Bak and Bax to inhibit the pro-apoptotic activity of these proteins (Chittenden *et al.*, 1995a; Fletcher *et al.*, 2008; Oltvai *et al.*, 1993; Sattler *et al.*, 1997; Wang *et al.*, 1998). Of the effector proteins, the Bak BH3 domain has a more restricted binding profile, with selectivity for Bcl-X_L, Mcl-1 and A1, whereas Bax binds to those pro-survival proteins as well as to Bcl-2 and Bcl-W (Simmons *et al.*, 2008; Willis *et al.*, 2005; Willis *et al.*, 2007). Though their binding repertoires are somewhat restricted, structural studies have demonstrated that the substantial structural plasticity of the hydrophobic groove of pro-survival proteins is likely what allows them to bind BH3 domains that differ in sequence (Lee *et al.*, 2009; Smits *et al.*, 2008).

Historically, it has proven difficult to produce and work with full-length multi-BH domain proteins and BH3-only proteins due to hydrophobic TM domains and lack of tertiary structure, respectively. In addition, working with these proteins in the physiologically relevant context of a phospholipid bilayer is challenging. Therefore, high-resolution structural studies of the BH3:groove interaction have been performed with C-terminally truncated pro-survival proteins and pro-apoptotic BH3 peptides. Due to this limited view, the BH3 domain:pro-survival protein interaction is often depicted as an α-helical BH3 domain binding to pro-survival protein that is largely unchanged from its apo form. However, some studies have suggested that in the biologically relevant context of a membrane, certain pro-survival proteins also change conformation in order to bind BH3 domains (Dlugosz *et al.*, 2006). Overall, the physiological relevance of conformational change in pro-survival proteins has received limited attention.

The various specificities of certain Bcl-2 family proteins and the promiscuity of others allow fine-tuning of the apoptotic response to the multitude of stresses that a cell may encounter. In addition, the potential for specificity in these interactions has facilitated the successful development of BH3 mimetic drugs that target a single pro-survival protein, circumventing the wide-reaching toxicity that would be associated with inhibiting all pro-survival proteins (Chen *et al.*, 2005; Pan *et al.*, 2014; Roberts *et al.*, 2016).

1.3.2 Activation and Dimerisation of Bak and Bax

The primary role of pro-survival proteins is to antagonise the function of the pro-apoptotic effector proteins Bak and Bax. In non-apoptotic cells, monomeric Bak and Bax shuttle between the mitochondria and the cytosol at different rates (Edlich *et al.*, 2011; Schellenberg *et al.*, 2013; Todt *et al.*, 2015). Bax exhibits a predominantly cytosolic localisation pattern while Bak is found primarily at the mitochondria, with its TM helix traversing the MOM (Griffiths *et al.*, 1999; Suzuki *et al.*, 2000). Bax is able to remain cytosolic because of its ability to sequester its TM helix in the canonical BH3-binding groove (Suzuki *et al.*, 2000). The TM domain appears to dictate localisation patterns, as swapping TM helices renders Bak cytosolic and Bax MOM-associated (Todt *et al.*, 2015).

Upon BH3-only protein upregulation following apoptotic stimuli, Bax accumulates on the MOM (Schellenberg *et al.*, 2013). A proposed initial activation site for Bax is formed by α-helices 1 and 6 on the side of the protein opposite to the canonical hydrophobic groove site (Gavathiotis *et al.*, 2008). This "rear site" was mapped using chemically stapled activator BH3 peptides, and it was suggested that binding triggers dissociation of the Bax TM helix from the canonical groove (Gavathiotis *et al.*, 2008). Such an event could increase Bax shuttling to the mitochondria, but mutation of residues in the rear site does not prevent apoptosis, suggesting that rear-site activation is dispensable for the pro-apoptotic activity of Bax (Okamoto *et al.*, 2013; Peng *et al.*, 2013).

Once at the mitochondria, both Bak and Bax are engaged by activator BH3-only proteins that bind transiently to the canonical hydrophobic groove and induce conformational change (Brouwer *et al.*, 2014; Czabotar *et al.*, 2013; Moldoveanu *et al.*, 2013). Structural details of this conformational change were first elucidated using a Bax construct lacking its TM domain by Czabotar and Westphal *et al.* in 2013. Addition of activator BH3 peptides to truncated Bax induced homodimerisation of the protein in the presence of detergent (Czabotar *et al.*, 2013). The crystal structure of the resulting homodimer revealed a domain-swapped conformation, with the "latch" domain (α6-8) of one Bax molecule wrapped around the "core" domain (α2-5) of a second Bax molecule, and vice versa (Czabotar *et al.*, 2013). The homodimer therefore contained

two Bax globules resembling the monomeric protein joined at the junction of α5 and α6 (Czabotar *et al.*, 2013). Though the domain-swapped dimer is likely an artefact of the use of truncated Bax in the absence of membrane, the domain-swapping event demonstrated that activator BH3 peptide binding had induced separation of the α5-6 helical hairpin (Czabotar *et al.*, 2013). This "unlatching" of monomeric Bax induced by activator BH3-only proteins and peptides was shown to be an essential event for MOMP, when full-length Bax with the α5 and α6 locked together via a disulphide bond failed to permeabilise mitochondria and release cytochrome *c* (Czabotar *et al.*, 2013).

Domain-swapped Bax dimers also presented a unique opportunity to study the BH3:groove interaction between BH3 domains and the Bax hydrophobic groove. In contrast to BH3:pro-survival protein complexes, BH3:groove interactions with Bax or Bak had proven difficult to study structurally due to the transient nature of BH3 domain binding to these proteins. As the domain-swapped dimer had already undergone conformational change but still resembled monomeric Bax protein, it provided a platform for stable binding of BH3 peptides. The structures of the Bid BH3 peptide and Bax BH3 peptide bound to the hydrophobic grooves of domain-swapped Bax dimers revealed the canonical BH3:groove interactions seen in pro-survival:BH3 peptide complexes (Czabotar *et al.*, 2013). The h1-h4 positions of the BH3 peptides bound deeply into the groove, and a salt-bridge was formed between the conserved aspartic acid residue of the BH3 peptides and Arg109 in the BH1 domain of Bax (Czabotar *et al.*, 2013). Apart from the canonical interactions, additional interactions were noted at the base of the hydrophobic groove involving two residues at the N-terminus of the BH3 domain (Czabotar *et al.*, 2013). Mutation of these residues, termed h0, drastically reduced the activating potency of both the Bid and Bim BH3 peptides (Czabotar *et al.*, 2013). Following this work, further structures of domain-swapped Bax bound to the Bim BH3 peptide and NMR structure of Bak bound to a stapled Bid BH3 peptide confirmed that the conserved BH3:groove binding interactions occurred in both of the multi-BH domain pro-apoptotic proteins (Moldoveanu *et al.*, 2013; Robin *et al.*, 2015). Interestingly, in cells lacking the 8 known BH3-only proteins, Bak and Bax activation occurred spontaneously when pro-survival proteins were neutralised (O'Neill *et al.*, 2016). The kinetics of cell death were similar when BH3-only proteins were present, suggesting Bak and Bax may be constitutively active, or that other undiscovered factors may influence their activation. This also suggests that Mode 1 inhibition may not play

an essential role in preventing apoptosis, and that Mode 2 complexes are critical for apoptosis inhibition. However, the genetic abnormality of the cells in this study preclude determination of the physiological relevance of BH3-only protein-mediated activation of Bax and Bak in genetically normal animals.

The separation of the latch and core domains induced by activator BH3-only proteins, as well as the requisite dissociation of α1, is posited to result in the collapse of initially globular full-length Bax onto the MOM, and Bax homodimerisation (Alsop *et al.*, 2015; Czabotar *et al.*, 2013; Westphal *et al.*, 2014). Bax and Bak homodimers on the MOM have been characterised by cysteine cross-linking studies in apoptotic cells (Dewson *et al.*, 2008; Dewson *et al.*, 2012). Unlike the domain-swapped dimers that form in solution, full-length membrane-bound Bax and Bak homodimerise via symmetric exchange of their BH3 domains into the hydrophobic grooves of a partner molecule (Dewson *et al.*, 2008; Dewson *et al.*, 2012).

Given that homodimerisation involved the BH3 domain (α2) and the hydrophobic groove (α3-5), the N-terminus of the newly coined core domain (α2-5) of Bax was fused to green fluorescent protein (GFP) for high-resolution structural studies. The rationale for the use of a fusion construct was that the core domain would likely exhibit large, exposed hydrophobic surfaces, and fusion to GFP could increase solubility, prevent aggregation and aid crystallisation of the core (Czabotar *et al.*, 2013). The fusion protein ran as a tetramer on gel filtration (GF) and crystallised in the presence of detergent (Czabotar *et al.*, 2013). The crystal structure revealed two GFP homodimers linked by homodimers of the Bax core domain, forming a fusion protein tetramer (Czabotar *et al.*, 2013). Bax core domains assumed a symmetric BH3:groove fold, where the BH3 domains of each monomer bound symmetrically to the hydrophobic groove of a partner Bax molecule (Czabotar *et al.*, 2013). The structure was in agreement with cysteine cross-linking data mentioned above, and has since been further validated by double electron-electron resonance (DEER) spectroscopy (Bleicken *et al.*, 2014; Czabotar *et al.*, 2013; Dewson *et al.*, 2012). Interestingly, the core homodimers presented hydrophilic (α2-3) and hydrophobic (α4-5) surfaces on opposite sides of the dimer. Given the enrichment of aromatic residues on the hydrophobic side of the dimer, it was proposed that this might represent a membrane-interacting surface (Czabotar *et al.*, 2013).

Subsequently determined crystal structures of Bak demonstrated identical core/latch separation and symmetric BH3:groove homodimerisation (Brouwer *et al.*, 2014). As with Bax, a GFP:Bak core domain fusion protein formed tetramers consisting of two GFP homodimers and two Bak BH3:groove core homodimers (Brouwer *et al.*, 2014). Again, the Bak core homodimers were consistent with cysteine cross-linking and EPR spectroscopy experiments (Aluvila *et al.*, 2014; Dewson *et al.*, 2008). The core homodimer of Bak also exhibited hydrophilic (α2-3) and hydrophobic (α4-5) surfaces with enrichment of aromatic residues on the hydrophobic side. The hydrophobic surface of the Bak dimer was curved in comparison to the Bax dimer, and was suggested to play a role in membrane disruption by inducing membrane curvature (Brouwer *et al.*, 2014). A schematic representation of the structural changes in Bax and Bak that lead to MOMP is presented in **Figure 5**, along with high-resolution structures that informed our understanding of these changes.

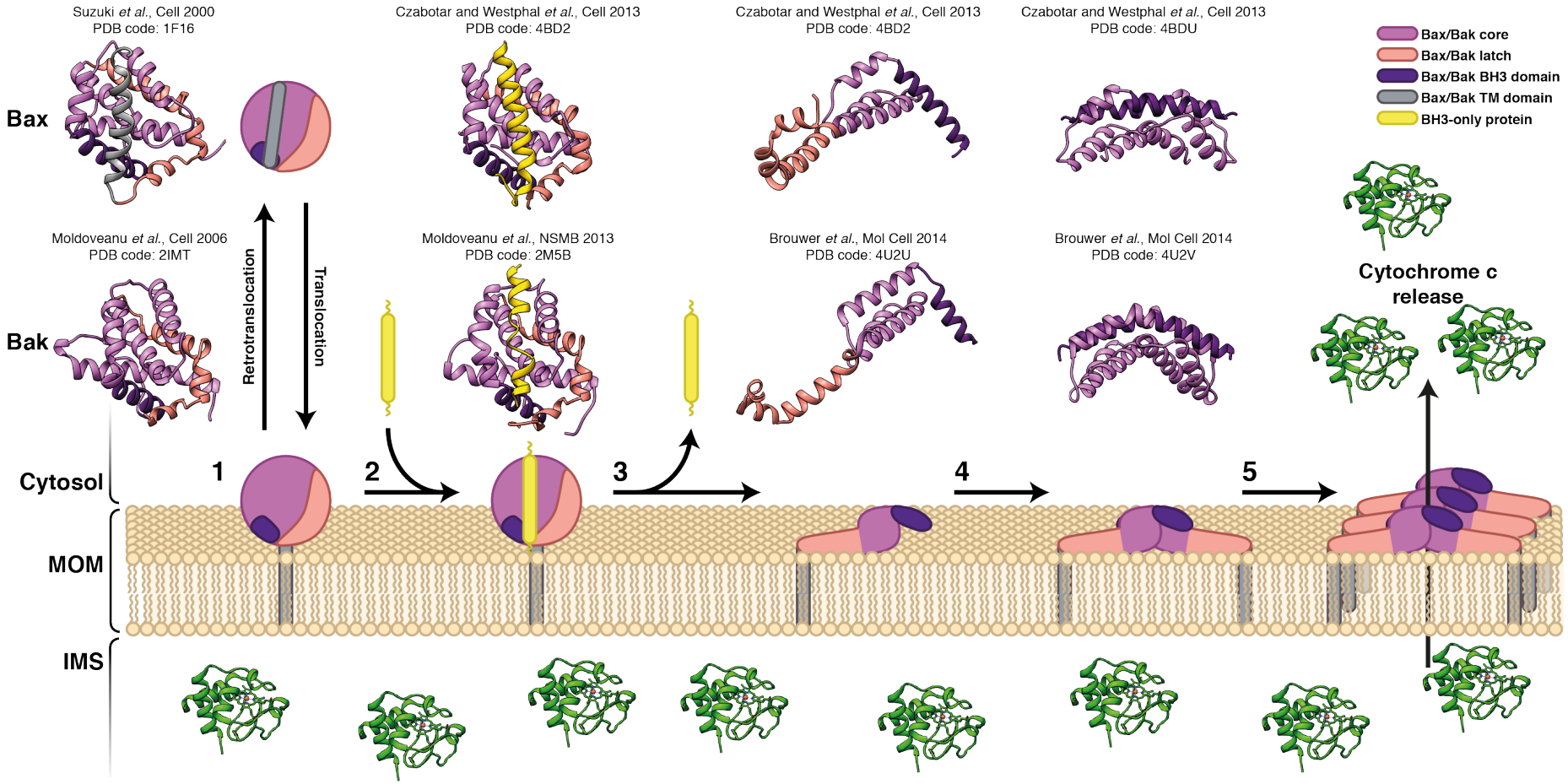
Suzuki et al., Cell 2000
PDB code: 1F16
Czabotar and Westphal et al., Cell 2013
PDB code: 4BD2
Czabotar and Westphal et al., Cell 2013
PDB code: 4BD2
Czabotar and Westphal et al., Cell 2013
PDB code: 4BDU
Bax/Bak core
Bax/Bak latch
Bax/Bak BH3 domain
Bax/Bak TM domain
BH3-only protein
Bax
Moldoveanu et al., Cell 2006
PDB code: 2IMT
Moldoveanu et al., NSMB 2013
PDB code: 2M5B
Brouwer et al., Mol Cell 2014
PDB code: 4U2U
Brouwer et al., Mol Cell 2014
PDB code: 4U2V
Cytochrome c release
Bak
Retrotranslocation
Translocation
1
2
3
4
5
Cytosol
MOM
IMS

Figure 5. Schematic and structural representation of the Bax/Bak-mediated MOMP pathway. *Schematic representation (see key at top right) and corresponding structures of Bax and Bak shown as ribbons (top and middle rows of structures, respectively), depicting conformational changes that occur along the MOMP pathway. The structure of cytochrome* c *(PDB code: 3ZCF (Rajagopal et al., 2013)) in the IMS is depicted as green ribbons in the bottom row of structures. Both Bax and Bak constantly shuttle between the cytosol and the MOM. In step* ***1****, Bax and Bak accumulate on the MOM following an apoptotic stimulus. Step* ***2*** *involves activation of Bax and Bak via transient binding of the BH3 domain of an activator BH3-only protein to the hydrophobic groove of Bax and Bak. BH3 binding induces separation of the core and latch domains in step* ***3****. In step* ***4****, the freed core domains homodimerise. Homodimers oligomerise and cause MOMP in step* ***5****.*

BH3:groove homodimers are now well accepted as the building blocks of the oligomers that permeabilise mitochondria (Aluvila *et al.*, 2014; Bleicken *et al.*, 2010; Bleicken *et al.*, 2014; Brouwer *et al.*, 2014; Cosentino and Garcia-Saez, 2017; Czabotar *et al.*, 2014; Czabotar *et al.*, 2013; Dewson *et al.*, 2009; Dewson *et al.*, 2012; Gilbert, 2016; Mandal *et al.*, 2016; Oh *et al.*, 2010; Subburaj *et al.*, 2015; Uren *et al.*, 2017; Zhang *et al.*, 2016). The nature of said oligomers, however, remains elusive. Several inter-dimer protein:protein interfaces have been proposed between Bax and/or Bak BH3:groove homodimers, including in the latch between α6 helices (Dewson *et al.*, 2009; Dewson *et al.*, 2012; Ma *et al.*, 2013), between the corners of core domain dimers consisting of the C-termini of α3 and α5 helices (hereafter referred to as the α3/α5 corners) (Aluvila *et al.*, 2014; Mandal *et al.*, 2016), and between the TM domain α9 helices (Iyer *et al.*, 2015; Zhang *et al.*, 2016). Despite the proximity of these linkage sites in oligomeric Bak or Bax on the membrane, detergent-solubilised Bak oligomers from the MOM collapse to homodimers on blue native PAGE (Ma *et al.*, 2013). The collapse of oligomers suggests that the protein:protein interactions at the inter-dimer interface are unstable when removed from the membrane environment (Ma *et al.*, 2013).

However it is that the homodimers assemble into an oligomer, a consequence of activation and oligomerisation of Bak and Bax is permeabilisation of the MOM.

Membrane permeabilisation likely occurs via the formation of pores by Bax and Bak oligomers.

1.4 Pore-forming Proteins

Cellular membranes are physical boundaries between both the cell and its environment and between different cellular compartments such as the cytosol and mitochondria. The lipid bilayers that constitute these membranes are impermeable to water and water-soluble molecules. Integral membrane proteins, including ion channels and transporters, allow passage of specific molecules across these barriers without compromising their integrity. Pore-forming proteins (PFPs), on the other hand, can allow non-specific passage of ions, small molecules, and even macromolecules by binding to membranes and forming pores through the bilayer. Pores formed by PFPs range in size from 1-2 nm across for *S. aureus* α-haemolysin to up to 500 nm for rings of Bax observed on mitochondria by stimulated emission depletion super-resolution microscopy (Grosse *et al.*, 2016; Song *et al.*, 1996). All kingdoms of life produce PFPs that can function as toxins, in the immune response to pathogens, and in other less lethal roles (Gilbert *et al.*, 2014).

Structurally, PFPs are a diverse group of proteins that are broadly divided into α-PFPs and β-PFPs (Iacovache *et al.*, 2010). In α-PFPs, the lumen of the pore is lined with α-helices, whereas pores created by β-PFPs are lined by β-hairpins that form a β-barrel. Common to both α- and β-PFPs is the conversion from a soluble form (usually monomeric) to a membrane-inserted, oligomeric form where each protomer may contribute one or more α-helices or β-hairpins to the pore. Bak and Bax are unusual and potentially unique among PFPs in that the building block of the oligomeric pores formed by these proteins are dimers that bear little structural resemblance to their inert monomeric forms.

1.4.1 Proteinaceous vs. Toroidal Pores

PFPs can also be categorised based on the type of pore that they form. Pores in which the lumen is lined entirely by protein are known as proteinaceous pores. Both α-PFPs and β-PFPs can form proteinaceous pores that are usually of a defined size (e.g. the

dodecameric α-helical pore formed by cytolysin A from *E. coli* (Mueller *et al.*, 2009)). Proteolipidic toroidal pores, on the other hand, incorporate lipid as well as protein into the pore structure. In toroidal pores, the lamellar structure of the bilayer is disrupted, resulting in the lipids of the inner and outer leaflets bending to fuse and form a continuous hydrophilic surface (**Figure 6A**). The hydrophilic surface, made up of lipid headgroups, protects the hydrophobic membrane core, reducing line tension (the biophysical force responsible for closing toroidal pores) at the pore edge (Karatekin *et al.*, 2003; May, 2000). Toroidal pores can be induced by different stimuli including the transition of electrical charge across membranes and by certain PFPs. Thus, the difference between proteinaceous and proteolipidic pores can be simply summarised: proteinaceous pores maintain the lamellar structure of the bilayer while proteolipidic pores disrupt it.

There are two known architectures of proteolipidic pores: arc-type pores and matrix-type pores (Gilbert, 2016; Gilbert *et al.*, 2014). In arc-type pores, such as those formed by the MACPF/CDC protein superfamily, a growing arc of oligomerising protein subunits line one side of the pore while the other side consists of a toroidal arrangement of lipids (**Figure 6C**). These pores may eventually form a closed, fully proteinaceous ring, but opening of a pore in the membrane precedes ring formation in some cases (Sonnen *et al.*, 2014). Matrix-type pores consist of protein interspersed with lipids at the pore lumen, and are thought to be formed by antimicrobial peptides such as melittin (**Figure 6D**) (Gilbert, 2016; Gilbert *et al.*, 2014). Despite what would at first appear to be a very energetically unfavourable pore structure, both arc- and matrix-type PFPs achieve pore stability by relieving the curvature stress at the pore edge, resulting in a reduction in line tension (Garcia-Saez *et al.*, 2007; Gilbert *et al.*, 2014).

Though clear examples exist of PFPs that form only arc- or matrix-type pores, these architectures are not necessarily mutually exclusive. It is possible that composite arc/matrix pores exist that exhibit features of both types, as well as other types of proteolipidic pores that are yet to be discovered (Gilbert *et al.*, 2014).

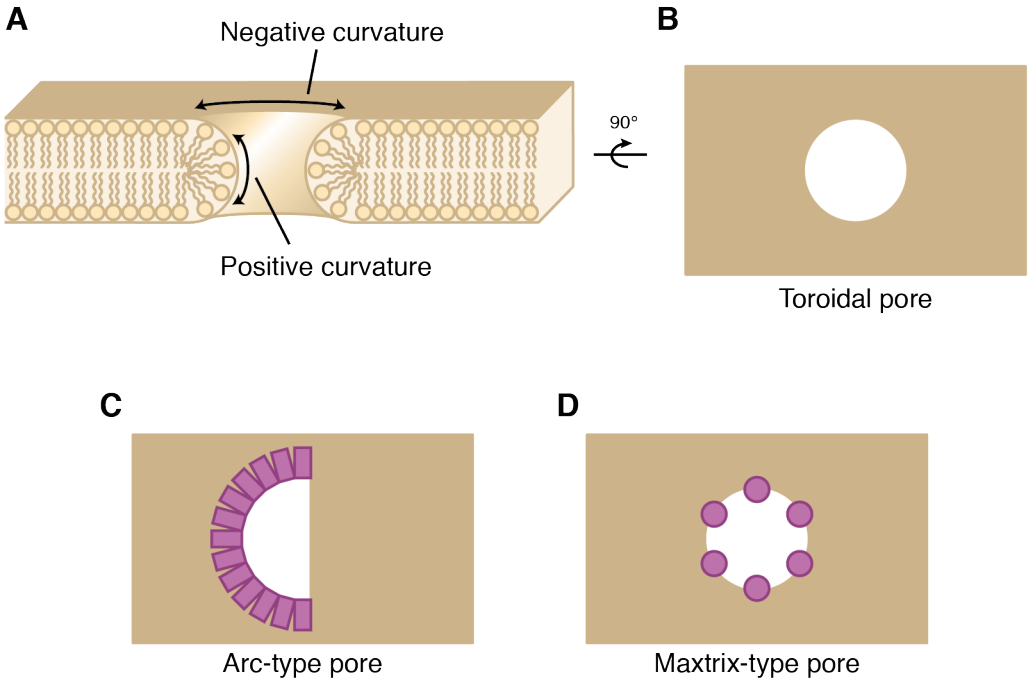

Figure 6. Architecture of toroidal pores and proteolipidic pores. **A)** *Cartoon cross-section of the membrane showing the architecture of a toroidal pore. Lipid headgroups bend around the pore lumen with negative curvature and positive curvature, parallel and perpendicular to the membrane plane, respectively.* ***B)*** *Top-down view of the toroidal lipidic pore in* ***A****.* ***C)*** *Top-down view of an arc-type proteolipidic pore lined by protein on one side (purple rectangles) and toroidal lipids on the other.* ***D)*** *Top-down view of a matrix-type proteolipidic pore lined by protein (purple circles) interspersed with toroidal lipids. Adapted from (Gilbert, 2016).*

1.4.2 Pore Formation by Bak and Bax

Overwhelmingly, data in the literature support the formation of toroidal proteolipidic pores by Bak and Bax. In early experiments, Bax decreased membrane planarity lifetime and line tension of the membrane (Basanez *et al.*, 1999). Intrinsic membrane curvature, along with line tension, is a property of membranes dependent on their lipid composition (Gruner, 1985; May, 2000). Certain lipids promote positive curvature while others promote negative curvature, both of which are favourable for stabilisation of toroidal lipidic and proteolipidic pores (see **Figure 6A**). Lysophospholipids have only one acyl chain and generally promote positive curvature by allowing closer packing of acyl chains as compared to diacyl phospholipids. In contrast, cardiolipin

possesses 4 acyl chains, expanding the hydrophobic portion of the molecule and promoting negative curvature. Artificial membranes with positive or negative intrinsic curvature were found to promote or inhibit Bax pore formation, respectively, supporting the proteolipidic pore hypothesis (Basanez *et al.*, 2002). Direct observation of Bak and Bax pores in liposomes by cryo-electron microscopy (cryo-EM) revealed pores sized between 25-100 nm (Bleicken *et al.*, 2010; Landeta *et al.*, 2011; Schafer *et al.*, 2009). The heterogeneity and concentration-dependency of Bak and Bax pore size is suggestive of toroidal proteolipidic pores, as opposed to proteinaceous pores such as those of tetanolysin, that are generally uniform in size at different concentrations and protein:lipid ratios (Bleicken *et al.*, 2013a; Bleicken *et al.*, 2013b; Landeta *et al.*, 2011). Nanogold-labelled Bax was observed incompletely lining the rim of pores in liposomes with gaps between the Bax particles, again suggesting a proteolipidic pore arrangement (Kuwana *et al.*, 2016).

Only recently, with the advent of super-resolution microscopy techniques, have the supramolecular structures formed by Bax on the MOM been revealed. Bax appears to form several distinct structures on the MOM after induction of apoptosis, including lines, double lines, arcs, rings and large aggregates (Grosse *et al.*, 2016; Salvador-Gallego *et al.*, 2016). In a similar study of Bak, only small and large clustered aggregates were observed, with no discernible lines, double lines, arcs or rings (Nasu *et al.*, 2016). This could be due to the comparatively lower fluorescence intensity fluorophore used in the Bak study that may have limited resolution (Nasu *et al.*, 2016). Large aggregates have previously been observed for both Bak and Bax (Zhou and Chang, 2008). Importantly however, apoptogenic molecules cytochrome *c* and Smac were released from mitochondria by small clusters of Bak/Bax prior to formation of larger aggregates (Zhou and Chang, 2008). Indeed, atomic force microscopy (AFM) experiments demonstrated that both the arc and ring structures lined pores formed by Bax in supported lipid bilayers (Salvador-Gallego *et al.*, 2016). That arcs of Bax were able to form pores is the first direct evidence that Bax pores are proteolipidic.

These microscopy studies have provided vital information, showing for the first time that Bax can form complex supramolecular structures, and that these structures are associated with membrane pores. Questions remain regarding the mechanism of initial

membrane disruption and how Bak and Bax homodimers interact with one another and with the membrane at a molecular level.

Disordered clustering of BH3:groove homodimers has recently been proposed to generate sufficient membrane tension to induce rupturing of the MOM (Uren *et al.*, 2017). Subsequent to membrane disruption and pore opening, models for stabilisation of growing pores by the stable core domains of BH3:groove homodimers have been proposed. The "clamp model" for Bax, based on DEER spectroscopy experiments, involves Bax homodimers forming a clamp at the pore rim, with the core dimer's hydrophobic α4-5 surface in contact with the hydrophobic membrane core and the α6 helices shallowly inserted parallel to the membrane plane on opposite leaflets (Bleicken *et al.*, 2014). A caveat of this model is that it assumes symmetry in the membrane plane and does not explain or provide evidence for flipping of the α6-9 helices from one side of the membrane to the other. Nevertheless, stabilisation of the pore edge is critical for maintaining an open toroidal pore, and the core dimer's polarity, in terms of hydrophilicity/hydrophobicity, makes it an attractive pore stabilising unit. In a different model, Bak core homodimers have been proposed to line the rim of pores (Aluvila *et al.*, 2014; Mandal *et al.*, 2016). In contrast to the clamp model, this model does not assume flipping of the α6-9 helices to the inner leaflet. Both models were created based on cysteine cross-linking and EPR spectroscopy experiments. While these techniques are valuable in informing the gross spatial and conformational arrangement of Bak and Bax in membrane pores, the dynamic nature and flexibility of Bak/Bax homodimers in the membrane can complicate interpretation of results. As such, the models remain our best guesses at the structure of Bak and Bax pores in lieu of high-resolution structural information from techniques such as X-ray crystallography and cryo-EM.

In general, it seems that pore formation by Bak and Bax likely involves two separate events: membrane disruption and pore stabilisation (Cosentino and Garcia-Saez, 2017). These two events may involve different conformations of Bak and Bax homodimers. However, the core homodimer at least seems to maintain its fold for all events subsequent to homodimerisation. The main barrier to determining a high-resolution structure of Bak or Bax pores is the difficulty of preparing a highly homogenous sample of Bak or Bax oligomers of a distinct size. Until such a sample can be prepared,

BH3:groove core domain homodimers remain our only high-resolution view of the activated forms of Bak and Bax.

While many questions surround the mechanism of pore formation by Bak and Bax, still less is clear in the case of the third multi-BH domain pro-apoptotic protein: Bok.

1.5 Bcl-2-related Ovarian Killer Protein

Of all known Bcl-2 family proteins, Bcl-2-related ovarian killer protein (Bok) remains one of the most enigmatic. Shortly after the discovery of Bak and Bax, Bok was identified in a yeast two-hybrid screen using the pro-survival protein Mcl-1 as bait (Hsu *et al.*, 1997). Bok also hybridised with A1 but not Bcl-2 or Bcl-X_L (Hsu *et al.*, 1997; Inohara *et al.*, 1998). Overexpression of Bok induced apoptosis in mammalian cells that could not be rescued by Bcl-2 or Bcl-X_L overexpression (Hsu *et al.*, 1997; Inohara *et al.*, 1998). Taken together with sequence similarity to Bak and Bax, these findings suggested that Bok could be a third pro-apoptotic effector protein (Hsu *et al.*, 1997; Inohara *et al.*, 1998).

In early studies, Bok appeared to show tissue-restricted expression in reproductive tissues as well as the liver, brain, appendix and lymphoid tissues (Hsu *et al.*, 1997; Inohara *et al.*, 1998). More recent studies confirmed higher expression levels in reproductive tissues and the brain, but also wider low-level expression in almost all tissues (Ke *et al.*, 2012). The pro-apoptotic effector function of Bok was called into question following findings that cells lacking Bak and Bax were highly resistant to most, if not all, intrinsic apoptotic stimuli (Lindsten *et al.*, 2000). Bak, Bax or Bok singly-deficient mice all developed relatively normally with minimal phenotypic abnormalities (Ke *et al.*, 2012; Knudson *et al.*, 1995; Lindsten *et al.*, 2000). However, while Bax can compensate during development for combined Bok/Bak loss, and Bak compensates for combined Bok/Bax loss, Bok cannot compensate for the combined loss of Bak and Bax that leads to a severe developmental phenotype resulting in perinatal death (Ke *et al.*, 2013; Lindsten *et al.*, 2000). Therefore, it appears that the roles of Bak and Bax largely overlap during development, while Bok function is likely non-essential or may be compensated for by an as yet unidentified protein.

Bok also differs from Bak and Bax in its subcellular localisation pattern. Bok localises primarily to the ER and Golgi membranes, with some protein at the nuclear outer membrane and the MOM (Bartholomeusz *et al.*, 2006; Echeverry *et al.*, 2013). This unique localisation pattern is due to an atypical TM domain. The Bok TM helix contains two positively charged residues and lacks the net positive charge on the C-terminus that acts as a mitochondrial targeting signal (Echeverry *et al.*, 2013; Horie *et al.*, 2002; Kaufmann *et al.*, 2003). At the ER membrane, Bok binds to the inositol 1,4,5-trisphosphate receptors (IP3Rs) and has been linked to the ER-associated degradation (ERAD) pathway (Llambi *et al.*, 2016; Schulman *et al.*, 2016; Schulman *et al.*, 2013). Further to this, $Bok^{-/-}$ mice and cells derived therefrom appeared to be resistant to intrinsic apoptosis induced by ER-stressing drugs such as thapsigargin (Carpio *et al.*, 2015, 2016). This finding is controversial, as $Bok^{-/-}$ cell lines and mice from two independent groups showed no defect in ER stress-related apoptosis (Echeverry *et al.*, 2013; Fernandez-Marrero *et al.*, 2016; Ke *et al.*, 2012; Llambi *et al.*, 2016). Whatever the case, the physiological role of Bok is certainly linked to its ER localisation. Overexpression of Bok causes early fragmentation of the ER and Golgi membranes prior to caspase activation, suggesting a membrane-related role for the protein (Echeverry *et al.*, 2013).

Whether Bok requires Bak and/or Bax for induction of the intrinsic apoptotic pathway is also controversial. In initial experiments with Bak and Bax doubly-deficient cells, Bok overexpression did not activate the intrinsic apoptotic pathway, nor did it sensitise the cells to intrinsic apoptotic stimuli such as etoposide (Echeverry *et al.*, 2013). It was thus hypothesised that Bok acts upstream of Bak and Bax. This notion has been challenged in experiments from other groups, demonstrating that in specific conditions Bok does induce intrinsic apoptosis independently of Bak and Bax (Einsele-Scholz *et al.*, 2016; Llambi *et al.*, 2016). Still, it is clear that cells lacking Bak and Bax are almost completely resistant to intrinsic apoptotic stimuli including ER-stress inducing agents, despite detectable Bok in these cells (Echeverry *et al.*, 2013; Lindsten *et al.*, 2000; Wei *et al.*, 2001).

Bok may be a non-canonical effector of apoptosis, regulated not by other Bcl-2 proteins but by components of the ERAD pathway (Llambi *et al.*, 2016). ERAD is part of the unfolded protein response (UPR) that is engaged when a cell is under ER stress

(Walter and Ron, 2011). In the proposed model (**Figure 7**), Bok is constantly produced by cells and is ubiquitylated by the E3 ubiquitin ligase AMFR/gp78, extracted from the ER by the AAA-ATPase VCP/p97, and then degraded by the proteasome (Llambi *et al.*, 2016). Proteasome inhibition or silencing of gp78 or VCP stabilised overexpressed Bok protein in Bak/Bax DKO mouse embryonic fibroblasts (MEFs) and endogenous Bok in HCT116 Bak/Bax DKO cells (Llambi *et al.*, 2016). Stabilisation of Bok led to caspase-mediated cell death, though cytochrome *c* release was not directly assayed (Llambi *et al.*, 2016). Interestingly, unlike Bak and Bax, recombinant Bok did not require BH3 peptide stimulation to permeabilise large unilamellar vesicles (LUVs), and permeabilisation was neither enhanced by treatment with several BH3 peptides nor inhibited by Bcl-2 and Bcl-X_L (Llambi *et al.*, 2016). Though Mcl-1 slightly inhibited Bok activity on liposomes, overexpression of Bcl-2, Bcl-X_L or Mcl-1 failed to inhibit apoptosis upon proteasome inhibition with MG132 in DKO MEFs with enforced Bok expression and in DKO HCT116 cells (Llambi *et al.*, 2016).

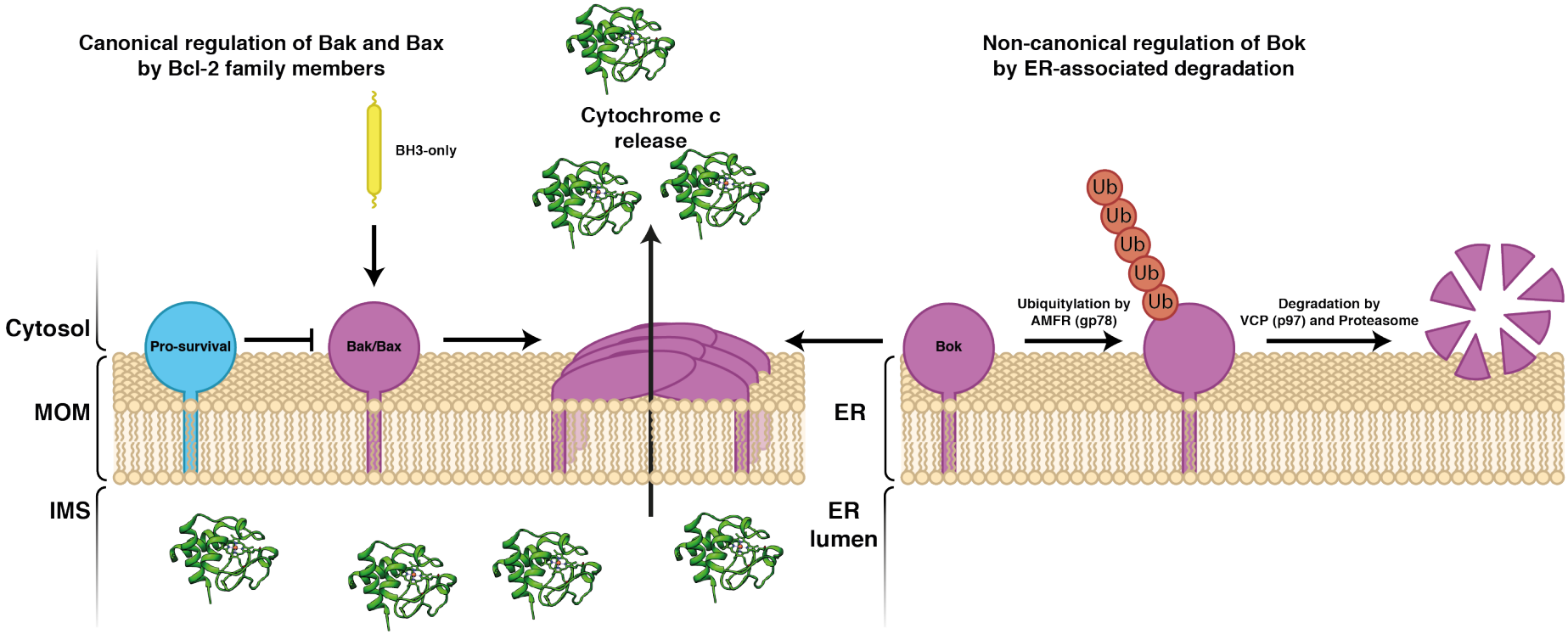
Canonical regulation of Bak and Bax
by Bcl-2 family members
BH3-only
Cytochrome c
release
Non-canonical regulation of Bok
by ER-associated degradation
Ub
Ub
Ub
Ub
Ub
Ubiquitylation by
AMFR (gp78)
Degradation by
VCP (p97) and Proteasome
Cytosol
MOM
IMS
Pro-survival
Bak/Bax
Bok
ER
ER
lumen

Figure 7. Model of Bok-mediated MOMP vs. canonical Bak/Bax-mediated MOMP. *MOMP by canonical Bcl-2 effector proteins Bak and Bax is regulated by other Bcl-2 proteins. Bok, on the other hand, initiates apoptosis when the ERAD pathway or the proteasome are inhibited (Llambi et al., 2016), leading to Bok accumulation followed presumably by MOMP and caspase activation.*

A model of constant Bok degradation in order to mitigate oligomerisation and cell death is difficult to reconcile with the fact that endogenous Bok protein is detectable in many different tissues (D'Orsi *et al.*, 2016; Echeverry *et al.*, 2013; Ke *et al.*, 2012; Llambi *et al.*, 2016; Schulman *et al.*, 2016). It has been suggested that most cellular Bok is stably bound to the IP3Rs, and that the constantly produced and degraded pool of free Bok is responsible for apoptosis observed in the Llambi *et al.* 2016 study (Schulman *et al.*, 2016). Although an apoptotic phenotype has been observed in cells lacking Bak and Bax but expressing Bok, whether Bok itself mediates cytochrome *c* release is contentious (Fernandez-Marrero *et al.*, 2017; Haschka and Villunger, 2017). Indeed, a C-terminally truncated form of Bok was unable to release cytochrome *c* from mitochondria isolated from Bak/Bax DKO MEFs, despite membrane association of the protein in Bok knockout MEFs (Fernandez-Marrero *et al.*, 2017). This may be due to some sort of inhibitory factor on the mitochondria, but it is also possible that Bak and Bax are required to recruit C-terminally truncated Bok to the MOM, as membrane association was only shown in the setting where Bak and Bax were present (Fernandez-Marrero *et al.*, 2017). Interestingly, this C-terminally truncated Bok can permeabilise liposomes and shows cooperativity in liposome permeabilisation with cBid but not Bid BH3 peptide, unlike Bak and Bax where peptide is sufficient (Fernandez-Marrero *et al.*, 2017). Whether the TM domain of Bok might be required for MOMP was not investigated in this study (Fernandez-Marrero *et al.*, 2017). It is also important to note that in experiments with recombinant C-terminally truncated Bok, the monomeric or oligomeric state of the protein was not known due to the lack of a gel filtration step during purification (Fernandez-Marrero *et al.*, 2017). Hence, the authors may have been experimenting with pre-oligomerised or aggregated, rather than monomeric, Bok.

Non-apoptotic cytoprotective roles have been proposed for Bok, including suppression of poly ADP-ribose polymerase-dependent cell death and maintenance of Ca^{2+} homeostasis in neurons (D'Orsi *et al.*, 2016). On top of this, and somewhat

counterintuitively, *Bok*$^{-/-}$ cells are more sensitive to cell death induced by Brefeldin A, a drug that causes collapse of the Golgi into the ER and activates the UPR (Echeverry *et al.*, 2013).

The literature on Bok is rife with perplexing contradictions, and the roles and physiological relevance of Bok remain murky. As a recent review so eloquently put it: "there is something about Bok we just don't get yet" (Haschka and Villunger, 2017). Determination of the 3D structure of the Bok protein would certainly be a boon to further research, and could reveal anomalies in the Bok fold that may explain its constitutive activity.

1.6 Thesis Outline

During apoptosis, Bak and Bax homodimerise and subsequently oligomerise on the MOM, leading to its permeabilisation. Recently, crystal structures of the core domains of both Bak and Bax have demonstrated that the proteins homodimerise via a reciprocal exchange of BH3 domains into the hydrophobic groove of a partner molecule, as predicted by earlier cysteine cross-linking studies (Brouwer *et al.*, 2014; Czabotar *et al.*, 2013; Dewson *et al.*, 2008; Dewson *et al.*, 2012). Formation of these BH3:groove homodimers is an essential step in MOMP.

How BH3:groove homodimers interact with the membrane and form oligomers remains an area of great interest in the field. In **Chapter 2**, I employ X-ray crystallography to examine these processes in molecular detail using a novel Bak core domain expression construct where the scaffolding GFP fusion protein is replaced by a cleavable purification tag.

The original structure of the Bak core homodimer was solved at high resolution, allowing precise characterisation of important molecular interactions (Brouwer *et al.*, 2014). The Bax core homodimer structure was solved at a much lower resolution, with particularly poor electron density in the Bax portions of the maps (Czabotar *et al.*, 2013). In **Chapter 3**, I aim to improve the resolution of the Bax core homodimer structure in order to gain a clearer picture of the Bax BH3:groove homodimer.

Pro-survival proteins inhibit apoptosis by sequestering pro-apoptotic proteins. In the case of Mode 1 inhibition, pro-survival proteins bind the BH3 domain of BH3-only proteins. In Mode 2 inhibition, pro-survival proteins bind the BH3 domain of Bak or Bax. Unlike the BH3-only proteins, Bak and Bax are multi-BH domain proteins, and it is possible that the interactions between Bak or Bax and a pro-survival protein are more extensive than just the BH3 domain binding to the pro-survival groove. The aim of **Chapter 4** is to investigate the possibility of pro-survival:Bax/Bak BH3:groove heterodimers similar to the Bax and Bak BH3:groove homodimers.

Bok is an enigmatic multi-BH domain pro-apoptotic Bcl-2 protein. One challenge in attempts to better understand this protein is the lack of a 3D structure. **Chapter 5** details the expression, purification and characterisation of recombinant human, rat and chicken Bok. The first crystal structure of Bok, from the chicken, is presented here.

Chapter 2

Investigation of Interactions Between Bak and Lipids

Bak is intimately associated with the MOM in localisation and function. Once activated by transient BH3-only protein binding, globular membrane-anchored Bak separates into the core (α2-5) and latch (α6-8) domains (Brouwer *et al.*, 2014). Subsequently, the freed core domain homodimerise with the core domain of a second Bak molecule via a symmetric exchange of the α2 BH3 helix of one Bak molecule into the α3-5 hydrophobic groove of another (Brouwer *et al.*, 2014; Dewson *et al.*, 2008). Bak BH3:groove homodimers nucleate formation of membrane-permeabilising Bak oligomers that incorporate more homodimers as they grow (see **Figure 5**) (Aluvila *et al.*, 2014; Brouwer *et al.*, 2014; Dewson *et al.*, 2009; Ma *et al.*, 2013; Mandal *et al.*, 2016; Uren *et al.*, 2017). Despite intense investigation, the molecular mechanisms by which Bak homodimers oligomerise and permeabilise the MOM remain unclear.

A well-defined and requisite protein:protein interface between Bak homodimers within an oligomer is yet to be described. Cysteine cross-linking and EPR spectroscopy studies have suggested that interactions between α6 helices (Dewson *et al.*, 2009; Ma *et al.*, 2013), between the α3/α5 corners of core domain dimers (Aluvila *et al.*, 2014; Mandal *et al.*, 2016), and between α9 TM helices may be involved in oligomerisation (Iyer *et al.*, 2015). However, any protein-mediated oligomerisation interfaces are unstable when removed from the membrane, as Bak oligomers dissociate to homodimers when extracted from the MOM with detergent (Ma *et al.*, 2013). In addition, no Bak mutations capable of disrupting oligomerisation without also disrupting homodimerisation have yet been found, suggesting that protein-mediated interactions may be dispensable for Bak homodimer oligomerisation. Disordered clustering of Bak homodimers has been proposed to cause membrane rupture and may explain the absence of well-ordered protein:protein oligomeric interfaces (Uren *et al.*, 2017).

The lack of evidence for a tight protein:protein interface between Bak homodimers suggests that the MOM itself may play a role in oligomerisation (Uren *et al.*, 2017). Indeed, other membrane proteins with few interactions at protein:protein interfaces

require lipids at interfacial regions for multimerisation (Gupta *et al.*, 2017). The possibility that lipids mediate or contribute to oligomerisation of Bak or Bax homodimers has not been investigated.

The core domains (α2-5) of BH3:groove homodimers are the most rigid, stable unit within Bak oligomers (Aluvila *et al.*, 2014; Mandal *et al.*, 2016; Uren *et al.*, 2017). As such, the truncated Bak core domain construct presents a unique opportunity to explore a component of activated Bak in high-resolution structural studies (Brouwer *et al.*, 2014). Of particular interest is the hydrophobic surface formed by the α4 and α5 helices of the core domain homodimer that could interact with the MOM.

To investigate the Bak core homodimer and its relationship with the membrane, I determined several X-ray crystal structures of Bak core homodimers in complex with lipids and detergents. The results described here have implications for Bak oligomerisation and its interactions with the membrane.

2.1 Crystal Structure of Bak Core Homodimers in Complex with Lipids

The crystal structure of the Bak core domain homodimer was originally solved by fusing the α2-5 core sequence to GFP to increase solubility and aid crystallisation (Brouwer *et al.*, 2014). The fusion protein crystallised in the presence of the detergent octyl glucoside, revealing a tetramer consisting of two pairs of GFP homodimers linked by two Bak BH3:groove core homodimers (Brouwer *et al.*, 2014). The arrangement of the core domain homodimers was consistent with previous cysteine cross-linking studies and has since been validated by EPR spectroscopy experiments (Aluvila *et al.*, 2014; Brouwer *et al.*, 2014; Dewson *et al.*, 2008; Mandal *et al.*, 2016).

It was thought that core domain homodimers would aggregate in the absence of a fusion protein partner because of large exposed hydrophobic surfaces (Brouwer *et al.*, 2014). Nevertheless, I attempted to move away from the potentially restrictive scaffolding of the GFP construct by instead fusing Bak(α2-5) to a cleavable N-terminal glutathione S-transferase (GST) tag. The fusion protein was expressed in *Escherichia coli* and purified on a glutathione column. Surprisingly, the Bak core domain remained soluble following cleavage from GST, and was further purified by anion exchange and GF

chromatography (**Figure 8**). The protein eluted from a Superdex 200 (S200) 10/300 GF column at a size consistent with a hexamer, based on the predicted monomer molecular weight of ~9.5 kDa (**Figure 8C**). This molecular weight is slightly outside the accurate resolution range of the SDS-PAGE gels used, hence it appeared smaller than expected on the gel with a relative mobility similar to the 6 kDa molecular weight marker (**Figure 8B** and **D**). Peak fractions containing Bak(α2-5) from the GF column were concentrated for crystallisation trials.

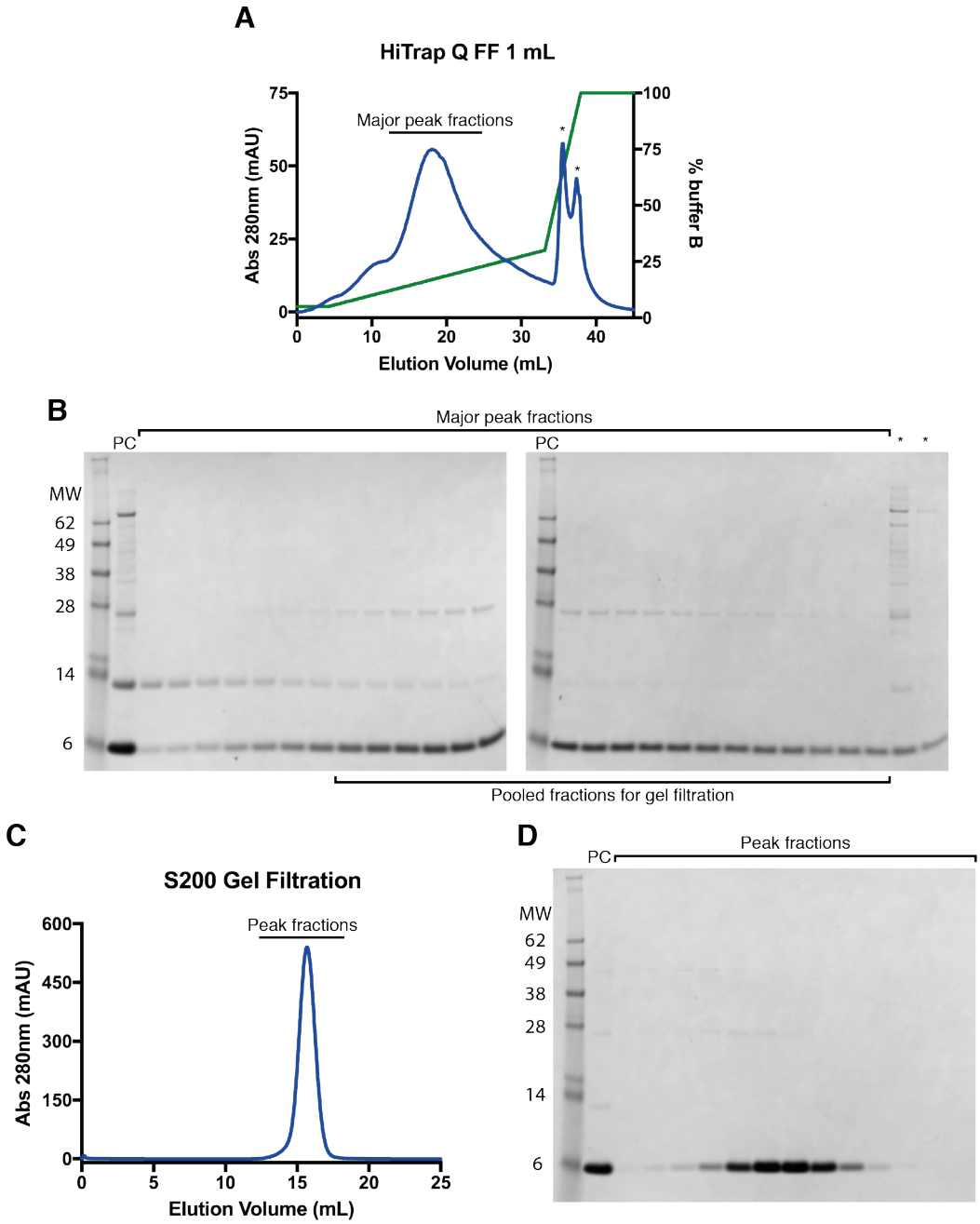

Figure 8. Purification of Bak(α2-5) following cleavage from GST. A) *Chromatogram trace of Bak(α2-5) cleaved from GST and run on a HiTrap Q FastFlow 1 mL column in Tris pH [8.0] with a NaCl gradient from 0.03 to 1 M (% buffer B gradient shown in green). Bak eluted in one major peak at ~25% buffer B and two smaller peaks at higher salt concentrations (labelled as *).* ***B)*** *SDS-PAGE analysis of peak fractions from* ***A****. Fractions from the major peak were pooled for further purification by GF (PC = pre-column sample).* ***C)*** *Pooled fractions were run on an S200 GF column.* ***D)*** *SDS-PAGE analysis of peak fractions from* ***C*** *show highly pure Bak(α2-5).*

The Bak(α2-5) core domain crystallised in the triclinic space group P1. Analysis with Xtriage in PHENIX predicted 5 copies of Bak(α2-5) in the unit cell of the crystal with ~50% solvent content (Adams *et al.*, 2010). Peaks in the self-rotation function of the data, 1 in the κ = 120º section and 3 at intervals of 60º in the κ = 180º section, were indicative of a particle with point group symmetry 32 (**Figure 9**). As the triclinic crystal system contains only lattice translations with no rotational symmetry, the symmetry arrangement in the self-rotation function was suggestive of three Bak homodimers in the unit cell related by a non-crystallographic 3-fold axis, consistent with the hexameric assembly predicted by elution volume from size exclusion chromatography.

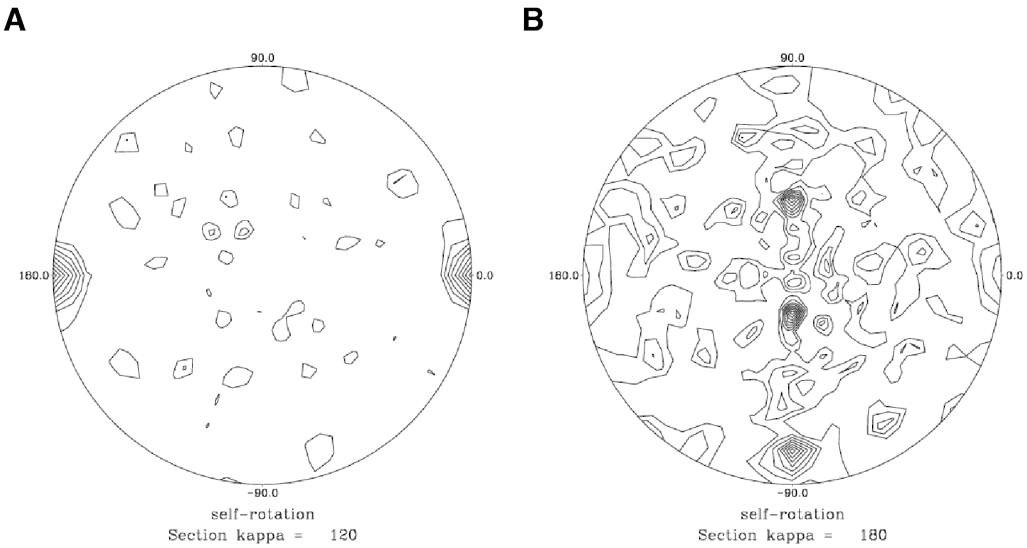

Figure 9. Self-rotation function of the Bak(α2-5) hexamer crystal. A) *and* ***B)*** *κ = 120º and κ = 180º sections, respectively, of the self-rotation function generated from the Bak(α2-5) hexamer crystal data with the UCLA Self Rotation Function Sever (http://services.mbi.ucla.edu/selfrot/). The single peak in the κ = 120º section and three peaks orthogonal to it at intervals of 60º in the κ = 180º section are suggestive of a particle with point group symmetry 32.*

Based on this, initial attempts at molecular replacement in PHASER were performed searching for 3 core homodimers from the GFP:Bak(α2-5) structure (PDB code: 4U2V) (Brouwer *et al.*, 2014; McCoy *et al.*, 2007). No solutions were found with this strategy. Therefore, a globular monomeric entity was constructed from the homodimer containing the α2 BH3 helix of one polypeptide of Bak in the α3-5 hydrophobic groove

of the partner. PHASER placed 6 copies of this search object into homodimer pairs with a translation function Z-score (TFZ) of 19.6 and a log-likelihood gain (LLG) value of 1460. The α2 and α3-5 helices of each copy of Bak were joined in COOT and the structure was refined by iterative rounds of building in COOT and refinement in PHENIX to 2.5 Å (data collection and refinement statistics are presented in **Table 1**) (Adams *et al.*, 2010; Emsley and Cowtan, 2004). Failure to find the core homodimers is attributable to the fact that the dimer structures discovered here are less bent than those described earlier.

The hexamer consisted of three BH3:groove homodimers in a cylinder-like arrangement with D3 symmetry, matching the interpretation of the self-rotation function (**Figure 10A-D**). One of the three homodimers is shown in **Figure 10E** demonstrating the BH3:groove fold where the α2 helices are reciprocally exchanged from one chain into the hydrophobic groove (α3-5) of the other. The three homodimers that formed the hexameric cylinder were highly similar in fold and are overlayed in **Figure 10F**. The hydrophilic α2-3 faces (depicted for one homodimer in **Figure 10G**) formed the outer surfaces of the cylinder while the hydrophobic α4-5 surfaces (depicted for one homodimer in **Figure 10H**) lined the cylinder interior.

Table 1. Data collection and refinement statistics for Bak(α2-5) hexamer.

Wavelength	0.9537
Resolution range	25.66 - 2.491 (2.58 - 2.491)
Space group	P 1
Unit cell	46.7 55.04 56.5 116.134 109.665 97.02
Total reflections	146199 (13487)
Unique reflections	15486 (1481)
Multiplicity	9.4 (9.1)
Completeness (%)	98.13 (93.03)
Mean I/sigma(I)	15.04 (1.45)
Wilson B-factor	66.40
R-merge	0.0905 (1.727)
R-meas	0.09588 (1.831)
CC1/2	0.999 (0.617)
CC*	1 (0.873)
Reflections used in refinement	15459 (1454)
Reflections used for R-free	1546 (142)
R-work	0.1931 (0.3049)
R-free	0.2521 (0.4012)
Protein residues	469
RMS(bonds)	0.002
RMS(angles)	0.35
Ramachandran favoured (%)	98.68
Ramachandran allowed (%)	1.32
Ramachandran outliers (%)	0.00
Rotamer outliers (%)	1.04
Clashscore	2.74
Average B-factor	94.68
macromolecules	94.79
ligands	91.77

Statistics for the highest-resolution shell are shown in parentheses.

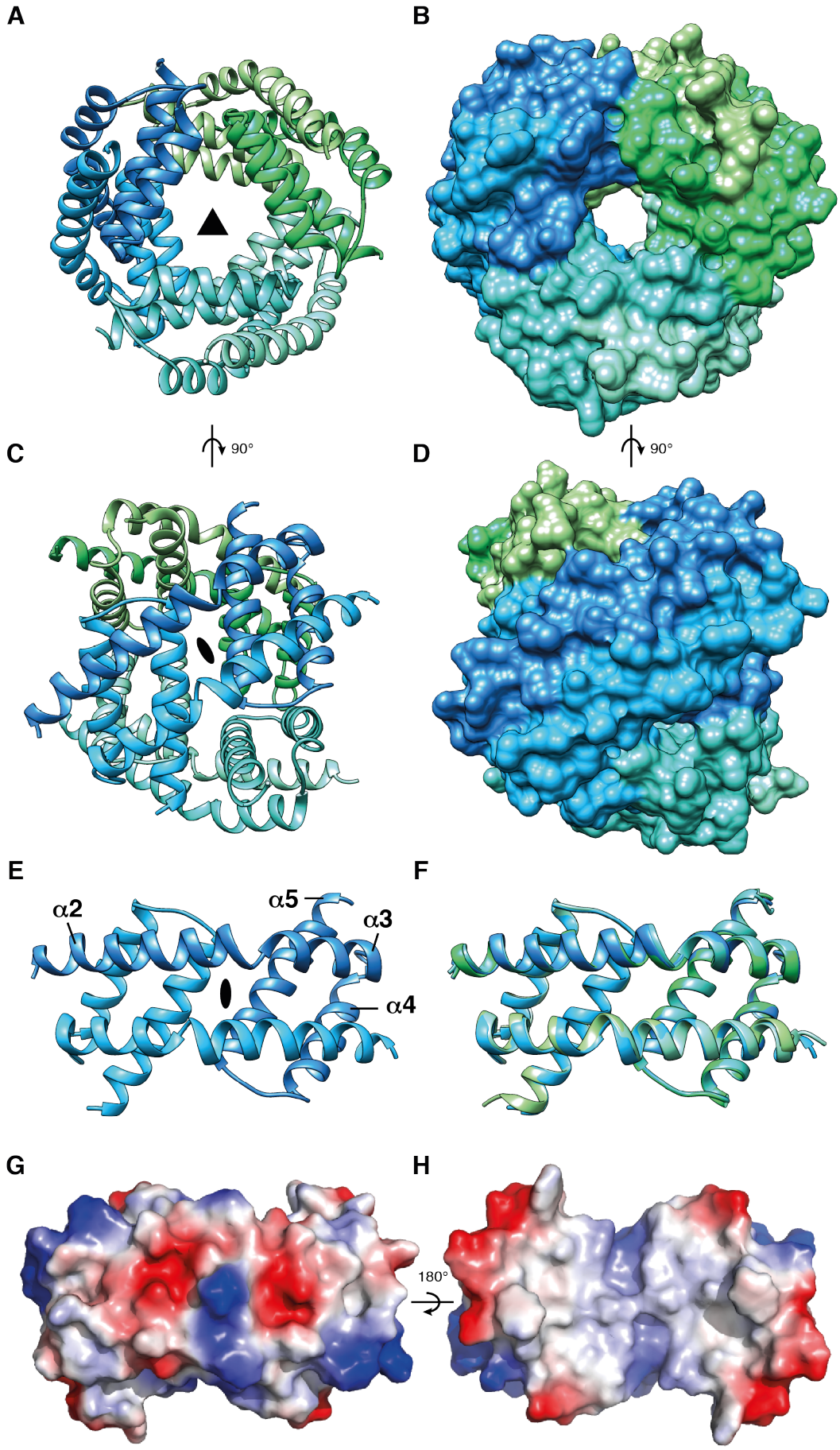
A
B
90°
C
90°
D
E
α2
α5
α3
α4
F
G
H
180°

Figure 10. X-ray crystal structure of the Bak(α2-5) hexamer. A) *and* ***B)*** *Asymmetric unit of the Bak(α2-5) hexamer crystal viewed down the non-crystallographic 3-fold axis shown in ribbon representation (**A**) and surface representation (**B**). The hexamer consists of three BH3:groove homodimer pairs (coloured dodger blue and deep sky blue, turquoise and aquamarine, and spring green and light green) with a hole through the assembly at the 3-fold axis.* ***C)*** *and* ***D)*** *90° rotation of structure as represented in **A** and **B**, respectively. One of three non-crystallographic 2-fold axes is labelled at the centre of the blue homodimer.* ***E)*** *One of the three homodimers with the α-helices of one chain labelled.* ***F)*** *Overlay of the three homodimers that form the hexamer.* ***G)*** *Vacuum electrostatic surface of the isolated homodimer in **E** generated in PyMOL (Delano, 2002) (blue positive potential (-60 kT), red negative potential (60 kT)).* ***H)*** *180° rotation of model in **G** shows the hydrophobic nature of the α4-5 surface.*

As mentioned above, the homodimers were flattened in the cylinder structure (**Figure 11A**) in comparison to the published GFP:Bak(α2-5) structure (PDB code: 4U2V) (**Figure 11B**) (Brouwer *et al.*, 2014). The arrangement of helices α2 and α3-5 in the globular BH3:groove entities used to solve the structure were similar between the two structures, but the angle between the globules increased in the flattened homodimers. As a consequence of dimer flattening, two symmetric hydrophobic indentations (hereafter referred to as the α5/5' grooves), delineated by residues I123, V128, L132 and Y136, opened up on the hydrophobic α4-5 surfaces of each homodimer of the cylinder structure (**Figure 11C** and **Figure 10H**). These were not present in the original GFP:Bak(α2-5) structure (**Figure 11D**). During refinement, large and distinctively shaped positive peaks were observed in the difference density maps at 6 equivalent positions in the α5/5' grooves (**Figure 11E**). The large peak with a forked tail was reminiscent of the phosphodiester group and fatty acid tails of a diacyl phospholipid. Endogenous lipids are known to copurify and crystallise with membrane proteins expressed in *E. coli* (Hunte and Richers, 2008).

Based on the difference density peaks, our collaborators at the Bio21 Molecular Science and Biotechnology Institute performed mass spectrometric analysis on purified Bak hexamer and dissolved Bak hexamer crystals to identify lipids present in the samples (for Methodology see Appendix) (**Figure 12**). Phosphatidylethanolamine (PE), phosphatidylglycerol (PG) and phosphatidylinositol (PI) were identified in the purified

Bak hexamer sample (**Figure 12A** and **C**). Both PE and PG were also present in the crystal sample but PI was completely excluded (**Figure 12B** and **D**). In both cases, there was no obvious preference for acyl chain length or saturation.

As the most abundant lipid in the crystal sample (85.8%), PE was chosen as the ligand to model into the difference density shown in **Figure 11E**. Adding lipids to the structure resulted in a significant improvement in R-factors after refinement. After several rounds of refinement, carbon atoms in the acyl chains that did not have convincing density in the 2Fo-Fc map contoured at 0.7 σ were set to zero occupancy. Ligands in all subsequent structures in this chapter were also treated in this way. To confirm the presence of lipids in the structure, the PE ligands were removed from the final model and refinement with simulated annealing was performed. Clear positive density for the phosphodiester and glycerol moieties was observed at all PE positions in the Fo-Fc map, with varying lengths for the acyl chains (**Figure 11F**). The final model containing lipid is shown in **Figure 11G** and **H**. The zero occupancy acyl chain atoms of the PE ligands were included in this depiction based on the chain lengths seen in the mass spec analysis. The acyl chains are likely flexible and disordered beyond a certain length in the crystal and are therefore not seen in the electron density. Each lipid headgroup sits between two adjacent homodimers, with the one acyl chain bound to the α5/5' groove of one homodimer and the other bound in a shallow groove created by the α4-5 surface of one Bak polypeptide in the second dimer.

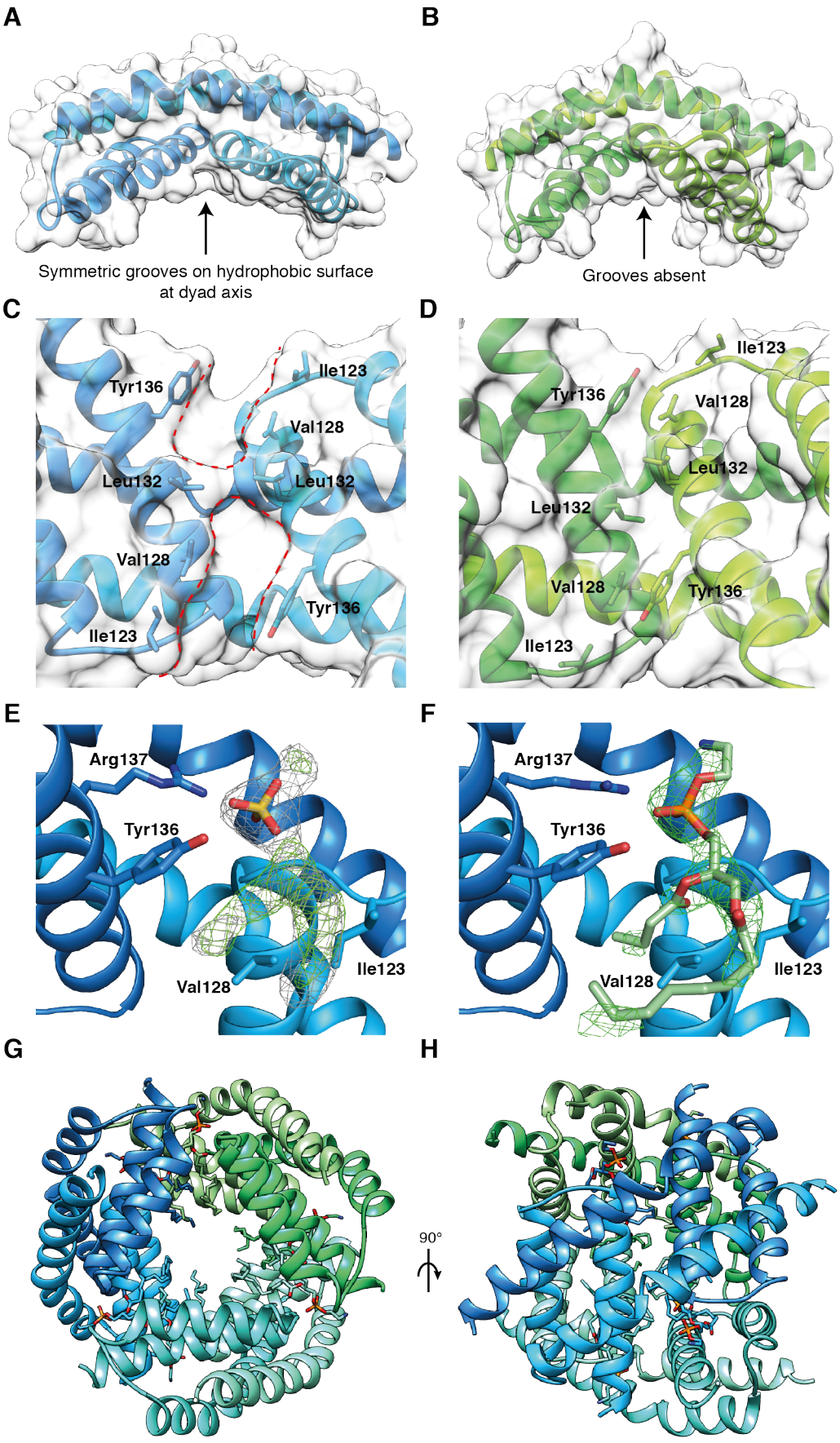
A
Symmetric grooves on hydrophobic surface
at dyad axis
B
Grooves absent
C
Tyr136
Ile123
Val128
Leu132
Leu132
Val128
Tyr136
Ile123
D
Ile123
Tyr136
Val128
Leu132
Leu132
Val128
Tyr136
Ile123
E
Arg137
Tyr136
Val128
Ile123
F
Arg137
Tyr136
Val128
Ile123
G
H
90°

Figure 11. Bak(α2-5) homodimer vs. published structure with evidence for bound phospholipid. **A*)*** *Bak(α2-5) homodimer (dodger blue and deep sky blue) from novel hexamer structure shown as ribbons with a transparent white surface. Two symmetric grooves (α5/5' grooves) are formed at the dyad axis on the hydrophobic α4-5 surface.* ***B)*** *Previously published structure of Bak(α2-5) homodimer (green and chartreuse, PDB code: 4U2V (Brouwer et al., 2014)) in the same orientation as* ***A*** *(N-terminal GFP fusion protein not shown).* ***C)*** *Structure in* ***A*** *focused on the hydrophobic α4-5 surface. The α5/5' grooves (red dotted line) formed between the α5 helices are delineated by residues Ile123, Val128, Leu132 and Tyr136 (labelled and shown as sticks).* ***D)*** *The Brouwer et al., 2014 structure displayed as in* ***C****. The α5/5' grooves observed in* ***C*** *are absent, due to the curved nature of the dimer in this structure.* ***E)*** *Density (2Fo-Fc in grey and Fo-Fc in green contoured at 1 and 3 σ, respectively) resembling a diacyl phospholipid (modelled at the time as a sulphate ion, yellow) was observed during the early stages of refinement at 6 identical positions in the α5/5' grooves of the 3 homodimers present in the hexamer.* ***F)*** *One homodimer from the final model of the hexamer overlayed with simulated annealing omit map (Fo-Fc contoured at 3 σ) generated from the model that had been refined with 6 PE ligands. All 6 PE ligands were removed to generate the map.* ***G)*** *and* ***H)*** *Final model with PE ligands shown as sticks.*

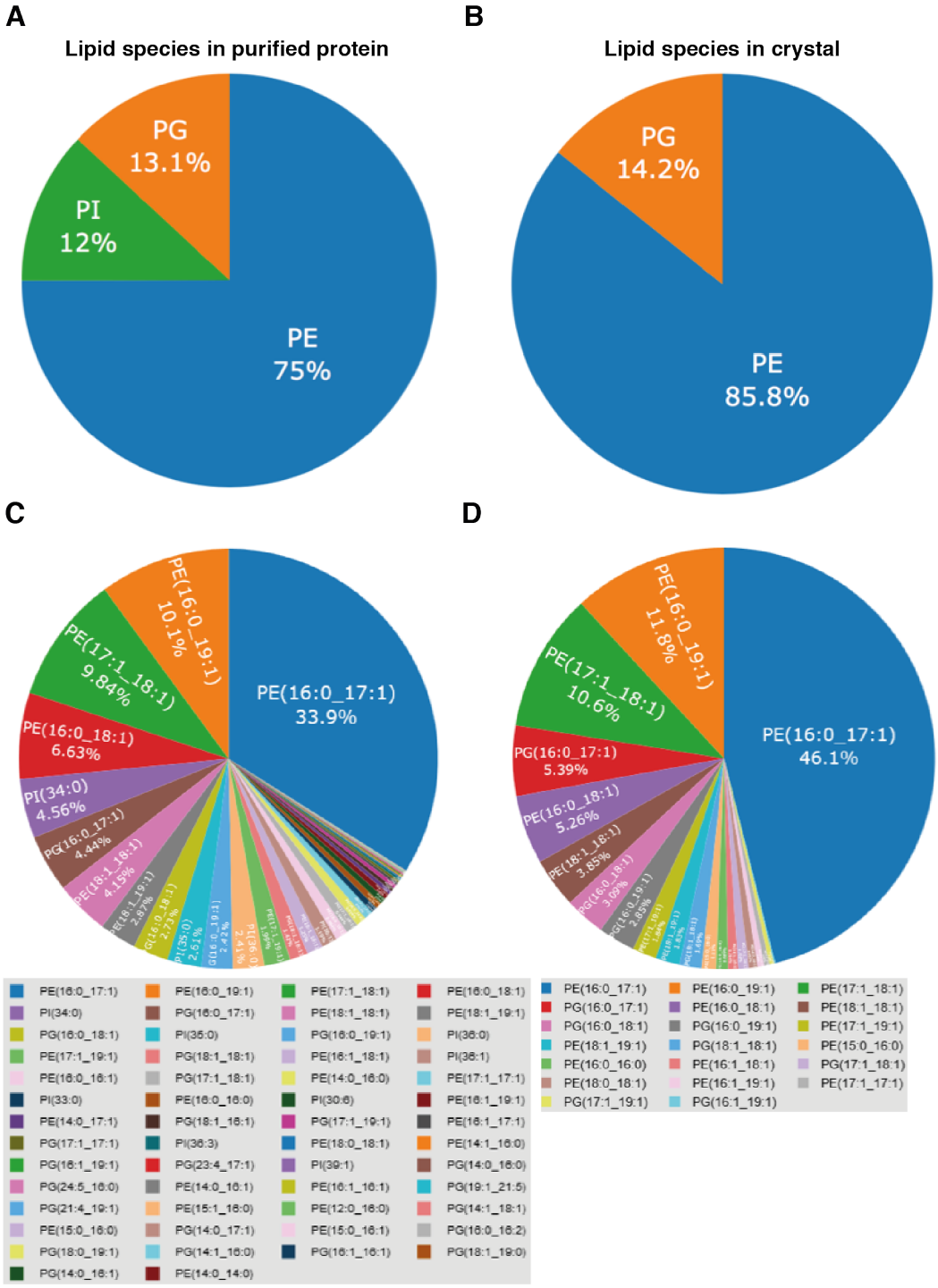

Figure 12. Lipid composition of purified and crystallised Bak(α2-5) samples. ***A)*** *and* ***B)*** *Mole percent composition of lipid classes identified in purified Bak(α2-5) (**A**) and Bak(α2-5) crystals (**B**).* ***C)*** *and* ***D)*** *Mole percent composition of individual lipid species identified in purified Bak(α2-5) (**C**) and Bak(α2-5) crystals (**D**). PE=phosphatidylethanolamine, PG=phosphatidylglycerol, PI=phosphatidylinositol.*

Small-angle X-ray scattering (SAXS) experiments were performed on purified Bak(α2-5) hexamer to further evaluate whether the presence of lipids in the structural model is most consistent with in solution structure (data collection and analysis statistics are presented in **Table 2**). The theoretical scattering curve generated in CRYSOL with the crystal structure coordinates for the Bax cylinder structure corresponded well with the measured experimental scattering curve (**Figure 13C**). In support of the presence of lipids in the Bak cylinder in solution, removing the PE ligands from the model diminished agreement with the experimental data (**Figure 13D**).

Table 2. SAXS data collection and analysis statistics for Bak(α2-5) hexamer.

Data-collection parameters	
Instrument	Australian Synchrotron SAXS/WAXS beamline
Beam geometry	120 micron point source
Wavelength (Å)	1.033
Exposure time	2 sec exposures
Temperature (K)	285
q range ($Å^{-1}$)[a]	0.0106 to 0.400
Protein concentration	50 µL of 17 mg/ml protein *via* inline gel filtration chromatography 0.2 M NaCl, 20 mM HEPES pH [7.5], 5% v/v glycerol
Structural parameters	
I(0) (cm^{-1}) [from P(r)]	0.03726 ± 0.0001
R_g (Å) [from P(r)]	24.59 ± 0.064
D_{max} (Å)	75
I(0) (cm^{-1}) (from Guinier)	0.03749 ± 0.0001
R_g (Å) (from Guinier)	25.10 ± 0.11
Software employed	
Primary data reduction	Scatterbrain (Australian Synchrotron)
Data processing	PRIMUS, GNOM
Computation of model intensities	CRYSOL

[a] q is the magnitude of the scattering vector, which is related to the scattering angle (2θ) and the wavelength (λ) as follows: $q = (4\pi/\lambda)\sin\theta$.

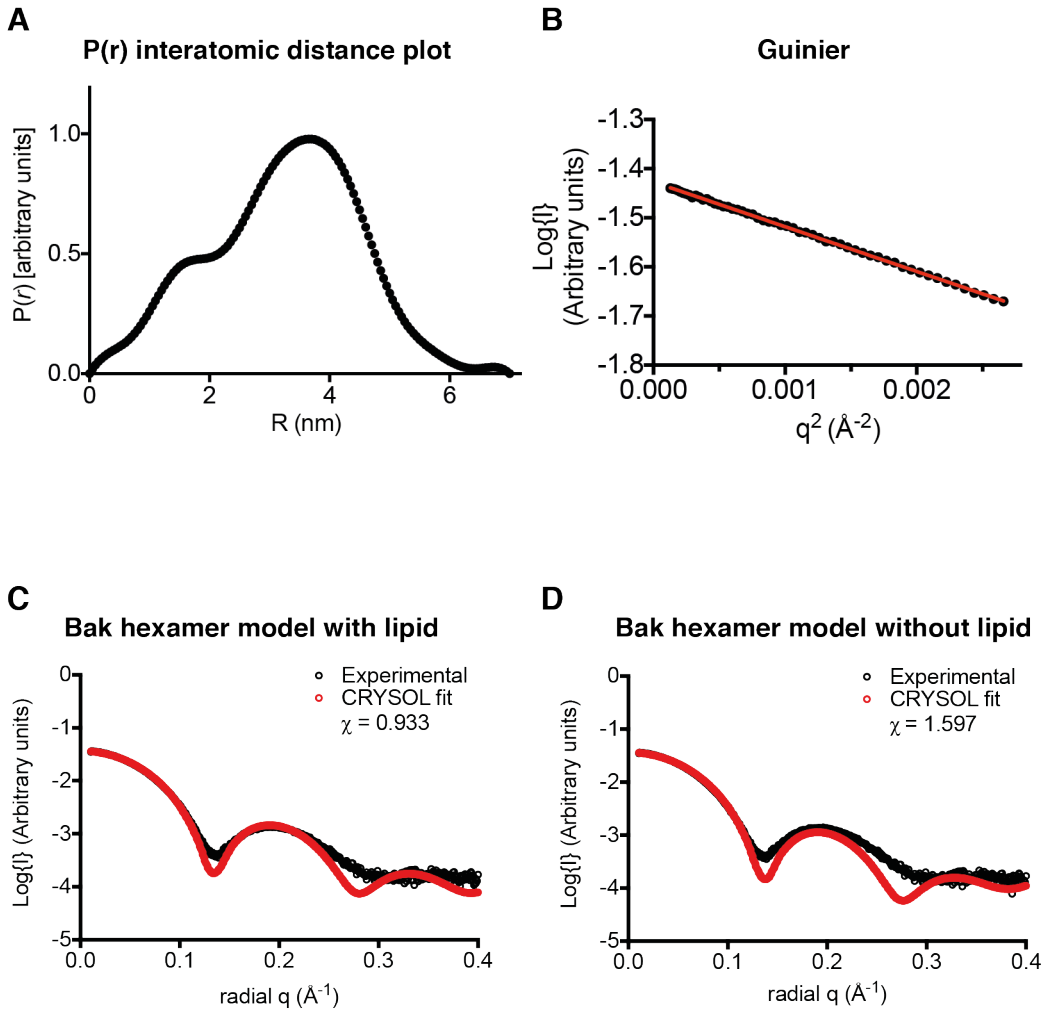

Figure 13. SAXS analysis of Bak(α2-5) hexamer. A) *Pairwise interatomic distance distribution (P(r)) determined with GNOM (Svergun, 1992).* ***B)*** *Guinier plot of the SAXS data for q.Rg ≤ 1.3 performed with PRIMUS (Konarev et al., 2003). The linearity of a Guinier plot of Bak α2-5 scattering data shows that higher molecular weight aggregates do not measurably contribute to scattering.* ***C)*** *and* ***D)*** *Experimental scattering curve measured for Bak α2-5 (black) overlayed with the theoretical scattering curve (red) generated with CRYSOL (Svergun et al., 1995) using the crystal structure of the Bak(α2-5) hexamer including PE lipids (**C**) and with lipids deleted from the model (**D**). The χ values of 0.933 and 1.597 indicate that the inclusion of lipids better represents the structure of the complex in solution.*

2.2 Investigation of Lipid Binding Site by X-ray Crystallography

Having demonstrated conclusively that Bak core domains associate with lipid, I went on to investigate the binding site further using X-ray crystallography. Concomitantly with refinement of the Bak hexamer structure and experiments to confirm the presence of lipid, an additive screen on a different set of conditions produced large crystals in a well containing the non-ionic detergent *n*-Dodecyl-β-D-maltoside (DDM). The structure was solved by molecular replacement using a homodimer from the cylinder structure as a search model and refined to 1.9 Å in the monoclinic space group C2 (data collection and refinement statistics are presented in **Table 3**). Six Bak core homodimers were present in the asymmetric unit, arranged in two near-identical hexameric funnel-like assemblies, one of which is depicted in **Figure 14A** and **B**. In contrast to the Bak hexamer cylinder, the inner and outer surfaces of the funnel were hydrophilic (α2-3 helices) and hydrophobic (α4-5 helices), respectively (**Figure 14C** and **D**). A sulphate ion coordinated by six Arg88 residues (two from each homodimer) plugged the funnel stem at a non-crystallographic 3-fold axis. The α5/5' grooves that bound *E. coli* lipids in the cylinder structure were replaced by DDM molecules that were well-resolved in the electron density, demonstrating for a second time the lipophilicity of the grooves (**Figure 14E**). DDM was also bound less consistently to secondary sites on the α4-5 surface (**Figure 14E**).

Table 3. Data collection and refinement statistics for Bak(α2-5) in complex with DDM.

Wavelength	0.9537
Resolution range	39.45 - 1.799 (1.863 - 1.799)
Space group	C 1 2 1
Unit cell	158.941 91.835 95.716 90 107.518 90
Total reflections	458431 (43684)
Unique reflections	121091 (11835)
Multiplicity	3.8 (3.7)
Completeness (%)	99.22 (94.54)
Mean I/sigma(I)	12.03 (0.58)
Wilson B-factor	31.44
R-merge	0.07763 (2.416)
R-meas	0.09051 (2.82)
CC1/2	0.999 (0.226)
CC*	1 (0.607)
Reflections used in refinement	120587 (11383)
Reflections used for R-free	1993 (188)
R-work	0.2129 (0.3515)
R-free	0.2487 (0.3789)
Protein residues	1019
RMS(bonds)	0.008
RMS(angles)	0.92
Ramachandran favoured (%)	99.46
Ramachandran allowed (%)	0.54
Ramachandran outliers (%)	0.00
Rotamer outliers (%)	1.65
Clashscore	6.58
Average B-factor	46.21
macromolecules	41.37
ligands	78.47
solvent	48.90

Statistics for the highest-resolution shell are shown in parentheses.

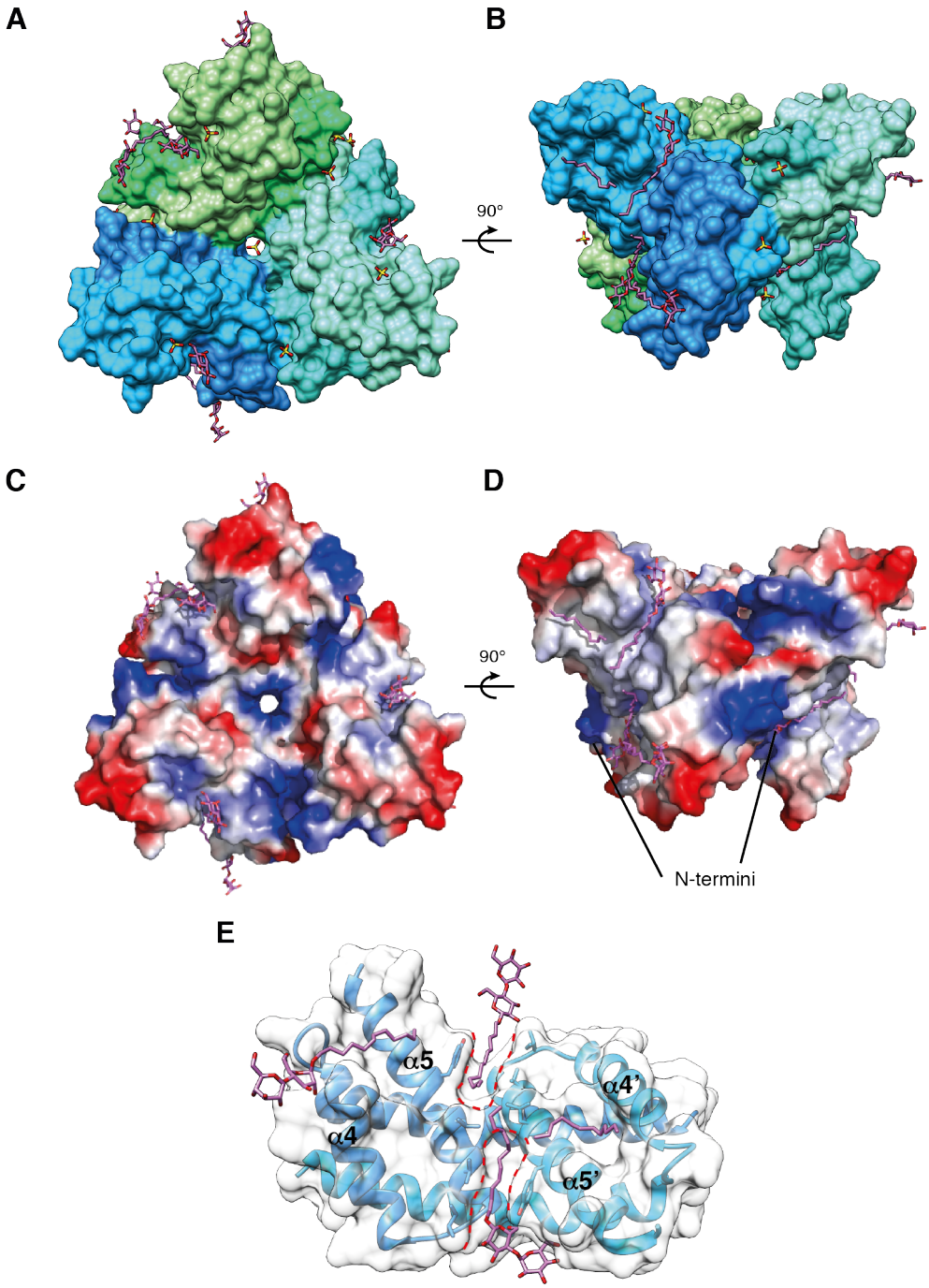
A
B
90°
C
D
90°
N-termini
E
α5
α4'
α4
α5'

Figure 14. Crystal structure of Bak(α2-5) funnel in complex with DDM. A-D) *Surface representation (**A** and **B**) and charge distribution (**C** and **D**, (blue positive potential (-63.5 kT), red negative potential (63.5 kT)) of three Bak(α2-5) homodimers (dodger blue and deep sky blue, spring green and light green, and turquoise and aquamarine) that formed a funnel in complex with DDM (purple, shown as sticks). The hydrophilic faces of the homodimers (α2-3) form the funnel's inner surface, with a sulphate ion, coordinated by several arginine residues, plugging the funnel stem at a non-crystallographic 3-fold symmetry axis. The exterior funnel surface made up of the α4-5 helices is hydrophobic and partially covered by detergent molecules.* ***E)*** *Ribbon diagram with transparent surface of one of the three homodimers in the funnel. DDM bound to the α5/5' grooves (red dotted lines) seen in the Bak cylinder structure and to secondary sites on the α4-5 surface.*

An analysis of the crystal packing of the Bak(α2-5):DDM funnels is presented in **Figure 15**. Layers of hexameric funnels build the crystal, exhibiting a packing arrangement similar to type-1 packing seen in crystals grown in lipidic cubic phase. In type-1 packing, the molecules are arranged in sheets as though inserted into a lipid bilayer, with transmembrane proteins traversing the hydrophobic core of the sheet and forming hydrophilic contacts between sheet layers. **Figure 15A** depicts two such sheets formed by the two funnels in the asymmetric unit, one of which is coloured while the other is shown in grey. The non-crystallographic 3-fold axes of the two hexamers in the asymmetric unit are antiparallel along the funnel axes, with a non-crystallographic 2-fold relating the two funnels (**Figure 15B**). Two dimers from each funnel partially enter the wide end of the other funnel in the asymmetric unit. The layering of hydrophilic and hydrophobic regions, as demonstrated by the positions of the hydrophilic sugar groups and hydrophobic alkyl chains, is reminiscent of a lipid bilayer with funnels inserted into and spanning the hydrophobic core. The distance of a detergent bilayer in the crystal (measured from sugar headgroups on one side of the hydrophobic region to the other side) is roughly commensurate with the thickness of a lipid bilayer. **Figure 15C** depicts the stacking of funnel layers that extends in the y direction, with sheets alternating between the two funnels in the asymmetric unit. In the XZ plane, the crystal grows via "hydrophobic sandwiching" of DDM molecules between pairs of homodimers on adjacent funnels (**Figure 15D**). As a consequence of the funnel asymmetry, each funnel in a layer is surrounded by three other funnels in an

antiparallel orientation (**Figure 15D**). In a single layer, the chain A/B and E/F dimers form sandwiches between adjacent funnels, while the C/D dimer forms a sandwich with itself through a crystallographic 2-fold axis. Similar interactions occur in the adjacent layers of funnels, with the chain G/H dimer at a crystallographic 2-fold axis and the I/J and K/L dimers forming sandwich pairs. The sandwiches overlay well with one another (**Figure 15E** and **F**), and the A/B E/F homodimer pair is shown in surface representation in **Figure 15G** and **H**).

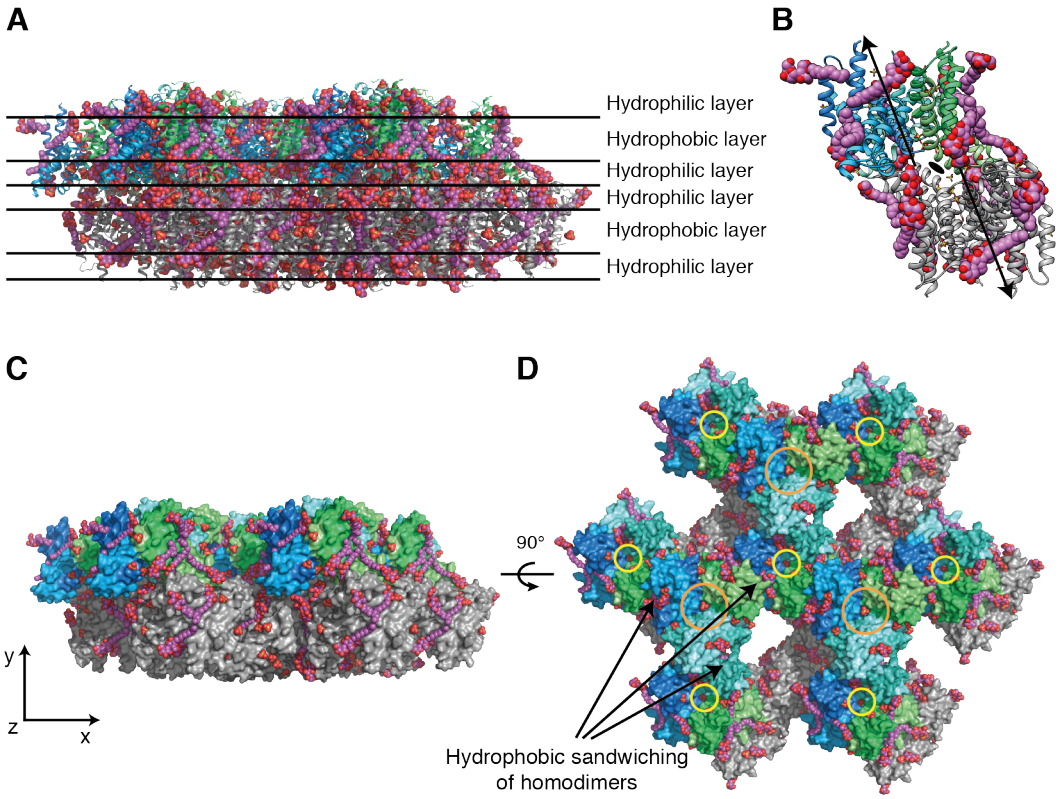
A
B
Hydrophilic layer
Hydrophobic layer
Hydrophilic layer
Hydrophilic layer
Hydrophobic layer
Hydrophilic layer
C
D
90°
y
z
x
Hydrophobic sandwiching
of homodimers
E
F
90°
G
H
90°

Figure 15. Packing analysis of the Bak(α2-5):DDM crystal structure. A) *Two layers of funnels from the crystal lattice demonstrating the hydrophilic/hydrophobic layering pattern. Chains A, B, C, D, E and F that make up one funnel are coloured dodger blue, deep sky blue, turquoise, aquamarine, spring green and light green, respectively. The second funnel in the asymmetric unit is coloured grey and DDM molecules are shown in purple as spheres.* ***B)*** *The asymmetric unit of the crystal coloured as in* ***A****. The non-crystallographic 2-fold that relates the two hexameric funnels is labelled. Arrows indicate the direction of non-crystallographic 3-fold axes down the centre of the funnels from the wide end to the narrow end.* ***C)*** *Surface representation of funnel layers depicted in* ***A****.* ***D)*** *90° rotation of funnel layers in* ***C****. Large orange circles and small yellow circles denote the wide and narrow ends of funnels, respectively. Each funnel is surrounded by 3 antiparallel funnels, extending the crystal in the XZ plane. The contacts between funnels in this plane are formed by the hydrophobic surfaces of dimers that sandwich DDM molecules between them.* ***E)*** *and* ***F)*** *Overlay of all the unique pairs of homodimers that form the sandwiches. The A/B, C/D, E/F, G/H, I/J, and K/L dimers are coloured dodger blue, turquoise, spring green, yellow, orange, and red orange, respectively. DDM molecules are shown as sticks and coloured according to which homodimer they are associated with.* ***G)*** *and* ***H)*** *Surface representation of the sandwich created by the A/B and E/F homodimers.*

Protein:lipid complexes of Bak and phospholipids would be of greater physiological relevance than the complex with the detergent DDM. Crystal screens of Bak(α2-5) with different lipids yielded crystals of complexes with the short chain diacyl phospholipid 1,2-dihexanoyl-*sn*-glycero-3-phosphocholine (6:0 DHPC), the monoacyl lysophospholipid 1-palmitoyl-2-hydroxy-*sn*-glycero-3-phosphocholine (16:0 LysoPC), and the physiologically relevant diacyl phospholipid 1-palmitoyl-2-oleoyl-*sn*-glycero-3-phosphocholine (16:0-18:1 POPC) dissolved in the non-ionic detergent tetraethylene glycol monooctyl ether (C8E4) (data collection and refinement statistics are presented in **Table 4**).

Table 4. Data collection and refinement statistics for Bak(α2-5):ligand complexes.

	Bak(α2-5):DHPC	Bak(α2-5):POPC/C8E4	Bak(α2-5):LysoPC
Wavelength	0.9537	0.9537	0.9537
Resolution range	38.34 - 2.703 (2.8 - 2.703)	42.6 - 1.696 (1.757 - 1.696)	30.04 - 1.8 (1.865 - 1.8)
Space group	C 1 2 1	C 2 2 21	C 2 2 21
Unit cell	126.73 96.344 52.939 90 91.651 90	84.318 150.086 51.749 90 90 90	55.921 89.949 77.572 90 90 90
Total reflections	63917 (6494)	263056 (23778)	267364 (25351)
Unique reflections	17437 (1713)	36562 (3405)	18436 (1785)
Multiplicity	3.7 (3.8)	7.2 (7.0)	14.5 (14.2)
Completeness (%)	99.53 (97.44)	99.19 (93.23)	99.41 (97.57)
Mean I/sigma(I)	10.02 (1.44)	11.70 (1.31)	28.11 (0.89)
Wilson B-factor	73.03	24.73	39.59
R-merge	0.08836 (0.9562)	0.1041 (1.741)	0.05922 (3.184)
R-meas	0.1039 (1.114)	0.1123 (1.88)	0.06139 (3.302)
CC1/2	0.997 (0.646)	0.999 (0.56)	1 (0.609)
CC*	0.999 (0.886)	1 (0.847)	1 (0.87)
Reflections used in refinement	17425 (1711)	36542 (3399)	18381 (1765)
Reflections used for R-free	1739 (162)	1992 (188)	1838 (191)
R-work	0.2134 (0.3142)	0.1828 (0.3888)	0.2094 (0.4933)
R-free	0.2470 (0.3427)	0.2099 (0.4242)	0.2394 (0.6021)
Protein residues	471	333	162
RMS(bonds)	0.002	0.003	0.005
RMS(angles)	0.43	0.61	0.71
Ramachandran favoured (%)	98.47	100.00	100.00
Ramachandran allowed (%)	1.53	0.00	0.00
Ramachandran outliers (%)	0.00	0.00	0.00
Rotamer outliers (%)	0.51	1.43	0.00
Clashscore	5.09	4.72	3.38
Average B-factor	91.34	34.12	58.82
macromolecules	90.86	32.17	56.17
ligands	107.02	56.60	86.66
solvent	73.40	41.60	56.53

Statistics for the highest-resolution shell are shown in parentheses.

Bak(α2-5) in complex with DHPC crystallised in the monoclinic space group C2. The structure was solved by molecular replacement using a Bak(α2-5) homodimer from the DDM structure as a search model, and was refined to 2.7 Å. As in the Bak:DDM crystal structure, the homodimers assembled into a funnel, with a single hexameric funnel in the asymmetric unit (**Figure 16A** and **B**). The packing of the crystal was identical to that observed in the DDM structure, except that the 2-fold axis (see **Figure 15B**) relating funnels on alternating layers of the crystal was a crystallographic 2-fold in this case (**Figure 16C** and **D**). Two unique hydrophobic sandwiches were formed in the crystal: one by the chain A/B and E/F homodimers, and one by the chain C/D homodimer at a crystallographic 2-fold.

Again, a sulphate ion plugged the funnel at the non-crystallographic 3-fold (**Figure 16A**). Four of the six α5/5' grooves were occupied by DHPC that bound in an analogous manner to the *E. coli* lipids in the cylinder structure (**Figure 16F**). The phosphodiester and glycerol moieties were within hydrogen bonding distance of the hydroxyl group of Y136 on α5 and the free backbone amide of W125 at the N-terminus of α5' (discussed below, **Figure 19C** and **D**). The aromatic ring of Y136 on α5 and residue V128 α5' acted as a brace for the hydrophobic acyl chain that bound to the hydrophobic region of the α5/5' grooves.

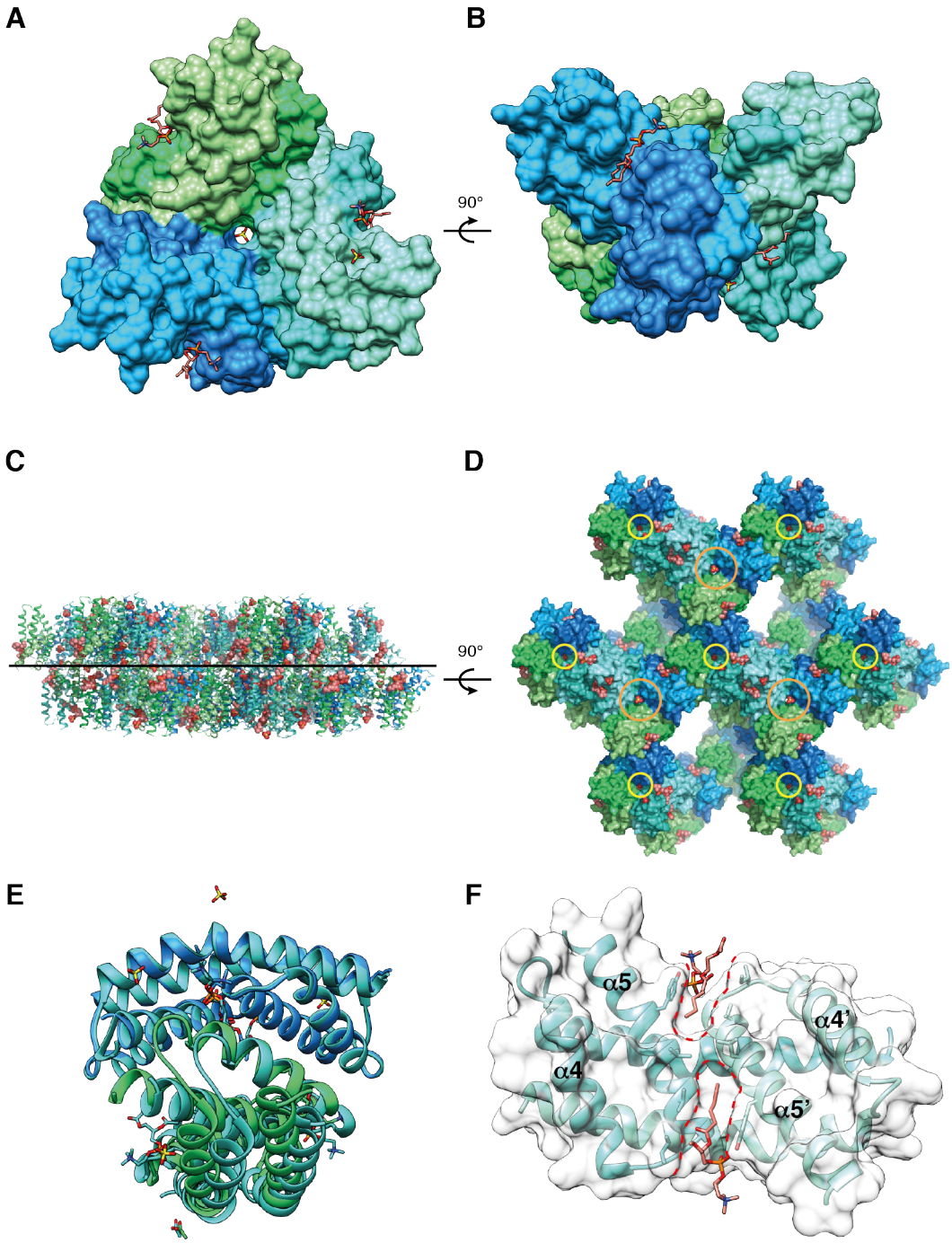
A
B
90°
C
D
90°
E
F
α5
α4'
α4
α5'

Figure 16. Crystal structure of Bak(α2-5) hexamer funnel in complex with DHPC. *A) and* ***B)*** *Bak core homodimers (coloured dodger blue and deep sky blue, turquoise and aquamarine, and spring green and light green) formed a hexameric funnel in complex with DHPC (salmon, shown as sticks) that is almost identical to the funnel seen in the Bak:DDM complex. The exterior surface of the funnel is hydrophobic, made up of the α4-5 helices of the homodimers with bound DHPC.* ***C)*** *and* ***D)*** *Two layers of funnels from* ***A*** *and* ***B*** *that make up the crystal lattice (divided by a black line in* ***C****) shown in cartoon and surface representation, respectively. In* ***D****, large orange circles and small yellow circles denote the wide and narrow ends of funnels, respectively. The arrangement of funnels is identical to that seen in the Bak(α2-5):DDM crystal structure.* ***E)*** *Overlay of the two unique hydrophobic sandwich structures formed by the homodimers which link in-plane, antiparallel funnels. The A/B, C/D, and E/F dimers are coloured dodger blue, turquoise, and spring green, respectively. DHPC molecules are shown as sticks and coloured according to which homodimer they are associated with.* ***F)*** *Ribbon diagram with transparent surface depicting the hydrophobic surface of the chain C/D Bak core homodimer. DHPC bound to the α5/5' grooves (red dotted lines) in a similar position to the* E. coli *lipids seen in the cylinder structure. The phosphate of the phosphodiester group is within hydrogen bonding distance of Y136 on α5 and the backbone amine at the N-terminal end of α5'.*

A third arrangement of homodimers appeared in tetragonal crystals grown in the presence of POPC and C8E4. The structure was solved by molecular placement using a Bak(α2-5) homodimer from the DDM structure as a search model and refined to 1.7 Å. Two homodimers in the asymmetric unit sat side-by-side with C8E4 detergent molecules at the homodimer junction (**Figure 17A** and **B**). The aliphatic chains of the C8E4 molecules bound to the adjacent α5/5' grooves of each homodimer, and the ethylene glycol moieties of each C8E4 formed hydrogen bonds with both homodimers, creating a protein:detergent:protein interface (**Figure 17B**). As with the funnel structures, both homodimers in the asymmetric unit formed a hydrophobic sandwich with a symmetry-related homodimer, sandwiching the aliphatic and acyl chains of C8E4 and POPC between them (**Figure 17C-F**). The homodimers differed in the distance to their symmetry-related sandwich partners and in the angle between the dyad axes of each homodimer in the sandwich (**Figure 17D** and **F**). The chain C/D homodimer in **Figure 17E** and **F** was close to its symmetry partner, whereas the chain

A/B homodimer in **Figure 17C** and **D** was further away from its symmetry partner. In the case of the C/D homodimer, the density in both α5/5' grooves clearly indicated the presence of C8E4 molecules. On the other hand, the density in α5/5' groove of the A/B homodimer distal to the junction between the homodimers was consistent with phospholipid. The larger area between the symmetry-related A/B homodimers also contained six detergent molecules running parallel to the POPC acyl chains (**Figure 17D**). Again, aliphatic chains of lipid and detergent were bound to the α5/5' grooves of the homodimers (**Figure 17G** and **H**). As with the cylinder and DHPC-bound structures, the phosphodiester and glycerol moieties of POPC were within hydrogen bonding distance of the hydroxyl group of Y136 on α5 and the N-terminus of α5' (**Figure 17G** and **Figure 19E** and **F**).

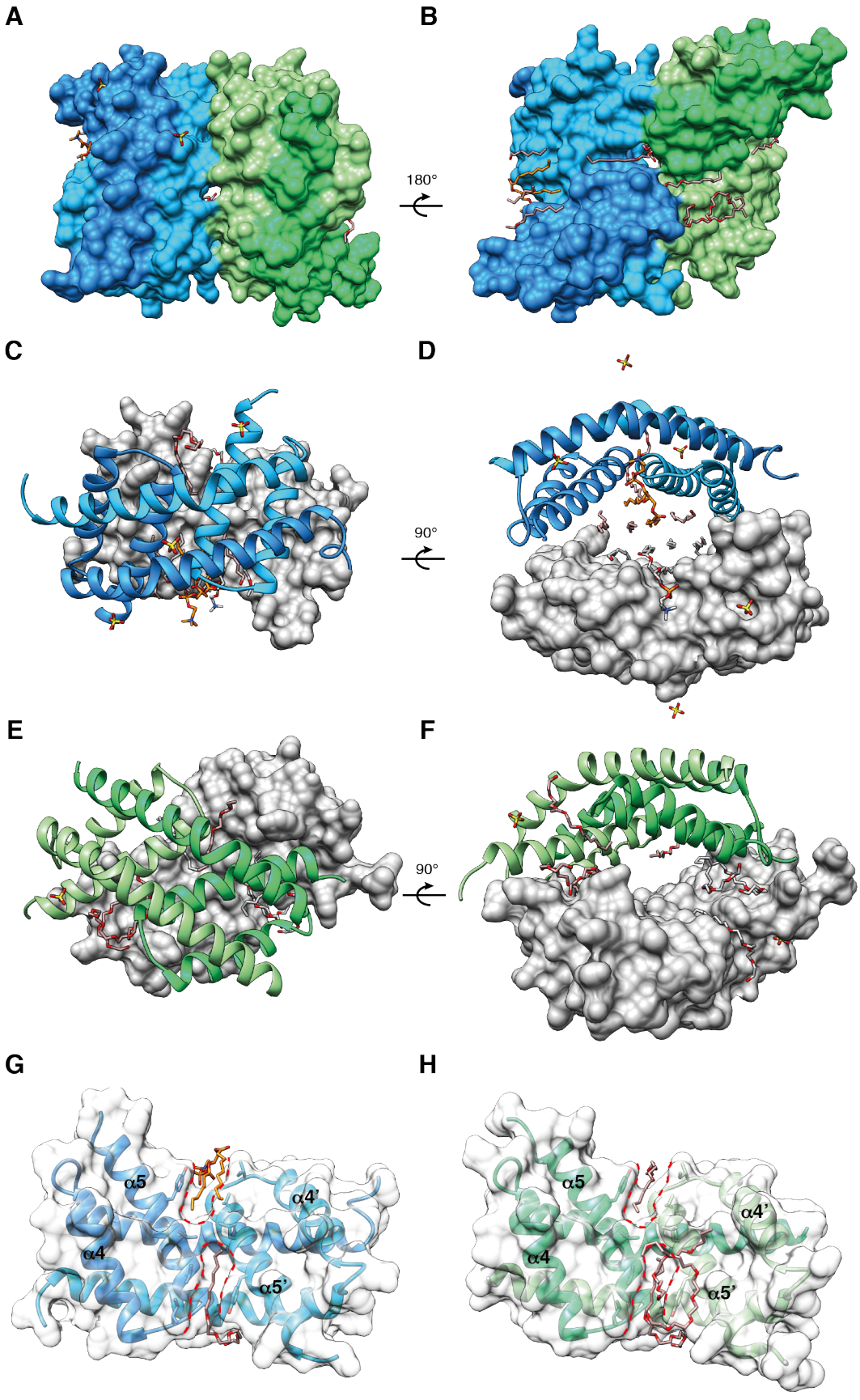
A
B
180°
C
D
90°
E
F
90°
G
H
α5
α4'
α4
α5'
α5
α4'
α4
α5'

Figure 17. Crystal structure of Bak(α2-5) in complex with POPC and C8E4. ***A)*** *and* ***B)*** *Surface representation of the α2-3 (**A**) and α4-5 (**B**) surfaces of Bak core homodimers (chains A and B in dodger blue and deep sky blue, chains C and D in spring green and light green) in the asymmetric unit of the crystal. Two C8E4 molecules (rosy brown, shown as sticks) sit at the junction of the dimers, each with its aliphatic chain bound to an α5/5' groove and the ethylene glycol moiety bridging the homodimers. At the α5/5' groove site distal to the dimer junction, POPC (orange, shown as sticks) and C8E4 are present on the left- and right-hand dimers, respectively. Additional C8E4 molecules surround the POPC and bind to shallow clefts on the right-hand dimer.* ***C-F)*** *Ribbon representation of each homodimer with their respective symmetry partners (coloured grey, surface representation).* ***G)*** *and* ***H)*** *Ribbon diagram with transparent surface of the A/B and C/D homodimers, respectively. POPC and C8E4 bound to the α5/5' grooves (red dotted lines) in a similar position to the* E. coli *lipids seen in the cylinder structure. The phosphate of the POPC phosphodiester group is within hydrogen bonding distance of the backbone amine at the N-terminal end of α5' and hydroxyl group of Y136 on α5.*

A hydrophobic sandwich arrangement of Bak homodimers also occurred within another tetragonal crystal grown from Bak core domains mixed with LysoPC. A Bak(α2-5) homodimer from the DDM structure was used as a search model for molecular replacement, and the structure was refined to 1.8 Å (**Figure 18**). Unlike the previous structure, only one homodimer was present in the asymmetric unit of the crystal, forming a sandwich with a symmetry-related homodimer (**Figure 18A** and **B**). The acyl chains of two LysoPC molecules bound to the α5/5' grooves while a third LysoPC bound along the α4-5 face of one chain of the homodimer (**Figure 18C**). Tubular density was also observed on the α4-5 face of the other chain. Polyethylene glycol (PEG) molecules were built into these positions, but the density could also correspond to acyl chains of LysoPC (**Figure 18C**). Despite the high resolution of this structure, and in contrast to the cylinder, DHPC, and POPC/C8E4 structures, the headgroups of the two lipids bound in the α5/5' grooves were not resolved in the electron density and are shown as lines in **Figure 18**. The density in the α5/5' grooves was modelled as LysoPC rather than PEG because of the hydrophobicity in the region and based on the binding of aliphatic chains to the grooves in previous structures.

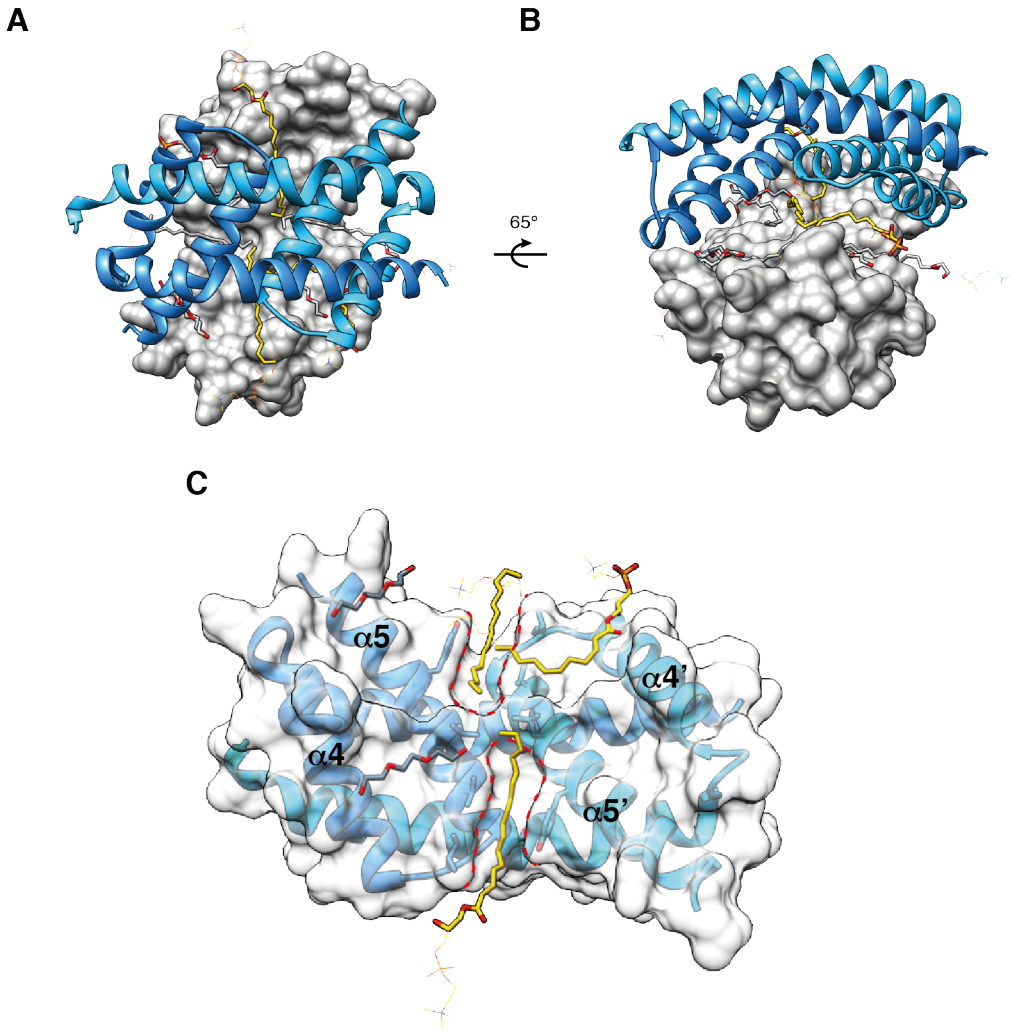

Figure 18. Crystal structure of Bak(α2-5) in complex with LysoPC. A) *and* ***B)*** *The Bak core homodimer in the asymmetric unit (dodger blue and deep sky blue) forms a hydrophobic sandwich in complex with LysoPC (yellow, shown as sticks, atoms with zero occupancy shown as lines) similar to the sandwiches seen in the Bak:POPC/C8E4 complexes.* ***C)*** *Ribbon diagram of the homodimer with transparent surface. The acyl chains of LysoPC bound to the α5/5' grooves (red dotted lines) but the headgroups were not resolved in this structure.*

Based on cysteine cross-linking and EPR spectroscopy data (discussed in Section 2.4), the quaternary arrangements of Bak homodimers observed in all of the structures presented in this chapter do not occur in the mature oligomer, and may be artefacts that arise due to both severe truncation of the protein and the lack of an orientating planar phospholipid bilayer. Importantly however, the symmetric α5/5' hydrophobic grooves were consistently occupied by the aliphatic hydrocarbon tails of lipid or detergent. In

addition, the phosphodiester and glycerol moieties of phospholipids bound to a similar position on the homodimers (excluding the Bak:LysoPC complex), forming hydrogen bonds with the backbone amide of residue W125 at the N-terminal end of α5 on one chain of the homodimer and the hydroxyl group of the Y136 side chain at the C-terminal end of α5 on the partner chain (**Figure 19**). The positively charged residue R137 was also in proximity to the phosphodiester group, though the position of the guanidinium group was inconsistent between structures and the electron density for the side chain was ambiguous in the cylinder structure. Whether this constitutes a *bona fide* headgroup binding site remains to be seen.

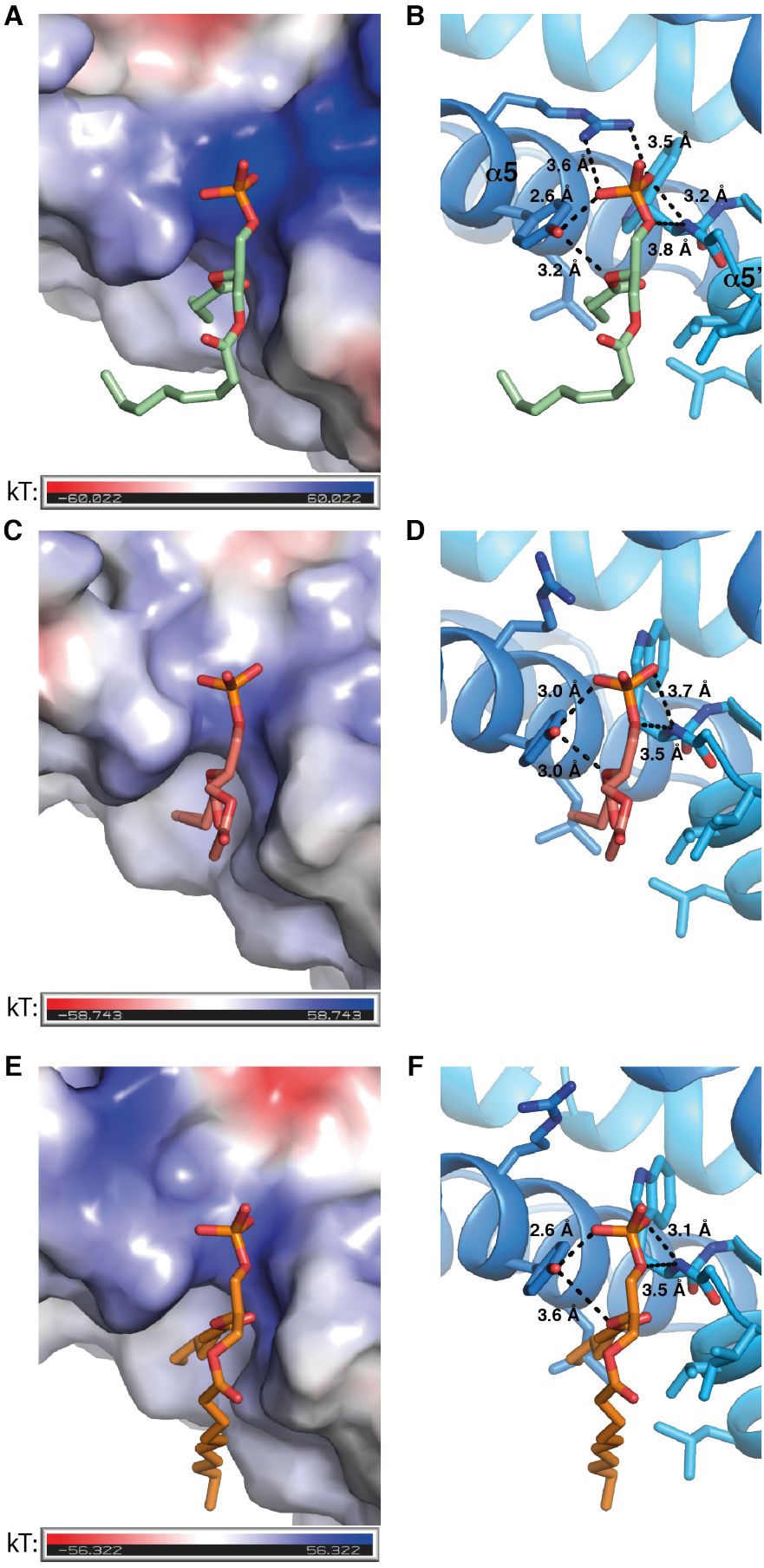
A
kT:
-60.022
60.022
B
α5
3.5 Å
3.6 Å
2.6 Å
3.2 Å
3.8 Å
3.2 Å
α5'
C
kT:
-58.743
58.743
D
3.0 Å
3.7 Å
3.5 Å
3.0 Å
E
kT:
-56.322
56.322
F
2.6 Å
3.1 Å
3.5 Å
3.6 Å

Figure 19. Phospholipid binding sites on Bak core homodimers. ***A), C)*** *and* ***E)*** *Vacuum electrostatic surface of phospholipid binding sites on a Bak core homodimer from the cylinder (**A**), DHPC (**C**), and POPC/C8E4 (**E**) structures. For clarity, the ethanolamine and choline headgroups have been removed from lipids in this depiction, as they do not form significant interactions with the protein. Bars show kT values for positive (blue) and negative (red) potential for each structure.* ***B), D)*** *and* ***F)*** *Ribbon representation of panels **A**, **C** and **E**, respectively. Hydrophobic α5/α5' groove-forming helices are labelled in **B**. The peptide backbone of W125 on α5', side chains of residues delineating the α5/5' grooves, and residues in proximity to the phosphodiester moiety of the lipids are shown as sticks. Bonding distances between the protein and lipid are shown as dotted black lines.*

2.3 Evidence for Lipid-mediated Oligomerisation of Bak

A robust secondary protein:protein interface between Bak homodimers within oligomers is yet to be identified. The homodimer structures presented here hint at a different type of oligomerisation that may be mediated by lipids. Lipid-mediated oligomerisation of membrane proteins with weak protein:protein interfaces has recently been demonstrated by native mass spectrometry experiments (Gupta *et al.*, 2017). Indeed, the acyl chains of lipids cross-link homodimers in the Bak(α2-5) hexameric cylinder structure (**Figure 20A-D**). The headgroup of each lipid sits at the interface between homodimers, with the first acyl chain bound to the α5/5' groove of one homodimer and the second chain running down a shallower hydrophobic groove between α4-5 helices of a Bak molecule in the adjacent homodimer (**Figure 20B** and **D**). The acyl chains of DHPC in the funnel structure are also positioned such that cross-linking could occur between Bak homodimers paired as hydrophobic sandwiches in a similar α5/5' to α4-5 groove fashion, if the chains were longer. These observations suggest diacyl phospholipids could act as bridges between homodimers via acyl chain binding to the α5/5' grooves and the hydrophobic α4-5 surface of adjacent homodimers (**Figure 20E**).

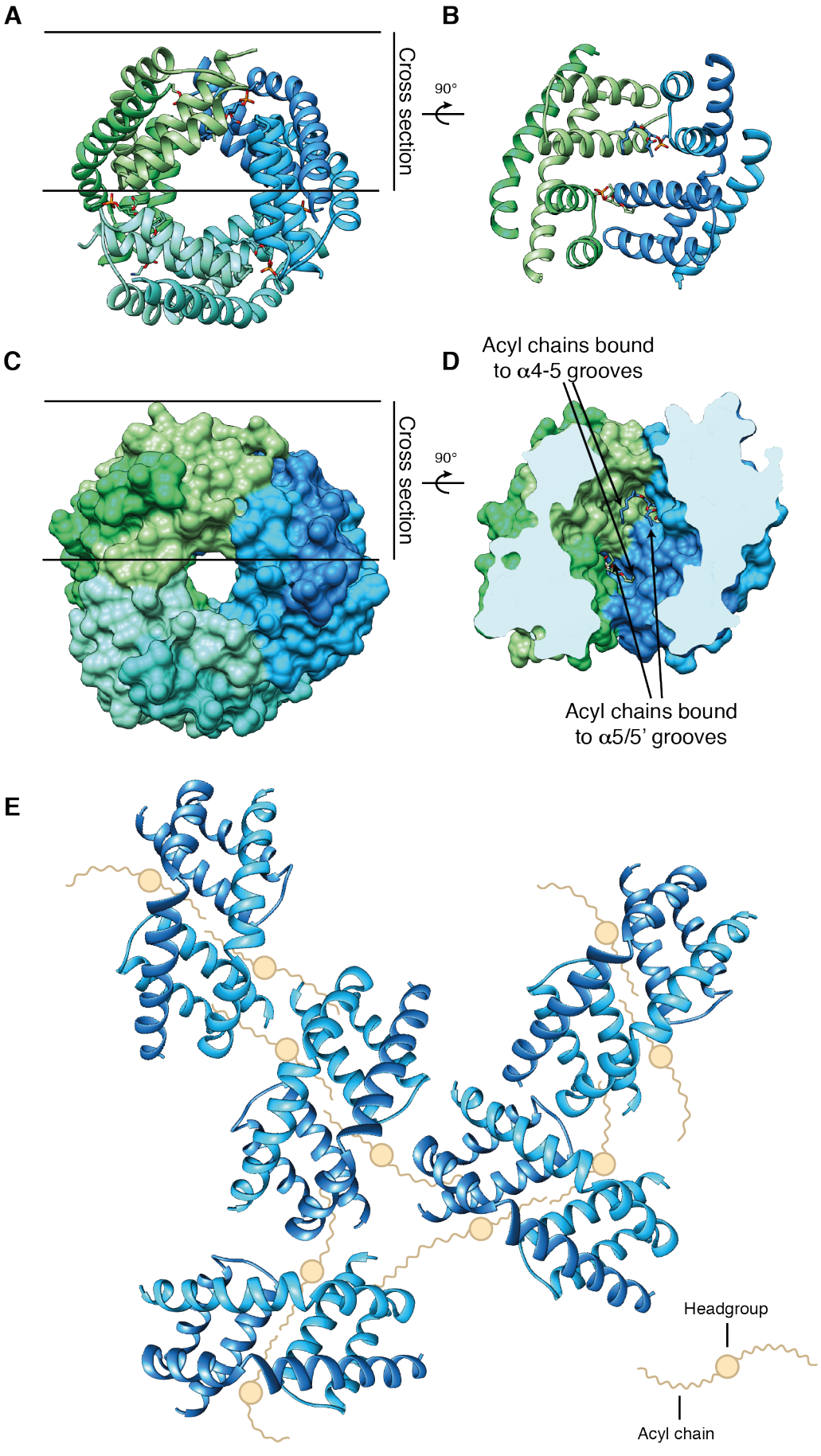
A
B
Cross section
90°
C
D
Cross section
90°
Acyl chains bound
to α4-5 grooves
Acyl chains bound
to α5/5' grooves
E
Headgroup
Acyl chain

Figure 20. Lipid cross-linking of Bak homodimers. ***A)*** *Bak(α2-5) cylinder structure depicted in ribbon representation with PE ligands shown as sticks (homodimers coloured dodger blue and deep sky blue, spring green and light green, and turquoise and aquamarine).* ***B)*** *Cross section of cylinder in* ***A*** *rotated 90°. The PE lipids cross-link the blue and green homodimers via their acyl chains.* ***C)*** *and* ***D)*** *Surface representation of* ***A*** *and* ***B****, respectively.* ***E)*** *A simple schematic model of Bak homodimers oligomerising through the acyl chains of diacyl phospholipids (core homodimer model taken from Bak(α2-5) cylinder structure). Oligomerisation could occur via acyl chains binding to the α5/5' and α4-5 grooves as depicted, or to other positions on the hydrophobic α4-5 surfaces of the homodimers.*

To investigate this possibility, I used the calcium-dependent enzyme phospholipase A2. Phospholipase A2 hydrolyses diacyl phospholipids at the *sn*-2 acyl bond, releasing a lysophospholipid and a free fatty acid (**Figure 21A**). Phospholipase A2 treatment would be expected to dissociate oligomeric Bak if the oligomerisation interface between homodimers required diacyl phospholipids.

Oligomeric Bak can be obtained in a minimal reconstituted liposomal system. Full-length Bak is difficult to express *in vitro* because of its hydrophobic TM anchor. Therefore, I used N- and C-terminally truncated Bak lacking its native cysteine (C166S) and with a C-terminal hexahistidine tag (His-tag), that expresses in high quantities. The C-terminal His-tag serves as a surrogate TM anchor by targeting the protein to liposomes incorporating 5% of the nickel-chelating lipid 1,2-dioleoyl-*sn*-glycero-3-[(*N*-(5-amino-1-carboxypentyl)iminodiacetic acid)succinyl] **(**DGS-NTA) (Oh *et al.*, 2010). Removal of the native cysteine increases protein yields and does not affect Bak function (Dewson *et al.*, 2008).

His-tagged Bak was added to liposomes made up of POPC and doped with 5% DGS-NTA at a molar ratio of ~1:20 protein:lipid, to ensure liposomes would be covered in protein. Oligomerisation was initiated by addition of human Bid BH3 peptide and the reaction was incubated at 37°C for two hours. Following incubation, EDTA was added to the reaction to release the protein from DGS-NTA and the mixture was injected into an S200 GF column to isolate oligomerised Bak from lipids not associated with the protein as well as any remaining intact liposomes (**Figure 21B**). Fractions

containing oligomeric Bak were pooled and treated with phospholipase A2 or left untreated. As a control for enzyme activity, EDTA was used to inactivate the calcium-dependent phospholipase in one sample. Following incubation, phospholipase-treated and untreated samples were rerun on the S200 column (**Figure 21C**).

A clear shift of the peak was observed in the sample treated with active phospholipase A2 (i.e. in the absence of EDTA) (red trace in **Figure 21C**). The presence of Bak in the peaks from each run was confirmed by Western blot (**Figure 21D**). Bak was not detected in the A2 peaks at the end of the S200 runs where phospholipase A2 was present (**Figure 21D**). These results demonstrate that the oligomeric species of Bak isolated in the experiments decreases in size following treatment with phospholipase A2.

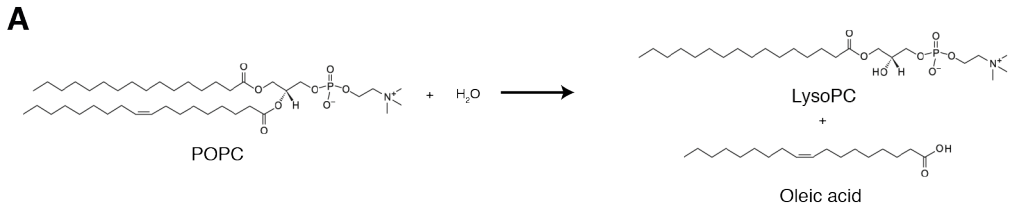
A
POPC
+ H2O
LysoPC
+
Oleic acid

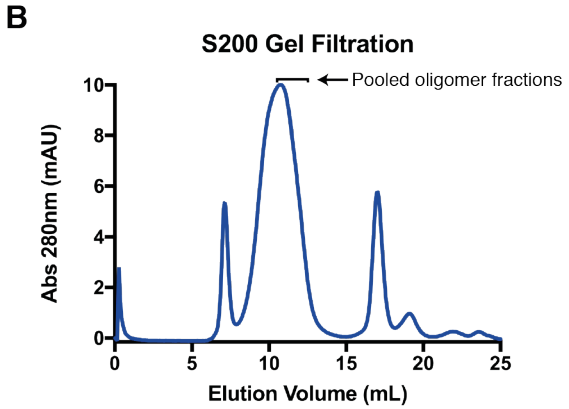
B
S200 Gel Filtration
Pooled oligomer fractions
Abs 280nm (mAU)
Elution Volume (mL)

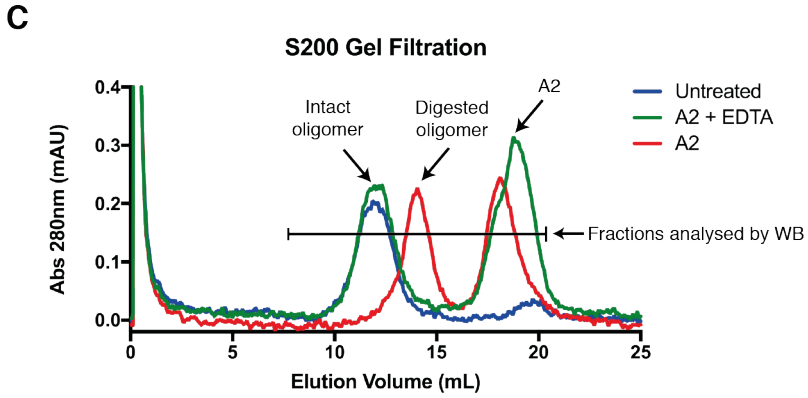
C
S200 Gel Filtration
Intact oligomer
Digested oligomer
A2
Untreated
A2 + EDTA
A2
Fractions analysed by WB
Abs 280nm (mAU)
Elution Volume (mL)

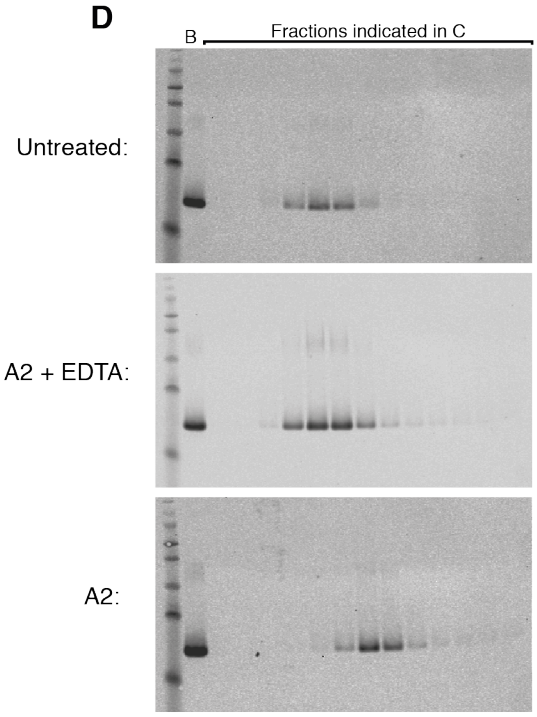
D
B
Fractions indicated in C
Untreated:
A2 + EDTA:
A2:

Figure 21. Phospholipase A2 treatment of oligomeric Bak. ***A)*** *Chemical reaction catalysed by phospholipase A2. The* sn-*2 acyl bond of POPC is hydrolysed to release LysoPC (16:0) and oleic acid.* ***B)*** *S200 GF chromatogram trace of oligomerised Bak. Indicated fractions were pooled for digestion with phospholipase A2.* ***C)*** *S200 GF chromatogram of oligomeric Bak either untreated (blue trace), treated with phospholipase A2 and EDTA (green trace) or treated with active phospholipase A2 (red trace). The peak shift to a smaller size indicates that the oligomer decreased in molecular weight following treatment with active phospholipase A2. Fractions marked by the black bar were analysed by Western blot.* ***D)*** *Western blot for Bak demonstrating that Bak was present in the corresponding peaks from the chromatograms in* ***C****. B=10 µg monomeric Bak as a positive control.*

2.4 Discussion

Structural and functional studies of Bak and Bax have provided great insight into the molecular mechanisms of activation and homodimerisation. However, despite a significant investment of research effort, details on oligomerisation of homodimers and the mechanism of membrane disruption remain largely elusive. In particular, the search for a secondary protein:protein interface between Bak or Bax homodimers has proven difficult, and random clustering of Bak homodimers has recently been proposed to facilitate MOMP (Uren *et al.*, 2017). Here, I have shown that lipids bind to Bak core domain homodimers on the hydrophobic α4-5 surface. The structures suggest that lipid binding may facilitate oligomerisation of Bak homodimers. In support of this, Bak oligomers decreased in size following treatment with phospholipase A2. These results could explain the lack of a robust protein:protein interface and are consistent with the idea of Bak forming toroidal proteolipidic pores.

A growing body of evidence has led to a general consensus that Bak and Bax oligomers form proteolipidic rather than proteinaceous pores (Bleicken *et al.*, 2013a; Epand *et al.*, 2002; Gillies *et al.*, 2015; Qian *et al.*, 2008; Salvador-Gallego *et al.*, 2016; Schafer *et al.*, 2009; Terrones *et al.*, 2004). The idea that lipids could contribute to the formation and structural integrity of the oligomer has not been explored previously.

Lipids were recently shown to be required for the multimerisation of α-helical membrane proteins with weak inter-subunit protein:protein interfaces (Gupta *et al.*, 2017). Among other α-helical pore-forming proteins, the crystal structure of the pore formed by the actinoporin FraC contained lipids at the oligomerisation interface (Tanaka *et al.*, 2015). The surface area contributed to the interface by lipid was almost equivalent to the buried protein:protein surface area between protomers (Tanaka *et al.*, 2015). Unlike the well-ordered octameric FraC pore, Bak and Bax pores have proven exceptionally difficult to produce for high-resolution structural studies, due to heterogeneity in form and variability in size (Bleicken *et al.*, 2013a; Salvador-Gallego *et al.*, 2016).

While the structure of the full-length oligomer remains undetermined, the truncated Bak core homodimer structure provided a high-resolution view of a part of activated Bak that could associate with the MOM (Brouwer *et al.*, 2014). Cysteine cross-linking studies had predicted what was observed in the structure: symmetric exchange of BH3 domains into the canonical hydrophobic groove of the two Bak chains in the homodimer (Brouwer *et al.*, 2014; Dewson *et al.*, 2008). A GFP fusion tag was used to express and crystallise the Bak core homodimer, as well as the Bax and mouse Bak core homodimers, based on the prediction that truncation of the protein would expose large hydrophobic surfaces (Brouwer *et al.*, 2014; Czabotar *et al.*, 2013; Mandal *et al.*, 2016). Indeed, growth of crystals of all three homodimers required detergent, and the structures revealed a large exposed hydrophobic surface made up of the α4 and α5 helices of the core domains.

It was therefore surprising that the Bak core domain remained soluble following cleavage of the GST solubility tag and grew crystals in the absence of detergent. The crystal structure explained how the core domains remained soluble, by forming a hexameric cylindrical complex of three homodimers with their α4-5 surfaces facing the centre of the cylinder. The disordered acyl chains of the lipids bound to the structure likely fill the central hole. Size exclusion chromatography and SAXS experiments agreed with the size and shape of the lipid-filled cylinder seen in the crystal structure. Mass spec analysis confirmed the presence of *E. coli* lipids of various classes and acyl chain lengths were present in both the purified and crystallised protein samples. Interestingly, of the lipids present, only PI was excluded from the crystal. The

headgroup of PI is bulkier than the other lipids detected and may have prevented incorporation of PI-containing Bak hexamers due to steric clashes at crystal contacts. Another possibility is that Bak homodimers do not directly bind PI lipids and that PI was only peripherally associated with purified hexamers. Commercially available lipid strips could be used to assay binding of Bak core homodimers to different lipid classes. The lipid class and chain length/saturation preference of the α5/α5' grooves could also be further investigated using techniques such as isothermal titration calorimetry, microscale thermophoresis or surface plasmon resonance with Bak core homodimers and different lipids.

The *E. coli* lipids present in α5/5' grooves of the cylinder structure could be exchanged for other lipids and detergents, resulting in vastly different quaternary arrangements of core homodimers. A hydrophobic sandwich arrangement formed in all crystals of Bak, excluding the cylinder, and is likely an artefact resulting from the use of truncated protein in the absence of membrane. The two homodimers in the asymmetric unit of the POPC/C8E4 crystal were side-by-side, with the PEG groups of the two C8E4 molecules forming hydrogen bonds with both homodimers and the aliphatic C8 chains binding to the α5/5' grooves. This is also unlikely to be a physiologically relevant interface, as cysteine cross-linking and EPR spectroscopy studies place the α3/α5 corners of Bak core domains in close proximity within Bak oligomers (Aluvila *et al.*, 2014; Mandal *et al.*, 2016).

At first glance, the hexameric funnel structure formed by Bak homodimers in the DDM and DHPC co-crystal structures appeared a good candidate for an intermediate arrangement assumed by oligomerising Bak homodimers on the pathway to pore formation. The polar lumen of the funnel and hydrophobic outer surfaces is reminiscent of an integral membrane protein channel. The distance between the DDM and DHPC headgroups at the top and bottom of the funnel is commensurate with the thickness of a bilayer, and the orientation of the hydrophilic headgroups and hydrophobic tails is consistent with insertion of the funnel into a planar bilayer. Models proposed for both Bak and Bax pores involve the core domains of BH3:groove homodimers lining the pore lumen, and this structure would be in rough agreement with these models (Aluvila *et al.*, 2014; Bleicken *et al.*, 2014; Mandal *et al.*, 2016). However, on closer inspection, the positions of the homodimers in relation to one another are inconsistent

with cysteine cross-linking and EPR spectroscopy data. For example, the H99 residues in the structure are isolated from one another but can be cross-linked in Bak homooligomers on mitochondria (Brouwer *et al.*, 2014). Conversely, I80 residues appear to be in favourable positions to cross-link Bak homodimers in the funnel structure, but did not form cysteine cross-links on the MOM (Brouwer *et al.*, 2014). The α3/α5 corners of core dimers, which are juxtaposed in the oligomer, are not proximal to one another in the funnel structure (Aluvila *et al.*, 2014; Mandal *et al.*, 2016).

Both crystals grew in similar conditions containing ammonium sulphate and sodium acetate at low pH. Three identical charge networks are formed at interfaces between homodimers in the funnel, involving D83 and R127 from one homodimer and Q77 and E92 of a second homodimer. The network is deficient by one proton and the deficiency is compounded by the presence of an acetate ion within bonding distance of the two negatively charged residues. Hence, funnel formation may be dependent on pH while also requiring a coordinating ion (a sulphate in both crystal structures) at the central 3-fold axis. Such requirements are unlikely to be met at the MOM. However, because most cysteine cross-linking and EPR spectroscopy experiments have been performed on mature oligomers, the possibility that the funnel represents an early pathway intermediate cannot be discounted. Further investigation of residue I80 could answer this question. Including an oxidant prior to induction of oligomerisation of Bak I80C expressed on isolated mitochondria may help to capture potential intermediate states such as the funnel that occur after Bak becomes activated but before the terminal oligomer is formed.

Regardless of the quaternary arrangement assumed by Bak core homodimers, their consistent fold and association with lipids and detergents across several structures is informative. In integral membrane protein structures, lipid molecules have been shown to bind to protein via their polar headgroups, hydrophobic acyl chains, or both (Yeagle, 2014). Both polar and non-polar interactions occur between phospholipid and the α5/5' grooves of Bak homodimers in the crystal structures containing *E. coli* lipids, POPC, and DHPC. Tyrosine residues are often found at lipid binding sites in membrane protein structures, coordinating acyl chains with its aromatic ring and hydrogen bonding via the hydroxyl group to the polar headgroup (Palsdottir and Hunte, 2004; Yeagle, 2014).

In the aforementioned structures, the phosphodiester group of the lipid forms hydrogen bonds with the hydroxyl group of Y136 on α5 and the free amide at the N-terminal end of α5' (**Figure 19**). Tyrosine 136 and other hydrophobic residues that line the α5/5' grooves coordinate the acyl chain of the lipid, which is ejected from the grooves by a bridge formed by L132 residues. Based on the crystal structures presented here, the α5/5' grooves may represent the first *bone fide* lipid binding sites observed in a Bcl-2 family protein.

The symmetric binding of lipid to two sides of the Bak core homodimer could facilitate oligomerisation of homodimers via the acyl chains of diacyl phospholipids (**Figure 20**). The acyl chains may bind to α5/5' grooves and/or other sites on the α4-5 surfaces of adjacent homodimers as observed in the cylinder crystal structure. Lipid cross-linking of membrane protein subunits has not been widely reported but is observable in some crystal structures. For example, the acyl chains of one of the integral lipids in the structure of bovine heart cytochrome *c* oxidase (PDB code: 2DYR) run at almost 180º in opposite directions, forming interactions with adjacent subunits (Shinzawa-Itoh *et al.*, 2007). There are other instances of acyl chains binding to different integral membrane protein subunits, though the example mentioned is particularly pertinent given the "split" conformation taken by the acyl chains that could facilitate cross-linking of Bak homodimers on the surface of, and in-plane with, the MOM. Promisingly, lipid-mediated stabilisation of weak protein:protein interfaces has been observed in multimeric membrane proteins, and the interface between Bak homodimers would certainly seem to fit this category (Gupta *et al.*, 2017).

In the model presented here, the diacyl nature of the phospholipid is integral to oligomer formation. Phospholipase A2 is specific for the *sn*-2 acyl bond of phospholipids, converting diacylglycerols into monoacyglycerols. Bak oligomers isolated from liposomes could be partially dissociated by phospholipase A2, lending weight to the lipid-mediated oligomerisation hypothesis. However, there are several important caveats to this experiment. While the oligomers decreased in size, the peak from GF suggested they were still much larger than dimers. It is possible that once lipid is digested away, the exposed hydrophobic surfaces of activated Bak homodimers collapse on one another, forming an artificial oligomer. The decrease in size could also be due to removal of large amounts of lipid peripherally associated with the oligomer,

rather than dissociation of homodimers from other homodimers. It is important to note that apparent molecular weight as measured by GF is also affected by the flexibility of proteins. A large flexible oligomer (or perhaps dimer) cannot be accurately sized by this method. While the results support a role for lipids in oligomerisation, more direct experiments are needed to determine whether lipids are required for oligomerisation. Native mass spectrometry experiments with oligomerised Bak, as in Gupta *et al.* 2017, could demonstrate conclusively the importance of lipids for Bak oligomerisation.

In addition to insights into oligomerisation, the structures presented here also have potential implications for pore formation. In the paper reporting the first structure of the Bak core homodimer, it was speculated that the curved nature of the dimer could be important for pore formation (Brouwer *et al.*, 2014). While, the structures presented here show less pronounced curvature, they provide another possible mechanism of curvature induction and membrane destabilisation. Monotopic membrane proteins bind to one side of the bilayer without traversing the membrane itself, often via shallow insertion of amphipathic α-helices and charged interactions with lipid headgroups. Certain monotopic membrane proteins such as cyclooxygenase(COX)-1 and -2 significantly perturb the local lamellar structure of bilayers in molecular dynamics simulations (Balali-Mood *et al.*, 2009; Fowler *et al.*, 2007).

The Bak BH3:groove homodimer is in many ways similar to monotopic membrane proteins, particularly for the core domain dimers. Binding of lipid to the α5/5' grooves and shallow in-plane insertion of the α4-5 surface (and potentially latch helices (Westphal *et al.*, 2014)) would displace headgroups from a large area (roughly 23 Å by 35 Å) of the outer leaflet of the MOM and thin the membrane underneath, bringing the inner and outer leaflets closer together. In-plane insertion of amphipathic helices creates curvature in membrane bilayers, particularly when multiple helices are inserted (Campelo *et al.*, 2008; McMahon and Boucrot, 2015). The effect could be compounded in areas of the MOM where Bak forms clusters, such that a rupturing event might occur as a result (Uren *et al.*, 2017). A possible schematic model for membrane disruption by Bak homodimers is presented in **Figure 22A** and **B**.

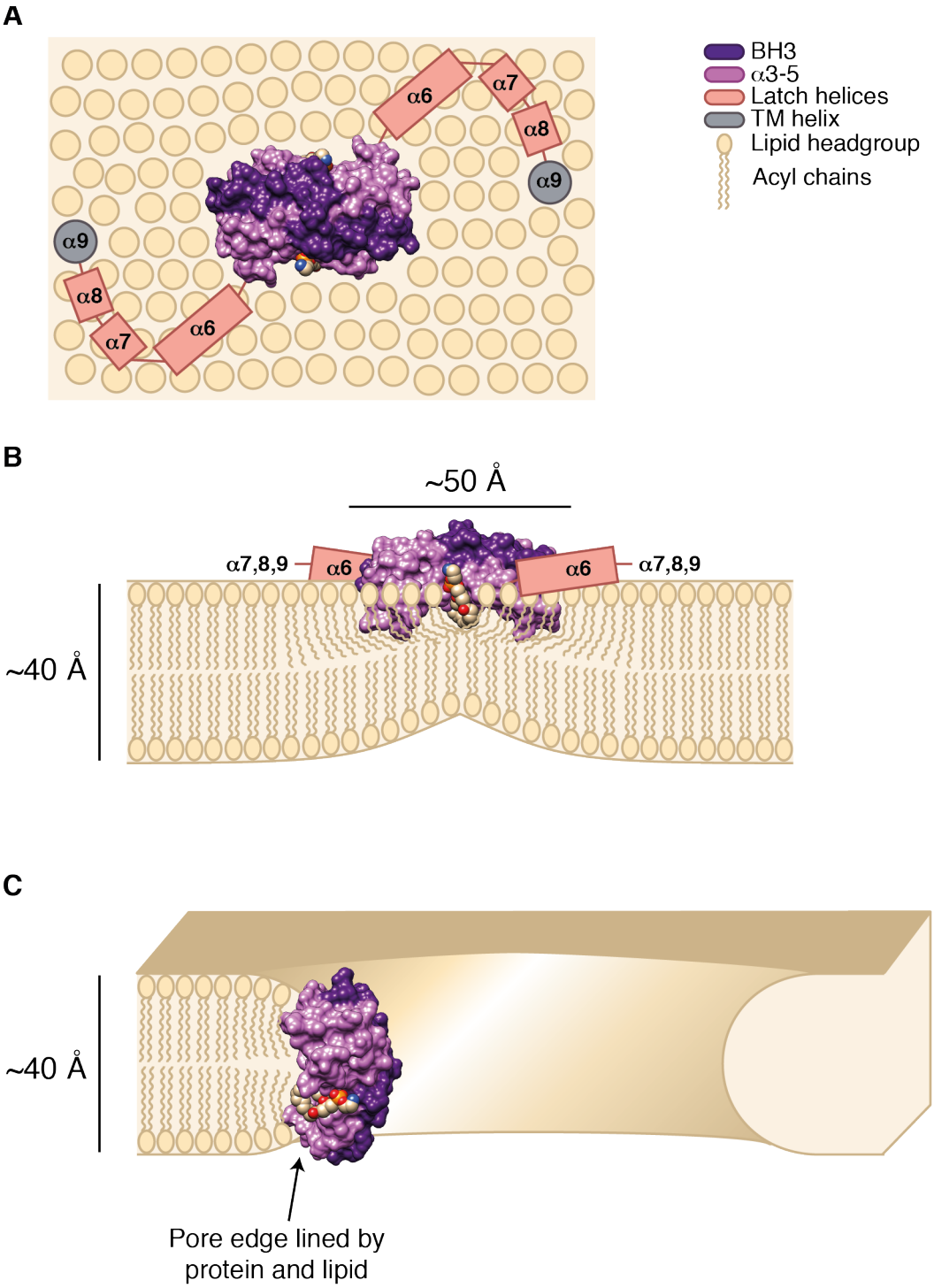
A
α6
α7
α8
α9
α9
α8
α7
α6
BH3
α3-5
Latch helices
TM helix
Lipid headgroup
Acyl chains
B
~50 Å
α7,8,9
α6
α6
α7,8,9
~40 Å
C
~40 Å
Pore edge lined by
protein and lipid

Figure 22. Possible models for membrane disruption and pore edge stabilisation by Bak. A) *Top-down view of a Bak BH3:groove homodimer on a patch of the MOM. One homodimer from the Bak(α2-5) cylinder structure is shown in surface representation with PE (tan, coloured by heteroatom) shown as spheres. Shallow in-plane insertion of the α4-5 surface could displace a large number of headgroups in the outer leaflet of the MOM. Positions of flexible latch helices (α6-8) and TM helix α9 are purely speculative.* ***B)*** *Cross section of membrane in* ***A****. The depth of insertion is based on the position of lipid headgroups in the structures and results in disruption of the lamellar structure of the bilayer and thinning of the membrane underneath the homodimer.* ***C)*** *Following disruption and rupture of the membrane, Bak core homodimers could reduce the stress of non-lamellar lipids arrangements at the pore edge. A Bak core homodimer is shown lining part of the pore lumen. The other side of the pore could be lined with more Bak, forming protein rings with interfacial lipids (i.e. matrix-type pore), or with toroidal lipids (i.e. arc-type pore). It is also possible that Bak could exhibit aspects of both the matrix- and arc-type pore. All components of each model are roughly to scale.*

Following membrane rupture, stabilisation of the pore edge is required to keep the pore open (Cosentino and Garcia-Saez, 2017; Gilbert, 2016). A model for pore stabilisation by Bak BH3:groove homodimers is presented in **Figure 22C**. Lining of the pore lumen with core homodimers has been proposed in pore models of both Bak and Bax to relieve stress caused by non-lamellar arrangements of lipids at the pore edge (Aluvila *et al.*, 2014; Bleicken *et al.*, 2014; Mandal *et al.*, 2016). The orientation of the homodimers shown in **Figure 22C** is loosely based on the model generated from EPR distance measurements on human and mouse Bak (Aluvila *et al.*, 2014; Mandal *et al.*, 2016).

Lipid-mediated oligomerisation and protein:lipid:protein interfaces could occur in both of the events depicted in **Figure 22**. Whatever the case, the lipid-binding capacity of the Bak core homodimer, demonstrated here for the first time in five crystal structures, is likely important in the interactions between BH3:groove homodimers and the MOM.

The structures presented here provide the first high-resolution details of the interactions between activated Bak and membrane lipids, with implications for oligomerisation, membrane destabilisation and proteolipidic pore formation.

2.5 Methodology

2.5.1 Recombinant Protein Cloning, Expression and Purification

The sequence encoding the core domain of Bak (α2-5, residues D68-T148) was cloned into the pGEX-6P-3 vector and transformed into BL21 (DE3) *E. coli* cells. Cells were grown at 37°C in Luria Super Broth (SB) to an Optical Density (O.D.) (600 nm) of ~1.0 and induced to express for 3 hours at 37°C with 1 mM isopropylthio-β-galactosidase (IPTG). Cells were lysed in GST buffer (100 mM Tris pH [8.0], 150 mM NaCl, 2 mM EDTA) and lysates were filtered through a 0.45 µm pore size filter then passed over glutathione agarose column. The column was washed with GST buffer and Bak(α2-5) was cleaved from the GST fusion partner on-column for at least 40 hours at 4°C with PreScission Protease (0.02 mg/mL). Bak(α2-5) was eluted from the column in GST buffer and buffer exchanged into a low-salt buffer (20 mM Tris pH [8.0], 30 mM NaCl). The protein was purified by anion exchange on a HiTrap Q FastFlow 1 mL column in 20 mM Tris pH [8.0] with a NaCl gradient of 0.03 to 1 M. All chromatogram trace images were generated in GraphPad Prism version 7 for Mac, GraphPad Software, La Jolla California USA, www.graphpad.com. The protein was further purified by GF (S200 10/300) in Tris-buffered saline (TBS) (20 mM Tris pH [8.0], 150 mM NaCl). Fractions containing Bak(α2-5) were concentrated and used in crystallisation trials.

The human Bak sequence lacking the dispensable N-terminus (ΔN22) (Moldoveanu *et al.*, 2006), native cysteine (C166S) and with a His-tag replacing the C-terminal TM anchor (ΔC25) was cloned into the pTYB1 vector and transformed into *E. coli* BL21 (DE3) cells. Cells were grown in SB to an O.D. (600 nM) of ~1.0 then cooled at 4ºC for 30 minutes. Expression was induced with 1 mM IPTG and cells were incubated with shaking overnight at 18ºC. Cells were lysed in TEN buffer (20 mM Tris pH [8.0], 1 mM EDTA, 500 mM NaCl) and lysate was passed over a column containing chitin resin. Cleavage of the C-terminal intein tag was initiated on-column with TEN buffer + 50 mM DTT and left to incubate at 4ºC for at least 40 hours. Bak was eluted from the column and further purified by GF on a Superdex 75 (S75) 10/300 column run in TBS. Fractions containing Bak were concentrated, frozen at -80ºC and thawed as required.

2.5.2 SDS-PAGE

Protein samples were heated at 95°C for 5 minutes with reducing protein-loading dye. After heating, samples were loaded into pre-cast NuPAGE 12% Bis-Tris gels (Life Technologies). Gels were submerged in 2-(*N*-morpholino)ethanesulfonic acid (MES) running buffer and electrophoresed for 40 minutes at 200V. Gels were fixed and stained with Coomassie stain (2% Coomassie R250 Brilliant Blue w/v, 10% acetic acid v/v, 40% ethanol v/v) for 30 minutes before removal of excess Coomassie with a destaining buffer (10% acetic acid v/v, 40% ethanol v/v). Molecular weight of protein bands was estimated using SeeBlue Plus2 Prestained Protein Standard (Life Technologies).

2.5.3 Bak(α2-5) Crystallisation, Data Collection and Processing

Crystallisation trials were performed in 96-well sitting drop plates at the CSIRO C3 facility in Parkville.

Bak(α2-5) crystallised at 10 mg/ml in 0.1 M ammonium sulphate, 15.3% PEG 10000, 90 mM sodium acetate, 90 mM bis-tris chloride pH [5.5] in the triclinic space group P1. The crystal was frozen in well solution supplemented with 20% ethylene glycol, and three X-ray datasets were collected at different positions along a single crystal at the MX2 beamline of the Australian Synchrotron. Diffraction images were processed with XDS and scaled with XSCALE (Kabsch, 2010). Data were converted to mtz format with POINTLESS and merged with AIMLESS (Evans and Murshudov, 2013). A self-rotation function was generated with the UCLA Self Rotation Function Server (http://services.mbi.ucla.edu/selfrot/). The structure was solved by molecular replacement in PHASER (McCoy *et al.*, 2007) by searching for six Bak core globules. The globules consisted of the α2 BH3 domain of one Bak core domain bound to the hydrophobic α3-5 groove of a partner core domain, and were constructed from a Bak core homodimer in the GFP:Bak(α2-5) structure, PDB code: 4BDU (Brouwer *et al.*, 2014). The PE ligand model and crystallographic information file (CIF) restraints used were taken from the PDB (PDB ligand ID: PEE), and chirality restraints were generated with eLBOW (Moriarty *et al.*, 2009).

Bak(α2-5) in complex with DDM crystallised at 7.7 mg/ml in 1.8 M ammonium sulphate, 0.5% DDM, 90 mM sodium acetate pH [4.6]. Crystals were frozen in well solution supplemented with 25% ethylene glycol, and data were collected at the MX2 beamline of the Australian Synchrotron. Data were processed with XDS, converted to mtz format with POINTLESS and merged and scaled with AIMLESS (Evans and Murshudov, 2013; Kabsch, 2010). The structure was solved by molecular replacement with PHASER (McCoy *et al.*, 2007). A Bak homodimer from the Bak cylinder structure was used as a search model, and six homodimers were placed.

DHPC was mixed with Bak(α2-5) to a final concentration of 10 mM and 5.5 mg/ml, respectively, to obtain crystals of the complex. Crystals grew in 100 mM sodium acetate pH [3.76], 172 mM ammonium sulphate and 24% PEG monomethyl ether 2000, and were frozen in well solution supplemented with 20% glycerol. Data were collected at the MX1 beamline of the Australian Synchrotron, processed with XDS and converted with XDSCONV (Kabsch, 2010). The structure was solved using a Bak homodimer from the Bak:DDM structure as a search model in PHASER (McCoy *et al.*, 2007). NCS restraints were used during refinement. The atomic model and CIF restraints for DHPC were taken from the PDB (PDB ligand ID: HXG) and chirality restraints were generated with eLBOW (Moriarty *et al.*, 2009).

To grow crystals of Bak(α2-5) in complex with POPC, I adapted a dry protein:compound co-crystallisation technique (developed by (Gelin *et al.*, 2015)) for protein:lipid co-crystallisation. First, 300 nL of 0.25% (w/v) POPC dissolved in ethanol was dispensed onto a 96-well sitting drop plates at the CSIRO C3 facility and allowed to dry. Bak(α2-5) at 5.5 mg/ml was dispensed on top of dried POPC and crystals grew in 150 mM trisodium citrate pH [5.5], 1.5 M ammonium sulphate and 80 mM C8E4. Crystals were frozen in well solution supplemented with 20% ethylene glycol, and diffraction data were collected at the MX2 beamline of the Australian Synchrotron. Data were processed with XDS and converted with XDSCONV (Kabsch, 2010). The structure was solved by molecular replacement with PHASER (McCoy *et al.*, 2007) by searching with a Bak homodimer from the Bak:DDM structure. The POPC ligand model and CIF restraints were generated by entering a SMILES string into the Grade Web Server (Global Phasing Ltd.). Chirality restraints were generated with eLBOW (Moriarty *et al.*, 2009).

Bak(α2-5) was mixed with 16:0 LysoPC to a final concentration of 5.5 mg/ml and 10 mM, respectively, prior to crystal tray setup. The protein:lipid mixture crystallised in 18 mM sodium acetate, 10 mM calcium chloride, 22.5% PEG 3350 and 90 mM HEPES pH [7.5]. Crystals were frozen in in well solution and data were collected at the MX2 beamline of the Australian Synchrotron. Data were processed with XDS and converted with XDSCONV (Kabsch, 2010). The structure was solved by molecular replacement with PHASER (McCoy *et al.*, 2007) searching using a single Bak homodimer from the Bak:DDM structure as a model. The LysoPC ligand PDB file and CIF were generated on the Grade Web Server using a SMILES string.

Models for all structures were refined with iterative rounds of building in COOT (Emsley and Cowtan, 2004) and refinement with PHENIX (Adams *et al.*, 2010).

2.5.4 Structure Analysis and Figure Generation

Molecular graphics images for structural figures were generated primarily with the USCF Chimera Package (Pettersen *et al.*, 2004). Models of qualitative electrostatic representation were generated in PyMOL with the vacuum electrostatics tool (Delano, 2002). Molecular graphics images containing electron density were generated in PyMOL (Delano, 2002).

2.5.5 Liposome Preparation

A mixture of lipids (95% POPC and 5% DGS-NTA(Ni)) were dissolved in chloroform and 0.01% butylated hydroxytoluene, then dried under N_2 gas before resuspension in Mg-free small unilamellar vesicle/liposome (SUV) buffer (10 mM HEPES pH [7.5], 135 mM KCl). Resuspended liposomes were extruded through a 100 nm pore size membrane and stored at 4°C.

2.5.6 Bak Oligomerisation and Purification

To prepare Bak oligomers for digestion with phospholipase A2, 100 µL of 85 µM Bak (ΔN22ΔC25 C166S C-terminal His-tag) was added to 67.6 µL of 2.5 mM liposomes and mixed gently. To initiate oligomerisation, 3.4 µL of 10 mM human Bid BH3

peptide was added to the reaction and gently mixed. The reaction was incubated for 2 hours at room temperature then stored at 4°C overnight. Twenty µL of 500 mM EDTA was added and the reaction was incubated for 10 minutes at room temperature to dissociate the His-tag from the DGS-NTA. The entire reaction was then injected and run on a S200 10/300 GF column in Mg-free SUV buffer, and fractions from a portion of the oligomeric peak were pooled.

2.5.7 Phospholipase A2 Treatment of Bak Oligomer

To test the effect of a lipase on the Bak oligomer, pooled oligomeric Bak was incubated with phospholipase A2 (from Honey Bee (*Apis mellifera)* venom, purchased as lyophilised powder from Sigma-Aldrich) in the presence (experimental) or absence (control 1) of EDTA. EDTA inactivates the calcium-dependent phospholipase A2 enzyme. As a second control, pooled oligomeric Bak was incubated with $CaCl_2$ in the absence of phospholipase A2 (control 2). Reactions all contained 150 µL of the pooled oligomer. $CaCl_2$ was added to the experimental and control 2 samples and EDTA was added to the control 1 sample to a final concentration of 500 nM and 20 µM, respectively. Phospholipase A2 (4.5 units) was added to the experimental and control 1 samples. All reactions were made up to 1 mL with Mg-free SUV buffer and incubated for 1 hour and 20 minutes at room temperature. Reactions were loaded onto a S200 10/300 GF column and run in Mg-free SUV buffer. Peak fractions were run on SDS-PAGE for immunoblotting.

2.5.8 Immunoblotting

SDS-PAGE gels were transferred to nitrocellulose membranes by Western transfer. Membranes were blocked overnight in 5% skim milk TBS-Tween (0.1% Tween 20) (TBS-T). Membranes were washed with TBS-T then incubated with anti-Bak rabbit antibody (DF9) at 1/2000 in 5% skim milk TBS-T for 1 hour at room temperature on a roller. After incubation, membranes were washed 4 times with 5% skim milk TBS-T over 30 minutes, then probed with anti-rabbit IRDye 800CW secondary antibody (Li-Cor) at 1/15000 for 1 hour in 5% skim milk TBS-T. Membranes were washed once

in 5% skim milk TBS-T, then 3 times over 30 minutes with TBS-T. Blots were scanned using the Odyssey Imaging System (Li-Cor).

Chapter 3

Structural Investigation of Bax Homodimerisation

Transient encounters between Bax and activator BH3-only proteins induce a large conformational change in Bax, causing separation of the latch (α6-8) from the core (α2-5) (Czabotar *et al.*, 2013). Dissociation of the latch from the core and exposure of the BH3 domain leads to core domain homodimerisation through the symmetrical exchange of BH3 domains (α2) into the hydrophobic groove (α3-5) of the partner molecule (see **Figure 5**) (Czabotar *et al.*, 2013; Dewson *et al.*, 2012). The resulting BH3:groove homodimer nucleates oligomerisation of Bax and growth of oligomers on the MOM, leading to MOMP (Czabotar *et al.*, 2013; Dewson *et al.*, 2012).

The structure of the Bax core homodimer was solved using a truncated construct of Bax(α2-5) with an N-terminal GFP fusion tag (Czabotar *et al.*, 2013). The fusion tag was used because the Bax core domain lacking the latch was predicted to have large exposed hydrophobic surfaces that could promote aggregation (Czabotar *et al.*, 2013). The GFP proteins dimerised and formed a scaffold with two Bax core homodimers bridging two GFP dimers (Czabotar *et al.*, 2013).

The electron density maps of the Bax component of the structure are of similar quality to maps at ~4 Å resolution. At this resolution, α-helices resemble tubes of density with little to no detail on side chain orientation. To improve the resolution of the Bax core homodimer structure, I took two approaches. The first was to crystallise the GFP:Bax tetramer in the presence of bicelles; the second was to express the Bax core as a GST fusion protein and remove the GST tag. While I had some success with the first approach, a significant improvement in resolution was achieved with the second. Here I describe the first crystal structure of a Bax core homodimer at atomic resolution.

3.1 Crystal Structures of GFP:Bax(α2-5) Tetramer

Czabotar and Westphal *et al.* 2013 determined the structure of the Bax core homodimer using a Bax core construct fused to GFP. Using the same expression and purification systems, I produced the GFP:Bax(α2-5) tetramer for crystallisation trials with lipid bicelles in an attempt to improve the resolution of the structure. Bicelles are small discs

of lipid in a planar bilayer arrangement ringed by detergent or short chain lipid that have been used as membrane mimetic systems in the successful crystallisation of a number of membrane proteins (Ujwal and Bowie, 2011). We reasoned that the planar hydrophobic surface presented by Bax core homodimers (consisting of α-helices 4 and 5) could be stabilised by associating with a bilayer mimetic like the bicelle.

Several different bicelle compositions were trialled in crystallisation conditions similar to the original hit, and data were collected on several crystals. A dataset from a crystal belonging to a novel space group ($P2_12_12$) was obtained at ~3.2 Å resolution. The crystal was grown from protein pre-incubated with bicelles made up of 1,2-ditetradecanoyl-*sn*-glycero-3-phospho-(1'-*rac*-glycerol) (DMPG) and 3-([3-cholamidopropyl]dimethylammonio)-2-hydroxy-1-propanesulfonate (CHAPSO). The structure was solved by molecular replacement and the GFP:Bax(α2-5) tetramer arrangement appeared similar to what was observed in the original $P6_4$ crystal form. However, the density for the Bax region of the structure and for two of the GFP molecules was extremely poor. Therefore, the structure was not pursued past some initial rounds of refinement.

The best diffraction data were obtained from a crystal of GFP:Bax(α2-5) pre-incubated with bicelles made up of 1,2-dioleoyl-*sn*-glycero-3-phosphocholine (DOPC) and CHAPSO. Like the original structure, the crystal belongs to the hexagonal space group $P6_4$ and the effective resolution was 2.7 Å (based on corresponding I/σ value of 1.9; data collection and refinement statistics are presented in **Table 5**). The structure was solved by molecular replacement by searching for and placing 4 GFP molecules initially, followed by searching for two Bax core homodimers from the published structure (PDB code: 4BDU) (Czabotar *et al.*, 2013). The electron density for the Bax regions of the structure was markedly improved from the published structure (**Figure 23**). However, the density was still not sufficient to accurately place the majority of amino acid side chains with confidence (**Figure 23D**). Further refinement of the structure was abandoned once it became clear that the density for the Bax(α2-5) homodimers did not reach atomic resolution.

Table 5. Data collection and refinement statistics for partially refined GFP-Bax(α2-5) crystal grown in the presence of DOPC:CHAPSO bicelles.

Wavelength	0.9537
Resolution range	44.58 - 2.407 (2.493 - 2.407)
Space group	P 64
Unit cell	112.314 112.314 293.27 90 90 120
Total reflections	927884 (91906)
Unique reflections	80637 (8083)
Multiplicity	11.5 (11.4)
Completeness (%)	99.31 (95.83)
Mean I/sigma(I)	17.09 (0.43)
Wilson B-factor	72.45
R-merge	0.09828 (5.718)
R-meas	0.1029 (5.986)
CC1/2	1 (0.226)
CC*	1 (0.607)
Reflections used in refinement	80172 (7758)
Reflections used for R-free	3972 (380)
R-work	0.2133 (0.4012)
R-free	0.2389 (0.4266)
Protein residues	1209
RMS(bonds)	0.008
RMS(angles)	1.29
Ramachandran favoured (%)	91.80
Ramachandran allowed (%)	6.51
Ramachandran outliers (%)	1.69
Rotamer outliers (%)	0.57
Clashscore	18.36
Average B-factor	120.92
macromolecules	121.37
ligands	99.61
solvent	81.75

Statistics for the highest-resolution shell are shown in parentheses.

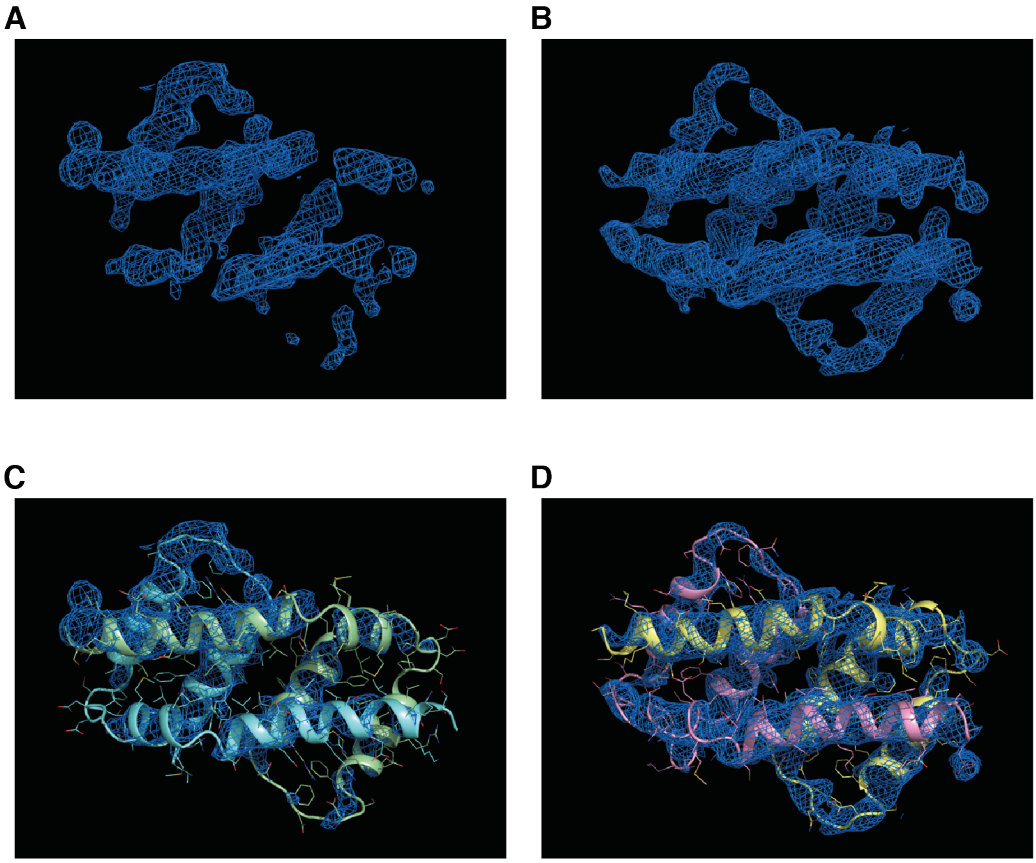

Figure 23. Electron density in the published GFP:Bax(α2-5) structure vs. newly solved structure. ***A)*** *and* ***B)*** *Equivalent 2Fo-Fc maps from the final refinement (contoured at 1 σ) of one Bax core homodimer in the published (PDB code: 4BDU (Czabotar et al., 2013)) (****A****) and novel (****B****) structures.* ***C)*** *and* ***D)*** *Homodimer chains from published (****C****, coloured pale green and aquamarine) and novel (****D****, coloured pale yellow and pink) structures built into electron density shown in cartoon representation with side chains shown as lines.*

3.2 Crystal Structure of the Bax Core Domain Tetramer

As bicelles produced only a modest improvement in resolution, I moved away from the scaffolding GFP construct and took a different approach. In this case, the same Bax core sequence was fused to a cleavable N-terminal GST tag. The protein expressed well, and after on-column cleavage the Bax core domain remained soluble. The Bax core domain was further purified by anion exchange chromatography and GF chromatography for crystallisation trials. Bax core domains eluted from the anion exchange column in two peaks (**Figure 24A** and **B**) sized at approximately 40 kDa and 63 kDa based on size exclusion GF elution volumes (**Figure 24C**). These peaks would be expected to contain tetramers and hexamers of Bax core domains, respectively, assuming BH3:groove homodimers are formed (predicted MW of homodimer: 17.9 kDa). The 40 kDa and 63 kDa peaks are hereafter referred to as the tetramer and hexamer, respectively.

Both the Bax core tetramer and hexamer crystallised in a number of conditions. The most promising crystals for the tetramer were obtained in 1.6 M trisodium citrate, and an additive optimisation screen yielded crystals for data collection. The best diffracting crystal belonged to the monoclinic space group $P2_1$. The structure was solved by molecular replacement using a Bax core homodimer from the published Bax core domain structure (PDB code: 4BDU) as a search model and refined to 2 Å (Czabotar *et al.*, 2013) (data collection and refinement statistics are presented in **Table 6**).

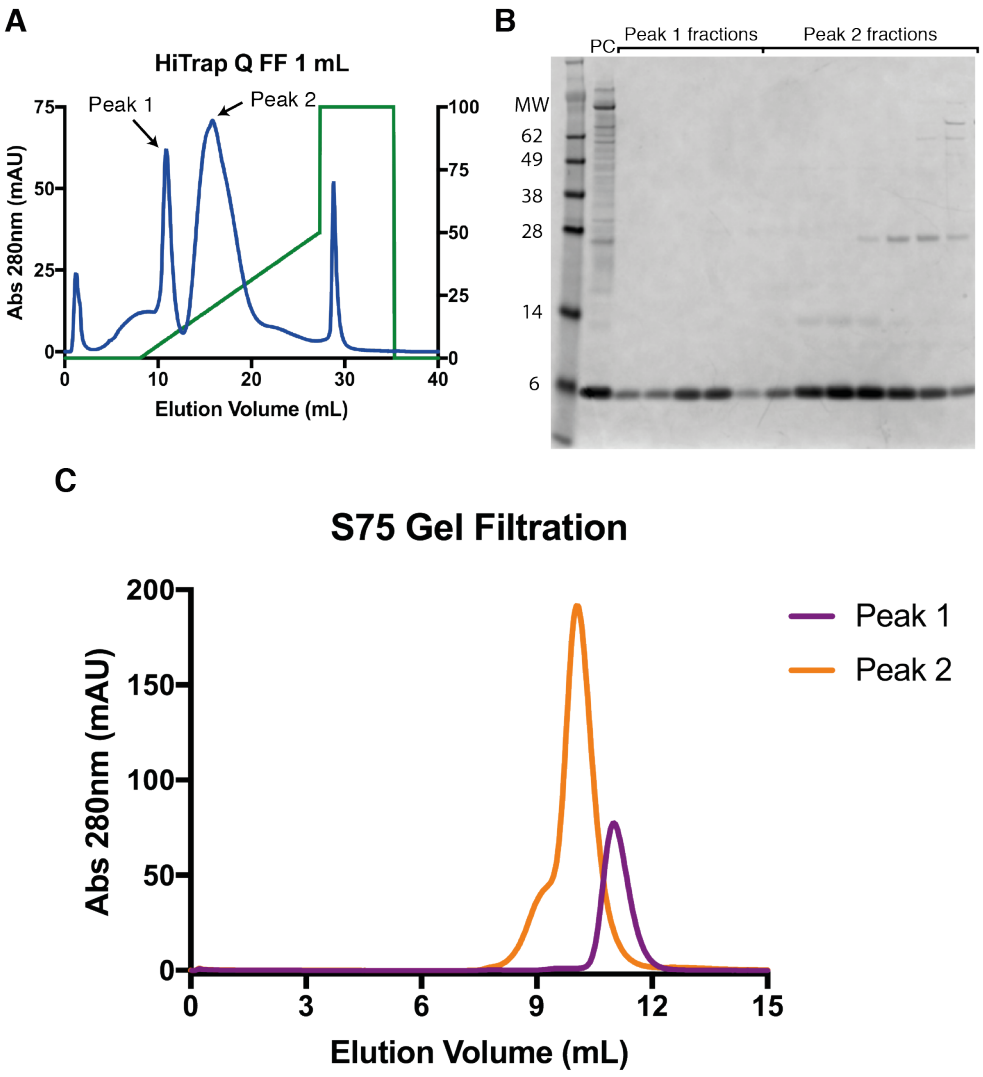

Figure 24. Purification of Bax(α2-5) following cleavage from GST. ***A)*** *Chromatogram trace of Bax(α2-5) cleaved from GST and run on a HiTrap Q FastFlow 1 mL column in Tris pH [8.0] with a NaCl gradient from 0 to 1 M (% buffer B gradient shown in green). Bax(α2-5) primarily eluted in two peaks labelled peak 1 and 2.* ***B)*** *SDS-PAGE analysis of peak fractions from* ***A****. Bax(α2-5) ran at a smaller than expected MW (predicted ~9 kDa) but was of a high purity in both peaks (PC = pre-column sample).* ***C)*** *Fractions from peak 1 (purple) and peak 2 (orange) were run separately on an S75 10/300 GF column. Molecular weights of 40 kDa and 63 kDa for peaks 1 and 2, respectively, were calculated from a standard curve derived from GF of proteins of known molecular weight.*

Table 6. Data collection and refinement statistics for Bax(α2-5) tetramer.

Wavelength	0.9537
Resolution range	30.4 - 2.092 (2.167 - 2.092)
Space group	P 1 21 1
Unit cell	60.363 70.374 62.784 90 90.139 90
Total reflections	112743 (10290)
Unique reflections	30871 (2935)
Multiplicity	3.7 (3.5)
Completeness (%)	98.85 (93.36)
Mean I/sigma(I)	9.05 (1.05)
Wilson B-factor	41.78
R-merge	0.1016 (1.811)
R-meas	0.1194 (2.129)
CC1/2	0.997 (0.33)
CC*	0.999 (0.705)
Reflections used in refinement	30812 (2881)
Reflections used for R-free	2029 (183)
R-work	0.2103 (0.3636)
R-free	0.2502 (0.3924)
Protein residues	556
RMS(bonds)	0.004
RMS(angles)	0.59
Ramachandran favoured (%)	97.17
Ramachandran allowed (%)	2.83
Ramachandran outliers (%)	0.00
Rotamer outliers (%)	0.42
Clashscore	5.96
Average B-factor	59.06
macromolecules	59.09
ligands	72.76
solvent	53.99

Statistics for the highest-resolution shell are shown in parentheses.

The asymmetric unit of the monoclinic crystal containing 8 Bax(α2-5) chains is presented in **Figure 25A**. In most chains, the α3-α4 loop could not be resolved. As the loop was resolved in the chain G and H homodimer, this homodimer was chosen as a comparative model and overlayed on the chain A and B homodimer of the GFP:Bax(α2-5) structure from Czabotar and Westphal *et al.*, 2013 in **Figure 25B** and **C**. The overall fold of the BH3:groove core domain homodimer is maintained between the two structures and between copies of the homodimer in the new structure.

The homodimers were further paired as tetramers, with the planar hydrophobic surfaces formed by the α4 and α5 helices of each of the homodimers (labelled in **Figure 25C**) sandwiched together (**Figure 25D**). The hydrophobic surface is enriched in aromatic residues and has been proposed to shallowly insert into the MOM in a similar manner to monotopic membrane proteins (Czabotar *et al.*, 2013). At the interface, the α4 and α5 helices of one homodimer run antiparallel with the α4 and α5 helices of the other homodimer, respectively. Interdigitating aromatic residues create a tight interface between homodimers. This protection of the hydrophobic surface allows the tetramers to remain soluble after cleavage of the GST tag. However, these tetramers are not likely to be physiologically relevant, because on the MOM the α4-5 surface becomes buried in the membrane (Westphal *et al.*, 2014).

The vast improvement in resolution allows for accurate placement of most sidechains in the new structure. As expected, the conserved h1-h4 residues of the BH3 domain sit in the hydrophobic groove of the partner Bax molecule (**Figure 25E**). Likewise, the conserved salt bridge between BH3 residue D68 and groove residue R109 was also observed (**Figure 25E**).

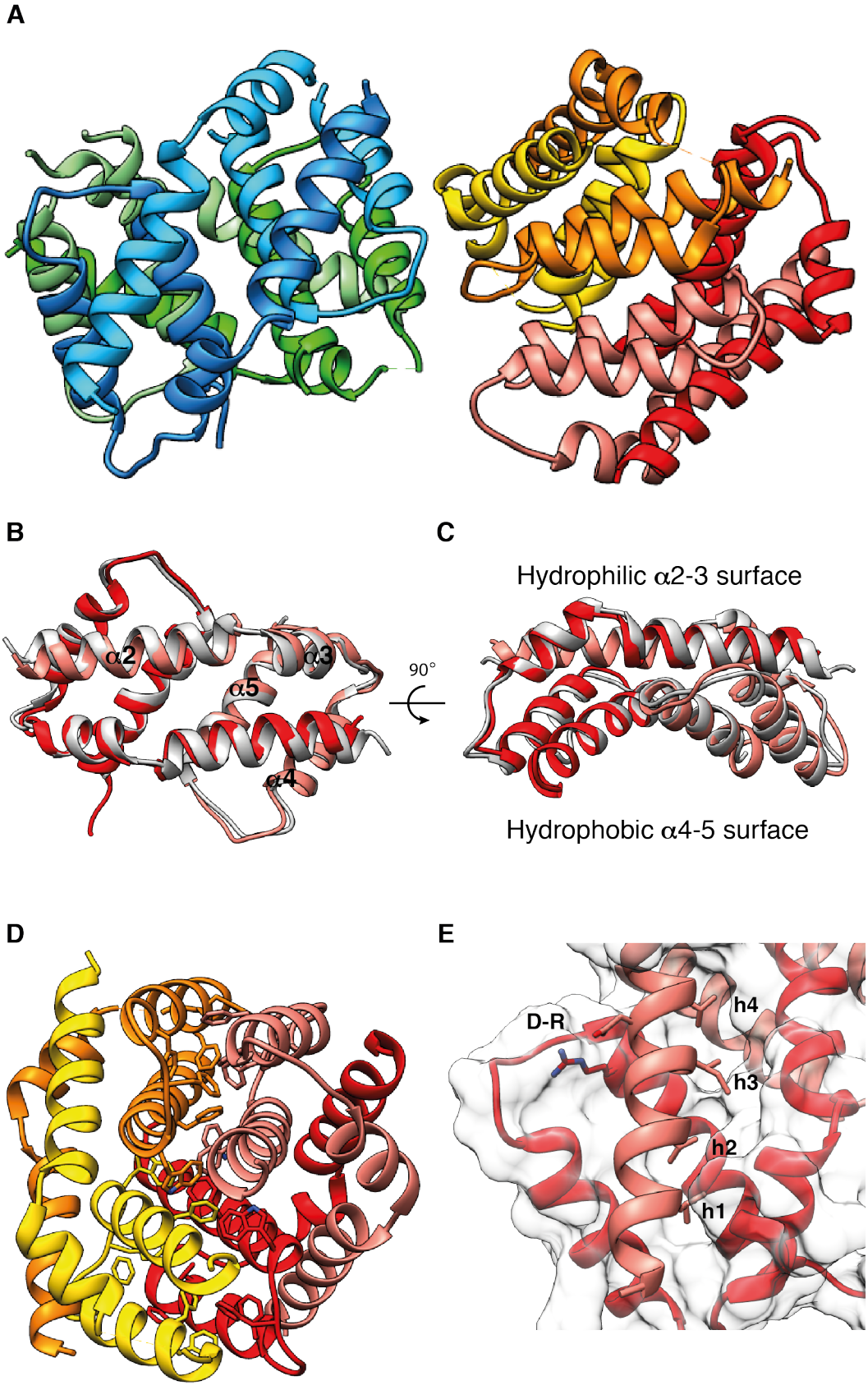
A
B
α2
α3
α5
α4
90°
C
Hydrophilic α2-3 surface
Hydrophobic α4-5 surface
D
E
D-R
h4
h3
h2
h1

Figure 25. X-ray crystal structure of the Bax(α2-5) tetramer. A) *The asymmetric unit of the crystal containing 2 tetramers that consist of 2 Bax core homodimers, shown in cartoon representation. The two chains of each homodimer are coloured in two shades of blue, green, yellow, or red.* ***B)*** *and* ***C)*** *The BH3:groove core homodimer consisting of chains G (salmon) and H (red) (representative of the other core homodimers in the structure) overlayed onto a Bax core homodimer from the GFP structure (grey, PDB code: 4BDU (Czabotar et al., 2013)). The BH3 domain (α2, labelled on chain G) is reciprocally exchanged into the hydrophobic groove (α3-5, labelled on chain G) of the partner chain. The hydrophilic/hydrophobic polarity of the homodimer is labelled in* ***C****.* ***D)*** *Tetramer consisting of the chains E (yellow) and F (orange) and chains G and H homodimers. The hydrophobic faces of the homodimers form an extensive interaction surface, with interdigitating aromatic residues (shown as sticks). The outer surface of the tetramer is largely polar.* ***E)*** *Canonical interactions occur between the BH3 domain (chain G) and the hydrophobic groove of the partner molecule (chain H, shown in cartoon representation with a transparent surface). Residues h1-4 sit in pockets in the hydrophobic groove, and a salt bridge is formed between D68 of the BH3 domain and R109 of the BH1 domain (labelled D-R).*

3.3 Twinned Crystal Structure of a Trimer of Bax Core Homodimers

The hexamer of Bax core domains is reminiscent of the Bak core domain hexamer cylinder presented in Chapter 2. Thin-layer chromatography (TLC) was performed to determine if *E. coli* lipids had copurified with Bax core domains as they had with Bak core domains. Solubilisation, separation and detection of lipids by this method revealed two identically migrating spots in the Bak(α2-5) and Bax(α2-5) hexamer samples that were absent in the Bax(α2-5) tetramer sample (**Figure 26**). Given that lipid mass spec analysis of the Bak(α2-5) hexamer revealed an abundance of PE and PG, the upper spot that is stainable with amine binding dye ninhydrin is likely PE, while the lower band could be PG based on approximate retardation factor values from the same solvent system (Fuchs *et al.*, 2011).

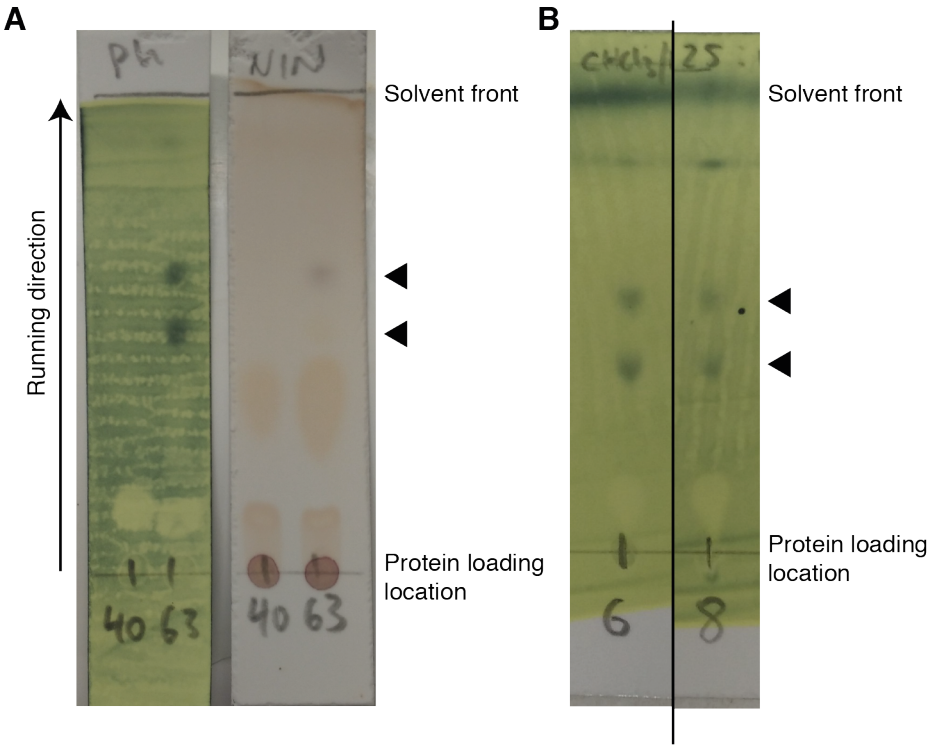

Figure 26. Thin layer chromatography of Bax(α2-5) tetramer and hexamer and Bak(α2-5) hexamer samples. A) *Phosphomolybdic acid (labelled Ph) and ninhydrin (labelled NIN) staining of purified Bax tetramer (labelled 40, referring to 40 kDa peak) and hexamer (labelled 63, referring to 63 kDa peak) samples run in chloroform/methanol/water (25:10:1 v/v) on TLC plates. Phosphomolybdic acid stains unsaturated bonds, revealing two spots (indicated with arrows) consistent with phospholipid in the hexamer sample but not the tetramer sample. Ninhydrin, which stains amines, reveals one spot consistent with the upper spot on the Ph stained plate that likely represents PE.* ***B)*** *Comparison of the phosphomolybdic acid stained spots in purified Bak hexamer (labelled 6) and Bax hexamer (labelled 8) samples run on a TLC plate in chloroform/methanol/water (25:10:1 v/v) demonstrates a consistent spot pattern between samples. The black line indicates where non-relevant samples have been cropped from the image.*

Crystals grown from the Bax(α2-5) hexamer peak diffracted to 2.2 Å but contained a significant twin fraction (estimated ~0.47-0.48 in PHENIX refine and REFMAC 5 (Adams *et al.*, 2010; Murshudov *et al.*, 1997)). Despite this, the structure was solved in the monoclinic space group $P2_1$ by molecular replacement using a Bax globule from a homodimer in the tetramer structure as a search model. The globule consisted of the

BH3 α2 helix of one Bax chain sitting in the α3-5 groove of the partner chain. Encouragingly, PHASER placed 6 of these globules in 3 homodimer pairs, an arrangement unlikely to be placed by chance, with a TFZ of 9.1 and an LLG value of 433 (McCoy *et al.*, 2007). The arrangement is also structurally and chemically sensible, with the 3 homodimers assuming a donut-like shape. The assembly is similar to the Bak core domain cylinder in that the hydrophobic α4-5 faces were all pointing towards the centre of the donut while the α2-3 hydrophilic faces were arrayed around the outside of the donut. Unfortunately, the structure could not be refined beyond an R-free value of 0.35, with no clear density for bound lipid. Nevertheless, lipid mass spectrometry was performed to identify any lipid in the crystals (for Methodology see Appendix). As with the Bak(α2-5) cylinder crystals, mass spec analysis detected both PE and PG, but not PI, in the Bax(α2-5) hexamer crystals, with a slightly lower ratio of PE to PG (**Table 7**).

Table 7. Mole percent composition of lipid classes in Bax(α2-5) and Bak(α2-5) samples. *Mole percentages of phosphatidylethanolamine (PE), phosphatidylglycerol (PG) and phosphatidylinositol (PI) identified by lipid mass spectrometry in Bax(α2-5) and Bak(α2-5) samples.*

	PE	**PG**	**PI**
Bax(α2-5) hexamer crystal	72.3%	27.7%	0%
Bak(α2-5) hexamer crystal	85.8%	14.2%	0%
Purified Bak(α2-5) hexamer	75%	13%	12%

3.4 Discussion

Bax/Bak-mediated MOMP is the point of no return for a cell. The molecular details of this event have slowly emerged over decades of research. Homodimerisation of activated Bax and Bak is an essential event. Homodimers nucleate and are sequentially added to the growing oligomers that are responsible for MOMP (Aluvila *et al.*, 2014; Bleicken *et al.*, 2014; Brouwer *et al.*, 2014; Czabotar *et al.*, 2013; Dewson *et al.*, 2009; Dewson *et al.*, 2008; Dewson *et al.*, 2012; Grosse *et al.*, 2016; Ma *et al.*, 2013; Mandal *et al.*, 2016; Salvador-Gallego *et al.*, 2016). The structures of the regions of Bax and Bak responsible for homodimerisation (the core domain α2-5) were solved by fusing them to GFP (Brouwer *et al.*, 2014; Czabotar *et al.*, 2013). The structures revealed what had been predicted by cysteine cross-linking studies: a reciprocal exchange of the BH3 α2 helix into the hydrophobic groove of a partner molecule (Dewson *et al.*, 2008; Dewson *et al.*, 2012).

The Bak core homodimer structure was of sufficient resolution to reveal the molecular interactions holding the two Bak core domains together in atomic detail (Brouwer *et al.*, 2014). Such details were missing from the Bax core homodimer structure that was solved at a lower resolution and in which the density for the Bax component was particularly poor (Czabotar *et al.*, 2013). The aim of this chapter was to gain a high-resolution picture of the Bax core homodimer.

Towards this goal, the first approach taken was to attempt to stabilise the hydrophobic aromatically-enriched surface of the Bax homodimers with a bilayer mimetic. Bicelles of different compositions produced crystals of GFP:Bax(α2-5) in the original $P6_4$ space group, as well as in a new space group, $P2_12_12$. Curiously, there was no evidence of bicelles in either crystal, and it is unclear why the addition of bicelles resulted in a new crystal form or an improvement in resolution. The $P2_12_12$ crystal, grown in the presence of DMPG:CHAPSO bicelles, diffracted to a lower resolution than the original crystal form and was therefore abandoned after some initial refinement. The $P6_4$ crystal grew in conditions similar to the original crystal with the addition of DOPC:CHAPSO bicelles. While the overall resolution improved, the density for the Bax portion of the structure was still very poor. The scaffolding by GFP in this crystal form leaves the Bax core homodimers suspended in the crystal lattice with few crystal contacts. Large

negative difference map peaks above 5 σ are present at the centre of the Bax core homodimers and may indicate cavities in the protein that could cause instability and thus limit diffraction.

In the original crystal structure of the Bax core domain, the degree of influence that the GFP molecules had on the fold of the BH3:groove core homodimers was not clear (Czabotar *et al.*, 2013). The work presented in this chapter demonstrates that their influence was minimal, with overall fold maintained between the core domain homodimers in the presence or absence of GFP. The tetramer structure without GFP provides high-resolution structural information on the Bax core homodimer to complement the high-resolution data for the Bak core homodimer. As with Bak, the canonical interactions between the BH3 domains and the hydrophobic groove are conserved in Bax.

The hydrophobic planar surface created by the α4-5 helices of both the Bax and Bak core homodimers has been proposed to be involved in membrane-binding (Brouwer *et al.*, 2014; Czabotar *et al.*, 2013). Indeed, based on the lipid-bound structures presented in Chapter 2, this appears likely to be the case with Bak. The preference of the Bax α4-5 surface for other hydrophobic surfaces is evident in the tetrameric Bax(α2-5) structure. In the crystal (and likely in solution, based on elution volume from a calibrated GF column), Bax core homodimers bury their hydrophobic surface by dimerising via said surface with a second Bax core homodimer. The resulting tetramer is likely an artefact of truncated protein expression in the absence of an orientating membrane and TM anchor. A similar tetrameric arrangement was seen in the case of Bak(α2-5) in complex with LysoPC, however apo Bak core domains only appeared as a hexamer on GF. Apo Bak core domains may be unable to assume the tetrameric assembly observed for Bax because the Bak α4-5 surface is more curved than the equivalent surface on Bax.

Like Bak, Bax core domains also formed hexamers based on the elution volume from GF. Thin-layer chromatography suggested these hexamers could be in complex with *E. coli* lipids, as the Bak and Bax hexamer samples produced identically migrating spots consistent with PE and PG while the Bax tetramer did not. Excitingly, crystals grew from purified Bax hexamer, and lipids were identified in the crystals by lipid mass

spectrometry. Unfortunately, the crystals were severely twinned. The twinning is likely the result of a non-crystallographic 2-fold axis formed by one of the 3 symmetric homodimers that make up the asymmetric unit of the $P2_1$ crystal. The dyad axis runs parallel to the C axis of the unit cell and is probably the cause of the crystal pathology. Consequently, a solution containing half of the same donut-shaped assembly can be found by PHASER with a crystallographic 2-fold along the C axis in the space group $P2_12_12$ (McCoy *et al.*, 2007). The R-free value for this solution did not dip below 0.42 during refinement, supporting the twinning conclusion. Even with a twin law (in this case -h, -k, l), twinned refinement is exceedingly difficult with a twin fraction approaching 50%. Optimising crystal growth conditions may therefore represent the best chance of obtaining a crystal that is not twinned or contains a smaller twinned fraction. Obtaining a refinable dataset of a Bax(α2-5):lipid complex could be very valuable. If a conserved lipid binding mechanism were found in both Bak and Bax, it would lend weight to the proposals made in Chapter 2 regarding the role of the α4-5 surface of Bak and Bax homodimers in MOMP.

In this chapter, I have provided the first high-resolution structure of the Bax core domain BH3:groove homodimer. The interactions in the structure are consistent with canonical BH3:groove interactions and provides structural information that will fuel further work, particularly in regard to the hydrophobic planar surface of the Bax and Bak core homodimers. The twinned crystal structure of a Bax core domain hexamer, potentially in complex with lipid, represents a good starting point for optimisation and will hopefully give greater insights into membrane and lipid interactions with Bax.

3.5 Methodology

3.5.1 GFP:Bax(α2-5) Expression and Purification

GFP:Bax(α2-5) was expressed and purified following the protocol described in (Czabotar *et al.*, 2013). The sequence encoding the core domain of Bax (α2-5, residues D53-K128, C62S, C126S) had been previously cloned into the pET28a-GFP vector and transformed into BL21 (DE3) *E. coli* cells (Czabotar *et al.*, 2013). Cells were grown at 37°C in SB to an O.D. (600 nm) of ~1.0 and induced to express for 3 hours at 37°C

with 1 mM IPTG. Cells were lysed in TBS pH [8.0] and lysates were filtered through a 0.45 μm pore size filter then passed over a Ni-NTA column. The column was washed with TBS containing 30 mM imidazole to remove non-specific binders, and bound protein was eluted with TBS containing 250 mM imidazole. The 6xHis-tag was not removed as in (Czabotar *et al.*, 2013). The protein was further purified by GF (S200 10/300) in TBS pH [8.0].

3.5.2 SDS-PAGE

Protein samples were heated at 95°C for 5 minutes with reducing protein loading dye. After heating, samples were loaded into pre-cast NuPAGE 12% Bis-Tris gels (Life Technologies). Gels were electrophoresed in MES running buffer for 40 minutes at 200V. Gels were fixed and stained with Coomassie stain (2% Coomassie R250 Brilliant Blue w/v, 10% acetic acid v/v, 40% ethanol v/v) for 30 minutes before removal of excess Coomassie with a destaining buffer (10% acetic acid v/v, 40% ethanol v/v). Molecular weight of protein bands was estimated using SeeBlue Plus2 Prestained Protein Standard (Life Technologies).

3.5.3 Bicelle Preparation

Bicelles were prepared as described in (Ujwal and Bowie, 2011). Briefly, different dried long chain lipids (such as DMPG or DOPC) were resuspended in detergent (CHAPSO or 3-[(3-cholamidopropyl)dimethylammonio]-1-propanesulfonate (CHAPS)) at different q ratios (q = ratio of long to short chain lipids which controls the bicelle diameter) and incubated at room temperature for 1 hour. Resuspended samples were frozen and thawed 5 times by cycling between liquid nitrogen and warm water, then sonicated in a water bath for 30-minutes. Final concentration of the bicelle mixture was 10% (w/v) lipid and detergent.

3.5.4 GFP:Bax(α2-5) Crystallisation, Data Collection and Processing

Crystals GFP-Bax α2-5 fusion protein samples were incubated with 0.5% (w/v) DMPG:CHAPSO bicelles (q=0.8) or 0.5% (w/v) DOPC:CHAPSO bicelles (q=0.6) for

20 minutes on ice before setting up in 24-well hanging drop plates. Proteins were crystallised in 10% (w/v) PEG 3350, 20% MPD, 0.1 M Tris pH [7.5]. Crystals were frozen in cryoprotectant (well solution supplemented with 10% ethylene glycol). Data were collected at the MX2 beamline of the Australian Synchrotron and processed with XDS (Kabsch, 2010). Molecular replacement was performed with PHASER (McCoy *et al.*, 2007) using GFP and the Bax core dimer from the published GFP-Bax α2-5 structure (PDB code: 4BDU (Czabotar *et al.*, 2013)) as search models. The structures were refined by iterative rounds of building in COOT (Emsley and Cowtan, 2004) and refinement with PHENIX (Adams *et al.*, 2010).

3.5.5 GST:Bax(α2-5) Cloning, Expression and Purification

The sequence encoding the core domain of Bax (α2-5, residues D53-K128, C62S, C126S) was cloned into the pGEX-6P-3 vector and transformed into BL21 (DE3) *E. coli* cells. Cells were grown at 37°C in SB to an O.D. (600 nm) of ~1.0 and induced to express for 3 hours at 37°C with 1 mM IPTG. Cells were lysed in GST buffer pH [8.0] and lysates were filtered through a 0.45 μm pore size filter then passed over a GST column. The column was washed with GST buffer and on-column cleavage was performed for 2 nights at 4°C with PreScission Protease (0.02 mg/mL). Bax(α2-5) cleaved from the GST fusion protein was eluted from the column in GST buffer, then purified by anion exchange on a HiTrap Q FastFlow 1 mL column in 20 mM Tris pH [8.0] with a NaCl gradient of 0 to 1 M. Anion exchange yielded two peaks, both of which were further purified by GF (S200 10/300) in TBS pH [8.0]. Based on elution volumes, the two different Bax(α2-5) species from anion exchange were approximately 40 kDa (tetramer) and 63 kDa (hexamer). Both species were taken forward for crystallisation.

3.5.6 Thin-layer Chromatography

Concentrated samples of the Bax core domain tetramer or hexamer or the Bak core domain hexamer were slowly pipetted onto marked spots near the base of aluminium-backed, Silica gel 60 TLC plates. Plates were placed in glass jars containing chloroform/methanol/water (25:10:1 (v/v)) to a level below where samples were

loaded. Samples were run until the solvent front was close to the top of the TLC plate, and plates were dried. Dried plates were stained with ninhydrin or phosphomolybdic acid, then dried and heated with a heat gun to reveal stained lipid species.

3.5.7 Bax(α2-5) Crystallisation, Data Collection and Processing

Crystallisation trials were performed in 96-well sitting drop plates at the CSIRO C3 facility in Parkville.

The Bax(α2-5) tetramer crystallised in 1.44 M trisodium citrate and 10 mM TCEP in the monoclinic space group $P2_1$. The crystal was frozen in well solution supplemented with 10% ethylene glycol and X-ray data were collected at the MX2 beamline of the Australian Synchrotron. Diffraction images were processed with XDS (Kabsch, 2010) and the structure was solved by molecular replacement with PHASER (McCoy *et al.*, 2007). The search model used was a Bax core homodimer from the published Bax core homodimer structure (PDB code: 4BDU) (Czabotar *et al.*, 2014). Four core homodimers were placed into a pair of near-identical tetramers. The model was refined with iterative rounds of building in COOT (Emsley and Cowtan, 2004) and refinement with PHENIX (Adams *et al.*, 2010).

The Bax(α2-5) hexamer crystallised in 0.1 M trisodium citrate [pH 3.5], 0.02 M sodium HEPES [pH 6.8], 2 M ammonium sulphate, 0.33% (w/v) 1,3,5 pentanetricarboxylic acid, 0.33% (w/v) 5-sulfosalicylic acid, 0.33% (w/v) trimesic acid in the monoclinic space group $P2_1$. The crystal was frozen in well solution supplemented with 25% ethylene glycol, and X-ray data were collected at the MX2 beamline of the Australian Synchrotron. Diffraction images were processed with XDS (Kabsch, 2010). A significant twinning fraction was predicted in Xtriage of approximately 34% (Adams *et al.*, 2010). The structure was solved by molecular replacement in PHASER (McCoy *et al.*, 2007) by searching for 6 Bax globules (consisting of α2 from one chain of the homodimer in the α3-5 groove of the partner chain) constructed from the tetramer structure. Refinement was attempted with iterative rounds of building in COOT (Emsley and Cowtan, 2004) and refinement with PHENIX (Adams *et al.*, 2010), but the R-free value did not drop below 0.35 with or without twinned refinement using the appropriate twin law of -h, -k, l. The twin fraction was estimated to be approximately

0.47 and 0.48 in PHENIX Refine and REFMAC5, respectively (Adams *et al.*, 2010; Murshudov *et al.*, 1997).

3.5.8 Structure Analysis and Figure Generation

Molecular graphics for structural figures were generated primarily with the USCF Chimera Package (Pettersen *et al.*, 2004). Molecular graphics containing electron density were generated in PyMOL (Delano, 2002).

Chapter 4

Mode 2 Inhibition of Bak and Bax by Bcl-X_L

Pro-survival proteins inhibit apoptosis by binding to and sequestering pro-apoptotic Bcl-2 family proteins. In the unified model of Bcl-2 family protein interactions, pro-survival proteins prevent apoptosis by two modes of action (see **Figure 3**) (Llambi *et al.*, 2011). Mode 1 involves binding of the BH3 domain of activator BH3-only proteins such as Bid or Bim to the conserved hydrophobic groove (made up of α-helices 3, 4 and 5) on a pro-survival protein, thereby preventing direct activation of Bak and Bax (Llambi *et al.*, 2011). Mode 2 inhibition occurs when pro-survival proteins bind to and sequester the BH3 domains of activated Bax and Bak in an analogous manner (Llambi *et al.*, 2011).

Many structures demonstrating these BH3:groove interactions have been solved using BH3 peptides in complex with pro-survival proteins that have been truncated to remove the C-terminal TM anchor (e.g. Refs (Czabotar *et al.*, 2007; Day *et al.*, 2008; Fire *et al.*, 2010; Follis *et al.*, 2013; Petros *et al.*, 2000; Rautureau *et al.*, 2012; Sattler *et al.*, 1997; Smits *et al.*, 2008)). Mutations to the hydrophobic groove of pro-survival proteins that abrogate BH3:groove binding also greatly impair pro-survival function, illustrating the importance of this interface for inhibition of apoptosis (Sattler *et al.*, 1997; Yin *et al.*, 1994). However, it is possible that the BH3:groove is not the only interaction interface between full-length proteins in complex on the membrane. Indeed, secondary sites of interaction have been proposed for both Bcl-2 and Bcl-X_L in complex with Bax (Ding *et al.*, 2014; Ding *et al.*, 2010). The α6 helix of Bax could be photocross-linked to the BH4 domain of Bcl-2, and α1 of Bax could be photocross-linked and cysteine cross-linked to α1 of Bcl-X_L (Ding *et al.*, 2014; Ding *et al.*, 2010). On top of this, Mode 1 complexes are more readily disrupted than Mode 2 complexes, implicating factors other than affinity for BH3 domains (Llambi *et al.*, 2011).

The relevance of large conformational change to pro-survival protein function has not been widely investigated. Disulphide tethering of α-helices 5 and 6 of Bax and Bak prevents dissociation of the core and latch domains and inhibits cytochrome *c* release from isolated mitochondria (Brouwer *et al.*, 2014; Czabotar *et al.*, 2013). Interestingly, a similarly tethered Bcl-2 disulphide mutant was impaired in its ability to prevent

cytochrome *c* release by Bax from isolated mitochondria (Dlugosz *et al.*, 2006). However, an oxidant was not used to induce the tether and it remains unclear whether Bcl-2 unlatches in a similar way to Bax and Bak.

Though the same tethering experiments have not been performed with Bcl-X_L, it is clear that Bcl-X_L can undergo core/latch separation based on several crystal structures (Denisov *et al.*, 2007; Follis *et al.*, 2013; O'Neill *et al.*, 2006; Rajan *et al.*, 2015; Tanaka *et al.*, 2013). The physiological relevance of this unlatching is ambiguous as it has only been observed in harsh conditions such as high pH, heat and the presence of isopropanol or detergent (Denisov *et al.*, 2007; Follis *et al.*, 2013; O'Neill *et al.*, 2006; Rajan *et al.*, 2015; Tanaka *et al.*, 2013).

Nevertheless, the potential of pro-survival proteins to unlatch does raise an interesting possibility. If Bcl-X_L could unlatch in cells, its core domain could heterodimerise with the core domains of Bax or Bak, forming a pseudo-symmetric BH3:groove heterodimer similar to the BH3:groove homodimers formed by Bax and Bak (discussed in Chapter 2 and Chapter 3). A schematic representation and structural models of core domain heterodimers of Bax:Bcl-X_L and Bak:Bcl-X_L are presented in **Figure 27**. The models were generated with SWISS-MODEL using one chain from the Bax or Bak core dimer structures (PDB codes: 4BDU and 4U2V) as templates (Biasini *et al.*, 2014; Brouwer *et al.*, 2014; Czabotar *et al.*, 2013). The Bcl-X_L chains generated from modelling were superposed in Chimera over one chain of the core homodimer structure it was generated from (Pettersen *et al.*, 2004).

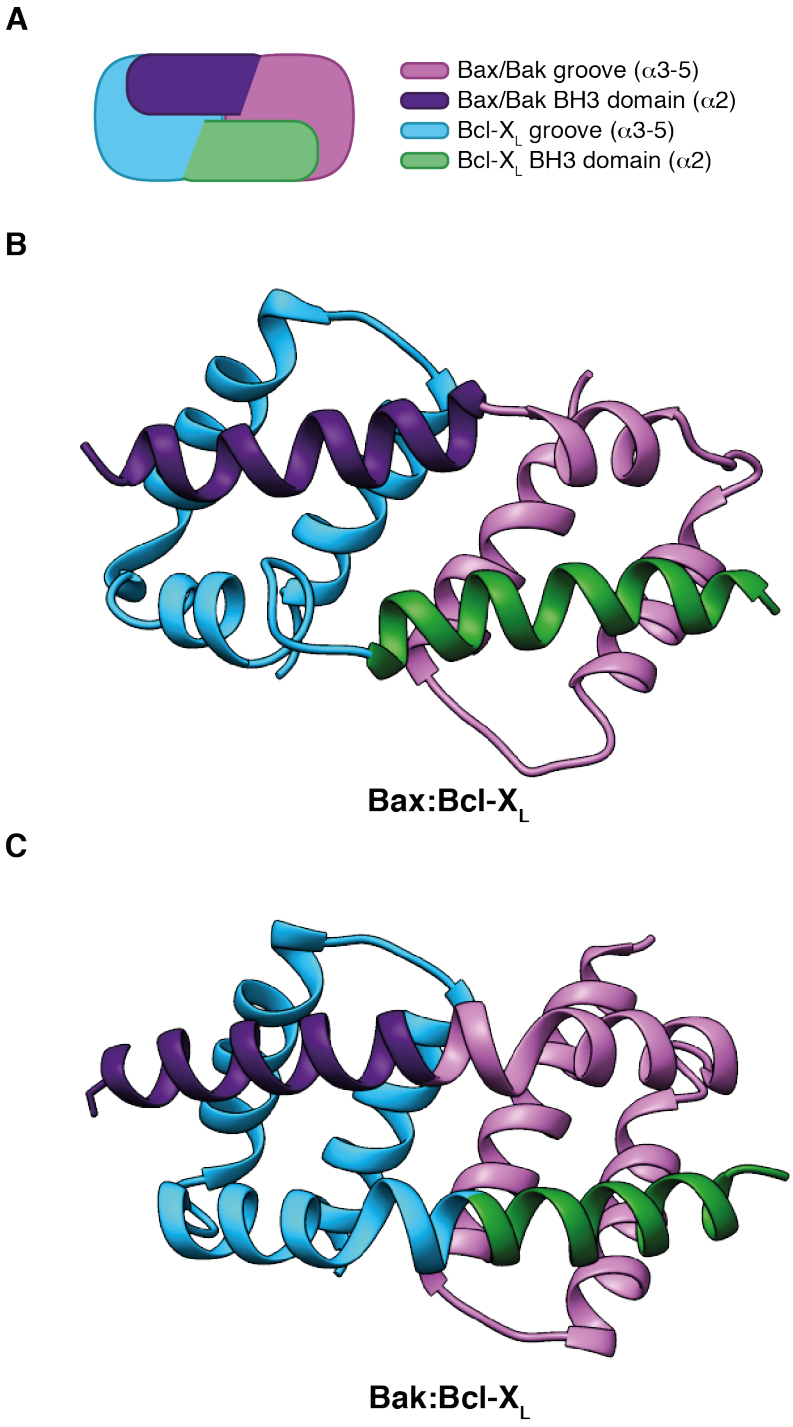

Figure 27. Structural models of Bax:Bcl-X_L and Bak:Bcl-X_L core domain heterodimers. ***A)*** *Schematic representation of a Bax/Bak:Bcl-X_L core domain heterodimer.* ***B)*** *Structural model of the proposed Bax:Bcl-X_L core domain heterodimer based on the structure of the Bax core dimer (PDB code: 4BDU).* ***C)*** *Structural model of the proposed Bak:Bcl-X_L core domain heterodimer based on the structure of the Bak core dimer (PDB code: 4U2V). The schematic and models are coloured as indicated in the figure key.*

To investigate the possibility of BH3:groove heterodimer formation, I used copper phenanthroline (CuPhe)-induced disulphide cross-linking of full-length proteins on mitochondria in attempts to cross-link the Bcl-X_L BH3 domain to the hydrophobic groove of Bax or Bak.

4.1 Disulphide Cross-linking of Bcl-X_L and Bax

To monitor possible Bax:Bcl-X_L BH3:groove heterodimerisation, I employed an established disulphide cross-linking methodology used to cross-link both the Bax and Bak BH3:groove homodimers (Dewson *et al.*, 2008; Dewson *et al.*, 2012). Combinations of single cysteine mutant Bax (hemagglutinin (HA)-tagged) or Bcl-X_L (FLAG-tagged) were co-transduced into Bak/Bax DKO MEFs. Cysteines were located in either the BH3 domain (Bax T56C, Bcl-X_L M83C) or the hydrophobic groove (Bax R94C or V95C, Bcl-X_L Q125C). The MEFs were permeabilised with digitonin detergent and the cytosol was discarded. The remaining heavy membrane fraction containing mitochondria was incubated with digitonin or Triton X-100. Triton X-100 detergent artificially increases the association of Bax with Bcl-X_L and was used to increase chances of detecting cross-linked heterodimers (Dewson, 2015; Hsu and Youle, 1998). Digitonin, on the other hand, does not appear to activate Bax, and thus more physiologically relevant complexes can be isolated with this detergent (Dewson, 2015). The proteins on the surface of the mitochondria were cross-linked using the oxidant CuPhe. Because only cysteines in close proximity are cross-linked, binding interfaces can be mapped with this technique (Pakula and Simon, 1992).

After cross-linking, Bcl-X_L was pulled down by immunoprecipitation (IP) using FLAG M2 affinity beads. Immunoprecipitated samples were heated in non-reducing loading dye to dissociate any non-covalently bound proteins and then run on SDS-PAGE. Immunoblotting for both Bcl-X_L and Bax or Bak in the same samples was performed to identify cross-linked heterodimers. Successful cross-links are demonstrated by a band shift from a monomer to a heterodimer.

The structural model and a schematic representation of a core domain heterodimer of Bax:Bcl-X_L are shown in **Figure 28A** and **B**, with cysteine mutant locations highlighted in yellow. In an initial pilot experiment, two Bax groove mutants (R94C and V95C)

were tested for cross-linking to the Bcl-X_L BH3 mutant M83C (**Figure 28C**). As mentioned above, pro-survival proteins such as Bcl-X_L bind to and sequester the BH3 domains of Bax or Bak in the hydrophobic groove on the pro-survival protein surface to inhibit apoptosis (Czabotar *et al.*, 2011). Therefore, the combination of the Bax BH3 domain mutant T56C and Bcl-X_L hydrophobic groove mutant Q125C was used as a positive control for heterodimer formation. Bax T56C was successfully cross-linked to the Bcl-X_L Q125C, as shown by the shift from monomer to heterodimer in both Bax and Bcl-X_L blots (**Figure 28C**). Negative control combinations of Bax BH3 to Bcl-X_L BH3 (M83C) and Bax groove to Bcl-X_L groove demonstrated that this cross-linking was specific (**Figure 28C**).

The experimental combination of Bax groove and Bcl-X_L BH3 cysteine mutants cross-linked to form a heterodimer band of the same molecular weight as the band seen for the Bax BH3 and Bcl-X_L groove cross-linked heterodimers (**Figure 28C**). The band was stronger for the V95C Bax groove mutant than the R94C mutant, again demonstrating specificity in cross-linking. Due to higher cross-linking efficiency, Bax groove mutant V95C was taken forward in subsequent experiments. As expected, samples incubated with Triton X-100 immunoprecipitated more total Bax and a larger amount of cross-linked heterodimer compared to samples incubated in digitonin.

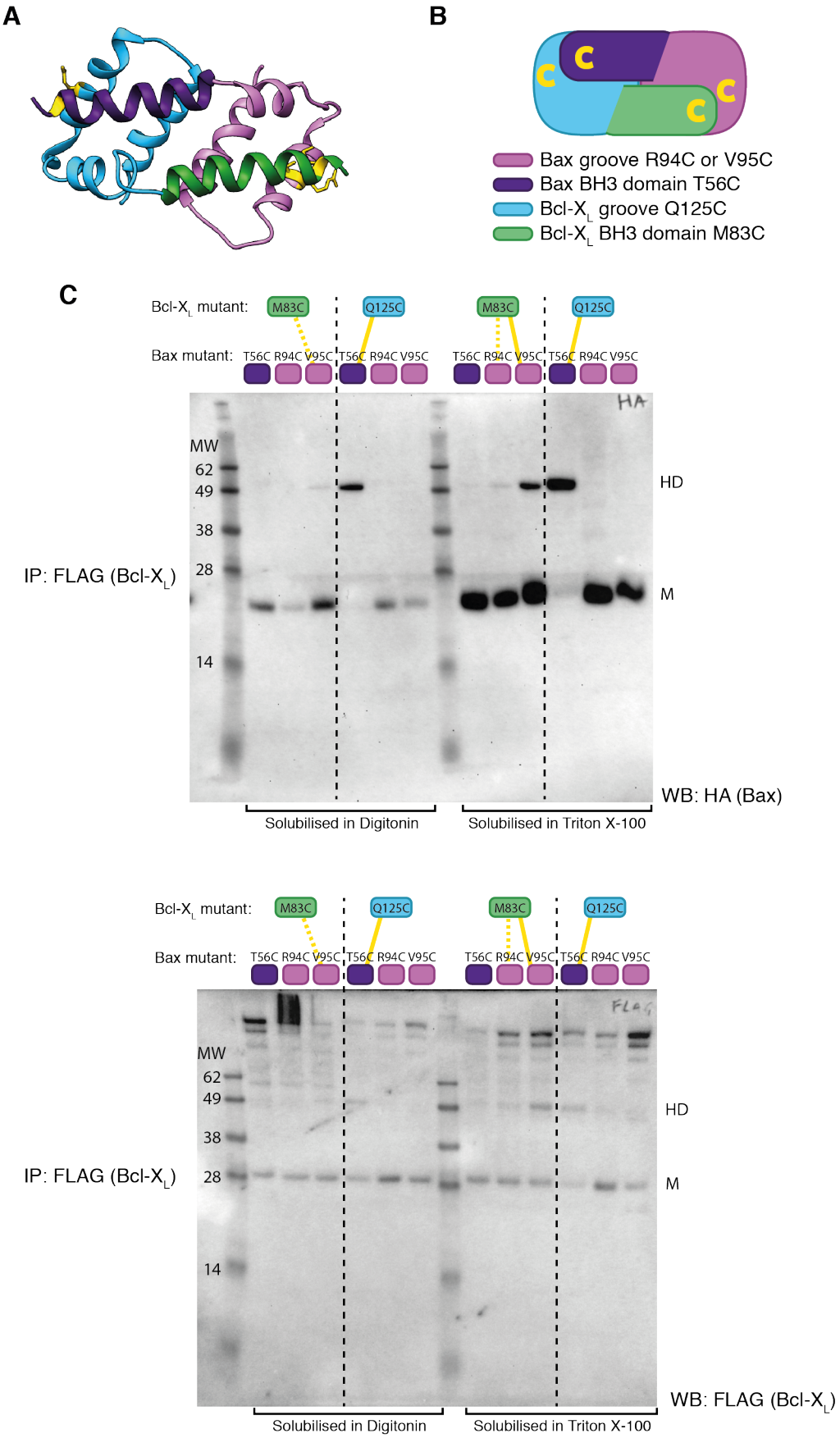
A
B
C
Bax groove R94C or V95C
Bax BH3 domain T56C
Bcl-X$_L$ groove Q125C
Bcl-X$_L$ BH3 domain M83C
Bcl-X$_L$ mutant:
M83C
Q125C
Bax mutant:
T56C R94C V95C
HA
MW
62
49
38
28
14
HD
M
IP: FLAG (Bcl-X$_L$)
WB: HA (Bax)
Solubilised in Digitonin
Solubilised in Triton X-100
FLAG
WB: FLAG (Bcl-X$_L$)

Figure 28. BH3:groove cysteine cross-linking of Bax and Bcl-X_L. A) *Structural model and* ***B)*** *schematic representation of the proposed Bax:Bcl-X_L core domain heterodimer based on the structure of the Bax core dimer (PDB code: 4BDU) coloured as indicated in the figure key. Sites of single cysteine mutations are shown as sticks in yellow.* ***C)*** *Immunoblots of protein samples immunoprecipitated with FLAG M2 beads from isolated heavy membranes of MEFs expressing different combinations of Bax and Bcl-X_L probed with anti-HA (to detect Bax, upper blot) or anti-FLAG (to detect Bcl-X_L, lower blot). Heavy membranes of the 6 sample lanes on the left- and right-hand sides of the blot were solubilised in digitonin and Triton X-100, respectively. Dashed black lines separate lanes containing either the Bcl-X_L BH3 (M83C, green) or groove (Q125C, cyan) mutants in combination with one of 3 Bax mutants (BH3 in dark purple, groove in light purple). Disulphide bond formation was induced with CuPhe. Successful cross-links between Bcl-X_L and Bax that result in a band shift from monomer (M) to heterodimer (HD) are represented schematically above their corresponding lanes. Complete cross-links (where all immunoprecipitated Bax runs as a heterodimer) and incomplete cross-links are indicated by solid and dashed yellow lines, respectively.*

To ensure cross-links seen in heterodimer complexes were physiologically relevant and not a detergent-induced artefact, digitonin-permeabilised cells were treated with two concentrations of tBid M97A prior to cross-linking and compared to samples incubated with Triton X-100 (**Figure 29**). The tBid M97A mutant is able to activate Bax, but has decreased affinity for Bcl-X_L and Mcl-1 and therefore favours Mode 2 complex formation (Czabotar *et al.*, 2013; Lee *et al.*, 2016). A cys null Bcl-X_L variant (C151S) lacking any cysteine residues was included as a negative control. As expected, it did not show any cross-link formation. The positive control combination of Bax BH3 (T56A) and Bcl-X_L groove (Q125C) mutants showed significant cross-link formation in both the Triton X-100 and tBid M97A treated samples. The combination of Bcl-X_L BH3 (M83C) and Bax groove (V95A) mutants again showed cross-link formation in the Triton X-100 solubilised sample, as well as a dose-dependent level of cross-linking in the tBid M97A treated samples (**Figure 29D**). Surprisingly, limited cross-linking was seen in the negative control combinations of Bax BH3 and Bcl-X_L BH3 mutants as well as Bax groove and Bcl-X_L groove mutants when the samples were treated with tBid M97A **(Figure 29C** and **D**). These cross-links could occur between heterodimers in a high-order complex or in a non-BH3:groove form of a Bax: Bcl-X_L heterodimer.

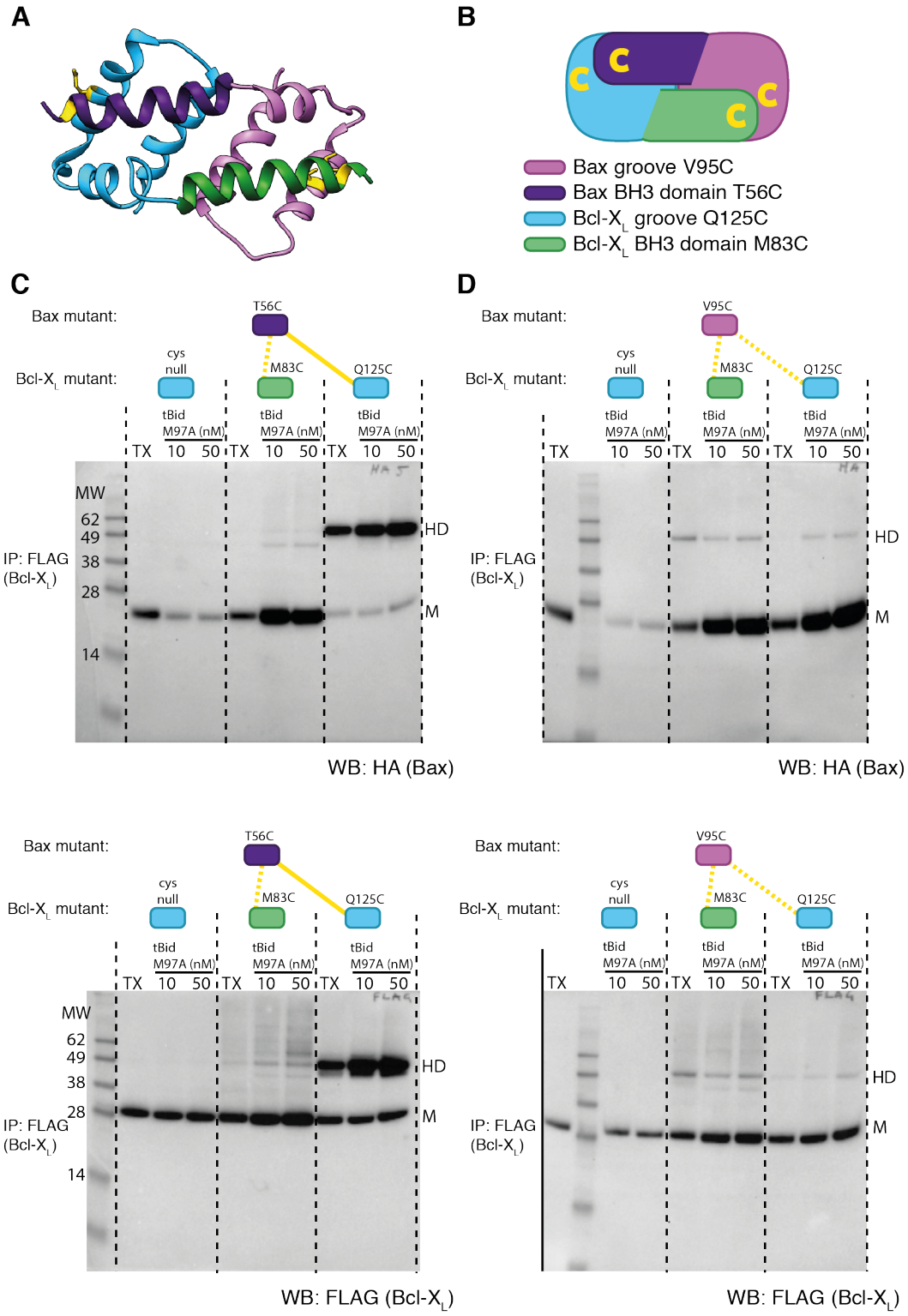
A
B
C
C
C
C
Bax groove V95C
Bax BH3 domain T56C
Bcl-X$_L$ groove Q125C
Bcl-X$_L$ BH3 domain M83C
C
Bax mutant:
T56C
Bcl-X$_L$ mutant:
cys null
M83C
Q125C
tBid M97A (nM)
TX 10 50 TX 10 50 TX 10 50
MW
62
49
38
28
14
IP: FLAG (Bcl-X$_L$)
HD
M
WB: HA (Bax)
D
Bax mutant:
V95C
Bcl-X$_L$ mutant:
cys null
M83C
Q125C
tBid M97A (nM)
TX 10 50 TX 10 50 TX 10 50
IP: FLAG (Bcl-X$_L$)
HD
M
WB: HA (Bax)
Bax mutant:
T56C
Bcl-X$_L$ mutant:
cys null
M83C
Q125C
tBid M97A (nM)
TX 10 50 TX 10 50 TX 10 50
MW
62
49
38
28
14
IP: FLAG (Bcl-X$_L$)
HD
M
WB: FLAG (Bcl-X$_L$)
Bax mutant:
V95C
Bcl-X$_L$ mutant:
cys null
M83C
Q125C
tBid M97A (nM)
TX 10 50 TX 10 50 TX 10 50
IP: FLAG (Bcl-X$_L$)
HD
M
WB: FLAG (Bcl-X$_L$)

Figure 29. Triton X-100- vs. tBid M97A-induced Bax:Bcl-X_L heterodimerisation. *A) Structural model and B) schematic representation of the proposed Bax:Bcl-X_L core domain heterodimer based on the structure of the Bax core dimer (PDB code: 4BDU) coloured as indicated in the figure key. Sites of single cysteine mutations are shown as sticks in yellow. C) and D) Immunoblots of proteins immunoprecipitated with FLAG M2 beads from isolated heavy membranes of MEFs expressing different combinations of Bax and Bcl-X_L mutants, probed with anti-HA (upper panels) or anti-FLAG (lower panels). C) Samples from cell lines co-expressing the Bax BH3 domain (T56C, dark purple) mutant and Bcl-X_L cys null (cyan), BH3 (M83C, dark green) or groove (Q125C, cyan) mutants. D) Samples from cell lines co-expressing the Bax groove (V95C, light purple) mutant and Bcl-X_L cys null, BH3 or groove mutants. Dashed black lines separate the different mutant combinations. Digitonin-permeabilised cells were treated with either 10 or 50 nM tBid M97A to induce formation of Mode 2 complexes. Following solubilisation and isolation of the heavy membranes with Triton X-100 (indicated by TX) or digitonin (in the case of tBid M97A-treated samples), disulphide bond formation was induced with the oxidant CuPhe. Successful cross-links between Bcl-X_L and Bax that resulted in a band shift from monomer (M) to heterodimer (HD) are represented schematically above their corresponding lanes. Near complete cross-links (where almost all immunoprecipitated Bax runs as a heterodimer) and incomplete cross-links are indicated by solid and dashed yellow lines, respectively.*

The tBid mutant M97A induced the formation of Mode 2 complexes of Bax and Bcl-X_L on mitochondria. Wild type (WT) tBid, on the other hand, should both activate Bax and inhibit Mode 2 complex formation of Bax with Bcl-X_L.

To compare the effect of tBid WT and tBid M97A, and to confirm the BH3:groove heterodimer formation in a third independent experiment, digitonin-permeabilised cells expressing reciprocal BH3:groove mutant combinations of Bax and Bcl-X_L were treated with increasing concentrations of tBid WT or M97A and cross-linked with CuPhe (**Figure 30**). As expected, samples treated with mutant tBid M97A immunoprecipitated more Bax than those treated with tBid WT (**Figure 30C**). A faint heterodimer band is present in the Bcl-X_L BH3 and Bax groove mutant combination samples treated with tBid M97A across all concentrations (**Figure 30C**). Poor IP of the

Bcl-X_L Q125C and Bax T56C samples treated with 50 nM tBid WT was likely due to experimental error, during either the IP step or gel loading (**Figure 30C**, lower panel).

Thus, a small population of Bax:Bcl-X_L heterodimers involve an interaction between the Bcl-X_L BH3 and the Bax groove. Because all Bax T56C (BH3 domain) is cross-linked to the Bcl-X_L groove after tBid M97A treatment, it seems likely that the small heterodimer population of Bcl-X_L BH3 linked to the Bax groove are indeed BH3:groove heterodimers. These BH3:groove heterodimers are rare in comparison to heterodimers that only exhibit the canonical Bax BH3 to Bcl-XL cross-link, as indicated by the different levels of cross-linking efficiency.

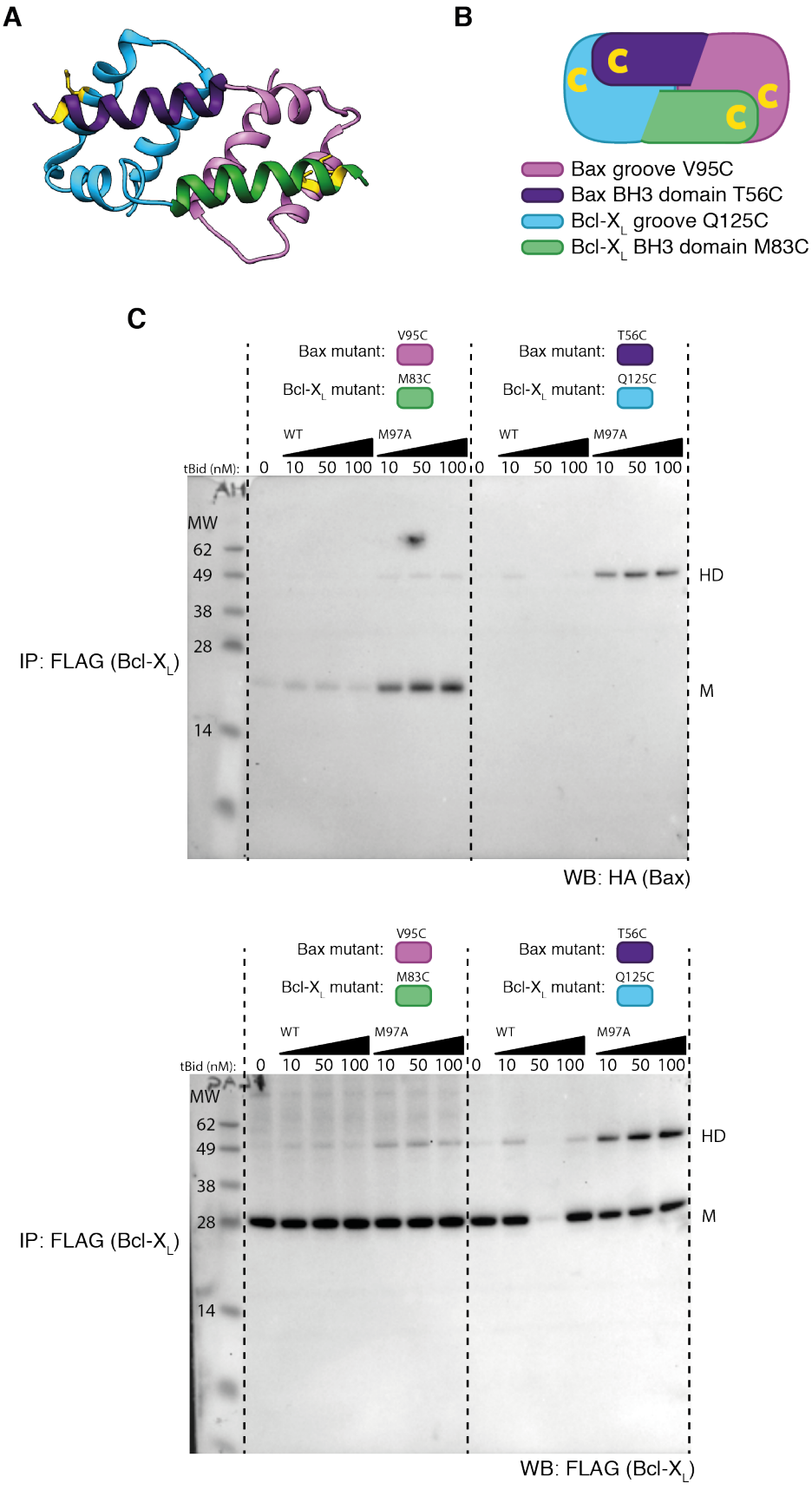
A
B
C
Bax groove V95C
Bax BH3 domain T56C
Bcl-X_L groove Q125C
Bcl-X_L BH3 domain M83C
Bax mutant:
V95C
T56C
Bcl-X_L mutant:
M83C
Q125C
WT
M97A
tBid (nM):
0 10 50 100 10 50 100 0 10 50 100 10 50 100
MW
62
49
38
28
14
HD
M
IP: FLAG (Bcl-X_L)
WB: HA (Bax)
WB: FLAG (Bcl-X_L)

Figure 30. tBid WT- vs. tBid M97A-induced Bax:Bcl-X_L heterodimerisation. ***A)*** *Structural model and* ***B)*** *schematic representation of the proposed Bax:Bcl-X_L core domain heterodimer based on the structure of the Bax core dimer (PDB code: 4BDU) coloured as indicated in the figure key. Sites of single cysteine mutations are shown as sticks in yellow.* ***C)*** *Immunoblots of proteins immunoprecipitated with FLAG M2 beads from isolated heavy membranes of MEFs expressing the combination of Bax groove (V95C, light purple) and Bcl-X_L BH3 (M83C, green) or Bcl-X_L groove (Q125C, cyan) and Bax BH3 (T56C, dark purple), probed with anti-HA (upper panel) or anti-FLAG (lower panel). Digitonin-permeabilised cells were untreated or treated with 10, 50 or 100 nM tBid WT or M97A, and heavy membranes were solubilised and isolated in digitonin. Disulphide bond formation was induced with CuPhe. Dashed black lines separate the different combinations of Bax and Bcl-X_L mutants. Successful cross-links between Bcl-X_L and Bax resulted in a band shift from monomer (M) to heterodimer (HD).*

Taken together, these three independent experiments reveal the existence of a minor population of Bax:Bcl-X_L BH3:groove heterodimers. Given the structural and functional homogeneity of Bax and Bak, I went on to look for a similar population of Bak:Bcl-X_L heterodimers.

4.2 Disulphide Cross-linking of Bcl-X_L and Bak

Like Bax, Bak is sequestered in Mode 2 complexes by Bcl-X_L (Willis *et al.*, 2005). To determine whether Bak also forms BH3:groove heterodimers with Bcl-X_L, I performed cysteine cross-linking studies using combinations of Bak and Bcl-X_L with single cysteine mutations in either their BH3 domains or hydrophobic grooves.

The structural model of a core domain heterodimer of Bak:Bcl-X_L is shown in **Figure 31A** along with a schematic representation in **Figure 31B**. As with Bax, MEFs expressing different combinations of Bak and Bcl-X_L single cysteine mutants were permeabilised with digitonin. Permeabilised cells were treated with 50 nM tBid M97A to induce Mode 2 complex formation (**Figure 31D**) or left untreated (**Figure 31C**). Heavy membranes were isolated and oxidised with CuPhe to induce disulphide bond

formation between cysteine pairs in close proximity. Immunoprecipitation was performed with FLAG M2 beads to pull down Bcl-X_L with any Bak associated.

Treatment with tBid M97A resulted in co-IP of Bak with Bcl-X_L (**Figure 31D**), whereas very little Bak was pulled down without tBid treatment (**Figure 31C**). The cys null Bcl-X_L variant failed to IP any Bak (**Figure 31C** and **D**, upper panels) in this experiment, despite detectable expression (**Figure 31C** and **D**, lower panels). This suggests that cys null Bcl-X_L may be unable to heterodimerise with Bak. Conversely, with Bcl-X_L acting as an internal loading control (**Figure 31D**, lower panel), it appeared that significantly larger amounts of Bak were pulled down by the Bcl-X_L BH3 (M83C) mutant (**Figure 31D**, upper panel). Interestingly, the M83C mutant also showed smearing and higher molecular weight band laddering (**Figure 31C** and **D**, lower panels). A band consistent with the molecular weight of a Bak:Bcl-X_L heterodimer demonstrated cross-link formation between the Bak BH3 domain and the Bcl-X_L groove, with a slightly more efficient cross-link between Bak M71C and Bcl-X_L S122C than with Q125C (**Figure 31D**). An extremely faint heterodimer band appeared in the sample containing the reciprocal Bcl-X_L BH3 domain (M83C) and Bak groove (Y110C) mutants in the HA blot (**Figure 31D**, upper panel). The band was clearer and of the correct size in the FLAG blot for Bcl-X_L (**Figure 31D**, lower panel, indicated with a *). Whether or not this constitutes a genuine Bak:Bcl-X_L BH3:groove heterodimer requires repetition of this experiment. A second band (indicated with a #) appeared at a lower molecular weight in some lanes of the Bcl-X_L blot where proteins had been treated with tBid M97A (**Figure 31D**, lower panel). Puzzlingly, the band did not appear in the Bak blots for the same samples (**Figure 31D**, upper panel), nor did it appear consistently for particular Bcl-X_L variants (**Figure 31D**, lower panel). What this band represents is unclear.

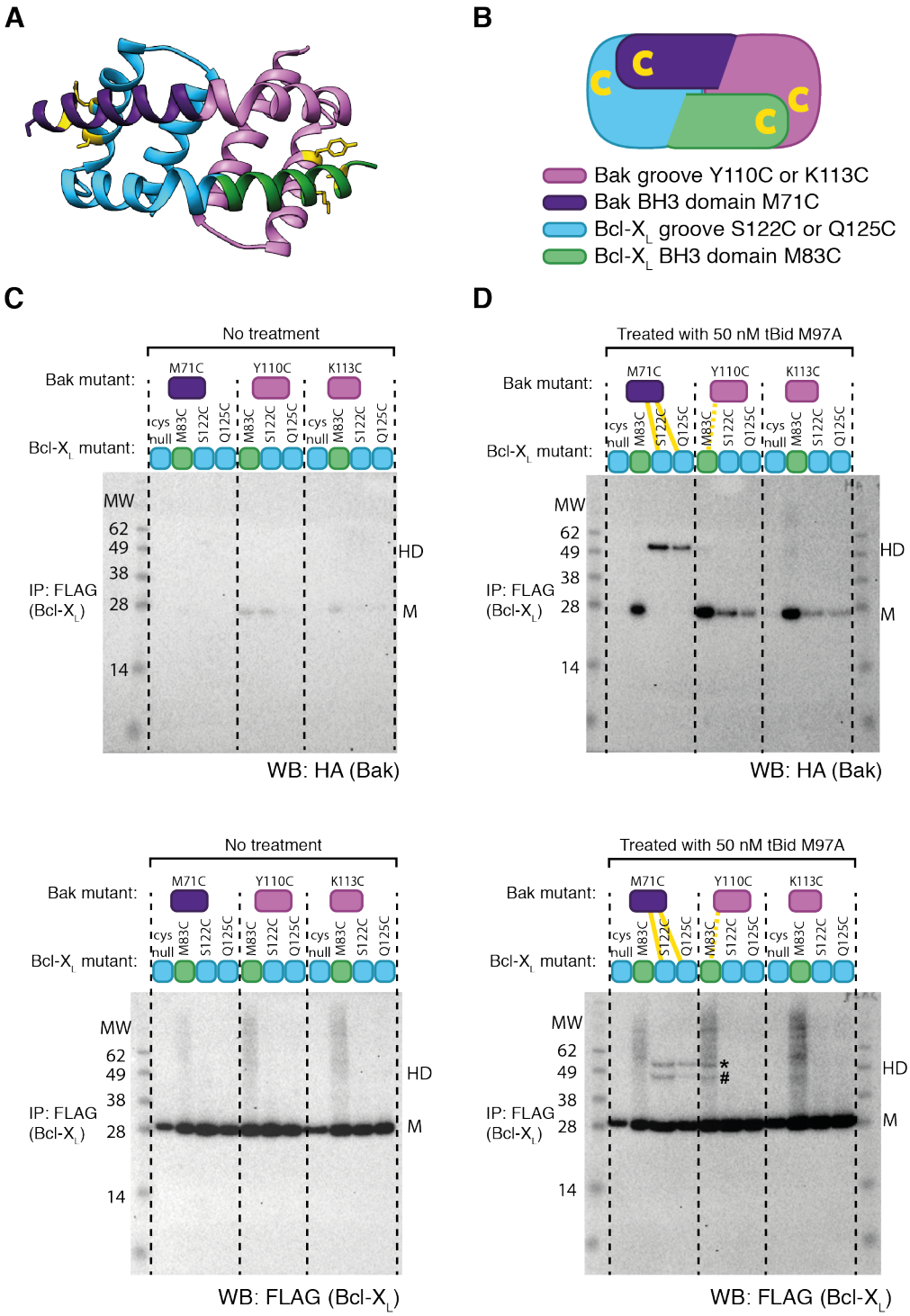
A
B
C
C
C
C
Bak groove Y110C or K113C
Bak BH3 domain M71C
Bcl-X$_L$ groove S122C or Q125C
Bcl-X$_L$ BH3 domain M83C
C
No treatment
Bak mutant:
M71C
Y110C
K113C
Bcl-X$_L$ mutant:
cys null
M83C
S122C
Q125C
MW
62
49
38
28
14
IP: FLAG (Bcl-X$_L$)
HD
M
WB: HA (Bak)
D
Treated with 50 nM tBid M97A
WB: HA (Bak)
No treatment
WB: FLAG (Bcl-X$_L$)
Treated with 50 nM tBid M97A
*
#
WB: FLAG (Bcl-X$_L$)

Figure 31. BH3:groove cysteine cross-linking of Bak and Bcl-X_L. A) *Structural model and* ***B)*** *schematic representation of the proposed Bak:Bcl-X_L core domain heterodimer based on the structure of the Bak core dimer (PDB code: 4U2V) coloured as indicated in the figure key. Sites of single cysteine mutations are shown as sticks in yellow.* ***C)*** *and* ***D)*** *Immunoblots of proteins immunoprecipitated with FLAG M2 beads from isolated heavy membranes of MEFs expressing the combination of Bak groove (Y110C or K113C, light purple) and Bcl-X_L BH3 (M83C, green) or Bcl-X_L groove (S122C or Q125C, cyan) and Bak BH3 (M71C, dark purple) mutants probed with anti-HA (upper panels) or anti-FLAG (lower panels). Dashed black lines separate different Bak and Bcl-X_L mutant combinations. Digitonin-permeabilised cells expressing cysteine mutant combinations were left untreated (**C**) or treated with 50 nM tBid M97A (**D**). Heavy membranes from these cells were solubilised and isolated in digitonin, and disulphide bond formation was induced with CuPhe. Successful cross-links between Bcl-X_L and Bak resulted in a band shift from monomer (M) to heterodimer (HD). Complete cross-links (where all immunoprecipitated Bak runs as a heterodimer) and incomplete cross-links are indicated by solid and dashed yellow lines, respectively.*

4.3 Discussion

Pro-survival proteins inhibit apoptosis in two ways. Mode 1 involves binding and sequestering of activator BH3-only proteins by the canonical binding of the BH3 domain to the pro-survival groove (Llambi *et al.*, 2011). In Mode 2, activated effector proteins Bax and Bak are sequestered, again via canonical binding of the Bax/Bak BH3 domain to the hydrophobic groove of the pro-survival proteins (Llambi *et al.*, 2011). Beyond pro-apoptotic BH3 domains binding to the hydrophobic groove of pro-survival proteins, little is known about the topology of Mode 2 complexes in the context of a membrane. Here, I provide novel insights into the topology of a small population of Mode 2 inhibitory complexes of the pro-survival protein Bcl-X_L and Bax or Bak with full-length proteins in their native environment on the MOM.

Despite a highly similar fold, pro-survival proteins and pro-apoptotic effector proteins exhibit opposing functions. A possible explanation for this difference in function is that BH3-binding could induce metastable states of Bax and Bak but form stable complexes with pro-survival proteins (Czabotar *et al.*, 2013). Evidence for this is seen in crystal

structures of Bax in complex with Bid, Bim or Bax BH3 peptides, where large internal cavities are created in the Bax protein (Czabotar *et al.*, 2013; Robin *et al.*, 2015). Such cavities can destabilise proteins and are not observed in structures of complexes of pro-survival proteins and BH3 peptides (Baase *et al.*, 2010; Czabotar *et al.*, 2013; Robin *et al.*, 2015).

Activator BH3-only protein binding induces large conformational changes in Bax and Bak (Brouwer *et al.*, 2014; Czabotar *et al.*, 2013; Robin *et al.*, 2015). One of these changes, essential for MOMP, is the separation of the core (α2-5) and latch (α6-8) domains. In solution and working with truncated protein, BH3 peptide-induced activation of Bax and Bak (in the presence of detergent) results in the formation of an off-pathway domain-swapped dimer where the latch of one molecule wraps around the core of an adjacent molecule. The resulting domain-swapped dimer consists of two monomer-like globules connected at the junction of α-helices 5 and 6. Of all the pro-survival proteins, only Bcl-X_L has been observed in the same domain-swapped conformation (Denisov *et al.*, 2007; Follis *et al.*, 2013; O'Neill *et al.*, 2006; Rajan *et al.*, 2015; Tanaka *et al.*, 2013).

The ability to unlatch may be unique to Bcl-X_L among pro-survival proteins, though whether it occurs in a physiological setting remains to be proven. If Bcl-X_L was able to unlatch in cells, it could form pseudo-symmetrical BH3:groove heterodimers with Bax and/or Bak, in the same fashion as Bax/Bak BH3:groove homodimers discussed in Chapter 2 and Chapter 3. The aim of this chapter was to identify these complexes if they exist on mitochondria.

The cysteine cross-linking data presented here agree with other cross-linking studies that show the BH3 domain of Bax binds to the hydrophobic groove of Bcl-X_L (**Figure 28**, **Figure 29** and **Figure 30**) (Ding *et al.*, 2014). Both that study and my work confirm that the canonical BH3:groove interaction seen in the crystal structure of the Bax BH3 domain with C-terminally truncated Bcl-X_L occurs between full-length proteins on the MOM (Czabotar *et al.*, 2011). In addition, I show for the first time that the BH3 domain of full-length Bak binds to the hydrophobic groove of full-length Bcl-X_L on the MOM (**Figure 31**), as predicted by the now 20-year old structure of the

first example of a BH3:groove complex between Bcl-X_L and the Bak BH3 peptide (Sattler *et al.*, 1997).

In initial experiments, heavy membrane fractions containing mitochondria were incubated with Triton X-100 detergent to increase association of Bax and Bcl-X_L (Hsu and Youle, 1998), thereby increasing the chance of detecting low abundance cross-links (**Figure 28** and **Figure 29**). The cross-linking pattern showed that the canonical Bax BH3 to Bcl-X_L groove interaction occurs in the Triton X-100-induced Bax:Bcl-X_L complexes. Heterodimer formation caused by this detergent therefore preserves the most important and physiologically relevant interaction. Digitonin was used as a control detergent, as it should not artificially promote Bax:Bcl-X_L association. Somewhat surprisingly, even in digitonin samples Bax was pulled down by Bcl-X_L and was bound via its BH3 domain to the groove of Bcl-X_L (**Figure 28C**). This was not the case in a later experiment where Bax was only pulled down in samples that had been treated with tBid (**Figure 30C**). Given that the Bax:Bcl-X_L complexes were more evident after an apoptotic stimulus (tBid M97A treatment), this indicates that cells in the experiment depicted in **Figure 28** were likely stressed prior to induction of cross-linking by CuPhe, possibly due to overgrowth. Together, these data suggest that Bax:Bcl-X_L complexes are limited in healthy cells and that Mode 2 complexes predominantly occur following apoptotic stress and activation of Bax.

Nevertheless, in all 3 experiments with Bax, a small population of Bax:Bcl-X_L heterodimers could be cross-linked via the Bcl-X_L BH3 to the Bax hydrophobic groove. Moreover, because the BH3 domain of all Bax pulled down with Bcl-X_L in samples treated with tBid M97A were linked to the Bcl-X_L groove (**Figure 30C**), it seems likely that this small population of heterodimers are BH3:groove heterodimers.

Whether these BH3:groove heterodimers form within endogenous populations of Bax:Bcl-X_L heterodimers requires further investigation. More importantly, whether they play a physiologically relevant role also remains unclear. One way to investigate this could be with core:latch-locked cysteine mutants of Bcl-X_L. The importance of dissociation of the Bax/Bak latch domain from the core was demonstrated by locking them together with a disulphide bond between α-helices 5 and 6 (Brouwer *et al.*, 2014; Czabotar *et al.*, 2013). Disulphide locked Bax and Bak could not release cytochrome *c*

from isolated mitochondria (Brouwer *et al.*, 2014; Czabotar *et al.*, 2013). A similar experiment could be performed by locking α-helices 5 and 6 of Bcl-X_L and assessing its ability to inhibit cytochrome *c* release from isolated mitochondria after treatment with BH3-only proteins.

The possibility of Bak:Bcl-X_L BH3:groove heterodimers has not been demonstrated conclusively in these experiments, despite a hint of a heterodimer band in **Figure 31C** and **D**. It is possible that Bcl-X_L only forms pseudo-symmetrical BH3:groove heterodimers with Bax but not Bak. Alternatively, the pairing of cysteine residues in the groove of Bcl-X_L and the BH3 domain of Bak may not be optimal to link these sites. Repeated experiments with these Bak mutants, and perhaps other BH3/groove mutants, are required to confirm BH3:groove heterodimers of Bak and Bcl-X_L.

Interestingly, far greater amounts of Bak seemed to be pulled down by the Bcl-X_L mutant M83C compared to groove mutants, and the cys null mutant did not pull down any Bak (**Figure 31D**). The cys null Bcl-X_L mutant also pulled down less Bax after treatment with tBid M97A compared to the BH3 and groove mutants (**Figure 29C** and **D**). Based on the relative levels of Bcl-X_L pulled down for each mutant, it appears that expression of cys null Bcl-X_L is lower in comparison to other variants. A blot of the total lysate with loading controls would be useful to determine whether this is actually the case, and future experiments could include Bcl-X_L WT as an additional control. In addition to pulling down more Bak, Bcl-X_L M83C showed laddering (lower panels of **Figure 29C** and **D**, **Figure 30C** and **Figure 31C** and **D**) and smearing (lower panels of **Figure 31C** and **D**), possibly indicating cross-links to proteins other than itself or Bax or Bak. Residue M83 is solvent exposed in structures of Bcl-X_L, and it would be interesting to identify any proteins that cross-link with Bcl-X_L before and after treatment with tBid via mass spectrometry.

Pseudo-symmetrical BH3:groove heterodimer formation has a number of implications for our understanding of Bcl-2 family protein dynamics on the MOM. Such heterodimers would presumably be significantly more difficult to disrupt than a simple pro-apoptotic BH3 in pro-survival groove complex. This could explain why Mode 2 complexes are less easily derepressed than Mode 1 complexes (Llambi *et al.*, 2011), as

BH3-only proteins would be unable to form reciprocal BH3:groove heterodimers. The structural features that distinguish the pro-apoptotic proteins Bak and Bax from their structurally similar pro-survival relatives are currently poorly understood. The fact that Bcl-X_L can also form (pseudo)symmetrical BH3:groove dimers suggests that the difference may lie in the inability of heterodimeric Bcl-X_L complexes to further oligomerise. BH3:groove heterodimers may even act to disrupt the growth of Bak and Bax oligomers by capping the ends of nascent oligomers such that they can no longer propagate. Bcl-X_L is implicated in retrotranslocation of Bax and Bak from the MOM to the cytosol (Edlich *et al.*, 2011; Todt *et al.*, 2015; Todt *et al.*, 2013). If BH3:groove heterodimers embed in the MOM similar to BH3:groove homodimers, their formation would presumably influence retrotranslocation. Further work is required to understand these heterodimers and their significance in the Bcl-2 protein family interactome.

The BH3-binding grooves of pro-survival proteins have been the subject of large drug discovery programs that aim to prevent Mode 1 and 2 inhibition of cell death by overexpressed pro-survival proteins in cancerous cells. Recently, the first clinical success story has emerged from these efforts in the form of ABT-199 (venetoclax/Venclexta), a Bcl-2-specific inhibitor recently approved for the treatment of relapsed 17p-deleted chronic lymphocytic leukaemia (Roberts *et al.*, 2016). Looking beyond the hydrophobic grooves of pro-survival proteins for other interactions that are targetable with drugs may lead to further development of therapeutics to target cells that are resistant to death. Other interaction surfaces that are specific to a single pro-survival protein may create opportunities for new drug classes that target only one type of pro-survival protein. The work presented here is one such attempt to look beyond the pro-survival groove, and provides a base for further research into BH3:groove heterodimers.

4.4 Methodology

4.4.1 Generation of Cell Lines

SV40-immortalised *bax*$^{-/-}$*bak*$^{-/-}$ MEFs were retrovirally co-transduced with combinations of human Bax or Bak single cysteine mutants with an N-terminal HA tag

in internal ribosome entry site (IRES)-GFP expression constructs and human Bcl-X_L single cysteine mutants with an N-terminal FLAG tag in IRES-hygromycin expression constructs. The Bax and Bak cysteine mutants used were from previous work (Dewson *et al.*, 2008; Dewson *et al.*, 2012). The Bcl-X_L BH3 mutant M83C was designed based on the structure of the Bax BH3:groove homodimer (PDB code: 4BDU (Czabotar *et al.*, 2013)) with the Bcl-X_L BH3 helix superposed over the Bax BH3 helix. Bcl-X_L groove mutant constructs had been previously designed by Grant Dewson and Ruth Kluck based on the BH3:groove homodimer cross-linking studies and structures of Bcl-X_L in complex with the BH3 domains of Bax and Bak (Czabotar *et al.*, 2011; Dewson *et al.*, 2008; Dewson *et al.*, 2012; Sattler *et al.*, 1997). Polyclonal GFP-positive, hygromycin-resistant cell lines were established by GFP-positive cell sorting by fluorescence activated cell sorting (FACS) in a flow cytometer followed by application of hygromycin selection as described previously (Dewson *et al.*, 2008).

4.4.2 Isolation of Heavy Membranes and Disulphide Cross-linking

MEF cell lines were grown to confluency, harvested by centrifugation at 1,500 rpm for 5 minutes at 4°C, and washed with ice cold phosphate buffered saline (PBS). The cells were permeabilised by resuspending in M-phase egg lysis buffer (MELB) + protease inhibitors with 0.025% digitonin and incubated on ice for 10 minutes. Permeabilisation was verified by trypan blue staining. At this point, where indicated, permeabilised cells were treated with tBid M97A or tBid WT for 30 minutes at 30°C. The samples were centrifuged at 13,000 rpm for 5 minutes at 4°C and the cytosolic fraction (supernatant) was discarded. The heavy membrane pellet fraction was resuspended in MELB + protease inhibitors with either 1% digitonin or 1% Triton X-100 and incubated on ice for 30 minutes to solubilise membranes. Samples were then centrifuged at 13,000 rpm for 5 minutes at 4°C to pellet cell debris. The supernatant was collected and the oxidant CuPhe was added to a concentration of 1 mM. Samples were incubated for 30 minutes on ice and the reaction was quenched with either 10 mM NEM or 10 mM EDTA and samples were stored at -80°C until IP.

4.4.3 Immunoprecipitation

Sepharose and FLAG M2 beads were washed 3 times in MELB with a final wash in MELB with 1% digitonin or Triton X-100. Samples were pre-cleared in a 1:1 slurry of sepharose:MELB for 1 hour at 4°C on a rotator. The samples were pulse spun in a centrifuge to pellet beads and the supernatant was transferred to a new tube. A 1:1 slurry of FLAG M2:MELB was added to the sample and incubated for 1 hour at 4°C on a rotator. Samples were pulse spun in a centrifuge to pellet beads and the supernatant was discarded. The beads were washed 3 times with MELB with a final wash in MELB with 1% digitonin or Triton X-100. The beads were incubated with 3xFLAG peptide for 30 minutes at 4°C on a rotator to elute bound protein. Samples were pulse spun to pellet beads and supernatant was retrieved for analysis by SDS-PAGE and immunoblotting.

4.4.4 SDS-PAGE

Proteins were heated at 95°C for 5 minutes in non-reducing protein loading dye. After heating, samples were loaded into pre-cast NuPAGE 12% Bis-Tris gels (Life Technologies). Gels were electrophoresed in MES running buffer for 40 minutes at 200 V. Molecular weight of protein bands was estimated using SeeBlue Plus2 Prestained Protein Standard (Life Technologies).

4.4.5 Immunoblotting

SDS-PAGE gels were transferred to polyvinylidene fluoride (PVDF) membranes by Western transfer. The PVDF membranes were blocked overnight in 5% skim milk in TBS-T. After incubation, membranes were washed with TBS-T then incubated with either in house anti-FLAG or Roche anti-HA primary antibodies at 1/1000 for 1 hour at room temperature on a roller. The membranes were washed 3 times over 30 minutes with TBS-T at room temperature on a rocker, then incubated for 1 hour at room temperature with an anti-rat secondary antibody at 1/3000 (Southern Biotech). The membranes were washed again 3 times over 30 minutes with TBS-T at room temperature on a rocker, then washed once with TBS. The Biorad Clarity developing

reagent was added to blots for 5 minutes. Excess reagent was removed and the immunoblots were developed in a Chemidoc system.

Chapter 5

Structural and Functional Characterisation of Bok

Among the Bcl-2 family of proteins, Bok is one of the most controversial in regard to its function. It shares sequence homology with Bak and Bax and induces apoptosis upon overexpression (Hsu *et al.*, 1997). As such, Bok was originally proposed to be a third pro-apoptotic effector protein.

Several groups working on Bok have reported conflicting data on Bok-induced apoptosis. Some groups report a dependency of Bok on Bak and Bax for MOMP (Carpio *et al.*, 2015, 2016; Echeverry *et al.*, 2013; Fernandez-Marrero *et al.*, 2016) while others report Bak/Bax-independent apoptosis (Einsele-Scholz *et al.*, 2016; Llambi *et al.*, 2016). Disentangling these results and establishing the physiological role of Bok has proven difficult.

Structural information is needed in order to better investigate the role of Bok. An X-ray crystal structure or NMR structure would pave the way for site-directed mutagenesis studies to help determine the function of Bok. In this chapter, I detail the expression of several human Bok (hBok) constructs, as well as the rat and chicken Bok homologues (rBok and cBok, respectively). I present the first X-ray crystal structure of the cBok homologue, as well as *in vitro* studies of cBok function.

5.1 Production of Recombinant Bok

Before I began my work on Bok, expression and purification of recombinant Bok had not been reported. Several vectors (pTYB1, pET28a-GFP, pWALDO, pET32a, pGEX-6P-3 and pET15b) containing full-length and truncated human, rat and chicken Bok constructs were tested for expression in *E. coli* (data not shown). Of the vectors tested, only pGEX-6P-3 successfully produced recombinant Bok protein. Using this vector, that encodes an N-terminal GST tag for solubility and purification, I expressed and purified several full-length and truncated constructs of hBok, rBok and cBok (listed in **Table 8**). In all cases, the removal of the hydrophobic C-terminal TM helix was necessary for expression. TM domain removal is a common tactic for recombinant expression of Bcl-2 family proteins. Replacing cysteine residues with serine has

improved yields and stability of constructs of Bak and Bax (Brouwer *et al.*, 2014; Czabotar *et al.*, 2013). The native hBok sequence contains 5 cysteine residues at positions conserved in rBok. Four of the 5 cysteines are conserved in cBok, with a serine replacing hBok residue C67 in the BH3 domain. Chicken Bok has a 5th cysteine, C35, that is a glycine is hBok and rBok. Cysteineless constructs of full length and truncated hBok, rBok and cBok did not express (data not shown).

Table 8. Bok constructs tested in the pGEX-6P-3 vector.

Originating organism	**N-terminal truncation**	**C-terminal truncation**	**Expression**	**Crystal trial attempted**	**Crystals obtained**
Homo sapiens	-	-	No	N/A	N/A
Homo sapiens	ΔN18	ΔC22	Yes	No	N/A
Homo sapiens	-	ΔC22	Yes	No	N/A
Homo sapiens	ΔN18	ΔC26	Yes	Yes	No
Homo sapiens	-	ΔC26	Yes	No	N/A
Homo sapiens	ΔN18	ΔC32	Yes	Yes	No
Homo sapiens	-	ΔC32	Yes	Yes	No
Rattus norvegicus	-	-	No	N/A	N/A
Rattus norvegicus	ΔN18	ΔC32	Yes	Yes	No
Rattus norvegicus	-	ΔC32	Yes	Yes	No
Gallus gallus	-	-	No	N/A	N/A
Gallus gallus	ΔN18	-	No	N/A	N/A
Gallus gallus	-	ΔC32	No	N/A	N/A
Gallus gallus	ΔN18	ΔC32	Yes	Yes	Yes

Proteins were purified by affinity chromatography on glutathione agarose bead columns. On-column cleavage was performed with PreScission protease to remove the GST tag, and proteins were further purified by GF on an S75 10/300 column. Representative chromatograms are presented along with SDS-PAGE gels of peak fractions in **Figure 32**. An extra purification step on a Mono S 5/50 GL cation exchange column was performed in some cases prior to crystallisation trials (e.g. for cBok ΔN18ΔC32 in **Figure 32G**).

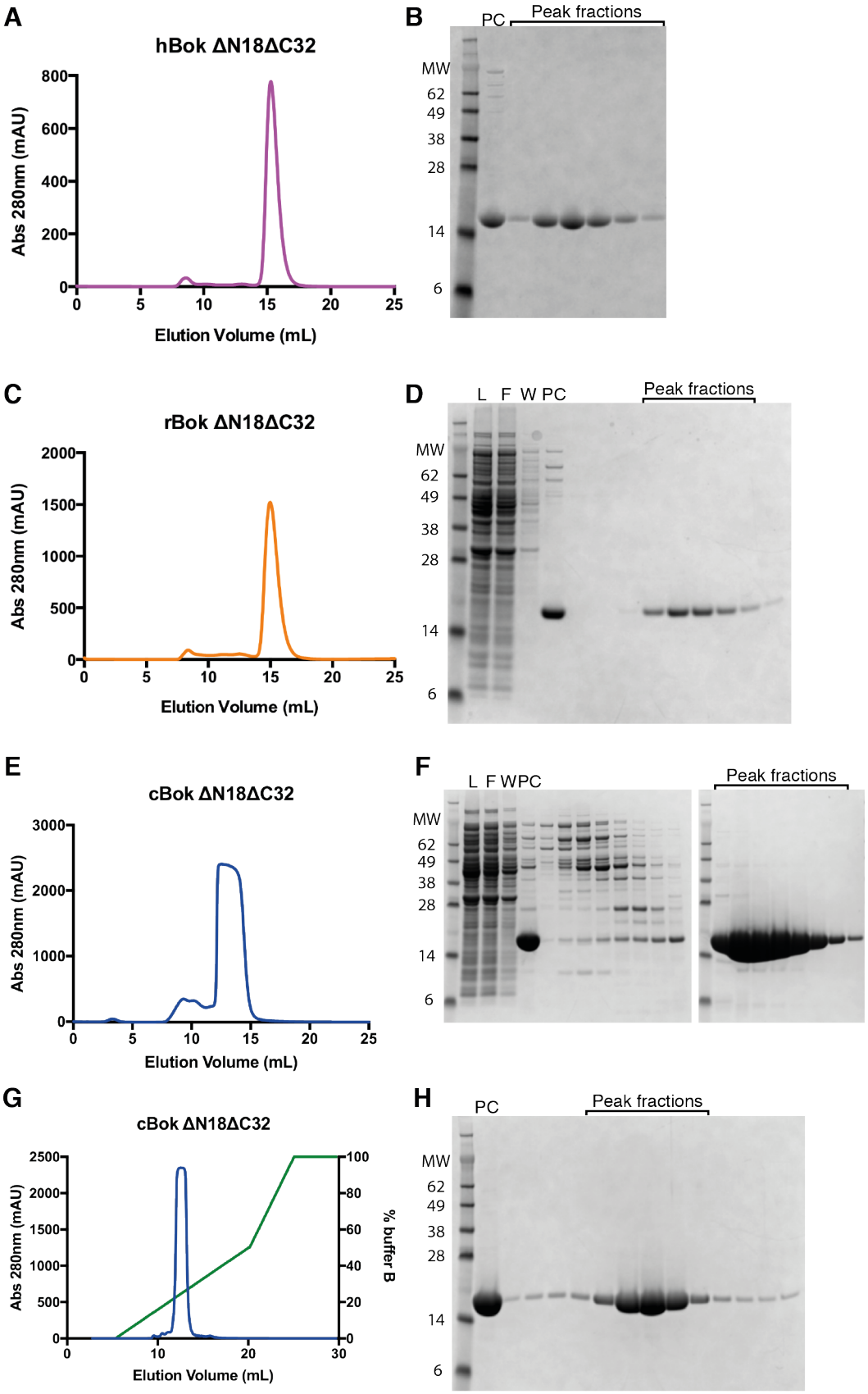
A
hBok ΔN18ΔC32
Abs 280nm (mAU)
Elution Volume (mL)
B
PC
Peak fractions
MW
62
49
38
28
14
6
C
rBok ΔN18ΔC32
Abs 280nm (mAU)
Elution Volume (mL)
D
L F W PC
Peak fractions
MW
62
49
38
28
14
6
E
cBok ΔN18ΔC32
Abs 280nm (mAU)
Elution Volume (mL)
F
L F WPC
Peak fractions
MW
62
49
38
28
14
6
G
cBok ΔN18ΔC32
Abs 280nm (mAU)
% buffer B
Elution Volume (mL)
H
PC
Peak fractions
MW
62
49
38
28
14
6

***Figure 32. Purification of recombinant Bok. A)**, **C)** and **E)** Chromatogram traces of hBok ΔN18ΔC32, rBok ΔN18ΔC32 and cBok ΔN18ΔC32 run on an S75 10/300 column. **G)** Chromatogram trace of cBok ΔN18ΔC32 eluted from a Mono S cation exchange column with an increasing salt gradient (% buffer B, green line). **B)**, **D)**, **F)** and **H)** Corresponding SDS-PAGE gels demonstrating purity of peak fractions from purification steps. Some gels also include the prior GST purification step, L = filtered lysate, F = GST column flowthrough, W = GST column wash, PC = pre-column sample prior to GF column run. In the case of cBok, the large amount of protein overloaded both columns in the purification steps. However, highly pure protein was still obtained.*

With access to pure recombinant protein, I began structural and functional characterisation of Bok.

5.2 X-ray Crystal Structure of Chicken Bok

Multi-BH domain containing pro-apoptotic and pro-survival Bcl-2 proteins share a remarkably similar fold despite their opposing functions. Bok possesses all four BH domains, but whether it assumes the Bcl-2 fold is unknown. To determine the structure of Bok, I performed crystallisation screens using several different constructs of hBok and rBok (**Table 8**). Additionally, I performed reductive lysine methylation on the hBok and rBok ΔN18ΔC32, but no crystals were obtained with this strategy.

After extensive trials with human and rat Bok failed to produce crystals, I turned to the cBok homologue. Bok shows high cross-species conservation, and cBok shares 81% sequence identity and 90% similarity with hBok (**Figure 33**) (Zhang *et al.*, 2000). Chicken Bok ΔN18ΔC32 expressed in large quantities and was purified by GF and cation exchange chromatography (**Figure 32E** and **G**). Following purification, cBok ΔN18ΔC32 readily crystallised within hours of setting up crystal trays. The best diffracting crystals were obtained from drops containing cBok at 7 mg/ml in 22.5% PEG 3350, 0.09 M trisodium citrate [pH 3.5] and 3% ethylene glycol. The crystal belonged to the monoclinic space group $P2_1$ and the structure was solved by molecular replacement. The model that produced the best solution was created from a domain-swapped Bax dimer (PDB code: 4BD8 (Czabotar *et al.*, 2013)). A monomeric globule of Bax was generated from the α1-5 helices (core domain plus α1) of one Bax

polypeptide and the α6-8 helices (latch domain) of the partner chain. Two copies of the search model were placed in the asymmetric unit. Initial model building was performed with PHENIX Autobuild (Terwilliger *et al.*, 2008) and once the majority of both copies was built the structure was refined by iterative rounds of building in COOT (Emsley and Cowtan, 2004) and refinement in PHENIX (Adams *et al.*, 2010) to 1.8 Å (crystallographic statistics are presented in **Table 9**).

Identities: 173/213 (81%)
Positives: 192/213 (90%)
Gaps: 1

```
                                ΔN18
                                ▼
human     1      MEVLRRSSVFAAEIMDAFDRSPTDKELVAQAKALGREYVHARLLRAGLSWSAPERAAPVP 60
consensus        MEVLRRSSVFAAE+M+ FDRSPTDKELV+QAKAL R+Y+++RL+RAG+SWS PE   PVP
chicken   1      MEVLRRSSVFAAEVMEVFDRSPTDKELVSQAKALCRDYINSRLIRAGVSWSKPEHNTPVP 60

human     61     G-RLAEVCAVLLRLGDELEMIRPSVYRNVARQLHISLQSEPVVTDAFLAVAGHIFSAGIT 119
consensus        G +LAEV A+LLRLGDELE IRP+VYRN+ARQL+ISL SE VVTDAFLAVA  IF+AGIT
chicken   61     GGKLAEVSAILLRLGDELEYIRPNVYRNIARQLNISLHSETVVTDAFLAVAAQIFTAGIT 120

human     120    WGKVVSLYAVAAGLAVDCVRQAQPAMVHALVDCLGEFVRKTLATWLRRRGGWTDVLKCVV 179
consensus        WGKVVSLYAVAAGLAVDCVR AQPAMVH +VDCLGEFVRKTL TWL+RRGGW D+ KCVV
chicken   121    WGKVVSLYAVAAGLAVDCVRHAQPAMVHTIVDCLGEFVRKTLVTWLKRRGGWADITKCVV 180
                                                                      ▲
                                                                      ΔC32
human     180    STDPGLRSHWLVAALCSFGRFLKAAFFVLLPER 212
consensus        STDP LRSHWLVAA+CSFG FLKA FFVLLPER
chicken   181    STDPSLRSHWLVAAVCSFGHFLKAIFFVLLPER 213
```

Figure 33. Sequence identity and similarity between human and chicken Bok. *The aligned sequences of human and chicken Bok demonstrate a high level of sequence identity and similarity. Identical residues between the two sequences are shown in the consensus sequence, while "+" indicates similar residues. The N- and C- terminal truncations of the cBok construct that crystallised are labelled.*

Table 9. Data collection and refinement statistics for cBok ΔN18ΔC32.

Wavelength	0.9537
Resolution range	36.53 - 1.799 (1.863 - 1.799)
Space group	P 1 21 1
Unit cell	41.559 59.62 64.083 90 96.258 90
Total reflections	110754 (10384)
Unique reflections	28655 (2803)
Multiplicity	3.9 (3.7)
Completeness (%)	98.50 (95.75)
Mean I/sigma(I)	12.93 (0.80)
Wilson B-factor	31.21
R-merge	0.06552 (2.155)
R-meas	0.0757 (2.503)
CC1/2	0.999 (0.593)
CC*	1 (0.863)
Reflections used in refinement	28603 (2797)
Reflections used for R-free	1996 (195)
R-work	0.1948 (0.4300)
R-free	0.2316 (0.4750)
Protein residues	309
RMS(bonds)	0.005
RMS(angles)	0.66
Ramachandran favoured (%)	97.03
Ramachandran allowed (%)	2.97
Ramachandran outliers (%)	0
Rotamer outliers (%)	0.78
Clashscore	11.49
Average B-factor	54.22
macromolecules	54.04
ligands	71.53
solvent	53.81

Statistics for the highest-resolution shell are shown in parentheses.

Both copies of cBok assumed the canonical Bcl-2 helical bundle fold. Chain B of the cBok structure is compared to Bak (PDB code: 2IMT (Moldoveanu *et al.*, 2006)) in an overlay of the two proteins presented in **Figure 34A**. Chains A and B of the cBok structure are overlayed in **Figure 34B**. The two copies are very similar in fold with notable exceptions at the junction of the α2 and α3 helices, the α3 helix and the canonical hydrophobic groove. Chain A displayed two helical turns separated by a convoluted fold at helix α3, whereas chain B possessed a recognisable α3 helix. Helix α2 of chain B was kinked near the α2/α3 junction and a hole through the protein was observed between this area and the hydrophobic α5 helix (**Figure 34C)**. The hole itself is hydrophobic and collapsed in chain A, resulting in distortion of α3 (**Figure 34D**). In chain B, the hydrophobic BH3-binding groove was occluded by residues Q92 and Q113 that form reciprocal hydrogen bonds between the donor and acceptor groups of each side chain (**Figure 35A**). Chain A adopted a more open conformation in the groove with the collapse of α3 (**Figure 35B**). B-factors in α3 and the loop to α4 were higher than the rest of the structure in both chain A and B (**Figure 34E** and **F**).

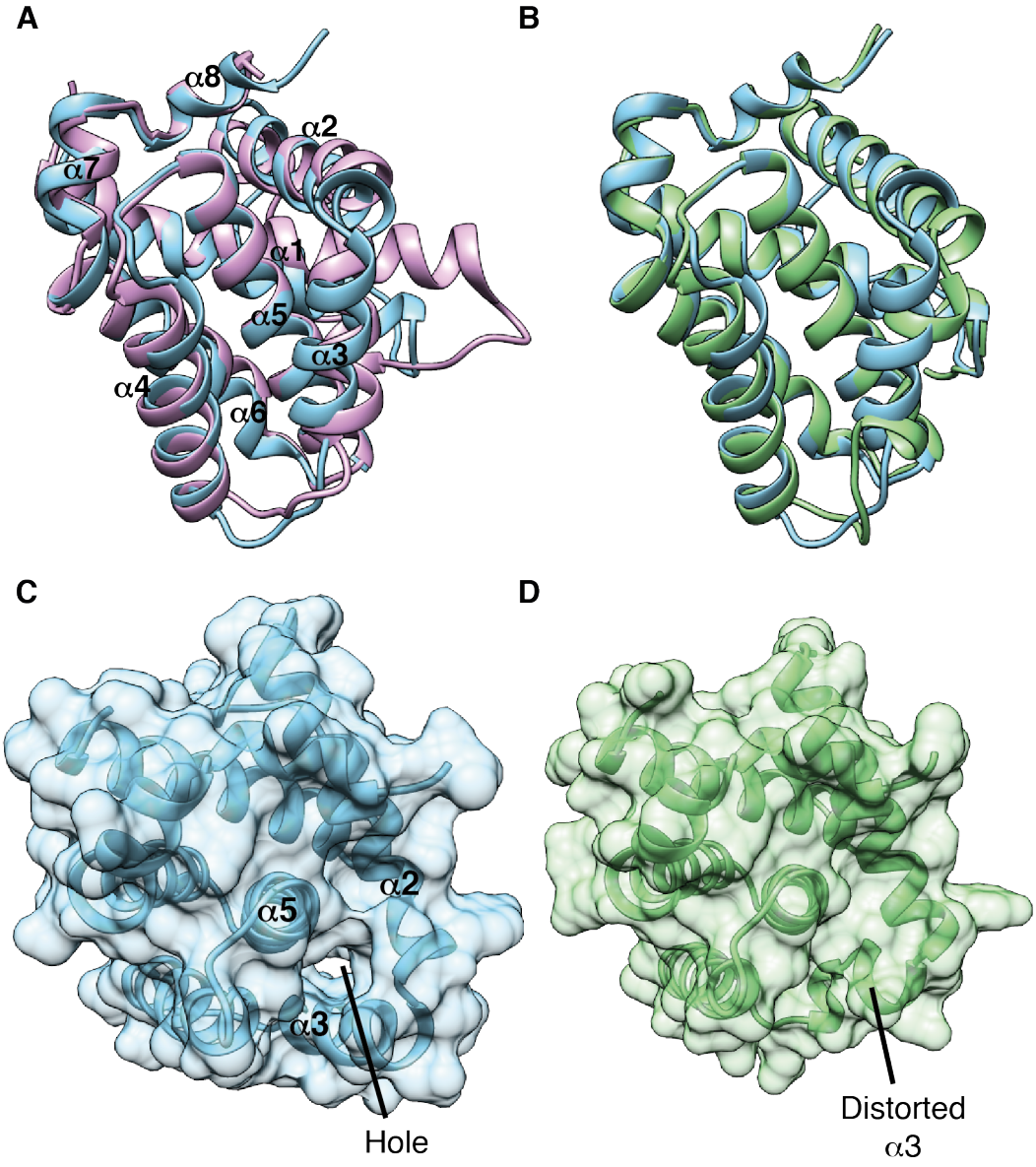
A
α8
α2
α7
α1
α5
α3
α4
α6
B
C
α2
α5
α3
Hole
D
Distorted
α3
E
α2
α3
F
α2
α3

Figure 34. X-ray crystal structure of chicken Bok ΔN18ΔC32. A) *Chain B from the crystal structure of cBok ΔN18ΔC32 (coloured sky blue) overlayed with Bak (coloured plum, PDB code: 2IMT (Moldoveanu et al., 2006)). Helices α1 to α8 are labelled.* ***B)*** *Overlay of chain A (coloured light green) and chain B from cBok ΔN18ΔC32 crystal structure.* ***C)*** *and* ***D)*** *Surface representation of chains B and A, respectively. A hole through chain B, bounded by α-helices 2, 3 and 5, is labelled.* ***E)*** *and* ***F)*** *Chains B and A, respectively, of the cBok structure coloured by B-factor from low (blue) to high (red). The highest B-factors are observed around α3 and the α3 to α4 loop.*

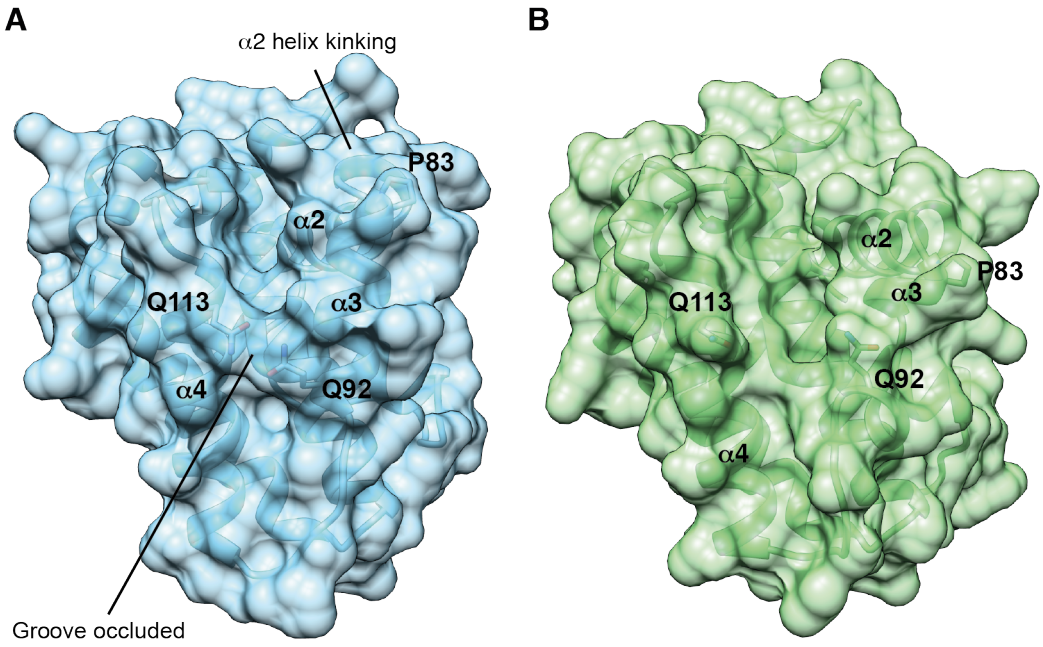

Figure 35. Differences in BH3 helix kinking and groove occlusion between the two copies of cBok. A) *Chain B from the crystal structure of cBok ΔN18ΔC32 shown in cartoon representation with a transparent surface. Residues P83, Q92 and Q113 are shown as sticks. The canonical hydrophobic groove of chain B is occluded by residues Q92 and Q113 that form hydrogen bonds between α3 and α4.* ***B)*** *Chain A represented in the same way as chain B. The collapse of α3 in chain A results in the breaking of hydrogen bonds between Q92 and Q113 and an open conformation for the hydrophobic groove. The collapse also relieves the severe kinking of the C-terminus of the α2 BH3 helix in chain B.*

Taken together, these observations suggest that cBok may be flexible and dynamic in this region. An atypical proline at position 83 could be the cause of instability (**Figure 35**). This proline is unique to Bok among human Bcl-2 family proteins, but is highly conserved among Bok homologues, even in evolutionarily distant organisms such as fruit flies and zebrafish.

The dynamic nature of the α2/α3 junction and α3 helix is potentially of interest because of its proximity to the BH3 domain. BH3 domain exposure is an important step in the activation of Bak and Bax (Dewson *et al.*, 2008; Dewson *et al.*, 2012). The BH3 domain helix α2 of both copies of cBok make crystal contacts and have low B-factors in the structure (**Figure 34E** and **F**). However, if this region were constantly being exposed in the cell it could provide a rationale for the proposed constitutive activity of Bok (Llambi *et al.*, 2016).

Liposome dye release assays have been used to demonstrate the constitutive activity of hBok (Fernandez-Marrero *et al.*, 2017; Llambi *et al.*, 2016). With the structure of cBok now available, I set out to compare the function of these homologous proteins and determine whether cBok recapitulates hBok auto-activity *in vitro*.

5.3 Membrane Permeabilisation by Bok

Liposomal systems are used to measure the membrane-permeabilising activity of both Bak and Bax *in vitro*. In these systems, self-quenching dyes such as carboxyfluorescein are encapsulated in liposomes with a lipid composition resembling the MOM. Membrane permeabilisation is measured by fluorescence increase as dye is released from the liposomes. Human Bok has been shown to form pores in liposomes mimicking the MOM or, to a lesser extent, the ER (Fernandez-Marrero *et al.*, 2017; Llambi *et al.*, 2016).

To investigate the membrane activity of cBok, I took a similar approach to that later outlined in Llambi *et al*. 2016. Because Bok could not be produced with an intact TM domain, I used a C-terminally truncated version of cBok where the TM anchor was replaced with a His-tag. This approach has also been used to target both Bak and hBok to MOM-mimicking liposomes doped with 5% nickel-chelating lipid (Llambi *et al.*,

2016; Oh *et al.*, 2010). The N-terminal 18 residues, predicted to be a region of disorder by secondary structure predictions, were removed in one of the constructs.

Given its pro-apoptotic activity but primarily ER-based localisation, cBok was tested on MOM- and ER-mimicking liposomes (MOMmix and ERmix, respectively). The composition of the MOMmix liposomes was based on a published protocol (Kuwana *et al.*, 2002). ERmix liposomes were based on the composition of rat liver ER (Keenan and Morre, 1970). Recombinant cBok or hBak constructs with C-terminal His-tags were added to MOMmix or ERmix liposomes doped with 5% nickel-chelating lipid and incubated for 2 hours with or without Bid BH3 peptide. Liposome permeabilisation was measured by fluorescence caused by release of the carboxyfluorescein dye from liposomes. Percentage maximum release was calculated by normalising with liposomes with or without Bid peptide as 0% release and liposomes with 3% CHAPS as 100% release.

On both MOMmix and ERmix liposomes, hBak ΔN22ΔC25-6xHis demonstrated Bid BH3 peptide-dependent permeabilisation (**Figure 36A** and **B**). Contrastingly, and in agreement with work on hBok, both cBok constructs caused the same level of permeabilisation of MOM-mimicking membranes regardless of the presence of Bid peptide (**Figure 36A**) (Fernandez-Marrero *et al.*, 2017; Llambi *et al.*, 2016). Interestingly, cBok permeabilised ERmix liposomes to a similar degree as unstimulated hBak, suggesting the constitutive BH3 peptide-independent activity of cBok is dependent on lipid composition (**Figure 36B**). Lipid composition dependence has also been observed in liposome permeabilisation experiments with hBok, where higher concentrations of hBok were required to permeabilise ER-mimicking membranes compared to MOM-mimicking membranes (Fernandez-Marrero *et al.*, 2017). A small difference was observed between hBak ΔN22ΔC25-6xHis and cBok ΔC32-6xHis on ERmix liposomes, though this result should be interpreted with caution due to the use of adjusted p-values.

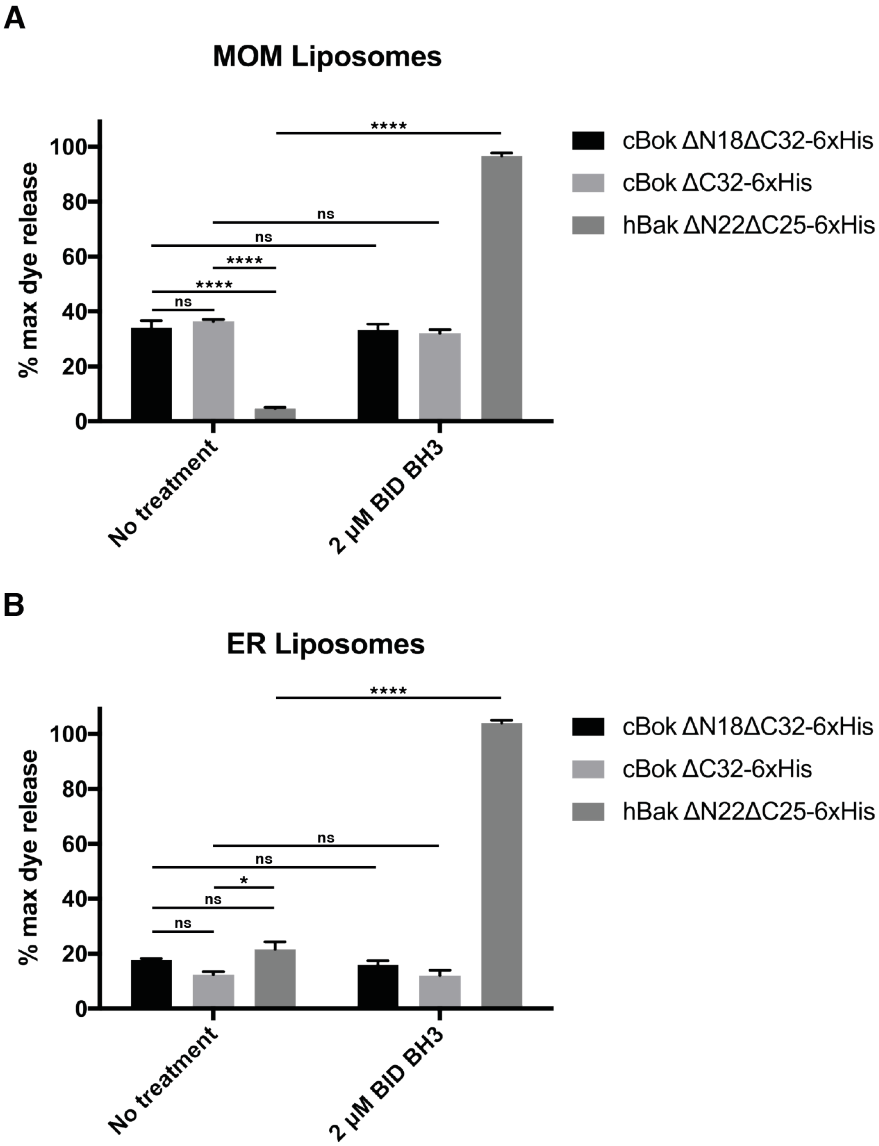

Figure 36. Membrane activity of Bok on liposomes. A) *and* ***B)*** *Liposome permeabilisation by cBok and hBak as measured by carboxyfluorescein dye release from MOMmix (**A**) and ERmix (**B**) liposomes, both doped with 5% NTA(Ni) lipid. 50 nM cBok ΔN18ΔC32-6xHis, cBok ΔC32-6xHis or hBak ΔN22ΔC25-6xHis was incubated with liposomes for 2 hours with or without Bid BH3 peptide followed by measurement of fluorescence. Data are represented as mean ± SEM of percentage maximum dye release, n=3. Data were analysed by two-way ANOVA comparing every mean to every other mean, and multiplicity adjusted p-values (Wright, 1992) were calculated with Tukey's test, 0.1234 (not significant, ns), 0.0332 (*), 0.0021 (**), 0.0002 (***), <0.0001 (****).*

Like hBok, cBok permeabilised liposomes mimicking the MOM and its activity was not enhanced by the activating BH3 peptide of Bid. ER-mimicking liposomes were permeabilised to a lesser degree with the same amount of cBok, and the level of permeabilisation was commensurate with unstimulated hBak. The similarity in sequence and function of hBok and cBok suggest that the crystal structure of the latter represents a good model of the former.

5.4 Discussion

The literature on Bok is plagued with apparent contradictions. Build-up of Bok upon proteasome inhibition leads to apoptosis in Bak/Bax DKO cells (Llambi *et al.*, 2016), but C-terminally truncated Bok that binds to isolated mitochondria does not cause MOMP (Fernandez-Marrero *et al.*, 2017). A role for Bok in induction of intrinsic apoptosis in response to ER stress has been reported but hotly disputed (Carpio *et al.*, 2015, 2016; Fernandez-Marrero *et al.*, 2016). These contradictions, compounded with a lack of structural information, have continued to dog the field even with the recent upturn in publications on Bok.

Here, I present the first structure of Bok that will contribute to understanding this perplexing protein. Chicken Bok adopted the canonical Bcl-2 alpha-helical bundle fold, consistent with the presence of all four BH domains. The structure overlayed well with the pro-apoptotic protein Bak, but displayed interesting deviations that may explain the constitutive activity of Bok. First and foremost, the two copies of cBok differed markedly around the α2/α3 junction and canonical hydrophobic groove. The difference between the copies suggests that the protein may be dynamic and flexible in this region in solution and potentially on the MOM or ER membrane.

An atypical proline (P83) in Bok at the α2/α3 junction may be the cause of instability. Proline is unique among amino acids in that the α-amino group is fused to the side chain, forming a pyrrolidine ring. The lack of a free amide proton to participate in hydrogen bonding and the steric bulk of the pyrrolidine ring causes proline residues to often break or kink helices if present beyond the 3rd or 4th position in the helix (Woolfson and Williams, 1990). In helix initiation, prolines are favoured at the Ncap + 1 position; that is, the residue following the residue whose backbone carbonyl

oxygen atom forms the first hydrogen bond with the amide of the *i* + 4 residue (Kim and Kang, 1999; Richardson and Richardson, 1988). Indeed, in both the A and B chains of the cBok structure, P83 is at the Ncap + 1 position of the α3 helix. The perturbations of the structure, including formation of a hole through chain B, kinking of the C-terminus of α2 in chain B, collapse of α3 in chain A, and high B-factors, point to dynamic flexibility in this region. The hydrophobic hole and the collapse or formation of α3 is unlikely to be due to crystal contacts, because the α3 is bordered by solvent and not in proximity to protein. Kinking of the BH3 domain helix α2 is particularly interesting given the importance of BH3 exposure in Bak and Bax activation and homodimer formation (Alsop *et al.*, 2015; Dewson *et al.*, 2008; Dewson *et al.*, 2012). In both copies of the cBok structure, the α2 BH3 helix of one copy is held in by the α1-2 loop of the other copy and α-helices 4 and 6 of a symmetry-related chain. Without these stabilising crystal contacts, it is possible that the BH3 domain of Bok may be constantly exposed in solution or on the membrane. Moreover, the hydrophobic hole seen through chain B next to the BH3 domain is potentially destabilising in a similar way to the cavities induced by activator BH3 peptides in Bax and Bak ((Czabotar *et al.*, 2013; Robin *et al.*, 2015) and unpublished work from the Czabotar and Colman labs by Jason Brouwer).

Another interesting disparity between the two cBok copies is the "openness" of the canonical hydrophobic groove. The α3 helix in chain B is in close proximity to α4, with glutamine residues Q92 and Q113 forming hydrogen bonds between the helices and occluding the groove. These hydrogen bonds are broken with the collapse of α3 in chain A, resulting in a more open groove. Whether cBok adopts both of these conformations in solution or at the membrane is unclear. Nevertheless, the possibility of switching between an open or occluded groove has implications for BH3 domain binding, be it to an activator BH3 domain or the BH3 domain of another Bok molecule. The groove of Bok would need to be able to receive the BH3 domain of a partner Bok molecule if, like Bak and Bax, Bok forms BH3:groove homodimers prior to oligomerisation.

The groove of Bok differs from other Bcl-2 proteins in the highly conserved BH1 domain. The primary sequence is NWGR in the BH1 domain of almost all other human multi-BH domain Bcl-2 proteins. Only Bok and another very poorly characterised Bcl-2

protein, Bcl-RAMBO, differ in the BH1 motif, with threonine and lysine replacing the asparagine and arginine, respectively. TWGK is also present in chicken Bok, as well as most other Bok homologues. The change in residues makes little difference in the fold when comparing the monomeric structures of hBak (PDB code: 2IMT (Moldoveanu *et al.*, 2006)) and cBok (both copies). However, on BH3 domain binding, the salt bridge formed with the conserved aspartate in the BH3 domain would have different geometry with lysine as opposed to arginine in the BH1 domain (Donald *et al.*, 2011). On top of this, the guanidinium group of arginine is able to form multiple interactions with different residues, whereas the lysyl side chain is more restricted in the number of interactions possible. Whether or not this difference would be significant enough to affect function requires further investigation, but may explain why Bok is not activated by BH3 peptides (Llambi *et al.*, 2016).

Human Bok permeabilises MOM-mimicking liposomes in the absence of BH3-peptide stimulation, and its activity is not enhanced by the BH3 peptides of Bid, Bim, PUMA, Bmf, Bad or Noxa (Llambi *et al.*, 2016). Here, I show that cBok also permeabilises MOM-mimicking liposomes, and its activity is not enhanced by the BH3 peptide of the activator BH3-only protein Bid. Furthermore, higher concentrations of hBok were required to permeabilise ER-mix liposomes compared to MOM-mix liposomes (Fernandez-Marrero *et al.*, 2017). I observed similar differences in permeabilisation by cBok. In the absence of Bid peptide, cBok was far more active than hBak on MOM-mimicking liposomes but not ER-mimicking liposomes. Differences in the lipid composition of MOM- and ER-mix liposomes may be responsible for the decreased pore-forming activity on ER-mimicking liposomes seen here for cBok and in published work for hBok (Fernandez-Marrero *et al.*, 2017). For example, MOM-mix liposomes contain cardiolipin, a mitochondrion-specific, negatively charged phospholipid that induces negative membrane curvature, while ER-mix liposomes contain LysoPC that induces positive curvature. The data presented here are consistent with the idea that Bok may form toroidal pores which are influenced by the intrinsic curvature of bilayers (Fernandez-Marrero *et al.*, 2017).

Given the similarities in sequence (81% identity) and function between hBok and cBok, the structure of cBok likely represents a good model in the absence of an hBok structure. With a structure of Bok in hand, structure-based site-directed mutagenesis becomes

possible. As discussed, the α2/α3 junction, hydrophobic groove and BH1 domains are regions of particular interest based on the cBok structure. In particular, mutation of proline 83 or replacing the α2/α3 junction with the equivalent region on Bak could be useful for understanding why Bok appears to be auto-active. Additionally, mutation of the lysine in the BH1 domain to arginine could provide interesting insights into the importance of conservation of salt bridge geometry to BH3 domain binding, BH3-mediated activation, and homodimerisation of pro-apoptotic effector proteins.

5.5 Methodology

5.5.1 Cloning, Expression and Purification of hBok, rBok and cBok

Different constructs of the wild type sequence of rBok and sequences of hBok and cBok codon-optimised for expression in *E. coli* were cloned into the pGEX-6P-3 expression vector and transformed into either Rosetta, ER2566 or BL21 (DE3) *E. coli* cells. Cells were grown at 37°C in SB to an O.D. (600 nm) of ~1.0 and induced to express overnight at 18°C with 1 mM IPTG. Cells were lysed in GST buffer pH [8.0] and lysates were filtered through a 0.45 μm pore size filter then passed over a glutathione agarose column. The column was washed with GST buffer and Bok was cleaved from the GST fusion partner on-column over 3 nights at 4°C with PreScission Protease (0.02 mg/mL). Bok was eluted from the column in GST buffer then purified by GF (S75 10/300) in TBS pH [8.0]. Purification of some constructs for crystallisation involved an extra purification step on a Mono S 5/50 GL cation exchange column in 20 mM HEPES pH [7.0] with a shallow gradient from 0.03 to 1 M NaCl.

5.5.2 SDS-PAGE

Proteins were heated at 95°C for 5 minutes with reducing protein loading dye. After heating, samples were loaded into pre-cast NuPAGE 12% Bis-Tris gels (Life Technologies). Gels were electrophoresed in MES running buffer for 40 minutes at 200V. Gels were fixed and stained with Coomassie stain (2% Coomassie R250 Brilliant Blue w/v, 10% acetic acid v/v, 40% ethanol v/v) for 30 minutes before removal of excess Coomassie with a destaining buffer (10% acetic acid v/v, 40% ethanol v/v).

Molecular weight of protein bands was estimated using SeeBlue Plus2 Prestained Protein Standard (Life Technologies).

5.5.3 Crystallisation, Data Collection, and Processing

Crystallisation trials were performed in 96-well sitting drop plates at the CSIRO C3 facility in Parkville. Chicken Bok ΔN18ΔC32 crystallized at 7 mg/ml in 22.5% PEG 3350, 90 mM trisodium citrate [pH 3.5], 3% ethylene glycol. Crystals were frozen in well solution supplemented with 20% ethylene glycol and X-ray data were collected at the MX2 beamline of the Australian Synchrotron. Data were processed with XDS (Kabsch, 2010) and the structure was solved by molecular replacement by searching for two monomeric globules created from the Bax domain-swapped dimer (PDB code: 4BD8 (Czabotar *et al.*, 2013)) in PHASER (McCoy *et al.*, 2007). The monomeric globule of Bax consisted of the α1-5 helices of one Bax polypeptide and the α6-8 helices of the partner chain. Initial model building was performed in PHENIX Autobuild (Terwilliger *et al.*, 2008) and the structure was refined with iterative rounds of building in COOT (Emsley and Cowtan, 2004) and refinement in PHENIX (Adams *et al.*, 2010).

5.5.4 Structure Analysis and Figure Generation

Molecular graphics for structural figures were generated in PyMOL (Delano, 2002).

5.5.5 Liposome Release Assay

Lipid mixtures mimicking the composition of the MOM (46% POPC, 25% 18:1 (Δ9-Cis) PE, 11% Liver PI, 10% 18:1 phosphatidylserine (PS) and 8% 18:1 cardiolipin) or the ER (61% POPC, 19% 18:1 (Δ9-Cis) PE, 9% Liver PI, 4% 16:0 LysoPC, 4% Brain, Porcine sphingomyelin, 3% 18:1 PS) were doped with 5% 18:1 DGS-NTA(Ni) lipid and dried in chloroform and 0.01% butylated hydroxytoluene under N_2 gas, and then resuspended in SUV buffer (10 mM HEPES pH [7.5], 135 mM KCl, 1 mM $MgCl_2$) containing 50 mM 5(6)-carboxy-fluorescein. Liposomes were extruded through a 100 nm pore size membrane and passed over a PD10 desalting column to remove excess dye. Liposomes (4 μg/mL) were incubated with recombinant

cBok or hBak with or without human Bid BH3 peptide for 2 hours at room temperature. 5(6)-carboxy-fluorescein fluorescence was measured with an excitation wavelength of 485 nm and an emission wavelength of 535 nm. Statistical analyses were performed with Tukey's test using GraphPad Prism version 7 for Mac, GraphPad Software, La Jolla California USA, www.graphpad.com, which was also used to generate the graphs.

Chapter 6

Conclusions and Future Directions

Multi-BH domain pro-apoptotic effector proteins play a pivotal role in development and tissue homeostasis, and their dysregulation is a feature of many diseases including cancer, autoimmunity and neurodegenerative disease (Czabotar *et al.*, 2014). Despite their importance, many questions remain surrounding the function and mechanisms of action of these proteins. While much progress has been made in understanding how Bak and Bax become activated and homodimerise at the molecular level, our knowledge of oligomerisation, interactions with the membrane and MOMP remains largely macromolecular. Far less still is known regarding Bok and its role in the cell. The aim of this thesis was to better understand the structure and function of these proteins and how they are regulated at the molecular level.

How Bak and Bax oligomerise and cause MOMP is one of the most outstanding unanswered questions in the field of intrinsic apoptosis. I therefore find the structures and results presented in **Chapter 2** to be the most exciting aspect of this thesis, as they could lead to a paradigm shift in a field that has traditionally focused on protein:protein interactions. Despite the primary localisation of most Bcl-2 family proteins at the MOM, structures of these proteins in complex with lipid were lacking before this work. Although the role of lipids has been explored to some extent, it is mainly in the context of the properties of the membrane bilayer rather than how individual lipid molecules could influence oligomerisation or pore formation (Basanez *et al.*, 2002; Bleicken *et al.*, 2013a; Kuwana *et al.*, 2002; Landeta *et al.*, 2011; Terrones *et al.*, 2004). The consistent binding of lipid to the α5/α5' grooves and the cross-linking of Bak homodimers by lipid acyl chains in the cylinder structure suggest that oligomerisation of Bak could be mediated by lipid. Inter-dimer interfaces mediated by lipid provide a sensible alternative to protein:protein interfaces in Bak (or Bax) oligomers that have been extensively searched for without success.

Phospholipase-induced dissociation of Bak oligomers supports a role for lipid in the structural integrity of the oligomers, but does not conclusively demonstrate a requirement for lipids at interfaces between homodimers. Experiments involving mutation of the lipid binding site or investigation of the requirement of lipid for

oligomerisation via native mass spectrometry would better confirm or disprove the lipid-mediated oligomerisation hypothesis (Gupta *et al.*, 2017). Mutation of the lipid binding site could also affect the way Bak interacts with the membrane in terms of membrane disruption and pore edge stabilisation, as theorised in **Figure 22**. Evidence that the membrane itself is likely just as important in the function of Bak and Bax as the proteins themselves continues to build. This work contributes to a more lipid-involved view of MOMP by Bak and Bax.

While the BH3:groove fold of Bax core homodimers had been confirmed by X-ray crystallography (Czabotar *et al.*, 2013), a picture of the molecular interactions that govern this fold at atomic resolution was missing before this work. The 2.4 Å structure in **Chapter 3** fills this gap in our knowledge of Bax homodimerisation. High-resolution structural information is almost mandatory for modern drug-design programs, and homodimerised Bax and Bak represent potentially unique targets. Stabilising or destabilising homodimers could be a novel therapeutic avenue for treating diseases such as cancer and autoimmune/degenerative disorders characterised by insufficient or excessive apoptosis, respectively.

Work with the Bax core domain construct also presented a tantalising piece of information; i.e. as with Bak, Bax core domains associate with lipid. It was both exciting and disappointing that crystals of these complexes could be produced but were heavily twinned. Future work to decrease or prevent twinning in these crystals could be very important, as demonstration of the existence of analogous lipid binding sites on Bax would lend weight to the lipid-mediated oligomerisation hypothesis proposed here for Bak.

Pro-survival proteins inhibit activated Bak and Bax by forming Mode 2 complexes. These complexes involve binding of the Bak/Bax BH3 domain to the pro-survival protein hydrophobic groove, but beyond this interaction little is known of the topology of Mode 2 complexes on membranes. In **Chapter 4**, I showed that the Bcl-X_L BH3 domain can be cross-linked to the Bax hydrophobic groove in cells, suggesting that some Mode 2 complexes may be pseudo-symmetrical BH3:groove heterodimers. The physiological relevance of conformational changes in Bcl-X_L during apoptosis, such as unlatching of the core and latch domains, could be investigated with cysteine-pinned

Bcl-X_L on isolated mitochondria, as performed previously for Bax and Bak (Brouwer *et al.*, 2014; Czabotar *et al.*, 2013). Is the ability to form BH3:groove heterodimers unique to Bcl-X_L? A more extensive cysteine cross-linking study with multiple pro-survival proteins and Bak and Bax would answer this question. In addition, assessing changes in susceptibility to digestion with specific proteases (such as proteinase K, as used to assess Bak conformational change (Iyer *et al.*, 2016)) would be useful for determining whether pro-survival proteins undergo significant conformational change before, during, or after activation of Bak and Bax. Finally, an X-ray crystal structure of a Bax:Bcl-X_L BH3:groove core heterodimer would be useful in better understanding these Mode 2 complexes.

The significance of such complexes in cells was not investigated here, but could provide novel targets for therapeutic manipulation of apoptosis. Cancer cells can become addicted to pro-survival Bcl-2 family proteins in order to restrain Bak and Bax at the MOM and prevent apoptosis. Mode 2 complexes represent the last line of defence in preventing MOMP and apoptosis. Recent studies hint at the importance of Mode 2 complex formation for the survival of certain cancers (Dai *et al.*, 2015; Inoue-Yamauchi *et al.*, 2017). The existence of such complexes may determine the drug sensitivity of a tumour (Dai *et al.*, 2015). Even in certain non-pathological settings, Mode 2 complex formation is essential for cell survival. For example, platelet survival and thymic T-cell development, two processes heavily reliant on Bcl-X_L (Ma *et al.*, 1995; Mason *et al.*, 2007; Motoyama *et al.*, 1995), are impaired when Mode 2 interactions are disrupted with a single point mutation in Bak that prevents it from binding to Bcl-X_L (Lee *et al.*, 2016). There is still much to learn with regard to topology of Mode 2 complexes that will inform our understanding of their physiological and pathophysiological roles. The work in **Chapter 4** contributes to this understanding and raises further questions for future work.

Of the multi-domain pro-apoptotic Bcl-2 family proteins, our understanding of Bok lags far behind Bak and Bax. This can be attributed in part to the lack of a clear phenotype in Bok knockout mice or cells, and the lack of a recombinant expression system to discern the function of Bok *in vivo* and *in vitro*, respectively. In **Chapter 5**, I provide a method for expressing and purifying recombinant human, rat and chicken Bok for functional and structural studies. I show that recombinant chicken Bok

recapitulates the constitutive activity of human Bok on liposomal membranes observed by other groups (Fernandez-Marrero *et al.*, 2017; Llambi *et al.*, 2016). The crystal structure of chicken Bok confirms that the protein adopts the canonical Bcl-2 fold with a few interesting anomalies that may explain its constitutive activity. In particular, the distorted fold around the α2/α3 junction and differences between Bok monomers in the asymmetric unit of the crystal suggest instability in the region. The hole observed through one monomer in the structure is reminiscent of the destabilising cavities seen in Bax and Bak upon activator BH3 binding ((Czabotar *et al.*, 2013; Robin *et al.*, 2015) Jason Brouwer, unpublished), and could result in constitutive exposure of the BH3 domain. Future work could involve mutational probing of this region to determine its functional significance. Alleviating the tension via mutation may prevent the constitutive activity of Bok and turn it into a Bak/Bax-like protein that responds to BH3-only protein activation.

We know Bok is able to permeabilise membranes, but does it unlatch and form BH3:groove homodimers like Bak and Bax? The development of an expression system for recombinant Bok detailed here will allow us to answer questions regarding its function, including what the similarities and differences are between Bok, Bak and Bax.

Dysfunction of the intrinsic apoptotic pathway is a feature common to many diseases and a better understanding of the molecular interactions and mechanisms that govern apoptosis is essential for the development of novel therapies. Taken together, the results in this thesis further our understanding of the multi-BH domain pro-apoptotic effector proteins that are central to the intrinsic apoptotic program.

Bibliography

Adams, P.D., Afonine, P.V., Bunkoczi, G., Chen, V.B., Davis, I.W., Echols, N., Headd, J.J., Hung, L.W., Kapral, G.J., Grosse-Kunstleve, R.W.*, et al.* (2010). PHENIX: a comprehensive Python-based system for macromolecular structure solution. Acta Crystallogr D Biol Crystallogr *66*, 213-221.

Alsop, A.E., Fennell, S.C., Bartolo, R.C., Tan, I.K., Dewson, G., and Kluck, R.M. (2015). Dissociation of Bak alpha1 helix from the core and latch domains is required for apoptosis. Nat Commun *6*, 6841.

Aluvila, S., Mandal, T., Hustedt, E., Fajer, P., Choe, J.Y., and Oh, K.J. (2014). Organization of the mitochondrial apoptotic BAK pore: oligomerization of the BAK homodimers. J Biol Chem *289*, 2537-2551.

Arbour, N., Vanderluit, J.L., Le Grand, J.N., Jahani-Asl, A., Ruzhynsky, V.A., Cheung, E.C., Kelly, M.A., MacKenzie, A.E., Park, D.S., Opferman, J.T.*, et al.* (2008). Mcl-1 is a key regulator of apoptosis during CNS development and after DNA damage. J Neurosci *28*, 6068-6078.

Baase, W.A., Liu, L., Tronrud, D.E., and Matthews, B.W. (2010). Lessons from the lysozyme of phage T4. Protein Sci *19*, 631-641.

Bakhshi, A., Jensen, J.P., Goldman, P., Wright, J.J., McBride, O.W., Epstein, A.L., and Korsmeyer, S.J. (1985). Cloning the chromosomal breakpoint of t(14;18) human lymphomas: clustering around JH on chromosome 14 and near a transcriptional unit on 18. Cell *41*, 899-906.

Bakhshi, A., Wright, J.J., Graninger, W., Seto, M., Owens, J., Cossman, J., Jensen, J.P., Goldman, P., and Korsmeyer, S.J. (1987). Mechanism of the t(14;18) chromosomal translocation: structural analysis of both derivative 14 and 18 reciprocal partners. Proc Natl Acad Sci U S A *84*, 2396-2400.

Balali-Mood, K., Bond, P.J., and Sansom, M.S. (2009). Interaction of monotopic membrane enzymes with a lipid bilayer: a coarse-grained MD simulation study. Biochemistry *48*, 2135-2145.

Bartholomeusz, G., Wu, Y., Ali Seyed, M., Xia, W., Kwong, K.Y., Hortobagyi, G., and Hung, M.C. (2006). Nuclear translocation of the pro-apoptotic Bcl-2 family member Bok induces apoptosis. Mol Carcinog *45*, 73-83.

Basanez, G., Nechushtan, A., Drozhinin, O., Chanturiya, A., Choe, E., Tutt, S., Wood, K.A., Hsu, Y.T., Zimmerberg, J., and Youle, R.J. (1999). Bax, but not Bcl-xL, decreases the lifetime of planar phospholipid bilayer membranes at subnanomolar concentrations. Proceedings of the National Academy of Sciences *96*, 5492-5497.

Basanez, G., Sharpe, J.C., Galanis, J., Brandt, T.B., Hardwick, J.M., and Zimmerberg, J. (2002). Bax-type apoptotic proteins porate pure lipid bilayers through a mechanism sensitive to intrinsic monolayer curvature. J Biol Chem *277*, 49360-49365.

Biasini, M., Bienert, S., Waterhouse, A., Arnold, K., Studer, G., Schmidt, T., Kiefer, F., Gallo Cassarino, T., Bertoni, M., Bordoli, L.*, et al.* (2014). SWISS-MODEL: modelling protein tertiary and quaternary structure using evolutionary information. Nucleic Acids Res *42*, W252-258.

Bleicken, S., Classen, M., Padmavathi, P.V., Ishikawa, T., Zeth, K., Steinhoff, H.J., and Bordignon, E. (2010). Molecular details of Bax activation, oligomerization, and membrane insertion. J Biol Chem *285*, 6636-6647.

Bleicken, S., Jeschke, G., Stegmueller, C., Salvador-Gallego, R., Garcia-Saez, A.J., and Bordignon, E. (2014). Structural model of active Bax at the membrane. Mol Cell *56*, 496-505.

Bleicken, S., Landeta, O., Landajuela, A., Basanez, G., and Garcia-Saez, A.J. (2013a). Proapoptotic Bax and Bak proteins form stable protein-permeable pores of tunable size. J Biol Chem *288*, 33241-33252.

Bleicken, S., Wagner, C., and Garcia-Saez, A.J. (2013b). Mechanistic differences in the membrane activity of Bax and Bcl-xL correlate with their opposing roles in apoptosis. Biophys J *104*, 421-431.

Boise, L.H., Gonzalez-Garcia, M., Postema, C.E., Ding, L., Lindsten, T., Turka, L.A., Mao, X., Nunez, G., and Thompson, C.B. (1993). bcl-x, a bcl-2-related gene that functions as a dominant regulator of apoptotic cell death. Cell *74*, 597-608.

Boot-Handford, R.P., Michaelidis, T.M., Hillarby, M.C., Zambelli, A., Denton, J., Hoyland, J.A., Freemont, A.J., Grant, M.E., and Wallis, G.A. (1998). The bcl-2 knockout mouse exhibits marked changes in osteoblast phenotype and collagen deposition in bone as well as a mild growth plate phenotype. Int J Exp Pathol *79*, 329-335.

Bouillet, P., Metcalf, D., Huang, D.C., Tarlinton, D.M., Kay, T.W., Kontgen, F., Adams, J.M., and Strasser, A. (1999). Proapoptotic Bcl-2 relative Bim required for certain apoptotic responses, leukocyte homeostasis, and to preclude autoimmunity. Science *286*, 1735-1738.

Brouwer, J.M., Westphal, D., Dewson, G., Robin, A.Y., Uren, R.T., Bartolo, R., Thompson, G.V., Colman, P.M., Kluck, R.M., and Czabotar, P.E. (2014). Bak core and latch domains separate during activation, and freed core domains form symmetric homodimers. Mol Cell *55*, 938-946.

Campelo, F., McMahon, H.T., and Kozlov, M.M. (2008). The hydrophobic insertion mechanism of membrane curvature generation by proteins. Biophys J *95*, 2325-2339.

Carpio, M.A., Michaud, M., Zhou, W., Fisher, J.K., Walensky, L.D., and Katz, S.G. (2015). BCL-2 family member BOK promotes apoptosis in response to endoplasmic reticulum stress. Proc Natl Acad Sci U S A *112*, 7201-7206.

Carpio, M.A., Michaud, M., Zhou, W., Fisher, J.K., Walensky, L.D., and Katz, S.G. (2016). Reply to Fernandez-Marrero et al.: Role of BOK at the intersection of endoplasmic reticulum stress and apoptosis regulation. Proc Natl Acad Sci U S A *113*, E494-495.

Certo, M., Del Gaizo Moore, V., Nishino, M., Wei, G., Korsmeyer, S., Armstrong, S.A., and Letai, A. (2006). Mitochondria primed by death signals determine cellular addiction to antiapoptotic BCL-2 family members. Cancer Cell *9*, 351-365.

Chautan, M., Chazal, G., Cecconi, F., Gruss, P., and Golstein, P. (1999). Interdigital cell death can occur through a necrotic and caspase-independent pathway. Curr Biol *9*, 967-970.

Chen, L., Willis, S.N., Wei, A., Smith, B.J., Fletcher, J.I., Hinds, M.G., Colman, P.M., Day, C.L., Adams, J.M., and Huang, D.C. (2005). Differential targeting of prosurvival Bcl-2 proteins by their BH3-only ligands allows complementary apoptotic function. Mol Cell *17*, 393-403.

Chittenden, T., Flemington, C., Houghton, A.B., Ebb, R.G., Gallo, G.J., Elangovan, B., Chinnadurai, G., and Lutz, R.J. (1995a). A conserved domain in Bak, distinct from BH1 and BH2, mediates cell death and protein binding functions. EMBO J *14*, 5589-5596.

Chittenden, T., Harrington, E.A., O'Connor, R., Flemington, C., Lutz, R.J., Evan, G.I., and Guild, B.C. (1995b). Induction of apoptosis by the Bcl-2 homologue Bak. Nature *374*, 733-736.

Cleary, M.L., Smith, S.D., and Sklar, J. (1986). Cloning and structural analysis of cDNAs for bcl-2 and a hybrid bcl-2/immunoglobulin transcript resulting from the t(14;18) translocation. Cell *47*, 19-28.

Cosentino, K., and Garcia-Saez, A.J. (2017). Bax and Bak Pores: Are We Closing the Circle? Trends Cell Biol *27*, 266-275.

Czabotar, P.E., Lee, E.F., Thompson, G.V., Wardak, A.Z., Fairlie, W.D., and Colman, P.M. (2011). Mutation to Bax beyond the BH3 domain disrupts interactions with pro-survival proteins and promotes apoptosis. J Biol Chem *286*, 7123-7131.

Czabotar, P.E., Lee, E.F., van Delft, M.F., Day, C.L., Smith, B.J., Huang, D.C., Fairlie, W.D., Hinds, M.G., and Colman, P.M. (2007). Structural insights into the degradation of Mcl-1 induced by BH3 domains. Proc Natl Acad Sci U S A *104*, 6217-6222.

Czabotar, P.E., Lessene, G., Strasser, A., and Adams, J.M. (2014). Control of apoptosis by the BCL-2 protein family: implications for physiology and therapy. Nat Rev Mol Cell Biol *15*, 49-63.

Czabotar, P.E., Westphal, D., Dewson, G., Ma, S., Hockings, C., Fairlie, W.D., Lee, E.F., Yao, S., Robin, A.Y., Smith, B.J.*, et al.* (2013). Bax crystal structures reveal how BH3 domains activate Bax and nucleate its oligomerization to induce apoptosis. Cell *152*, 519-531.

D'Orsi, B., Engel, T., Pfeiffer, S., Nandi, S., Kaufmann, T., Henshall, D.C., and Prehn, J.H. (2016). Bok Is Not Pro-Apoptotic But Suppresses Poly ADP-Ribose Polymerase-Dependent Cell Death Pathways and Protects against Excitotoxic and Seizure-Induced Neuronal Injury. J Neurosci *36*, 4564-4578.

Dai, H., Ding, H., Meng, X.W., Peterson, K.L., Schneider, P.A., Karp, J.E., and Kaufmann, S.H. (2015). Constitutive BAK activation as a determinant of drug sensitivity in malignant lymphohematopoietic cells. Genes Dev *29*, 2140-2152.

Day, C.L., Smits, C., Fan, F.C., Lee, E.F., Fairlie, W.D., and Hinds, M.G. (2008). Structure of the BH3 domains from the p53-inducible BH3-only proteins Noxa and Puma in complex with Mcl-1. J Mol Biol *380*, 958-971.

Delano, W.L. (2002). The PyMOL Molecular Graphics System.

Denisov, A.Y., Sprules, T., Fraser, J., Kozlov, G., and Gehring, K. (2007). Heat-induced dimerization of BCL-xL through alpha-helix swapping. Biochemistry *46*, 734-740.

Dewson, G. (2015). Investigating Bak/Bax activating conformation change by immunoprecipitation. Cold Spring Harbor protocols *2015*, 472-476.

Dewson, G., Kratina, T., Czabotar, P., Day, C.L., Adams, J.M., and Kluck, R.M. (2009). Bak activation for apoptosis involves oligomerization of dimers via their alpha6 helices. Mol Cell *36*, 696-703.

Dewson, G., Kratina, T., Sim, H.W., Puthalakath, H., Adams, J.M., Colman, P.M., and Kluck, R.M. (2008). To trigger apoptosis, Bak exposes its BH3 domain and homodimerizes via BH3:groove interactions. Mol Cell *30*, 369-380.

Dewson, G., Ma, S., Frederick, P., Hockings, C., Tan, I., Kratina, T., and Kluck, R.M. (2012). Bax dimerizes via a symmetric BH3:groove interface during apoptosis. Cell Death Differ *19*, 661-670.

Ding, J., Mooers, B.H., Zhang, Z., Kale, J., Falcone, D., McNichol, J., Huang, B., Zhang, X.C., Xing, C., Andrews, D.W.*, et al.* (2014). After embedding in membranes antiapoptotic Bcl-XL protein binds both Bcl-2 homology region 3 and helix 1 of

proapoptotic Bax protein to inhibit apoptotic mitochondrial permeabilization. J Biol Chem *289*, 11873-11896.

Ding, J., Zhang, Z., Roberts, G.J., Falcone, M., Miao, Y., Shao, Y., Zhang, X.C., Andrews, D.W., and Lin, J. (2010). Bcl-2 and Bax interact via the BH1-3 groove-BH3 motif interface and a novel interface involving the BH4 motif. J Biol Chem *285*, 28749-28763.

Dlugosz, P.J., Billen, L.P., Annis, M.G., Zhu, W., Zhang, Z., Lin, J., Leber, B., and Andrews, D.W. (2006). Bcl-2 changes conformation to inhibit Bax oligomerization. EMBO J *25*, 2287-2296.

Donald, J.E., Kulp, D.W., and DeGrado, W.F. (2011). Salt bridges: geometrically specific, designable interactions. Proteins *79*, 898-915.

Dzhagalov, I., St John, A., and He, Y.W. (2007). The antiapoptotic protein Mcl-1 is essential for the survival of neutrophils but not macrophages. Blood *109*, 1620-1626.

Echeverry, N., Bachmann, D., Ke, F., Strasser, A., Simon, H.U., and Kaufmann, T. (2013). Intracellular localization of the BCL-2 family member BOK and functional implications. Cell Death Differ *20*, 785-799.

Edlich, F., Banerjee, S., Suzuki, M., Cleland, M.M., Arnoult, D., Wang, C., Neutzner, A., Tjandra, N., and Youle, R.J. (2011). Bcl-x(L) retrotranslocates Bax from the mitochondria into the cytosol. Cell *145*, 104-116.

Einsele-Scholz, S., Malmsheimer, S., Bertram, K., Stehle, D., Johanning, J., Manz, M., Daniel, P.T., Gillissen, B.F., Schulze-Osthoff, K., and Essmann, F. (2016). Bok is a genuine multi-BH-domain protein that triggers apoptosis in the absence of Bax and Bak. J Cell Sci *129*, 2213-2223.

Ekert, P.G., Read, S.H., Silke, J., Marsden, V.S., Kaufmann, H., Hawkins, C.J., Gerl, R., Kumar, S., and Vaux, D.L. (2004). Apaf-1 and caspase-9 accelerate apoptosis, but do not determine whether factor-deprived or drug-treated cells die. J Cell Biol *165*, 835-842.

Ellis, H.M., and Horvitz, H.R. (1986). Genetic control of programmed cell death in the nematode C. elegans. Cell *44*, 817-829.

Emsley, P., and Cowtan, K. (2004). Coot: model-building tools for molecular graphics. Acta Crystallogr D Biol Crystallogr *60*, 2126-2132.

Epand, R.F., Martinou, J.C., Montessuit, S., Epand, R.M., and Yip, C.M. (2002). Direct evidence for membrane pore formation by the apoptotic protein Bax. Biochem Biophys Res Commun *298*, 744-749.

Evans, P.R., and Murshudov, G.N. (2013). How good are my data and what is the resolution? Acta Crystallogr D Biol Crystallogr *69*, 1204-1214.

Fahy, E., Cotter, D., Sud, M., and Subramaniam, S. (2011). Lipid classification, structures and tools. Biochim Biophys Acta *1811*, 637-647.

Farrow, S.N., White, J.H., Martinou, I., Raven, T., Pun, K.T., Grinham, C.J., Martinou, J.C., and Brown, R. (1995). Cloning of a bcl-2 homologue by interaction with adenovirus E1B 19K. Nature *374*, 731-733.

Fedorov, L.M., Schmittwolf, C., Amann, K., Thomas, W.H., Muller, A.M., Schubert, H., Domen, J., and Kneitz, B. (2006). Renal failure causes early death of bcl-2 deficient mice. Mech Ageing Dev *127*, 600-609.

Fernandez-Marrero, Y., Bleicken, S., Das, K.K., Bachmann, D., Kaufmann, T., and Garcia-Saez, A.J. (2017). The membrane activity of BOK involves formation of large, stable toroidal pores and is promoted by cBID. Febs J *284*, 711-724.

Fernandez-Marrero, Y., Ke, F., Echeverry, N., Bouillet, P., Bachmann, D., Strasser, A., and Kaufmann, T. (2016). Is BOK required for apoptosis induced by endoplasmic reticulum stress? Proc Natl Acad Sci U S A *113*, E492-493.

Fire, E., Gulla, S.V., Grant, R.A., and Keating, A.E. (2010). Mcl-1-Bim complexes accommodate surprising point mutations via minor structural changes. Protein Sci *19*, 507-519.

Fletcher, J.I., Meusburger, S., Hawkins, C.J., Riglar, D.T., Lee, E.F., Fairlie, W.D., Huang, D.C., and Adams, J.M. (2008). Apoptosis is triggered when prosurvival Bcl-2 proteins cannot restrain Bax. Proc Natl Acad Sci U S A *105*, 18081-18087.

Follis, A.V., Chipuk, J.E., Fisher, J.C., Yun, M.K., Grace, C.R., Nourse, A., Baran, K., Ou, L., Min, L., White, S.W.*, et al.* (2013). PUMA binding induces partial unfolding within BCL-xL to disrupt p53 binding and promote apoptosis. Nat Chem Biol *9*, 163-168.

Fowler, P.W., Balali-Mood, K., Deol, S., Coveney, P.V., and Sansom, M.S. (2007). Monotopic enzymes and lipid bilayers: a comparative study. Biochemistry *46*, 3108-3115.

Fuchs, B., Suss, R., Teuber, K., Eibisch, M., and Schiller, J. (2011). Lipid analysis by thin-layer chromatography--a review of the current state. J Chromatogr A *1218*, 2754-2774.

Garcia-Saez, A.J., Chiantia, S., Salgado, J., and Schwille, P. (2007). Pore formation by a Bax-derived peptide: effect on the line tension of the membrane probed by AFM. Biophys J *93*, 103-112.

Gavathiotis, E., Suzuki, M., Davis, M.L., Pitter, K., Bird, G.H., Katz, S.G., Tu, H.C., Kim, H., Cheng, E.H., Tjandra, N.*, et al.* (2008). BAX activation is initiated at a novel interaction site. Nature *455*, 1076-1081.

Gelin, M., Delfosse, V., Allemand, F., Hoh, F., Sallaz-Damaz, Y., Pirocchi, M., Bourguet, W., Ferrer, J.L., Labesse, G., and Guichou, J.F. (2015). Combining 'dry' co-crystallization and in situ diffraction to facilitate ligand screening by X-ray crystallography. Acta Crystallogr D Biol Crystallogr *71*, 1777-1787.

Ghavami, S., Shojaei, S., Yeganeh, B., Ande, S.R., Jangamreddy, J.R., Mehrpour, M., Christoffersson, J., Chaabane, W., Moghadam, A.R., Kashani, H.H.*, et al.* (2014). Autophagy and apoptosis dysfunction in neurodegenerative disorders. Prog Neurobiol *112*, 24-49.

Gilbert, R.J. (2016). Protein-lipid interactions and non-lamellar lipidic structures in membrane pore formation and membrane fusion. Biochim Biophys Acta *1858*, 487-499.

Gilbert, R.J., Dalla Serra, M., Froelich, C.J., Wallace, M.I., and Anderluh, G. (2014). Membrane pore formation at protein-lipid interfaces. Trends Biochem Sci *39*, 510-516.

Gillies, L.A., Du, H., Peters, B., Knudson, C.M., Newmeyer, D.D., and Kuwana, T. (2015). Visual and functional demonstration of growing Bax-induced pores in mitochondrial outer membranes. Mol Biol Cell *26*, 339-349.

Glucksmann, A. (1951). Cell deaths in normal vertebrate ontogeny. Biol Rev Camb Philos Soc *26*, 59-86.

Griffiths, G.J., Dubrez, L., Morgan, C.P., Jones, N.A., Whitehouse, J., Corfe, B.M., Dive, C., and Hickman, J.A. (1999). Cell damage-induced conformational changes of the pro-apoptotic protein Bak in vivo precede the onset of apoptosis. J Cell Biol *144*, 903-914.

Grosse, L., Wurm, C.A., Bruser, C., Neumann, D., Jans, D.C., and Jakobs, S. (2016). Bax assembles into large ring-like structures remodeling the mitochondrial outer membrane in apoptosis. EMBO J *35*, 402-413.

Gruner, S.M. (1985). Intrinsic curvature hypothesis for biomembrane lipid composition: a role for nonbilayer lipids. Proc Natl Acad Sci U S A *82*, 3665-3669.

Gupta, K., Donlan, J.A.C., Hopper, J.T.S., Uzdavinys, P., Landreh, M., Struwe, W.B., Drew, D., Baldwin, A.J., Stansfeld, P.J., and Robinson, C.V. (2017). The role of interfacial lipids in stabilizing membrane protein oligomers. Nature *541*, 421-424.

Hanahan, D., and Weinberg, R.A. (2011). Hallmarks of cancer: the next generation. Cell *144*, 646-674.

Happo, L., Strasser, A., and Cory, S. (2012). BH3-only proteins in apoptosis at a glance. J Cell Sci *125*, 1081-1087.

Haschka, M.D., and Villunger, A. (2017). There is something about BOK we just don't get yet. Febs J *284*, 708-710.

Hengartner, M.O., and Horvitz, H.R. (1994). C. elegans cell survival gene ced-9 encodes a functional homolog of the mammalian proto-oncogene bcl-2. Cell *76*, 665-676.

Horie, C., Suzuki, H., Sakaguchi, M., and Mihara, K. (2002). Characterization of signal that directs C-tail-anchored proteins to mammalian mitochondrial outer membrane. Mol Biol Cell *13*, 1615-1625.

Hsu, S.Y., Kaipia, A., McGee, E., Lomeli, M., and Hsueh, A.J. (1997). Bok is a pro-apoptotic Bcl-2 protein with restricted expression in reproductive tissues and heterodimerizes with selective anti-apoptotic Bcl-2 family members. Proc Natl Acad Sci U S A *94*, 12401-12406.

Hsu, Y.T., and Youle, R.J. (1998). Bax in murine thymus is a soluble monomeric protein that displays differential detergent-induced conformations. Journal of Biological Chemistry *273*, 10777-10783.

Hunte, C., and Richers, S. (2008). Lipids and membrane protein structures. Curr Opin Struct Biol *18*, 406-411.

Iacovache, I., Bischofberger, M., and van der Goot, F.G. (2010). Structure and assembly of pore-forming proteins. Curr Opin Struct Biol *20*, 241-246.

Inohara, N., Ekhterae, D., Garcia, I., Carrio, R., Merino, J., Merry, A., Chen, S., and Nunez, G. (1998). Mtd, a novel Bcl-2 family member activates apoptosis in the absence of heterodimerization with Bcl-2 and Bcl-X-L. Journal of Biological Chemistry *273*, 8705-8710.

Inoue-Yamauchi, A., Jeng, P.S., Kim, K., Chen, H.C., Han, S., Ganesan, Y.T., Ishizawa, K., Jebiwott, S., Dong, Y., Pietanza, M.C*., et al.* (2017). Targeting the differential addiction to anti-apoptotic BCL-2 family for cancer therapy. Nat Commun *8*, 16078.

Iyer, S., Anwari, K., Alsop, A.E., Yuen, W.S., Huang, D.C., Carroll, J., Smith, N.A., Smith, B.J., Dewson, G., and Kluck, R.M. (2016). Identification of an activation site in Bak and mitochondrial Bax triggered by antibodies. Nat Commun *7*, 11734.

Iyer, S., Bell, F., Westphal, D., Anwari, K., Gulbis, J., Smith, B.J., Dewson, G., and Kluck, R.M. (2015). Bak apoptotic pores involve a flexible C-terminal region and juxtaposition of the C-terminal transmembrane domains. Cell Death Differ *22*, 1665-1675.

Kabsch, W. (2010). Xds. Acta Crystallogr D Biol Crystallogr *66*, 125-132.

Karatekin, E., Sandre, O., Guitouni, H., Borghi, N., Puech, P.H., and Brochard-Wyart, F. (2003). Cascades of transient pores in giant vesicles: line tension and transport. Biophys J *84*, 1734-1749.

Kaufmann, T., Schlipf, S., Sanz, J., Neubert, K., Stein, R., and Borner, C. (2003). Characterization of the signal that directs Bcl-x(L), but not Bcl-2, to the mitochondrial outer membrane. J Cell Biol *160*, 53-64.

Ke, F., Bouillet, P., Kaufmann, T., Strasser, A., Kerr, J., and Voss, A.K. (2013). Consequences of the combined loss of BOK and BAK or BOK and BAX. Cell Death Dis *4*, e650.

Ke, F., Voss, A., Kerr, J.B., O'Reilly, L.A., Tai, L., Echeverry, N., Bouillet, P., Strasser, A., and Kaufmann, T. (2012). BCL-2 family member BOK is widely expressed but its loss has only minimal impact in mice. Cell Death Differ *19*, 915-925.

Keenan, T.W., and Morre, D.J. (1970). Phospholipid class and fatty acid composition of golgi apparatus isolated from rat liver and comparison with other cell fractions. Biochemistry *9*, 19-25.

Kerr, J.F. (1971). Shrinkage necrosis: a distinct mode of cellular death. J Pathol *105*, 13-20.

Kerr, J.F., Wyllie, A.H., and Currie, A.R. (1972). Apoptosis: a basic biological phenomenon with wide-ranging implications in tissue kinetics. Br J Cancer *26*, 239-257.

Kiefer, M.C., Brauer, M.J., Powers, V.C., Wu, J.J., Umansky, S.R., Tomei, L.D., and Barr, P.J. (1995). Modulation of apoptosis by the widely distributed Bcl-2 homologue Bak. Nature *374*, 736-739.

Kim, M.K., and Kang, Y.K. (1999). Positional preference of proline in alpha-helices. Protein Sci *8*, 1492-1499.

Kirby, N.M., Mudie, S.T., Hawley, A.M., Cookson, D.J., Mertens, H.D.T., Cowieson, N., and Samardzic-Boban, V. (2013). A low-background-intensity focusing small-angle X-ray scattering undulator beamline. J Appl Crystallogr *46*, 1670-1680.

Kluck, R.M., Bossy-Wetzel, E., Green, D.R., and Newmeyer, D.D. (1997). The release of cytochrome c from mitochondria: a primary site for Bcl-2 regulation of apoptosis. Science *275*, 1132-1136.

Knudson, C.M., Tung, K.S., Tourtellotte, W.G., Brown, G.A., and Korsmeyer, S.J. (1995). Bax-deficient mice with lymphoid hyperplasia and male germ cell death. Science *270*, 96-99.

Konarev, P.V., Volkov, V.V., Sokolova, A.V., Koch, M.H.J., and Svergun, D.I. (2003). PRIMUS: a Windows PC-based system for small-angle scattering data analysis. J Appl Crystallogr *36*, 1277-1282.

Kozopas, K.M., Yang, T., Buchan, H.L., Zhou, P., and Craig, R.W. (1993). MCL1, a gene expressed in programmed myeloid cell differentiation, has sequence similarity to BCL2. Proc Natl Acad Sci U S A *90*, 3516-3520.

Kuwana, T., Bouchier-Hayes, L., Chipuk, J.E., Bonzon, C., Sullivan, B.A., Green, D.R., and Newmeyer, D.D. (2005). BH3 domains of BH3-only proteins differentially regulate Bax-mediated mitochondrial membrane permeabilization both directly and indirectly. Mol Cell *17*, 525-535.

Kuwana, T., Mackey, M.R., Perkins, G., Ellisman, M.H., Latterich, M., Schneiter, R., Green, D.R., and Newmeyer, D.D. (2002). Bid, Bax, and lipids cooperate to form supramolecular openings in the outer mitochondrial membrane. Cell *111*, 331-342.

Kuwana, T., Olson, N.H., Kiosses, W.B., Peters, B., and Newmeyer, D.D. (2016). Pro-apoptotic Bax molecules densely populate the edges of membrane pores. Sci Rep *6*, 27299.

Kvansakul, M., and Hinds, M.G. (2013). Structural biology of the Bcl-2 family and its mimicry by viral proteins. Cell Death Dis *4*, e909.

Lamkanfi, M., and Dixit, V.M. (2010). Manipulation of host cell death pathways during microbial infections. Cell Host Microbe *8*, 44-54.

Landeta, O., Landajuela, A., Gil, D., Taneva, S., Di Primo, C., Sot, B., Valle, M., Frolov, V.A., and Basanez, G. (2011). Reconstitution of proapoptotic BAK function in liposomes reveals a dual role for mitochondrial lipids in the BAK-driven membrane permeabilization process. J Biol Chem *286*, 8213-8230.

Lee, E.F., Grabow, S., Chappaz, S., Dewson, G., Hockings, C., Kluck, R.M., Debrincat, M.A., Gray, D.H., Witkowski, M.T., Evangelista, M.*, et al.* (2016). Physiological restraint of Bak by Bcl-xL is essential for cell survival. Gene Dev *30*.

Lee, E.F., Sadowsky, J.D., Smith, B.J., Czabotar, P.E., Peterson-Kaufman, K.J., Colman, P.M., Gellman, S.H., and Fairlie, W.D. (2009). High-resolution structural characterization of a helical alpha/beta-peptide foldamer bound to the anti-apoptotic protein Bcl-xL. Angew Chem Int Ed Engl *48*, 4318-4322.

Lindsten, T., Ross, A.J., King, A., Zong, W.X., Rathmell, J.C., Shiels, H.A., Ulrich, E., Waymire, K.G., Mahar, P., Frauwirth, K.*, et al.* (2000). The combined functions of

proapoptotic Bcl-2 family members bak and bax are essential for normal development of multiple tissues. Mol Cell *6*, 1389-1399.

Llambi, F., Moldoveanu, T., Tait, S.W., Bouchier-Hayes, L., Temirov, J., McCormick, L.L., Dillon, C.P., and Green, D.R. (2011). A unified model of mammalian BCL-2 protein family interactions at the mitochondria. Mol Cell *44*, 517-531.

Llambi, F., Wang, Y.M., Victor, B., Yang, M., Schneider, D.M., Gingras, S., Parsons, M.J., Zheng, J.H., Brown, S.A., Pelletier, S.*, et al.* (2016). BOK Is a Non-canonical BCL-2 Family Effector of Apoptosis Regulated by ER-Associated Degradation. Cell *165*, 421-433.

Lockshin, R.A., and Williams, C.M. (1965). Programmed Cell Death--I. Cytology of Degeneration in the Intersegmental Muscles of the Pernyi Silkmoth. J Insect Physiol *11*, 123-133.

Lydic, T.A., Busik, J.V., and Reid, G.E. (2014). A monophasic extraction strategy for the simultaneous lipidome analysis of polar and nonpolar retina lipids. J Lipid Res *55*, 1797-1809.

Ma, A., Pena, J.C., Chang, B., Margosian, E., Davidson, L., Alt, F.W., and Thompson, C.B. (1995). Bclx regulates the survival of double-positive thymocytes. Proc Natl Acad Sci U S A *92*, 4763-4767.

Ma, S., Hockings, C., Anwari, K., Kratina, T., Fennell, S., Lazarou, M., Ryan, M.T., Kluck, R.M., and Dewson, G. (2013). Assembly of the Bak apoptotic pore: a critical role for the Bak protein alpha6 helix in the multimerization of homodimers during apoptosis. J Biol Chem *288*, 26027-26038.

Mandal, T., Shin, S., Aluvila, S., Chen, H.C., Grieve, C., Choe, J.Y., Cheng, E.H., Hustedt, E.J., and Oh, K.J. (2016). Assembly of Bak homodimers into higher order homooligomers in the mitochondrial apoptotic pore. Sci Rep *6*, 30763.

Mason, K.D., Carpinelli, M.R., Fletcher, J.I., Collinge, J.E., Hilton, A.A., Ellis, S., Kelly, P.N., Ekert, P.G., Metcalf, D., Roberts, A.W.*, et al.* (2007). Programmed anuclear cell death delimits platelet life span. Cell *128*, 1173-1186.

May, S. (2000). A molecular model for the line tension of lipid membranes. Eur Phys J E *3*, 37-44.

McCoy, A.J., Grosse-Kunstleve, R.W., Adams, P.D., Winn, M.D., Storoni, L.C., and Read, R.J. (2007). Phaser crystallographic software. J Appl Crystallogr *40*, 658-674.

McMahon, H.T., and Boucrot, E. (2015). Membrane curvature at a glance. J Cell Sci *128*, 1065-1070.

Moldoveanu, T., Grace, C.R., Llambi, F., Nourse, A., Fitzgerald, P., Gehring, K., Kriwacki, R.W., and Green, D.R. (2013). BID-induced structural changes in BAK promote apoptosis. Nat Struct Mol Biol *20*, 589-597.

Moldoveanu, T., Liu, Q., Tocilj, A., Watson, M., Shore, G., and Gehring, K. (2006). The X-ray structure of a BAK homodimer reveals an inhibitory zinc binding site. Mol Cell *24*, 677-688.

Moriarty, N.W., Grosse-Kunstleve, R.W., and Adams, P.D. (2009). electronic Ligand Builder and Optimization Workbench (eLBOW): a tool for ligand coordinate and restraint generation. Acta Crystallogr D Biol Crystallogr *65*, 1074-1080.

Motoyama, N., Wang, F., Roth, K.A., Sawa, H., Nakayama, K., Nakayama, K., Negishi, I., Senju, S., Zhang, Q., Fujii, S.*, et al.* (1995). Massive cell death of immature hematopoietic cells and neurons in Bcl-x-deficient mice. Science *267*, 1506-1510.

Muchmore, S.W., Sattler, M., Liang, H., Meadows, R.P., Harlan, J.E., Yoon, H.S., Nettesheim, D., Chang, B.S., Thompson, C.B., Wong, S.L.*, et al.* (1996). X-ray and NMR structure of human Bcl-xL, an inhibitor of programmed cell death. Nature *381*, 335-341.

Mueller, M., Grauschopf, U., Maier, T., Glockshuber, R., and Ban, N. (2009). The structure of a cytolytic alpha-helical toxin pore reveals its assembly mechanism. Nature *459*, 726-730.

Murshudov, G.N., Vagin, A.A., and Dodson, E.J. (1997). Refinement of macromolecular structures by the maximum-likelihood method. Acta Crystallogr D Biol Crystallogr *53*, 240-255.

Nasu, Y., Benke, A., Arakawa, S., Yoshida, G.J., Kawamura, G., Manley, S., Shimizu, S., and Ozawa, T. (2016). In Situ Characterization of Bak Clusters Responsible for Cell Death Using Single Molecule Localization Microscopy. Sci Rep *6*, 27505.

O'Neill, J.W., Manion, M.K., Maguire, B., and Hockenbery, D.M. (2006). BCL-XL dimerization by three-dimensional domain swapping. J Mol Biol *356*, 367-381.

O'Neill, K.L., Huang, K., Zhang, J., Chen, Y., and Luo, X. (2016). Inactivation of prosurvival Bcl-2 proteins activates Bax/Bak through the outer mitochondrial membrane. Gene Dev *30*, 973-988.

Oh, K.J., Singh, P., Lee, K., Foss, K., Lee, S., Park, M., Lee, S., Aluvila, S., Park, M., Singh, P.*, et al.* (2010). Conformational changes in BAK, a pore-forming proapoptotic Bcl-2 family member, upon membrane insertion and direct evidence for the existence of BH3-BH3 contact interface in BAK homo-oligomers. J Biol Chem *285*, 28924-28937.

Okamoto, T., Zobel, K., Fedorova, A., Quan, C., Yang, H., Fairbrother, W.J., Huang, D.C.S., Smith, B.J., Deshayes, K., and Czabotar, P.E. (2013). Stabilizing the Pro-Apoptotic Bim BH3 Helix (BimSAHB) Does Not Necessarily Enhance Affinity or Biological Activity. Biopolymers *100*, 308-308.

Oltvai, Z.N., Milliman, C.L., and Korsmeyer, S.J. (1993). Bcl-2 heterodimerizes in vivo with a conserved homolog, Bax, that accelerates programmed cell death. Cell *74*, 609-619.

Opferman, J.T., Iwasaki, H., Ong, C.C., Suh, H., Mizuno, S., Akashi, K., and Korsmeyer, S.J. (2005). Obligate role of anti-apoptotic MCL-1 in the survival of hematopoietic stem cells. Science *307*, 1101-1104.

Opferman, J.T., Letai, A., Beard, C., Sorcinelli, M.D., Ong, C.C., and Korsmeyer, S.J. (2003). Development and maintenance of B and T lymphocytes requires antiapoptotic MCL-1. Nature *426*, 671-676.

Ottina, E., Grespi, F., Tischner, D., Soratroi, C., Geley, S., Ploner, A., Reichardt, H.M., Villunger, A., and Herold, M.J. (2012). Targeting antiapoptotic A1/Bfl-1 by in vivo RNAi reveals multiple roles in leukocyte development in mice. Blood *119*, 6032-6042.

Pakula, A.A., and Simon, M.I. (1992). Determination of transmembrane protein structure by disulfide cross-linking: the Escherichia coli Tar receptor. Proc Natl Acad Sci U S A *89*, 4144-4148.

Palsdottir, H., and Hunte, C. (2004). Lipids in membrane protein structures. Biochim Biophys Acta *1666*, 2-18.

Pan, R., Hogdal, L.J., Benito, J.M., Bucci, D., Han, L., Borthakur, G., Cortes, J., DeAngelo, D.J., Debose, L., Mu, H.*, et al.* (2014). Selective BCL-2 inhibition by ABT-199 causes on-target cell death in acute myeloid leukemia. Cancer Discov *4*, 362-375.

Peng, R., Tong, J.S., Li, H., Yue, B., Zou, F., Yu, J., and Zhang, L. (2013). Targeting Bax interaction sites reveals that only homo-oligomerization sites are essential for its activation. Cell Death Differ *20*, 744-754.

Petros, A.M., Nettesheim, D.G., Wang, Y., Olejniczak, E.T., Meadows, R.P., Mack, J., Swift, K., Matayoshi, E.D., Zhang, H., Thompson, C.B.*, et al.* (2000). Rationale for Bcl-xL/Bad peptide complex formation from structure, mutagenesis, and biophysical studies. Protein Sci *9*, 2528-2534.

Pettersen, E.F., Goddard, T.D., Huang, C.C., Couch, G.S., Greenblatt, D.M., Meng, E.C., and Ferrin, T.E. (2004). UCSF Chimera--a visualization system for exploratory research and analysis. Journal of computational chemistry *25*, 1605-1612.

Plotly Technologies Inc. (2015). Collaborative data science (Montreal, QC).

Print, C.G., Loveland, K.L., Gibson, L., Meehan, T., Stylianou, A., Wreford, N., de Kretser, D., Metcalf, D., Kontgen, F., Adams, J.M.*, et al.* (1998). Apoptosis regulator bcl-w is essential for spermatogenesis but appears otherwise redundant. Proc Natl Acad Sci U S A *95*, 12424-12431.

Qian, S., Wang, W., Yang, L., and Huang, H.W. (2008). Structure of transmembrane pore induced by Bax-derived peptide: evidence for lipidic pores. Proc Natl Acad Sci U S A *105*, 17379-17383.

R Core Team (2016). R: A language and environment for statistical computing (Vienna, Austria: R Foundation for Statistical Computing).

Rajagopal, B.S., Edzuma, A.N., Hough, M.A., Blundell, K.L., Kagan, V.E., Kapralov, A.A., Fraser, L.A., Butt, J.N., Silkstone, G.G., Wilson, M.T.*, et al.* (2013). The hydrogen-peroxide-induced radical behaviour in human cytochrome c-phospholipid complexes: implications for the enhanced pro-apoptotic activity of the G41S mutant. Biochem J *456*, 441-452.

Rajan, S., Choi, M., Nguyen, Q.T., Ye, H., Liu, W., Toh, H.T., Kang, C., Kamariah, N., Li, C., Huang, H.*, et al.* (2015). Structural transition in Bcl-xL and its potential association with mitochondrial calcium ion transport. Sci Rep *5*, 10609.

Rautureau, G.J., Day, C.L., and Hinds, M.G. (2010). The structure of Boo/Diva reveals a divergent Bcl-2 protein. Proteins *78*, 2181-2186.

Rautureau, G.J., Yabal, M., Yang, H., Huang, D.C., Kvansakul, M., and Hinds, M.G. (2012). The restricted binding repertoire of Bcl-B leaves Bim as the universal BH3-only prosurvival Bcl-2 protein antagonist. Cell Death Dis *3*, e443.

Richardson, J.S., and Richardson, D.C. (1988). Amino-Acid Preferences for Specific Locations at the Ends of Alpha-Helices. Science *240*, 1648-1652.

Rinkenberger, J.L., Horning, S., Klocke, B., Roth, K., and Korsmeyer, S.J. (2000). Mcl-1 deficiency results in peri-implantation embryonic lethality. Genes Dev *14*, 23-27.

Roberts, A.W., Davids, M.S., Pagel, J.M., Kahl, B.S., Puvvada, S.D., Gerecitano, J.F., Kipps, T.J., Anderson, M.A., Brown, J.R., Gressick, L.*, et al.* (2016). Targeting BCL2 with Venetoclax in Relapsed Chronic Lymphocytic Leukemia. N Engl J Med *374*, 311-322.

Robin, A.Y., Krishna Kumar, K., Westphal, D., Wardak, A.Z., Thompson, G.V., Dewson, G., Colman, P.M., and Czabotar, P.E. (2015). Crystal structure of Bax bound to the BH3 peptide of Bim identifies important contacts for interaction. Cell Death Dis *6*, e1809.

Salvador-Gallego, R., Mund, M., Cosentino, K., Schneider, J., Unsay, J., Schraermeyer, U., Engelhardt, J., Ries, J., and Garcia-Saez, A.J. (2016). Bax assembly into rings and arcs in apoptotic mitochondria is linked to membrane pores. EMBO J *35*, 389-401.

Sattler, M., Liang, H., Nettesheim, D., Meadows, R.P., Harlan, J.E., Eberstadt, M., Yoon, H.S., Shuker, S.B., Chang, B.S., Minn, A.J.*, et al.* (1997). Structure of Bcl-xL-Bak peptide complex: recognition between regulators of apoptosis. Science *275*, 983-986.

Saunders, J.W., Jr. (1966). Death in embryonic systems. Science *154*, 604-612.

Schafer, B., Quispe, J., Choudhary, V., Chipuk, J.E., Ajero, T.G., Du, H., Schneiter, R., and Kuwana, T. (2009). Mitochondrial outer membrane proteins assist Bid in Bax-mediated lipidic pore formation. Mol Biol Cell *20*, 2276-2285.

Schellenberg, B., Wang, P., Keeble, J.A., Rodriguez-Enriquez, R., Walker, S., Owens, T.W., Foster, F., Tanianis-Hughes, J., Brennan, K., Streuli, C.H.*, et al.* (2013). Bax exists in a dynamic equilibrium between the cytosol and mitochondria to control apoptotic priming. Mol Cell *49*, 959-971.

Schulman, J.J., Wright, F.A., Han, X., Zluhan, E.J., Szczesniak, L.M., and Wojcikiewicz, R.J. (2016). The Stability and Expression Level of Bok Are Governed by Binding to Inositol 1,4,5-Trisphosphate Receptors. J Biol Chem *291*, 11820-11828.

Schulman, J.J., Wright, F.A., Kaufmann, T., and Wojcikiewicz, R.J. (2013). The Bcl-2 protein family member Bok binds to the coupling domain of inositol 1,4,5-trisphosphate receptors and protects them from proteolytic cleavage. J Biol Chem *288*, 25340-25349.

Shinzawa-Itoh, K., Aoyama, H., Muramoto, K., Terada, H., Kurauchi, T., Tadehara, Y., Yamasaki, A., Sugimura, T., Kurono, S., Tsujimoto, K.*, et al.* (2007). Structures and physiological roles of 13 integral lipids of bovine heart cytochrome c oxidase. EMBO J *26*, 1713-1725.

Simmons, M.J., Fan, G., Zong, W.X., Degenhardt, K., White, E., and Gelinas, C. (2008). Bfl-1/A1 functions, similar to Mcl-1, as a selective tBid and Bak antagonist. Oncogene *27*, 1421-1428.

Smits, C., Czabotar, P.E., Hinds, M.G., and Day, C.L. (2008). Structural plasticity underpins promiscuous binding of the prosurvival protein A1. Structure *16*, 818-829.

Song, L., Hobaugh, M.R., Shustak, C., Cheley, S., Bayley, H., and Gouaux, J.E. (1996). Structure of staphylococcal alpha-hemolysin, a heptameric transmembrane pore. Science *274*, 1859-1866.

Sonnen, A.F., Plitzko, J.M., and Gilbert, R.J. (2014). Incomplete pneumolysin oligomers form membrane pores. Open Biol *4*, 140044.

Souers, A.J., Leverson, J.D., Boghaert, E.R., Ackler, S.L., Catron, N.D., Chen, J., Dayton, B.D., Ding, H., Enschede, S.H., Fairbrother, W.J*., et al.* (2013). ABT-199, a potent and selective BCL-2 inhibitor, achieves antitumor activity while sparing platelets. Nat Med *19*, 202-208.

Subburaj, Y., Cosentino, K., Axmann, M., Pedrueza-Villalmanzo, E., Hermann, E., Bleicken, S., Spatz, J., and Garcia-Saez, A.J. (2015). Bax monomers form dimer units in the membrane that further self-assemble into multiple oligomeric species. Nat Commun *6*, 8042.

Sulston, J.E., and Horvitz, H.R. (1977). Post-embryonic cell lineages of the nematode, Caenorhabditis elegans. Dev Biol *56*, 110-156.

Suzuki, M., Youle, R.J., and Tjandra, N. (2000). Structure of Bax: coregulation of dimer formation and intracellular localization. Cell *103*, 645-654.

Svergun, D., Barberato, C., and Koch, M.H.J. (1995). CRYSOL - A program to evaluate x-ray solution scattering of biological macromolecules from atomic coordinates. J Appl Crystallogr *28*, 768-773.

Svergun, D.I. (1992). Determination of the Regularization Parameter in Indirect-Transform Methods Using Perceptual Criteria. J Appl Crystallogr *25*, 495-503.

Tanaka, K., Caaveiro, J.M., Morante, K., Gonzalez-Manas, J.M., and Tsumoto, K. (2015). Structural basis for self-assembly of a cytolytic pore lined by protein and lipid. Nat Commun *6*, 6337.

Tanaka, Y., Aikawa, K., Nishida, G., Homma, M., Sogabe, S., Igaki, S., Hayano, Y., Sameshima, T., Miyahisa, I., Kawamoto, T*., et al.* (2013). Discovery of potent Mcl-1/Bcl-xL dual inhibitors by using a hybridization strategy based on structural analysis of target proteins. J Med Chem *56*, 9635-9645.

Terrones, O., Antonsson, B., Yamaguchi, H., Wang, H.G., Liu, J., Lee, R.M., Herrmann, A., and Basanez, G. (2004). Lipidic pore formation by the concerted action of proapoptotic BAX and tBID. J Biol Chem *279*, 30081-30091.

Terwilliger, T.C., Grosse-Kunstleve, R.W., Afonine, P.V., Moriarty, N.W., Zwart, P.H., Hung, L.W., Read, R.J., and Adams, P.D. (2008). Iterative model building, structure refinement and density modification with the PHENIX AutoBuild wizard. Acta Crystallogr D Biol Crystallogr *64*, 61-69.

Thomas, R.L., Roberts, D.J., Kubli, D.A., Lee, Y., Quinsay, M.N., Owens, J.B., Fischer, K.M., Sussman, M.A., Miyamoto, S., and Gustafsson, A.B. (2013). Loss of MCL-1 leads to impaired autophagy and rapid development of heart failure. Genes Dev *27*, 1365-1377.

Todt, F., Cakir, Z., Reichenbach, F., Emschermann, F., Lauterwasser, J., Kaiser, A., Ichim, G., Tait, S.W., Frank, S., Langer, H.F., *et al.* (2015). Differential retrotranslocation of mitochondrial Bax and Bak. EMBO J *34*, 67-80.

Todt, F., Cakir, Z., Reichenbach, F., Youle, R.J., and Edlich, F. (2013). The C-terminal helix of Bcl-x(L) mediates Bax retrotranslocation from the mitochondria. Cell Death Differ *20*, 333-342.

Tsujimoto, Y., Finger, L.R., Yunis, J., Nowell, P.C., and Croce, C.M. (1984). Cloning of the chromosome breakpoint of neoplastic B cells with the t(14;18) chromosome translocation. Science *226*, 1097-1099.

Ujwal, R., and Bowie, J.U. (2011). Crystallizing membrane proteins using lipidic bicelles. Methods *55*, 337-341.

Uren, R.T., O'Hely, M., Iyer, S., Bartolo, R., Shi, M.X., Brouwer, J.M., Alsop, A.E., Dewson, G., and Kluck, R.M. (2017). Disordered clusters of Bak dimers rupture mitochondria during apoptosis. Elife *6*.

Vaux, D.L., Cory, S., and Adams, J.M. (1988). Bcl-2 gene promotes haemopoietic cell survival and cooperates with c-myc to immortalize pre-B cells. Nature *335*, 440-442.

Vaux, D.L., Weissman, I.L., and Kim, S.K. (1992). Prevention of programmed cell death in Caenorhabditis elegans by human bcl-2. Science *258*, 1955-1957.

Veis, D.J., Sorenson, C.M., Shutter, J.R., and Korsmeyer, S.J. (1993). Bcl-2-deficient mice demonstrate fulminant lymphoid apoptosis, polycystic kidneys, and hypopigmented hair. Cell *75*, 229-240.

Vick, B., Weber, A., Urbanik, T., Maass, T., Teufel, A., Krammer, P.H., Opferman, J.T., Schuchmann, M., Galle, P.R., and Schulze-Bergkamen, H. (2009). Knockout of myeloid cell leukemia-1 induces liver damage and increases apoptosis susceptibility of murine hepatocytes. Hepatology *49*, 627-636.

Walter, P., and Ron, D. (2011). The unfolded protein response: from stress pathway to homeostatic regulation. Science *334*, 1081-1086.

Wang, K., Gross, A., Waksman, G., and Korsmeyer, S.J. (1998). Mutagenesis of the BH3 domain of BAX identifies residues critical for dimerization and killing. Mol Cell Biol *18*, 6083-6089.

Wang, X., Bathina, M., Lynch, J., Koss, B., Calabrese, C., Frase, S., Schuetz, J.D., Rehg, J.E., and Opferman, J.T. (2013). Deletion of MCL-1 causes lethal cardiac failure and mitochondrial dysfunction. Genes Dev *27*, 1351-1364.

Wei, M.C., Zong, W.X., Cheng, E.H., Lindsten, T., Panoutsakopoulou, V., Ross, A.J., Roth, K.A., MacGregor, G.R., Thompson, C.B., and Korsmeyer, S.J. (2001). Proapoptotic BAX and BAK: a requisite gateway to mitochondrial dysfunction and death. Science *292*, 727-730.

Weijman, J.F., Kumar, A., Jamieson, S.A., King, C.M., Caradoc-Davies, T.T., Ledgerwood, E.C., Murphy, J.M., and Mace, P.D. (2017). Structural basis of autoregulatory scaffolding by apoptosis signal-regulating kinase 1. Proc Natl Acad Sci U S A *114*, E2096-E2105.

Westphal, D., Dewson, G., Menard, M., Frederick, P., Iyer, S., Bartolo, R., Gibson, L., Czabotar, P.E., Smith, B.J., Adams, J.M.*, et al.* (2014). Apoptotic pore formation is associated with in-plane insertion of Bak or Bax central helices into the mitochondrial outer membrane. Proc Natl Acad Sci U S A *111*, E4076-4085.

Willis, S.N., Chen, L., Dewson, G., Wei, A., Naik, E., Fletcher, J.I., Adams, J.M., and Huang, D.C. (2005). Proapoptotic Bak is sequestered by Mcl-1 and Bcl-xL, but not Bcl-2, until displaced by BH3-only proteins. Genes Dev *19*, 1294-1305.

Willis, S.N., Fletcher, J.I., Kaufmann, T., van Delft, M.F., Chen, L., Czabotar, P.E., Ierino, H., Lee, E.F., Fairlie, W.D., Bouillet, P.*, et al.* (2007). Apoptosis initiated when BH3 ligands engage multiple Bcl-2 homologs, not Bax or Bak. Science *315*, 856-859.

Woolfson, D.N., and Williams, D.H. (1990). The influence of proline residues on alpha-helical structure. FEBS Lett *277*, 185-188.

Wright, S.P. (1992). Adjusted P-Values for Simultaneous Inference. Biometrics *48*, 1005-1013.

Yeagle, P.L. (2014). Non-covalent binding of membrane lipids to membrane proteins. Biochim Biophys Acta *1838*, 1548-1559.

Yin, X.M., Oltvai, Z.N., and Korsmeyer, S.J. (1994). BH1 and BH2 domains of Bcl-2 are required for inhibition of apoptosis and heterodimerization with Bax. Nature *369*, 321-323.

Zhang, H., Holzgreve, W., and De Geyter, C. (2000). Evolutionarily conserved Bok proteins in the Bcl-2 family. FEBS Lett *480*, 311-313.

Zhang, Z., Subramaniam, S., Kale, J., Liao, C., Huang, B., Brahmbhatt, H., Condon, S.G., Lapolla, S.M., Hays, F.A., Ding, J.*, et al.* (2016). BH3-in-groove dimerization initiates and helix 9 dimerization expands Bax pore assembly in membranes. EMBO J *35*, 208-236.

Zhou, L., and Chang, D.C. (2008). Dynamics and structure of the Bax-Bak complex responsible for releasing mitochondrial proteins during apoptosis. J Cell Sci *121*, 2186-2196.

Appendix

Methodology for Mass Spectrometric Analysis of Bak Samples

Mass spectrometric analysis of purified Bak(α2-5), crystallised Bak(α2-5), and crystallised Bax(α2-5) samples was performed by Yepy Rustam (Bio21 Molecular Science and Biotechnology Institute) under the supervision of Gavin Reid (Bio21 Molecular Science and Biotechnology Institute).

Monophasic Lipid Extraction

Lipids were extracted from samples of purified Bak(α2-5) hexamer, crushed Bak(α2-5) crystals, and crushed Bax(α2-5) crystals using a modified monophasic lipid extraction procedure (Lydic *et al.*, 2014). Methanol and water were added to each sample and a blank to a final volume of 200 µL containing 40% methanol. Internal standards (25 pmol each) dissolved together in 60 µL of Milli-Q water, 460 µL of methanol, and 285 µL of chloroform were then added to all tubes. Samples were incubated on a ThermoMix at 1,000 rpm for 30 minutes at room temperature. The precipitate was separated by centrifugation at 14,000 rpm for 15 minutes and supernatants were transferred into new tubes. Solvent was completely evaporated under vacuum and lipid extracts were resuspended in 500 µL of 2-propanol/methanol/chloroform (4/2/1 v/v/v). Lipid extracts were transferred into 2 mL glass vials and stored in a -80°C freezer prior to mass spectrometry analysis.

Mass Spectrometry Analyses

Lipid extracts were introduced to an ultrahigh-resolution/accurate mass Thermo Scientific model Orbitrap Fusion™ Lumos™ Tribrid™ Mass Spectrometer (San Jose, CA) using an Advion Triversa Nanomate nESI source (Advion, Ithaca, NY) with a spray voltage of 1.0 kV and a gas pressure of 0.3 psi. The Ion Transfer Tube temperature was set to 150°C and RF Lens was set to 40%. Mass spectra were acquired in positive ionisation mode using orbitrap detector with maximum mass resolving power of

500,000 in the m/z range of 300-2000 for 2 minutes (approximately 115 scans). To confirm the glycerophospholipid headgroups and elucidate the acyl-chain structure of the lipids, higher-energy collision-induced dissociation (HCD) was applied to monoisotopically isolated precursor ions in negative ionisation mode (120,000 mass resolving power), using an optimised collision energy for each lipid class.

Peak Finding, Lipid Identification, and Quantification

Lipid identification and peak quantification were performed with LipidSearch 5.0α software (Thermo Fisher Scientific, USA and Mitsui Knowledge Industry, Japan). The program assigned lipid sum composition based on exact mass and ^{13}C isotope distribution found in mass spectra. Lipid classification and nomenclature based on the LIPID MAPS consortium were used (Fahy *et al.*, 2011). Lipid identification parameters used were 1 ppm of parent tolerance and parent threshold of 10 times of noise background intensity. Product ions in HCD-MS/MS spectrum were analysed to determine acyl chain structure. Further data analysis using R was performed to calculate molar ratio of lipids/protein by normalising peak intensity against corresponding internal standard peak intensity and protein content (R Core Team, 2016). Charts were produced using the plotly package for R (Plotly Technologies Inc., 2015).

Methodology for Small-angle X-ray Scattering Experiment on Bak

Small-angle X-ray scattering data were collected with James Murphy (Walter and Eliza Hall Institute) and analyses performed by James Murphy.

Small-angle X-ray Scattering Measurements and Analysis

SAXS data collection was performed at the Australian Synchrotron SAXS/WAXS beamline using an inline GF chromatography setup with co-flow (Kirby *et al.*, 2013), as detailed in (Weijman *et al.*, 2017). Fifty µL of purified recombinant Bak(α2-5) at 17 mg/mL was injected onto an inline S200 5/150 GF column and eluted at a flow rate of 0.2 mL/min via a 1.5 mm glass capillary positioned in the X-ray beam in 200 mM NaCl, 20 mM HEPES [pH 7.5], 5% v/v glycerol at 12°C. Scattering data were collected

in 2 second exposures over the course of the elution, and nine 2D intensity plots with superimposable scatter intensities from the peak of the size exclusion chromatography run were radially averaged, normalised to sample transmission, and background subtracted (as estimated from 20 averaged scatter profiles from earlier in the elution) using the Scatterbrain software (Stephen Mudie, Australian Synchrotron). Guinier analysis of data was performed using PRIMUS (Konarev *et al.*, 2003). An indirect Fourier transform was performed with GNOM to obtain the pairwise distance distribution function, P(r), and the maximum dimension, Dmax, of the scattering particle (Svergun, 1992). Theoretical scattering curves were calculated in CRYSOL from atomic coordinates of the Bak(α2-5) cylinder crystal structure lacking lipids or containing modeled *E. coli* lipids, and compared with the experimental scattering curve (Svergun *et al.*, 1995).